NSTX

CENTER STACK UPGRADE PRELIMINARY DESIGN REPORT STRUCTURAL ANALYSIS

August 2010

Prepared By:
P. Titus, H.Zhang, A. Zolfaghari, S.Avasarala, A. Brooks, R. Ellis, R.Woolley, J.Boales, A.Khodak, D. Mangra; M. Smith, R. Hatcher
PPPL Mechanical Engineering
L. Myatt, Myatt Consulting

Reviewed By:

Peter Titus Digitally signed by Peter Titus
DN: cn=Peter Titus, o, ou, email=ptitus@pppl.gov, c=US
Date: 2010.08.11 10:53:38 -04'00'

Peter Titus, Branch Head, Engineering Analysis Division

Approved By:

____

Phil Heitzenroeder, Head, Mechanical Engineering

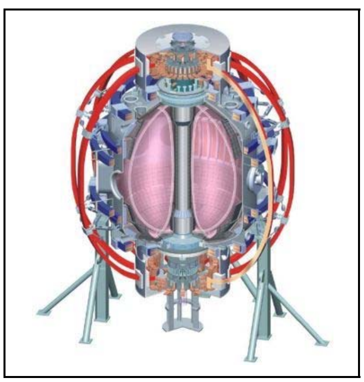

NSTX CENTER STACK UPGRADE PRELIMINARY DESIGN REPORT
STRUCTURAL ANALYSIS

Table of Contents

1 Introduction, Summary, and Design Input 4
1.1 Introduction 4
1.2. Summary of the CDR Analysis Status 5
1.3. Design Point 6
1.4 Criteria 8
1.4.1 Monotonic Stress Criteria 8
1.4.1.1 Allowables for Coil Copper Stresses 8
1.4.2 Room Temperature Allowables for 316 and 304 SST 8
1.4.2.1 Mill Certifications for the 304 Vessel Show a 45 ksi Yield........ 10
1.4.2.2 Insulation Shear Stress Allowable 11
1.4.2.3 NSTX Fatigue Criteria Document Content 14
1.4.3 Design Loads 15
1.4.3.1 Lorentz Loads 15
1.4.3.2 Criteria Document Paragraph I-2.0 LOAD COMBINATIONS .. 16
1.4.3.3 Criteria Document Paragraph I-2.6 Damage Limits & Recovery From Events 17
1.4.3.4 Machine Protection System Input
1.4.3.5 Monte Carlo Analysis 19
1.5 List of References 22
2. Global Modeling 23
2.1. Status of the Global Model 23
3. Plasma Facing Components (WBS 1.1.1) 24
3.1. Heat Balance and Heat Loads on PFCs 25
3.2 Tile Stress Analysis 27
3.2.1 Divertor Tile Thermal and Stress Analysis
3.2.2 Generic Tile Qualification Spreadsheet and ANSYS Script
3.2.3 Centerstack tiles
3.3. Disruption Analysis, Disruption Specifications 32
3.4. Passive Plate Disruption Analyses 37
3.4.1 Applying the Background Field
3.5 Disruption Analysis of the Detailed ProE model of the Passive Plates
3.5.1 Analysis of Ron Hatcher's PPP or Primary Passive Plate File
3.5.2 Analysis of Ron Hatcher's VDE Plasma 1 to 5........
4. Vacuum Vessel & Support Structure (WBS 1.1.2) ....
4.1. Overview ....
4.2 Port L modification
4.3. Vessel Outer Leg Connection ....
4.4. Upper Diaphragm/Cover/Flex ....
4.5. Umbrella Structure 54
4.5.1 Aluminum Block Connection of the TF to the Umbrella Structure
4.5.2 Umbrella Structure Support Feet
4.6 Support Ribs on the dished head
4.7. Center Stack Casing 60
4.7.1. Centerstack Casing Thermal Loads 64

4.7.2. Centerstack Casing Halo Loads ... 66
5. Magnet Systems (WBS 1.1.3) ... 69
5.1. Coil Builds ... 69
5.2. PF Currents ... 70
5.3. Fields and Forces ... 72
5.3.1 Lorentz Force Plots – TF and TF+OH
5.3.2 TF Current Profile
5.3.3 Toroidal Field Plots
5.3.4 TF Out-of Plane Force Plots
5.3.5 Poloidal Field Plots
5.4 Toroidal Field Coils ... 79
5.4.1. Coupled Electromagnic-Thermal Analysis ... 79
5.4.2 Analysis Method ... 81
5.4.3. Extended Hub Structural Pass ... 88
5.4.4 Joint Option Studies ... 91
5.4.4.1 Concept Options ... 91
5.4.4.2 TF Joint Qualification and Model ... 92
5.4.4.2.1. TF Joint Qualification Boundary Conditions ... 92
5.4.4.2.2. TF Joint Local Model ... 93
5.4.4.2.3. Joint Mechanical Parameters Comparison ... 96
5.4.4.2.4. Joint Electrical/ Thermal Parameters Comparison ... 96
5.4.4.2.5. Static Bolt Strengths and Insert Pull-Out Loads Comparison . 97
5.4.4.2.6. Comparison Summary ... 97
5.4.5. Global Torques ... 103
5.4.6 TF Coil Analyses
5.4.6.1 TF Inner Leg Torsional Shear ... 104
5.4.6.2 Global Model Results ... 104
5.4.6.3 Simplified Analysis ... 105
5.4.6.4 TF Outer Leg Reinforcement ... 111
5.4.6.5 TF Outer Leg Bond Shear ... 121
5.4.6.6 TF Outer Leg Bake-Out Stress
5.4.6.7 Stress at Friction Stir Weld at TF Extension
5.4.6.8 TF flash shield
5.4.7 OH and CenterStack
5.4.7.1. OH Analyses in the Centerstack Assembly ... 130
5.4.7.2 OH Conductor Fatigue Evaluation ... 136
5.4.7.3 OH Preload System
5.4.7.4 OH Coolant Hole Optimization ... 138
5.4.7.5 Stress Analysis of the Cooldown process.
5.4.7.6 OH Coax Connection
5.4.8 PF Coil and PF Support Analyses
5.4.8.9. Inner PF Support Design and Analysis ...
PF1a - OH Lateral Stability
PF1a, b Lead Support

5.4.8.11 Pedestal Analysis

5.4.8.12. PF 2, and 3 Support Design and Analysis 153
5.4.8.11. PF Coil Hoop Stresses 152
5.4.8.12. PF 4 and 5 Supports System 153
5.4.8.12.2.3 PF 4 and 5 Supports
5.4.8.12.2.2 PF 4 and 5 Supports Existing and Upgrade Welds
5.4.8.12.2.3 PF 4/5 Supports Dynamic Response to Normal Scenario Loading
5.4.9 Bus Bar Analyses
5.4.9.1 TF Bus Bar Support Analyses
6 Plasma Heating & Current Drive System (WBS 2) 164
6.1 High Harmonic Fast Wave (HHFW) – WBS 2.1 166
6.2 Electron Cyclotron Heating (ECH) – WBS 2.3 168
6.3 Neutral Beam Injection (NBI) – WBS 2.4 168
6.3.1 Net Pressure loads on the Vessel Due to NBI Bellows Vacuum
6.3.2 NBI Armor Backing Plate Disruption Eddy Current Loads
6.4 Foundation Loads
6.4.1 Angle Brace Hilti Anchor Loads
6.5 Seismic Analysis
7 Diagnostics

1 Introduction, Summary, and Design Input

1.1 Introduction

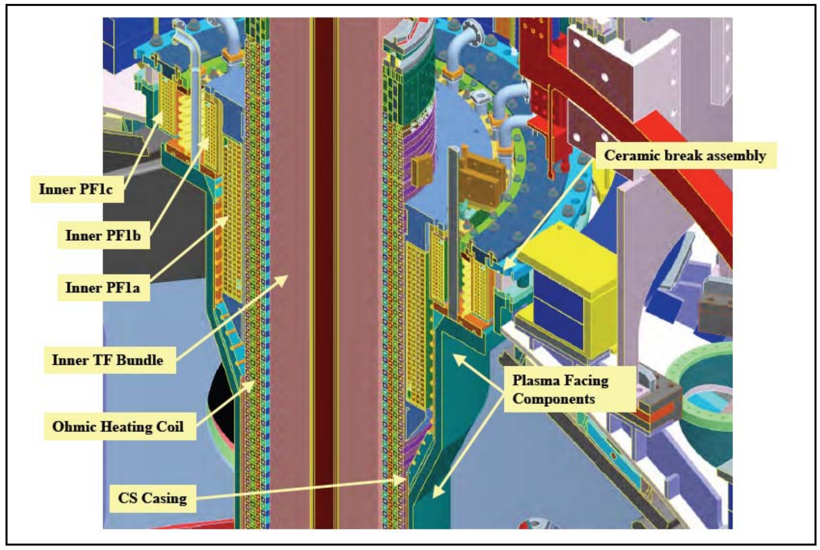

The NSTX [1] is the world's highest performance spherical torus (ST) research facility and is the centerpiece of the U.S. ST research program. Since starting operation in 1999, NSTX has established the attractiveness of the low-aspect-ratio tokamak ST concept characterized by strong intrinsic plasma shaping and enhanced stabilizing magnetic field line curvature. Figure 1.1- shows the major exterior features of the NSTX Center Stack Upgrade. Figure 1.1-3 shows some of the new features of the upgraded centerstack design

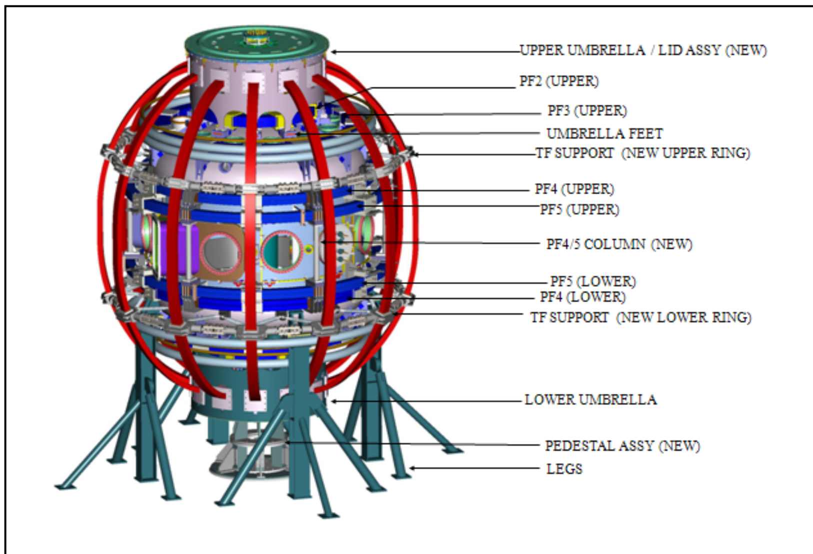

Figure 1.1-2 External Features of the Centerstack Upgrade

The purpose of the NSTX Center Stack Upgrade project is to expand the NSTX operational space and thereby the physics basis for next-step ST facilities. The plasma aspect ratio (ratio of major to minor radius) of the upgrade is increased to 1.5 from the original value of 1.26. The higher value of A matches the value found to be optimal in studies of future ST devices, and also increases the cross sectional area of the center stack by a factor of ~ 3 and makes possible higher levels of performance and pulse duration. The new center stack will provide a toroidal magnetic field at the major radius R_0 of 1 Tesla (T) compared to 0.55T in the existing NSTX device, and will enable operation at plasma current I_p up to 2 Mega-Amp (MA) compared to the 1MA rating of the existing. Plasma flat top duration is extended to 5.0 seconds from the present 0.5 second capability. This extension benefits substantially from another upgrade project which will add a second

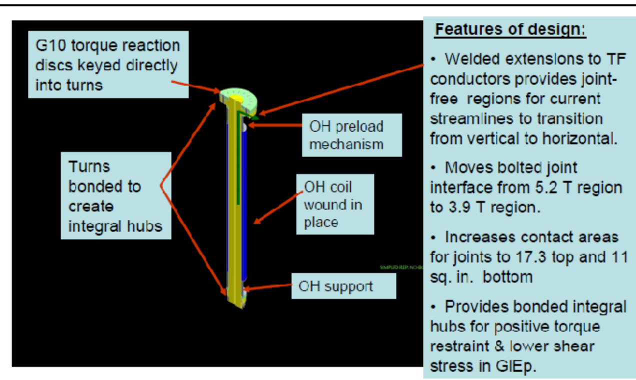

Figure 1.1-3 Features of the NSTX Center Stack Upgrade

Neutral Beam Injection (NBI) line to NSTX such that flat-top current sustainment can be achieved non-inductively using NBI current drive.

The NSTX center stack (CS) consists of the inner legs of the toroidal field (TF) coil surrounded by an ohmic heating (OH) solenoid and a several poloidal field (PF) shaping coils, all encased in a vacuum-tight metallic center stack casing (CSC) covered by plasma facing tiles. Since the TF coils include a demountable joint between the inner and outer legs, and the CSC includes a bellows and vacuum seal connection to the outer vacuum vessel, the entire center stack assembly is removable as a modular unit. Thus the upgrade will be accomplished by replacing the existing CS with an entirely new assembly with new TF inner legs, OH and PF coils, CSC, and plasma facing tiles. The TF outer legs, originally designed with an upgrade in mind, are retained but with enhancements to their structural supports. One substantial improvement, born out by recent (May 2010) operating experience, is the relocation of all coolant connections to the bottom of the centerstack. The bottom of the centerstack is connected through the TF flags to the pedestal and the OH is seated against the flags. The thermal excursions that occur each pulse are directed upward. and the large differential motions in the centerstack occur at the top. In the present operating version of NSTX, coolant connections are at the top and may have caused a leak in the lead.

This document describes the analytic effort performed to support the conceptual design effort. Analyses build on a strong document package qualifying the original NSTX design. Operational history also contributed to understanding weaknesses in the design and afforded an opportunity to expand the engineering qualification more uniformly throughout the machine. Calculations which support the original design may be found at:

http://nstx.pppl.gov/nstx/Engineering/NSTX_Eng_Site/Technical/General/Calculations/NSTX_Engr_Calcs.html

Calculations that support the conceptual design of the centerstack upgrade may be found at:

http://nstx-upgrade.pppl.gov/Engineering/WBS_Specific_Info/Design_Basis_Documentation/Calculations/index_Calcs.htm

1.2.Summary of the PDR Analysis Status

The design basis loading is evolving because of GRD guidance on Worst Case vs Normal +Machine Protection System. Cost savings have been realized extreme load scenarios have been removed via inclusion in the Digital Coil Protection System (previously called the Machine Protection System or MPS.) Much of the effort in the last six months has been dedicated to qualifying existing components of NSTX for the higher loads, and providing minimal modifications to support the higher loads.

TF Inner Joint Field and displacement boundary conditions have been passed to a detailed model of the joint (T. Willard's Calculation [4])

TF reinforcements for in-plane and out-of plane loads have been designed to Worst Case loads and remain in the territory currently used by the present TF supports – Loosening or disassembly is not required for bake-out. Reinforcements of the umbrella structure are needed.

Centerstack TF and OH assembly meets normal operational loads,. The Belleville support system maintains OH coil contact at lower support to eliminate motion at leads and coolant connections. This preload system is being optimized to meet the requirements of the design point which has only an 9000 max net upward load specified for the OH coil. The system is being designed to resist a 20,000 lb "launching" load to provide some headroom for nominal loads that will be used as a basis for the DCPS set points. The faulted loading is potentially very large - 400,000 lbs. A sacrificial bumper system is being considered to mitigate the effects of the faulted loading.

As of the CDR no modifications of the vessel or passive plates were anticipated for disruption loads. During the PDR, detailed modeling of the support hardware has been initiated and local details - brackets and bolts, have been identified that requireupgrade. More disruption cases are being run, and more detailed models of the passive plate support hardware are being modeled.

Active cooling being incorporated into the new center stack divertor areas has been sized. Tile surface temperatures for long pulse full power operation are high and require further evaluation.

Inner PF's and structure are undergoing improvements as a part of the normal design process to meet Normal and Halo loads.

Analysis work continues to complete treatment of all details of the design and optimize and economize the design concepts.

1.3. Design Point

Some of the CSU Upgrade parameters are repeated here for convenience (Table 1.3-1). An up-to-date complete listing of the these CSU Upgrade characteristics is provided in the design point spreadsheet available on the NSTX Upgrade engineering website at:

http://www.pppl.gov/~neumeyer/NSTX_CSU/Design_Point.html

Table 1.3-1Summary of CSU Upgrade Design Point Data

		NSTX BASE	NSTX CSU
Ro	m	0.854	0.934
Ip	MA	1.0	2.0

Bt@Ro	T	0.6	1.0
OH Flux Swing Total	Wb	0.7	1.9
Initiation Vloop	V	2.9	4.7
Ip Flat Top Time	s	0.5	5.0
Ip Ramp Up Rate	MA/s	5.0	2.0
Ip Ramp Down Rate	MA/s	10.0	4.0
Ro+a	m	1.477	1.504
A_95		1.4	1.6
a	m	0.623	0.570
R0-a	m	0.231	0.365
Zmax	m	1.371	1.424
Rzmax	m	0.480	0.593
Ip Duration	s	0.8	6.5
OH Single Swing Flux	Wb	0.4	1.4
OH Flux Initiation	Wb	0.1	0.1
OH Flux Ramp	Wb	0.5	1.3
OH Flux Flat Top	Wb	0.1	0.5
TF Rcuinner	m	0.0072	0.0260
TF Rcuouter	m	0.0977	0.1941
TF �Zcu	m	5.3300	5.3300
TF #turns	turns	36	36
TF #layers	layers	2	1
TF Ground insulation	m	0.0014	0.0024
TF Turn insulation	m	0.0008	0.0008
TF Cooling hole diameter	m	0.0047	0.0047
TF Conductor corner radius	m	0.0010	0.0010
TF Packing fraction		0.8169	0.8900
TF Voltage	V	1013	1013
TF Current	Amp	71168	129778
TF Tesw (L/R Decay)	s	1.38	7.57
TF Action (L/R Decay)	A^2-s	7.01E+09	1.27E+11
TF Voltage stress max turn-turn	kv/mm	0.6231	0.6231
TF Voltage stress max turn-ground	kv/mm	0.4637	0.3190
TF Inlet Coolant Temp	C	12	12
TF Inner leg maximum temp (L/R Decay)	C	99	100
TF Outer leg maximum temp (L/R Decay)	C	17	50
Total Copper Mass TF Inner Legs	Tonne	1.2	0.0
Total Copper Mass TF Outer Legs	Tonne	8.4	0.0
TF Rcuinner	in	0.2819	1.0220
TF Rcuouter	in	3.8469	7.6398
TF �Zcu	in	209.8425	209.8425
TF #turns	turns	36	36
TF #layers	layers	2	1
TF Cooling hole diameter	in	0.1860	0.1860
TF Conductor corner radius	in	0.0390	0.0390
TF Packing fraction		0.8169	0.8900

TF Current	Amp	71168	129778
TF Tesw (L/R Decay)	s	1.38	7.57
TF Action (L/R Decay)	A^2-s	7.01E+09	1.27452E+11
TF Voltage stress max turn-turn	volt/mil	16	16
TF Voltage stress max turn-ground	volt/mil	12	8
TF Inlet Coolant Temp	C	12	12
TF Inner leg maximum temp (L/R Decay)	C	99	100
TF Outer leg maximum temp (L/R Decay)	C	17	50
Total Copper Mass TF Inner Legs	lbs	2560	0
Total Copper Mass TF Outer Legs	lbs	18495	0

1.4 Criteria

For the conceptual design of NSTX Centerstack Upgrade, a structural criteria specific to the project, has been adopted. This and the General Requirements document provide the criteria for design of the upgrade. Both the GRD and the criteria document may be accessed through the NSTX Upgrade engineering web page. Summaries are included in the following sections.

1.4.1 Monotonic Stress Criteria

1.4.1.1 Allowables for Coil Copper Stresses

The TF copper ultimate is 39,000 psi or 270 MPa . The yield is 38ksi (262 MPa). Sm is 2/3 yield or 25.3ksi or 173 MPa – for adequate ductility, which is the case with this copper which has a minimum of 24% elongation. Note that the ½ ultimate is not invoked for the conductor (It is for other structural materials) . These stresses should be further reduced to consider the effects of operation at 100C. This effect is estimated to be 10% so the Sm value is 156 MPa. From NSTX Design Criteria Document [NSTX_DesCrit_IZ_080103], Sections I-4.1.1 and I-4.1.2:

- For conventional (i.e., non-superconducting) conductor materials, the design Tresca stress values (Sm) shall be 2/3 of the specified minimum yield strength at temperature, for materials where sufficient ductility is demonstrated (see Section I-4.1.2). *
- It is expected that the CS would be a similar hardness to the TF so that it could be wound readily. For the stress gradient in a solenoid, the bending allowable has been used for initial sizing. The bending allowable is 1.5*156 or 233MPa, Membrane or average tresca stress in the coil section should meet the membrane stress allowable.

1.4.2 Room Temperature Allowables for 316 and 304 SST

Table 1.4-1 below shows the room temperature allowables for 316 and 304 stainless steels.

Table 1.4-1 Room Temperature Allowables for 316 and 304 SST

Material	Sm	1.5Sm
316 LN SST	183Mpa (26.6 ksi)	275Mpa (40ksi)
316 LN SST weld	160MPa(23.2ksi)	241MPa(35ksi)

1.4.2.1 Mill Certifications for the 304 Vessel Show a 45 ksi Yield

Figure 1.4-1 is represents the mill certifications for the 304 vessel. This shows a 45 ksi yield.

05/19/1998 13:53 6174720409 NEWENGLANDSTEELTANK PAGE 03

Avesta Sheffield Plate Inc.

Certificate of Analysis and Tests

OUR ORDER 106101 - 01 HEAT & PIECE 87893-3B 5/13/98

PSI MIC NO. C9923

SOLD TO: PROCESS SYSTEMS INTERNATIONAL
20 WALKUP DRIVE
WESTBOROUGH MA 01581

SHIP TO: NEW ENGLAND STEEL TANK
111 BROOK ROAD
SOUTH QUINCY MA 02169
737001-06

YOUR ORDER & DATE

558635 3/18/98 TAG# PART #V077P001

ITEM DESCRIPTION

HEAT & PIECE 87893 - 3B 3A
WEIGHT 3002
FINISH 1
GRADE 304 UNS-S30400
DIMENSIONS .625 X 76.000 X 212.000 EXACT

SPECIFICATIONS

THE PRODUCTS LISTED ON THIS MILL TEST REPORT SATISFY PREFERENCE CRITERION B AS DEFINED IN ARTICLE 401 OF THE NORTH AMERICAN FREE TRADE AGREEMENT. COUNTRY OF ORIGIN IS USA

ASTM A240-96A ASMESA240-96AD
NO WELD REPAIR ON MATERIAL
ASTM A262-93A PRAC A

ASTM A480-96,ASMESA480-96AD
MAG PERM <1.05 ASTM A342 (6)
ASTM A262-93A PRAC E

PLATES & TEST PCS SOLUTION ANNEALED @ 1950 DEGREES FARENHEIT MINIMUM.
THEN WATER COOLED OR RAPIDLY COOLED BY AIR
FREE OF MERCURY CONTAMINATION
HOT ROLLED, ANNEALED & PICKLED (HRAP)

MECHANICAL & OTHER TESTS

HARDNESS RB	81
GRAIN SIZE	5
YIELD STRENGTH (PSI)	45256
TENSILE STRENGTH (PSI)	91368
BEND	OK
INTERGRANULAR CORROSION	OK
ELONGATION % IN 2"	63.6
REDUCTION OF AREA %	72.5

Figure 1.4-1 Material Certification for 304 Stainless Steel

1.4.2.2 Insulation Shear Stress Allowable

From Dick Reed (Cryogenic Materials, Inc.) reports and conversations concerning stress allowables at room temperature, shear strength, short-beam-shear, and interlaminar shear, the results are:

- Without Kapton: 65 Mpa (for TF, PF1 a,b,c)
- With Kapton: 40 MPa (CS)
- Estimated Strength at Copper Bond: 65 MPa/2 = 32.5 MPa (All Coils)

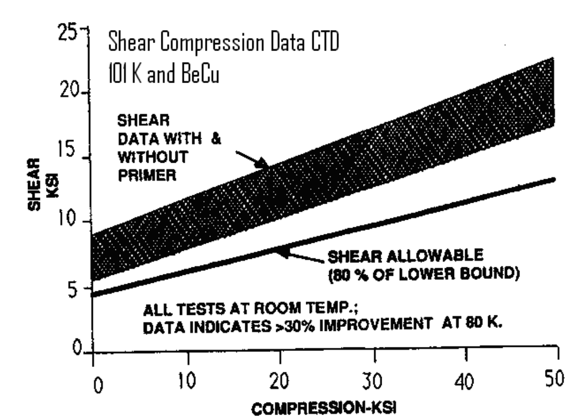

Figure 1.4-2 Shear Compression Data

From the NSTX Criteria Document***: SectionI-5.2.1.3 Shear Stress Allowable***

The shear-stress allowable, Ss, for an insulating material is most strongly a function of the particular material and processing method chosen, the loading conditions, the temperature, and the radiation exposure level. The shear strength of insulating materials depends strongly on the applied compressive stress. Therefore, the following conditions must be met for either static or fatigue conditions:

Ss = [2/3 to]+ [c2 x Sc(n)]

2/3 of 32.5 MPa = 21.7 MPa

5ksi=34 MPa
2/3 of this is 23 MPa
C2~=.1 (not .3)

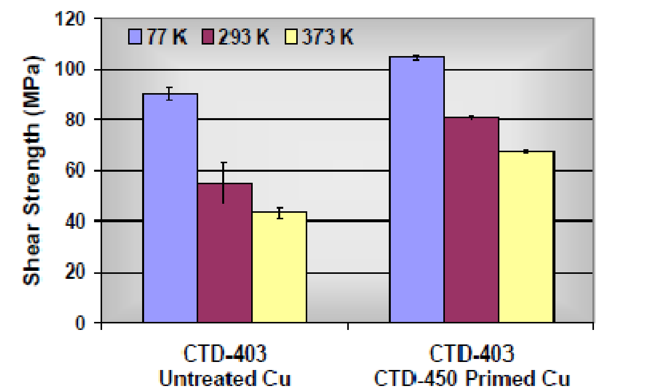

Shear Strength with binder

Figure 1.4-2 at right shows the shear compression data from CTD for 101 K and BeCu.

The fatigue strength for the required 60000 cycles based on the Cyanate Ester primer at 100C is 21.5 MPa. The allowable without compression is 2/3*21.5= 14.33 MPa

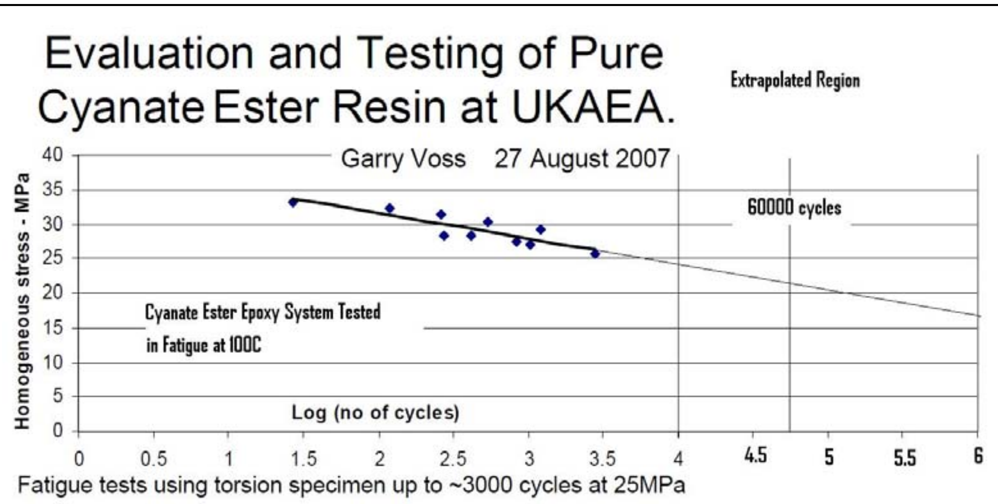

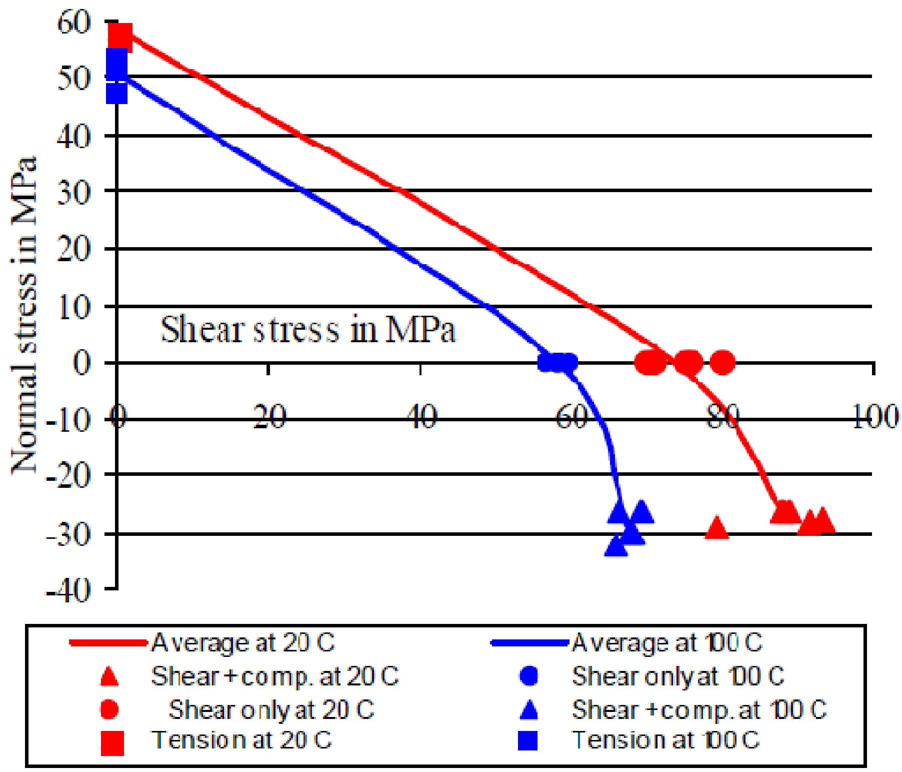

From Gary Voss Paper on Cyanate Ester

Criteria – Stress Allowables

	Sm	Sb	
TF Copper	156 MPa	233MPa,	
OH Copper	156 MPa	233MPa	
Vessel 304 Away from weld	30 ksi 207 MPa	45 ksi 310 MPa	Mill Certs for the 304 Vessel Show a 45 ksi Yield
304 Vessel in Heat Effected Zone	20 ksi 138 MPa	30 ksi 206MPa	
316	183 MPa	275 MPa	
316 weld	160MPa	241MPa	
AISC/ASME/AWS 304 weld	20 ksi (w/PT)	14ksi (w/Visual)	

	Static	Fatigue	
TF Insulation	2/3 of 24 - **16 MPa**	16 Mpa Qualified by Component Test	Existing TF Prepreg CTD 12P
CS Insulation CTD 101K	***2/3 of 32.5 MPa*** = ***21.7 MPa***	2/3*21.5MPa=14.3 Mpa based on primer	With high temp binder CTD-450

1.4.2.3 NSTX Fatigue Criteria Document Content

- NSTX CSU is designed for approximately 3000 full power and 30,000 two-thirds power pulses.
- A fatigue strength evaluation is required for those NSTX CSU components with undetectable flaws that are either cycled over 10,000 times or are exposed to cyclic peak stresses exceeding yield stress.
- Any NSTX component without cyclic tensile loading and loaded only in compression shall not require a fatigue evaluation.

For engineering purposes, number of NSTX pulses, after implementing the Center Stack Upgrade, shall be assumed to consist of a total of ~ 60,000 pulses based on the GRD specified pulse spectrum.

Fatigue had not been considered extensively during the CDR, For the PDR, the Criteria document and GRD, which had different life requirements, have been reconciled. A definition of the aged condition for "used" components has been developed. This largely depends on pre-service inspection and in-service inspection. Because of the increase in loads, Minors rule and non-linearity of fatigue, previous stress cycles will add little in the cumulative damage evaluation, but there are some indications of fatigue issues, for example the OH lead failure and OH strap fatigue. These have led to a commitment to develop an inspection regimen for components that have been identified as sensitive to fatigue. The next run period (June 2010) includes revisions in the PF4 and 5 currents that will increase weld stresses in the brackets that supports these coils. The corners of the square weld patterns that attach the brackets to the vessel shell were inspected visually and no indication of cracking or weld failure was found. Similar inspections will be done on similarly highly stressed components.

There will be a formal list of required in-service inspection locations.
Here are a few:

1. Weld under the Umbrella Foot.

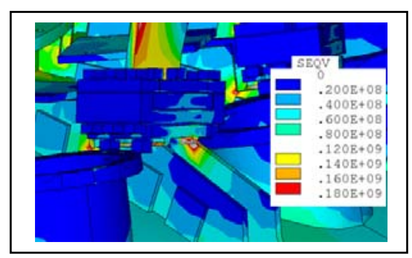

2. PF4/5 Corners of the bracket weld to the vessel

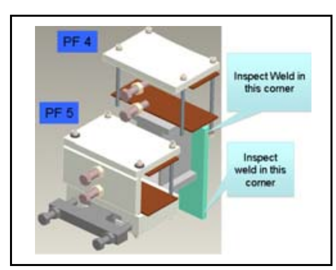

1.4.3 Design Loads

1.4.3.1 Lorentz Loads

Lorentz Loads from coil currents are a major loading on NSTX. A range of identified operational current equilibria constitute the normal operating loads. These are included in the published design point, accessed through the NSTX Upgrade web page[1]. A plot of the currents is included in Figure 1.4-3 and Figure 1.4-4.

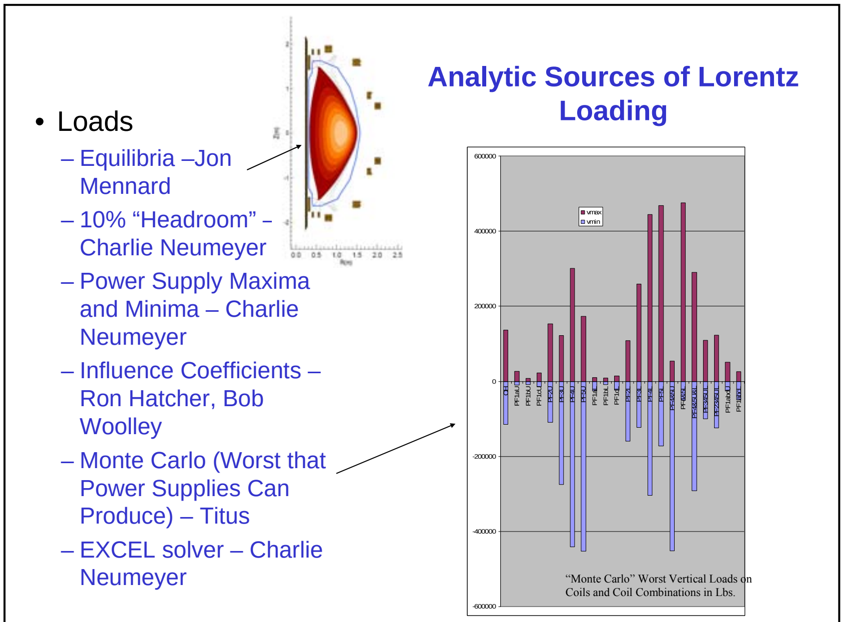

Figure 1.4-3 Analytic Sources of Lorentz Loading

A modest 10% “headroom is used in the current specs to provide for some scenario flexibility.

A challenging requirement in the GRD was to evaluate worst power supply loads and attempt to design to these. If the resulting designs are difficult or costly to implement, then the load combination that produces the “onerous” loading is to be addressed in the Machine Protection System (MPS). The magnitudes of the worst case combinations of loads have made it hard to design any of the structures to meet the worst case load criteria.

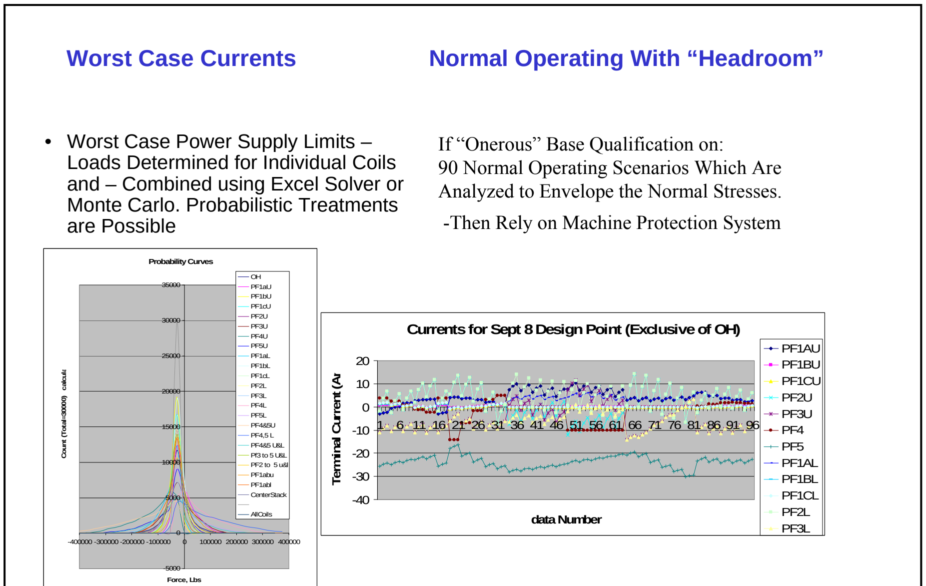

Figure 1.4-4 Worst Case and Normal Operating Conditions

The TF self load effects i.e. the centering load in the centerstack and the tension loads in the outer legs have been designed with the maximum terminal current planned for the upgrade. It is the poloidal field coils that potentially combine in uncertain ways to produce large unanticipated loads. The outer leg reinforcements had been designed to the worst out-of-plane loads, and the hardware needed to react these loads did not appear excessive, however even minimal improvements in the clevises that are attached to the knuckle region of the vessel were judged difficult. Reliance on the digital coil protection system and adherence to the limits of the 96 scenarios in the design point has allowed TF support concepts that do not require alteration to the existing hardware. Support of the outer PF coils to resist the worst possible extremes in loading appeared to be a costly and time consuming proposition. This area is one of the prime candidates for relaxing load requirements and obtaining some significant cost savings. In order to utilize the full capacity of PF4 and 5 extra columns have been added, spaced between the existing columns.

The specifics of the load spec for the poloidal field coils were still evolving at the time of the CDR. One approach is to rely exclusively on the digital coil protection system, and abandon designing to coil current overage, If this is chosen , the criteria, and the GRD had to be changed. One proposal was to add a probabilistic approach. This would remain within the GRD, and Criteria framework by describing what a reasonable level of over current loading should be. - essentially putting a spec on "onerous" During the CDR, J. Minerviini suggested a ITER like categorization of loads – MED is working to this on the ELM coils, port plugs etc. Excerpts from our NSTX criteria document were provided to the review committee. ITER uses a load spec that assigns "Anticipated" "Unlikely" etc. to loading - but no probabilities. The present NSTX Centerstack Upgrade criteria quotes probabilities. The NSTX CSU GRD and Criteria provides a better framework to categorize loads than ITER, but there is some consistency in approach and there would be an advantage in retaining a framework of load qualification used on other projects. The solution for these difficulties is to commit to building a robust Machine Protection System and shifting the worst case currents evaluation from an “Unlikely” category to an “Extremely Unlikely Category” In the structural design criteria, the load spec will be clarified. Load categorizations will be based on an update of the NSTX Failure Modes and Effects Analysis (FMEA) Numerical probabilities will not be assessed. A rigorous reliability analysis is not judged appropriate for the NSTX CSU experimental device.

A draft proposal **(red text)** follows in the following two sections.

1.4.3.2 Criteria Document Paragraph I-2.0 LOAD COMBINATIONS

The NSTX structural systems shall be designed for both normal operating conditions and off-normal events. These conditions are:

- Normal Events - Events that are planned to occur regularly in the course of facility operation. ***Normal EM loading shall consist of the 96 currently (Nov 2009) defined current scenarios, identified in the NSTX Upgrade Design Point, and other normal operating current scenarios identified as required for the NSTX Centerstack Upgrade mission, and included in the Design Point.***
- Anticipated Events - Events of moderate frequency which may occur once or more in the lifetime of a facility. ***Anticipated EM loading shall consist of Normal loads plus disruptions judged to be common or anticipated.***
- Unlikely Events - Events which are not anticipated but may occur during the lifetime of a facility.

EM Loading for Unlikely Events can result from:

- ***TBD – The Failure Modes and Effects Analysis (FMEA) will be re-evaluated by WAF cognizant Engineers for the Upgrade Design Point. A qualitative evaluation of the likelyhood of the failure and the severity of the consequences will be combined in a qualitative manner and be assigned to the list of "Unlikely" and "Extremely Unlikely" events***
- ***Disruption Events that are judged to be unlikely***

- Extremely Unlikely Events - Events which are not expected to occur during the lifetime of a facility but are postulated because of their safety consequences.

  EM Loading for Extremely Unlikely Events can result from
  - ***Machine Protection System(MPS) failure. Lower level power supply controls remaining intact, with random or pegged currents resulting, Consequences of current control failure shall be within the damage limits described in the table in section 1.2.6***
  - ***Other TBD events from the FMEA***
  - ***Catastrophic Disruption Events if identified for NSTX***
  - Incredible Events - Events of extremely low probability of occurrence or of non-mechanistic origin.

1.4.3.3 Criteria Document Paragraph I-2.6 Damage Limits & Recovery From Events

Table 1.4-2 Damage Limits and Recovery from Events

Condition	Functional and damage limit for the experimental facility	Damage limits to component or support	Recovery from damage
Normal	All the safety related structures, systems, and components are functional.	The component or support should maintain specified service function.	Within specified operational limit. Anticipated maintenance and minor adjustment.
Anticipated	All the safety related structures, systems, and components are functional.	The component or support must withstand this loading without significant damage requiring repair.	Within specified operational limit. Anticipated maintenance and minor adjustment
Unlikely	In addition to the challenged component, inspection may reveal localized large damage, which may call for repair of the affected components.	Material plasticity, local insulation failure or local melting which may necessitate the removal of the component from service for inspection or repair of damage to the component or support.	The facility may require major replacement of faulty component or repair work.

Extremely Unlikely	Gross damage to the affected system or component. Nevertheless the facility maintains the specified minimum safety function.	Gross general deformations, local melting and extensive insulation damage requiring repair, which may require removal of component from service.	Magnet system may be so damaged that repair is not considered economic.

1.4.3.4 Digital Coil Protection System (DCPS)

The proposed DCPS is described in detail in a draft requirements document by Robert Woolley ref [13]. In the description of the DCPS, the "systems code" will actually be the analyses described in the filed structural calculations. There is a global model which is the closest thing we have to a single systems code, but this is augmented in many ways by separate calculations to address specific stress locations and components and support hardware. During the final design activity, Each preparer of a calculation will be assigned the development of "mini algorithms" Some examples are:

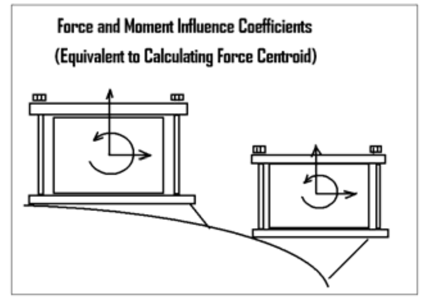

Figure 1.4.3.4-1

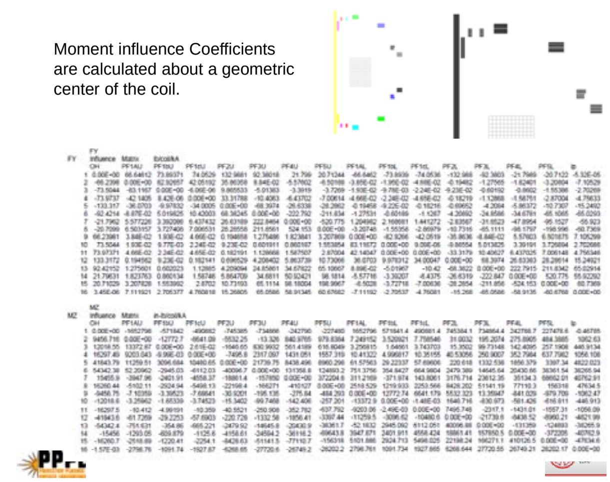

Figure 1.4.3.4-2 Moment Influence Coefficients. These are computed by P. Titus. R.Woolley has also calculated these

.

PF1,2,3 supports, welds bolts – At this stage, These are just calculated from influence coefficient matrix loads divided by weld or bolt area. Addition of moment influence coefficients has been proposed to address the difference between the centroid of the Lorentz force and the support reaction location.

- PF 4/5 support weldment (see section 5.4.6.12.2.2)
- PF4/5 Conductor stress - Hoop + bending + thermal
- OH Preload-Launch-TF temperature dependence
- PF1a-OH interaction Stress
- Vertical Loads on pedestal load path (TF Flag Bolts, Pedestal hilti's), (Ali)
- TF Strap (T. Willard)
  - Mostly designed to TF max Current. DCPS should trip if vertical field exceeds limit (.24T?)
- -More – As a Guide on Scope: Use the number of calculations each with a few sensitive areas

The DCPS is ultimately intended to address shorter times between shots, i.e. starting the next pulse before the coils are fully cooled. For low current short shots, the thought is that the heat-up will be small and the internal temperature differences will not produce unacceptable stress. A better way is to run multiple short shots and let the temperatures accumulate until a limit (100C) is reached then pause for the 20 minutes for cooldown. It is possible to run a number of conditioning shots or shots that explore start-up, etc. of the same scale run now, then cool and then have a long pulse shot. If thermal gradients in any of the coils, can be avoided that would be best. Otherwise you have to postulate all kinds of gradients based on how far the "wave" has progressed in each coil.

The DCPS requirements document assumes the individual stress components are subject to linear superposition. There are some number of areas where non-linear dependencies will be important. The double pancakes of PF4 and 5 develop beam strength via friction between the pancakes resulting from the self attraction of the two pancakes. There are coulomb friction and geometric non-linearities.

The DCPS requirements document assumes shear stresses are small. This is not always true in PF and OH coils. Long narrow coils like the OH and to a lesser degree the PF1 coils see radial and vertical field gradients that cause non-uniform distributions of Lorentz forces, and resulting shears. In a long thin solenoid this causes the “bellmouthing” at the ends and can produce sizeable shears, with only self field gradients. The interaction between PF1a and the OH could produce interesting shears. This is an interesting problem for the DCPS. Shear capacity is improved by compressive stress. For a self field in a solenoid, the compressive stress goes as the square of the coil current – if it sees a shear stress due to the attraction to a neighboring coil, the shear stress is related to the product of the two coil currents. You could have a situation where ramping down currents uniformly could diminish the shear capacity faster than you diminish the applied shear. For the OH, the local shear stress dependencies are evident in and ultimately will be addressed in centerstack Ali Zolfaghari’s calculation.

Examples of Algorithms for the DCPS

The Latest Coil Current Spec allows the OH current to go from -24kA to +24kA, but limits currents in the OH and PF1a via a limit on:
f1*OH Current^2 + f2*PF1a * OH currents.

PF4/5 support bracket weld - A new, separate control system has been added to the current operation (2010). This system has a small computer mounted on a control board that calculates loads from PF3,4,5,U/L then multiplies these by linear transforms to weld stress and the stress is limited. Implementation of this was troublesome because a conservative stress limit based on peak weld stress in the weld corner limited operation below previous test currents. Stress requirements were relaxed and an inspection of the corner stresses was performed. No weld cracks or other indications of overstress were observed.

1.4.3.5 Monte Carlo Analysis and Other Coil Load Maximizers

Maximized loads from individual coil current maximums have been calculated in a few different ways. Charlie Neumeyer uses the EXCEL optimizer. Ron Hatcher varies coil currents to their individual max and min current and finds the max load This analysis and the procedures for quantifying worst case loads may still find some usefulness in identifying loads for the “Extremely Unlikely” Category.

Vertical and Radial force influence matrices were provided by Ron Hatcher(1). These were used in a Monte Carlo simulation which varied the coil current’s within their allowable ranges and computed forces on the individual coils. The maximums and minimums were determined for 10,000 sets of randomly selected coil currents. This yields the worst case loading the power supplies can produce, and ignores the likely loading during plasma shots. The resulting loads and hoop stresses are useful in providing an upper limit on the mechanical loads on the coils. Forces on coil groups, such as PF4 and 5 upper can be summed and maxima and minima determined to provide design loads for specific structural elements or regions.

The "random" results are similar to those obtained in the design point spreadsheet with EXCEL solver or Hatchers procedure to rack up max loads. Typically the Monte Carlo simulation with 10,000 simulations misses some of the peaks and captures more with a higher number of simulations. Modeling "pegged" currents extends the likelihood that the Monte Carlo simulation will capture the low probability max loads because currents are modeled as either at a max or a min, rather than simulations many intermediate currents. Figure 1.4-5 shows a typical Monte Carlo current assignment routine. Figure 1.4-6 shows a graphical representation of the Monte Carlo simulation run by Ron Hatcher.

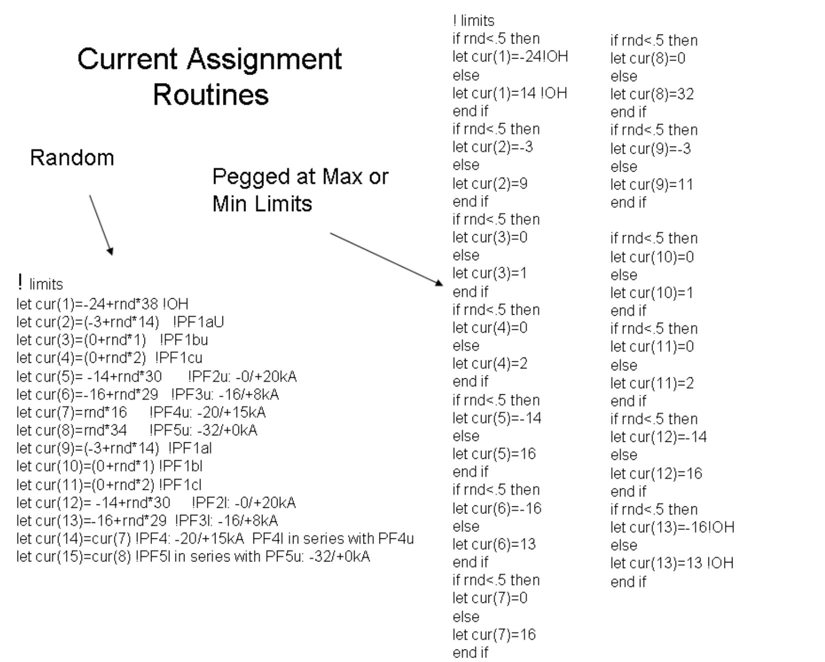

Figure 1.4-5 Monte Carlo Simulation Current Assignment Routine

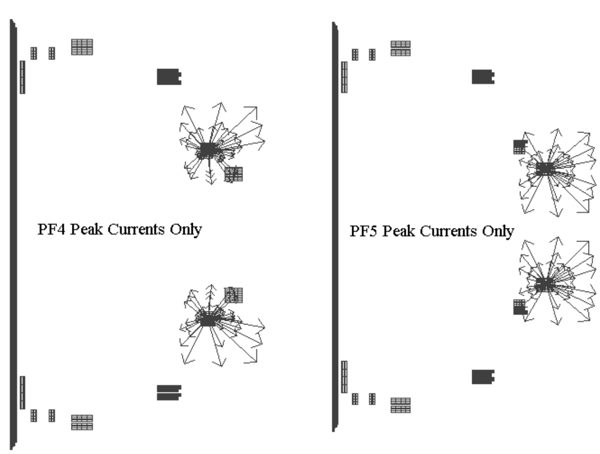

Figure 1.4-6 Monte Carlo Graphical Representation

1.5 List of References

[1] Design Point by Charles L. Neumeyer, http://www.pppl.gov/~neumeyer/NSTX_CSU/Design_Point.html, dated 7-29-2009.

[2] NSTX-CALC-13-001-00, Global Model – Model Description, Mesh Generation, Results

[3] Disruption Analysis Of Vacuum Vessel and Passsive Plates NSTX-CALC-12-001-00, S. Avasarala

[4] Tom Willard, "TF Flex Joint and TF Bundle Stub", NSTX-CALC-132-06-00, 2009.

[5] Robert D. Woolley, "TF Joint Pressure VS Temperature In NSTX CSU Upgrade", CSU-CALC-132-090211-RDW-01, 2009.

[6] Peter Titus, "Coupled Electromagnetic-Thermal Analysis (04072009)", *NSTX-CALC-132-01-00*, 2009.

[7] Peter Titus, "Coupled Electromagnetic-Thermal Analysis (04202009)", NSTX-CALC-132-02-00, 2009.[8] Robert D. Woolley, "TF Out-Of-Plane (OOP) PF/TF Torques on TF Conductors in NSTX CSU", CSU-CALC-132-03-00, July 26 2009

[9] P. Titus, "Maximum TF Torsional Shear" CSU-CALC-132-07-00

[10] JOINT PRESSURE VS TEMPERATURE IN NSTX CS UPGRADE, 132-090211-RDW-01 R. WOOLLEY 11 February 2009
TO: DISTRIBUTION Date:

[11] Reference 1: R. Woolley memo, "NSTX TF Flag Joint Relationship between Contact Electrical Resistance and Contact Pressure",1 June 2004;[Included herein as Appendix B]

[12] N.J.Simon, E.S.Wexler, R.J.Reed, NIST Monograph 177, "Properties of Copper and Copper Alloys at Cryogenic Temperatures", 1992

[13] DIGITAL COIL PROTECTION SYSTEM (DCPS) REQUIREMENTS DOCUMENT (DRAFT)**,** NSTX-CSU-RD-DCPS for the National Spherical Torus Experiment Center Stack Upgrade, February 5, 2010 R. Woolley

[14] NSTX SEISMIC DESIGN ANALYSIS REPORT, 71-990611-JHC-01, Revision 00,June 11, 1999, Prepared By: James H. Chrzanowski, Douglas G. Loesser, Mike Kalish, Bob Parsells, Approved By Charlie Neumeyer, NSTX Engineering Project Head

[25] Disruption specification were provided by Jon Menard as a spreadsheet: disruption_scenario_currents_v2.xls, July 2010

2. Global Modeling

2.1. Status of the Global Model

The Global model of the NSTX machine and Center Stack Upgrade (NSTX-CSU) provides a simulation of the overall behavior of the machine. It provides boundary conditions for local models and sub Models , or allows inclusion of the detailed models of components in the global model. The CDR version is shown in (figure 2.1-1). In many cases it has been built from other available model segments – The upper and lower head sections of the vessel model come from H.M. Fan's early vessel models. The cylindrical shell that contains the mid plane ports comes from a vessel model built by Srinivasa Avasarala from the Pro–E model of the vessel. In some instances parts of the global model were exported to be evaluateds in more detail. Multiple scenarios from the NSTX design point are run using the global model. The design points are publized on the web and are maintained by C. Neumeyer.

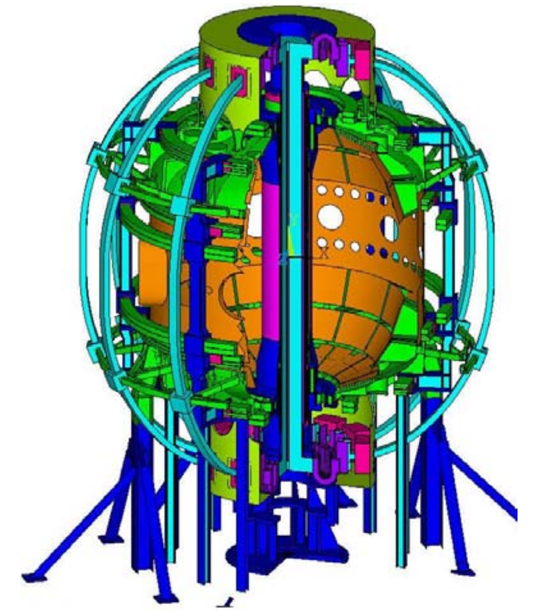

Figure 1.5-1 Global Model With External PF Cage

As of this issue of the calculation, all 96 normal operating current sets published in the July 2009 design point have been run in the global model (Figure 2.1-2).

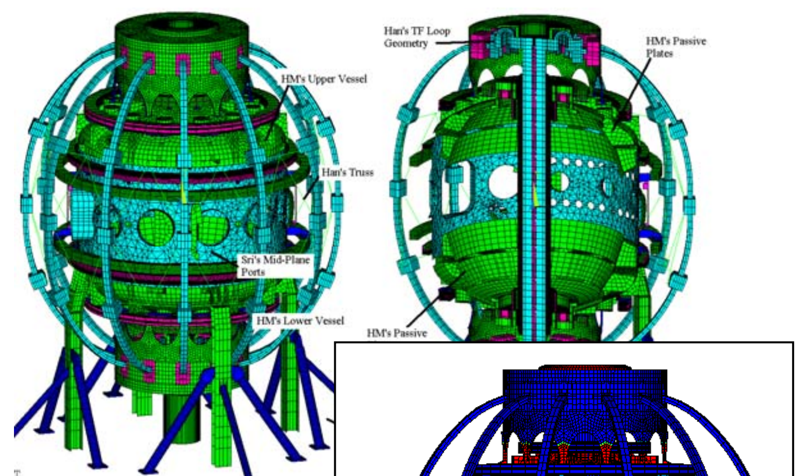

Figure 2.1-2 Global Mod

The September 8 2009 design point has a revision to the OH current variations limiting the currents to +24kA and -13.8 kA. These were never run. During the PDR, the OH currents were returned to the earlier +24, -24kA spec. The loads from normal operating current sets are in general are much less severe than loads that are based on worst case power supply currents. In order to compare the global model results with some of the local models that have been run, some of the "worst case" currents have been run in the global model. The outer TF reinforcements are an example of this.

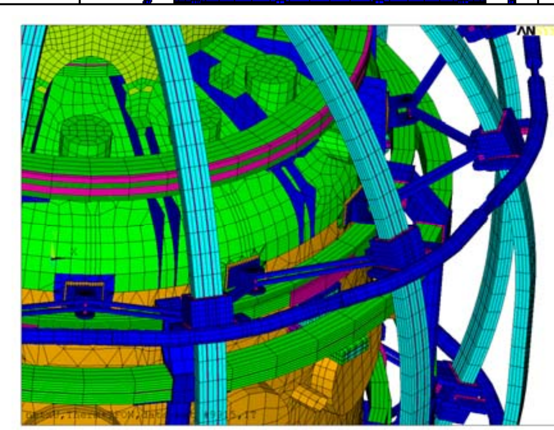

Conditions

Results reported in sub paragraphs of section 8 have been used to qualify components, check results and guide the need for further analyses. The outer TF leg reinforcements discussed in section 8.3 and in NSTX calculation number 132-04-00 are based on two pairs of current sets. These are intended to maximize the out-of-plane loading on the TF outer legs for an up-down symmetric loading and an up-down asymmetric loading that causes large net torques on the outer legs. These two current sets were included in the loading analyzed in the global model. Behavior of the two analyses is consistent. Section 8.3 of Ref [2] discusses these results and adds a qualifiucationn of the bending related bond shear in the TF outer leg. Section 8.1 documents the acceptable stresses in the diaphram plate that replaces the gear tooth torsional connection between the centerstack and the outer umbrella structure.Section 8.5 of Ref [2] provided global displacements to the detailed analysis of the flex joint [4] Section 1.3.2.3 or Secion 8.6 of Ref [2] is to date, the only treatment that shows acceptability of the torsional shear in the inner leg. Other sections of Ref [2] similarly profided guidance on global twist in the evaluation of the centerstack OH support details. Section 8.8 shows the stresses and loading around the I beam column attachmeents to the vessel and points to the need to evaluate the weld details of this connection.

Figure 2.1-3 shows the global model at 350 C bakeout conditions. Figure 2.1-4 shows the bakeout vertical displacements of the CDR \version of the machine. Note that the outer PF support "cage" is not connected to the vessel during normal operation or bake-out. The global model allowed studies of various alternative configurations of the PF and TF supports throughout the PDR, the global model has been updated to reflect support of the PF coils off the vessel as well as support of teh TF out-of-plane (OOP) loads off the vessel.

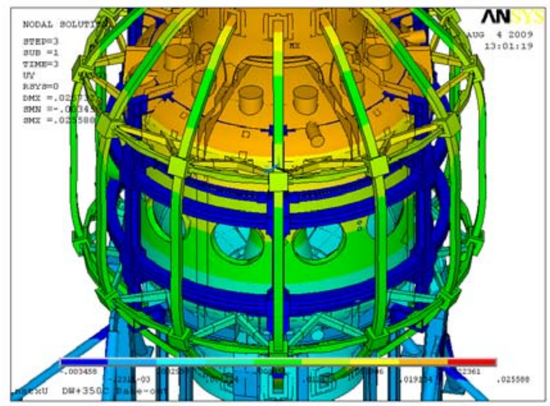

Figure 2.1-4 Bake-out Vertical Displacements

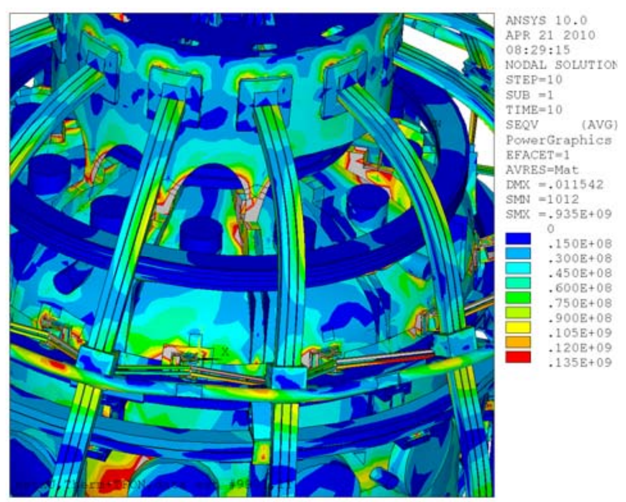

Figure 2.1-5 Stress levels in the outer structures from the global model

3. Plasma Facing Components (WBS 1.1.1)

3.1. Heat Balance and Heat Loads on the Vessel and PFCs

A thermal analysis of the NSTX CSU was done to demonstrate that the adequacy of proposed active cooling of the CS, in conjunction with radiation cooling to outboard components, to limit the maximum temperatures and thermal gradients in the CS Casing to protect the CS coils and O-rings joints. The analysis and analysis models is described in figure 3.1.2. Output of the thermal analysis (Figure 3.1-1, and 3) was used in a first cut thermal stress analysis of the graphite tiles. The impact of anticipated lithium coating on ratcheted temperatures was also investigated by varying the emissivity

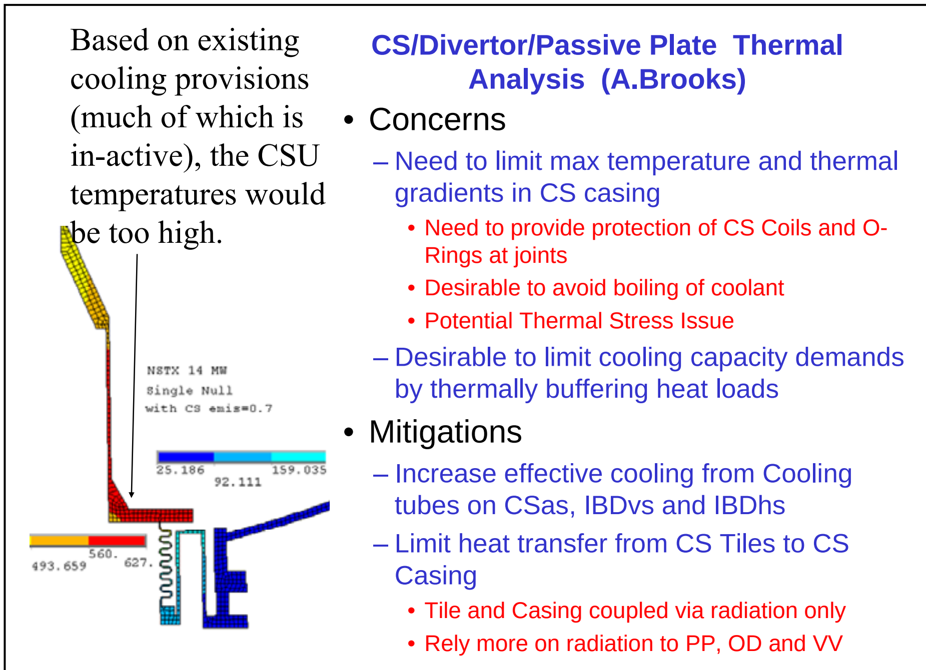

Figure 2.1-1 Heat Balance Summary Slide from the CDR

Results of the analysis were used to guide the design. In particular, it was found advantageous to thermally isolate as much as possible the CS tiles from the CS casing to limit the thermal ratcheting of the casing and thermal gradients with the actively cooled inboard divertor region. This does lead to higher temperatures in the graphite (in excess of 2000 C) which needs to be assessed by the project as to whether the increased carbon sublimation can be tolerated or if alternate materials (ie molybdenum) should be considered. Figure 3.1-3 shows the heat balance summary and the critical areas requiring cooling. Figure 3.1- also shows the end of pulse temperature distribution.

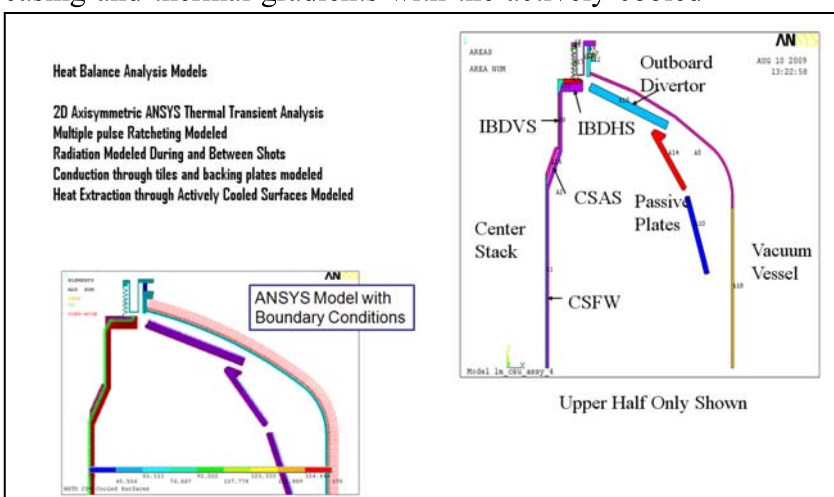

Figure 3.1-2 Thermal Analysis Models

NSTX currently does not use many of the provisions for active cooling. The upgrade will have more heat addition with the addition of the second neutral beam more RF, higher plasma current and longer pulses. This will require activation of minimally used cooling systems and design of cooling systems for the new centerstack.

Figure 3.1.4 is a representation of the operating envelope that will be available to NSTX operations. Single Operation will be limited depending on the allowd tile surface temperature, surface heat load and emissivity. The tile temperature limit based on stresses and sublimation is discussed in the following section.

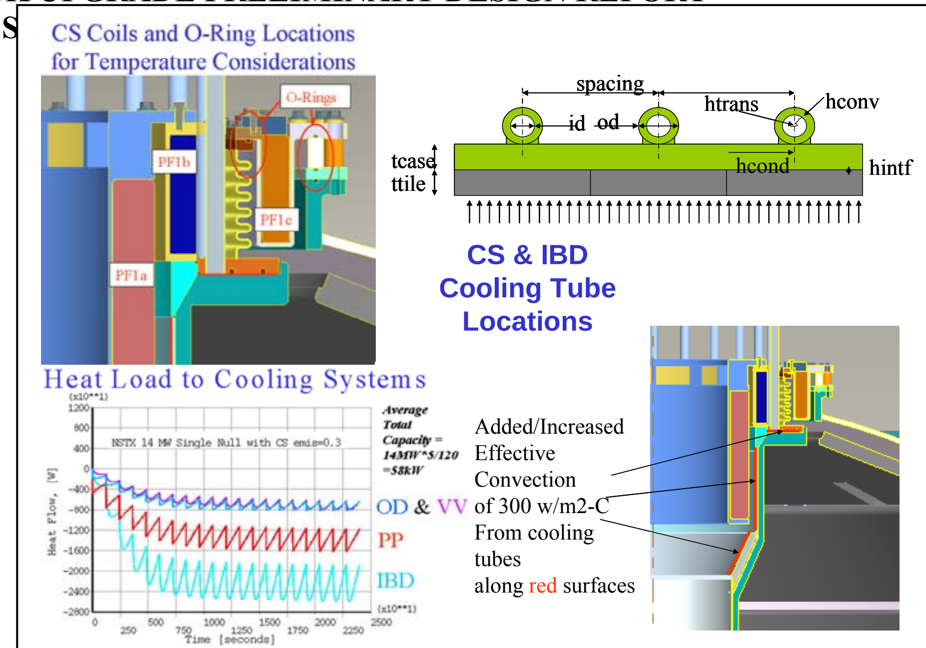

Figure 3.1-3 Heat Balance Summary Slide – Critical Areas Requiring Cooling

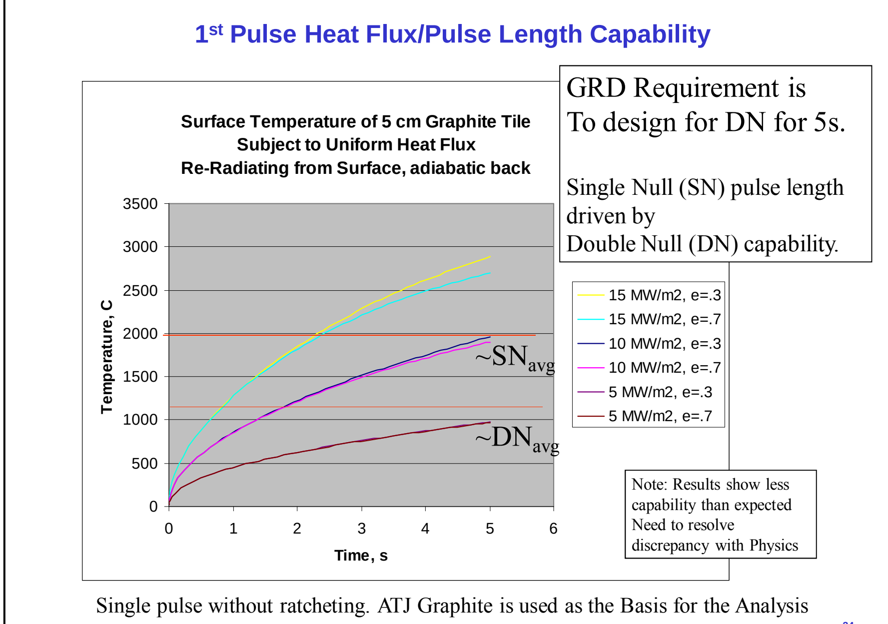

Figure 3.1-4 Pulse Length vs Heat Load Parametric Study

3.2 Tile Thermal and Stress Analysis

3.2.1 Divertor Tile Temperatures and Stress

The initial thermal stress analysis the inboard divertor tile assuming ATJ graphite at those temperatures appear marginally adequate. Efforts to increase margin by considering CFC's or by better characterizing the ATJ thermal-stress properties at temperature are needed. Figure 3.2-1 shows the end of pulse temperature distribution. This is a single pulse, single null result. The thermal gradient evident in this plot gives rise to a shear stress distribution with peak "islands" near the edges shown in Figure 3.2.1-3. Other shear stresses have strong geometric or stress concentration components that may be relieved by introducing radii. Shear stresses are critical to the design because they can lead to a spalling failure, and the allowables for the tiles have still not been obtained. Note also that the "islands" of shear stress are below the surface of eth tile, away from the peak stress. Graphite gets stronger with higher temperature. It is unfortunate that the improvement in stength may be at teh tile surface away from the peak shear stress. Figures 3.2.1-3 through 6 are all for the first pulse at 10.54 MW/m2 for 5s which gets up to 2058 C. Figure 3.2.1-4 shows the skin compression that results from the high temperature of the tile facing the plasma. Figure 3.2-5 shows the Divertor Tile Thermal Stress - Plasma Facing Side at Left and Back Side at Right. Figure 3.2-2 Tabulates the results for the full series of analyses.

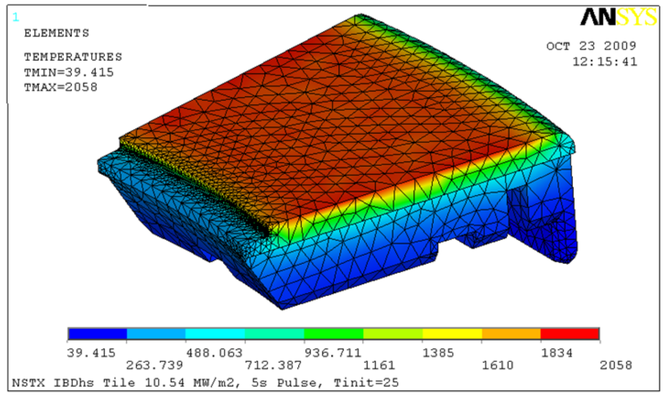

Figure 3.2.1-1 Inboard Divertor Horizontal Section End of Pulse Temperature Distribution

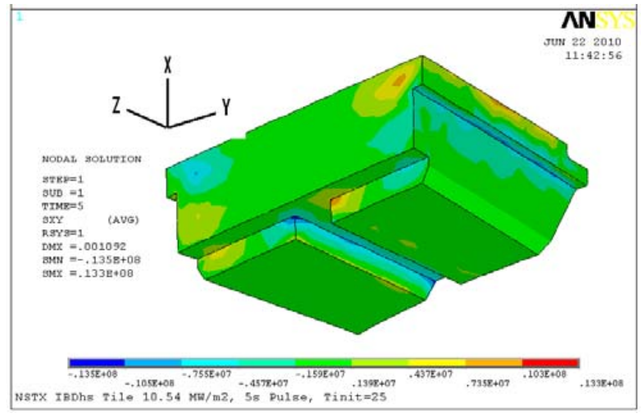

Figure 3.1 Shear Stress, Vertical face, theta direction, half section cut

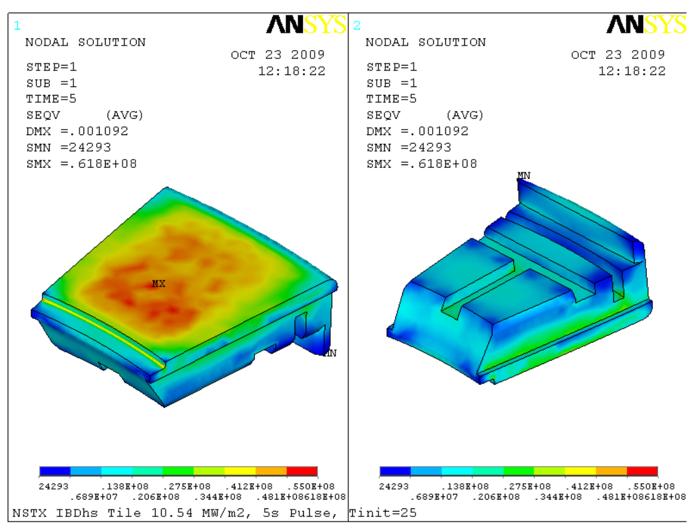

Figure 3.1 Inboard Divertor Horizontal Section Tile Thermal Stress - Plasma Facing Side at Left and Back Side at Right.

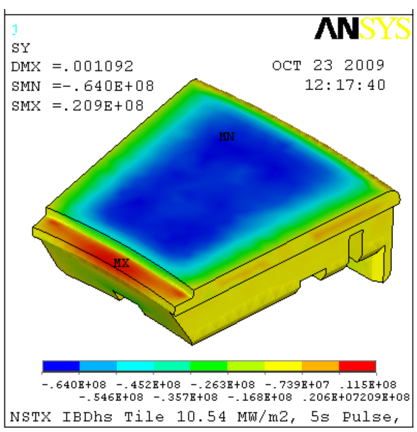

Figure 3.1

Tile Stress Results Summary

	Inboard Divertor Horizontal Section Tile		
	Thermal and Structural Response Summary		
		Max	Min
1st Pulse	Temp, C	2058	39
	Sx, Mpa	9.5	-51.7
	Sy	20.9	-64.0
	Sz	15.6	-63.7
	Sxy	13.3	-13.5
	Syz	13.6	-13.5
	Sxz	18.2	29.6
	Seqv	61.8	0.0
		Max	Min
Last Pulse	Temp, C	2516	623
	Sx, Mpa	11.1	-60.2
	Sy	25.0	-71.8
	Sz	20.0	-72.4
	Sxy	15.8	-16.0
	Syz	15.7	-15.6
	Sxz	21.8	-35.4
	Seqv	72.2	0.0
	Note: y is normal to tile, z is radial, x is toroidal		

No Data on Shear Stress Limit

	Ten Str. (//)	Comp. Str.
units	MPa	MPa
GraphTech ATJ Graphite	26	66
CGW Iso Graphite	31.4	77.5
CGC Iso Graphite	34.3	86.3

RT Tensile and Compressive Strength Values From Kelsey Tresemer

Flexural Strength vs T (below) suggests Graphite gets stronger at higher T

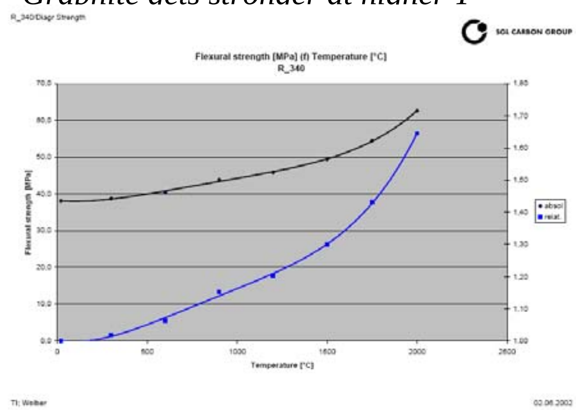

Figure 3.2.1.2 Stress Results Summary

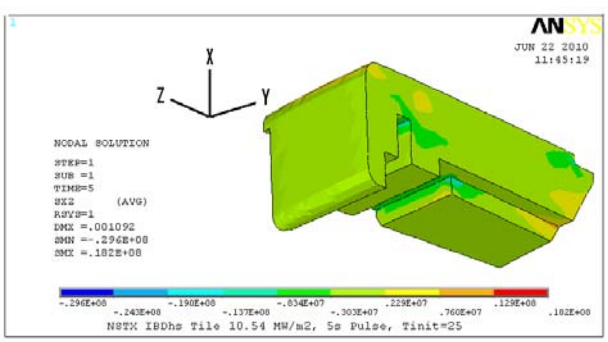

Figure 3.1

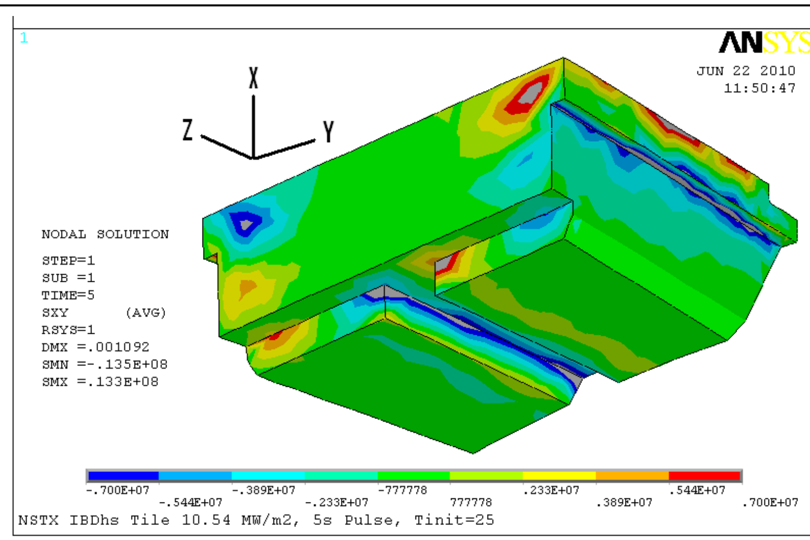

Figure 3.1

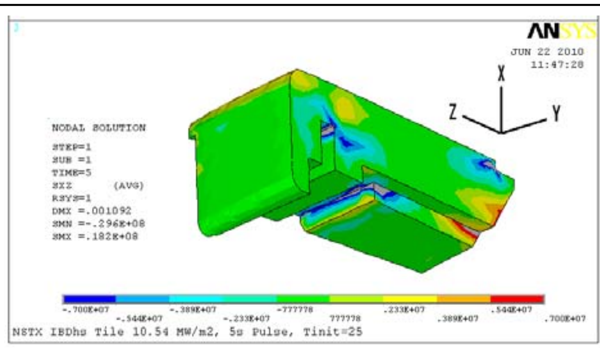

Figure 3.1

Tile Temperature Limit

Currently the NSTX project puts a temperature limit on the graphite tiles of 1200C. If the limit is based on sublimation of the graphite then there is data that indicates that NSTX could be run with the temperature limit increase substantially without unacceptable loss of material. If the concern is the carbon content in the plasma, then operation will dictate the appropriate temperature limits.

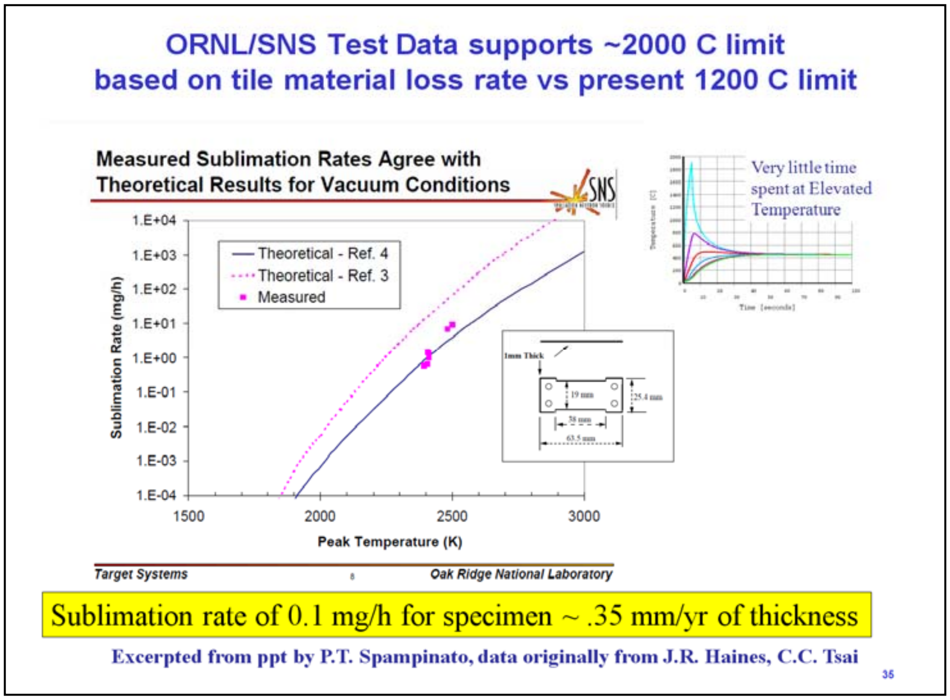

3.2.2 "Generic" Tile Qualification

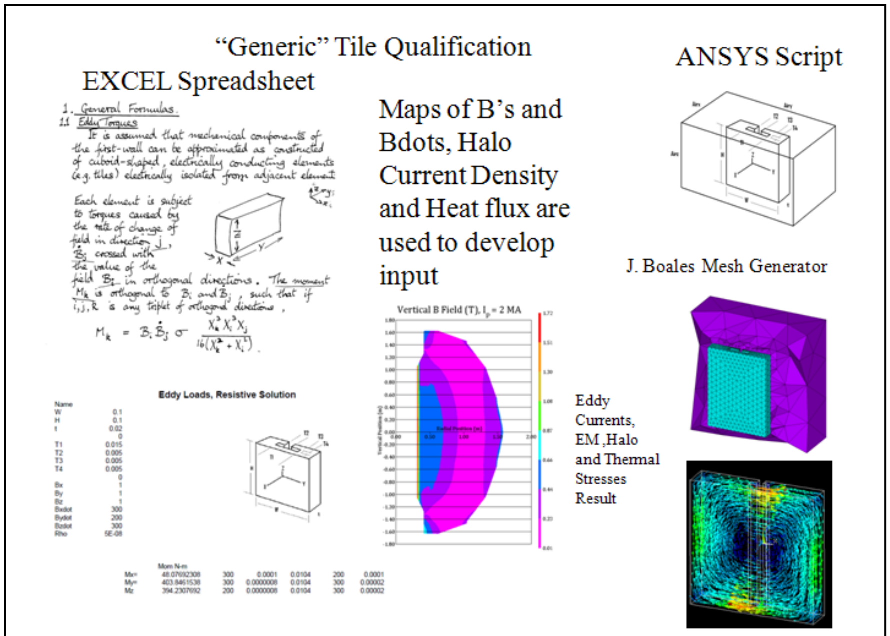

Generic Tile Qualification Procedures

Tiles see loads from a number of sources. Heating from plasma particle interaction and radiative heating produce thermal gradients that cause stress. Electromagnetic transients cause eddy currents in the conducting tiles such as the carbon-carbon and ATJ graphite used in NSTX. These eddy currents crossed with the toroidal and poloidal fields load the tiles. There are two regimes of electromagnetic response of the tiles. If the transient is short with respect to the tile time constant, then the tiles develop only the inductively driven currents. If the event is a bit longer, the initial currents which oppose flux penetration will decay allowing a resistive solution. In the spreadsheet version of the "Generic" Tile Qualification, both the inductive and resistive solutions are computed. In the ANSYS script the transient is simulated and inductive and resistive effects are included. Halo currents also load the tiles by entering from the plasma side, passing through the tiles and exiting at some electrical connection at the back of the tiles. In NSTX this can be through grafoil between the tile and backing plate, or through mounting hardware where grafoil is not used. Electrical connections between the tiles and the backing structures will allow currents in the backing structures to be shared with the tiles. These currents also will cross field lines and develop loads. The spreadsheet

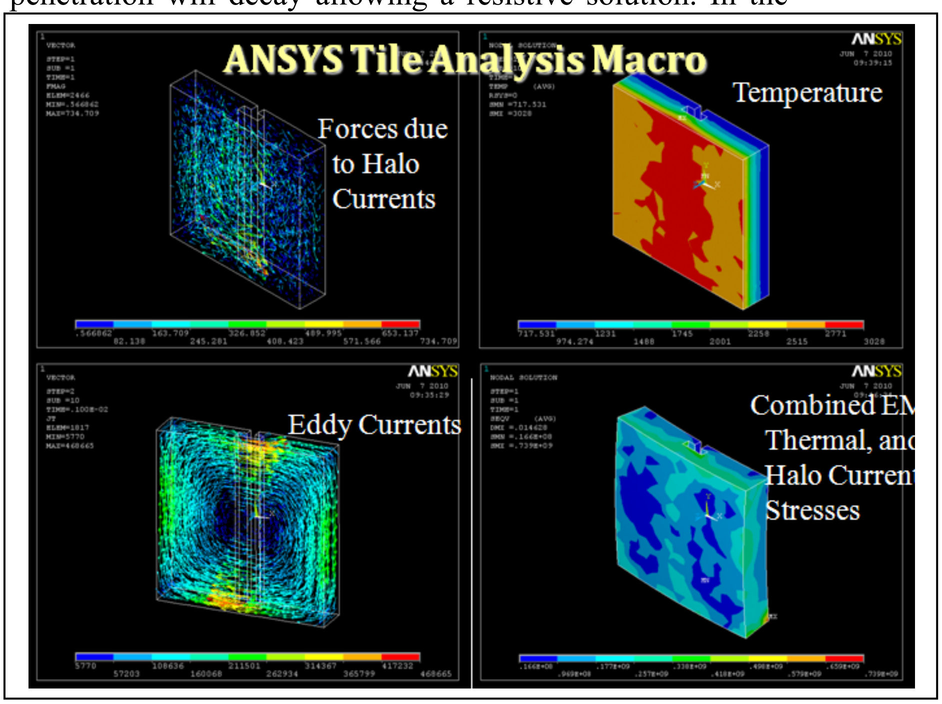

solution and the ANSYS macro include this effect where the currents in the backing structures are available from disruption simulations.

3.2.3 Centerstack tiles

All tiles are CFC. The centerstack tiles were expanded in size with the radius of the centerstack, plus some height adjustment that produces 600 tiles total vs. 900. This has the potential of increasing the stress in the tile. Tiles grow in size at the surface or "mushroom" The strain differential causes a stress. There is a "size effect" that comes from the constraint of growth. Art Brooks investigated this and found a significant increase in stress in the size ranges being considered for NSTX Upgrade. As a result the centerstack coils were analyzed in the "generic" tile qualification procedure (Section 3.2.2). The ANSYS script was employed to better model the constraints at the backside of the tiles. Figure 3.2.3-2 shows the backing plate/fixture, and Figure 3.2.3-3 the constraints intended to model the tile support.

Figure 3.2.3-2 Backing Plate/Fixture

Figure 3.2.3-3

Figure 3.2.3-1

Initial stress analysis of the centerstack tiles has been performed. The run included thermal, halo current and eddy current loads on the tiles on the CS cylindrical section. The results indicate the stresses in the CFC material is low, approximately 10% of the allowables (2D material). This allows the use of the less expensive CFC materials in this area as planned.

Figure 3.2.3-5

Figure 3.2.3-5

Figure 3.2.3-4

3.3. Disruption Analyses, Disruption Specifications

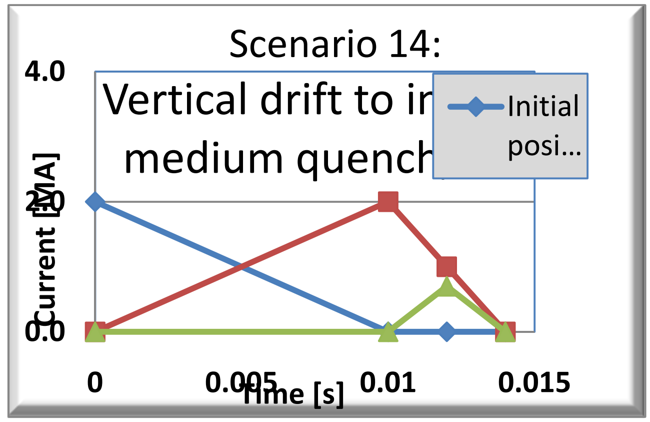

Figure 3.3-1 Time phasing of the plasma current changes that induce currents in the vessel and vessel components; and the halo currents. From J. Menard

The latest (August 2010) disruption specification were provided by Jon Menard as a spreadsheet:
disruption_scenario_currents_v2.xls
This is a substantial update of the CDR GRD discussed in section 4.7.2 which included 5 plasma positions, some quenches and some with halo currents.

The CS casing has been analyzed (see section 4.7.2) for inductively driven currents from a toroidal current quench. Halo loads have been analyzed for a mid plane entry and exit. We have done dynamic analyses based on GRD quench times. Based on PDR results, CS casing stresses are acceptable. We have done "first pass analyses on the bellows, ceramic break and pedistal, and their stresses are acceptable. The passive plates and divertors have been analyzed for a major mid-plane disruption and a VDE. Both with conservative "power supply limit" background poloidal fields from Ron Hatcher. Only small hardware upgrades are needed. We have not yet imposed Halo loads. Between the max power supply poloidal field and the 1/r correction (see below) there should be margin to accept the halo loads. Macros developed by Srinavas Avasarala have been used for other models to simulate disruption stresses. This method (of imposing Vector Potentials) circumvents the modeling of air and other complexities involving complex 3-D geometry.

Larry Bryant has analyzed the neutral beam armor backing plate for the mid plane disruption, but with Ron Hatcher's poloidal fields maximized at the passive plates. Stresses are low. Joe Boales has analyzed diagnostic shutters for Mid plane disruption with poloidal fields based on "worst case power supply limits" maximized for PPP and OBD – Shutter stresses are acceptable. Joe Boales is working on tiles as well. The centerstack carbon-carbon tiles have been analyzed and stresses are low.

New High Priority Disruption Analyses
Centered disruption, fast quench
Initiated shifted to CS, fast quench, no halo
Inward drift to CS, very slow quench, halo
Initiated shifted down to inboard, fast quench, no halo
Vertical drift to inboard, very slow quench, halo
Initiated shifted down to middle, fast quench, no halo
Vertical drift to middle, very slow quench, halo
Initiated shifted down to outboard, fast quench, no halo
Vertical drift to outboard, very slow quench, halo

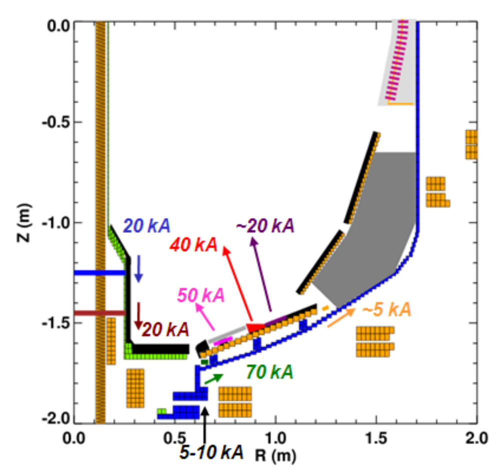

Figure 3.3-3 A plot from Stefan Gerhardt's report on halo currents

During the CDR, we identified a mistake in the conversion from OPERA axisymmetric vector potential to 3D ANSYS vector potential. While the conversion from one formulation to the other is more complex, basically we need to divide the ANSYS results by the radius to the component.

Han has analyzed the HHFW Antenna for a 2 MA mid-plane disruption, and is running the other GDR plasma quenchs – independent of Ron's Opera Simulations. Ron's simulations were based on "max power supply limits" which were conservative, but also required OPERA runs with background fields specific to a component location. We are investigating de-coupling the plasma disruption from the assignment of the background field at the specific component location.

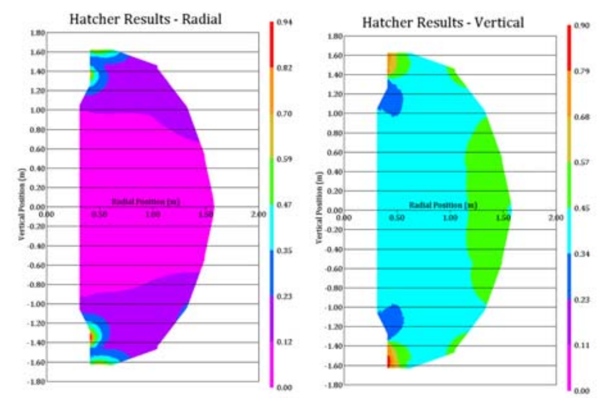

Figure 3.3-4 Maximum Poloidal Fields

The VDE specified by the CDR GRD did not include a final quench – This was a reasonable assumption for a fast VDE (a flux conserved solution would attempt to preserve the original flux state of the centered mid-plane plasma). This may not be appropriate for a slow VDE followed by a quench. The GRD content is being updated.

We did not run all plasma quenches at the passive plates. Quenches of plasmas 3,4, and 5 at the surface of the plates could be worse – but are tangent to the plate surface and have a small Bdot-normal, and may not increase the eddy currents.

Halo current distributions and timing are being updated based on experimental results.

During the PDR there was confusion about the files that Ron Hatcher provided and how we were using them. Ron included the background field in his OPERA solution and he maximized the background field for the specific location for the component that he understood was being qualified. We used the files for components other than those Ron intended. For smaller components the background fields can be separated from the disruption simulation and added when the local part is analyzed. Poloidal field maps can be used such as those in section 5.3 to choose an appropriate maximum for the component analysis.

3.3.1 Disruption Analysis, Passive Plate Disruption Analysis

The objective of this analysis is to estimate the stresses in the vacuum vessel and passive plates (Figure 3.3-1) caused by the plasma disruption. The Vector Potential solution for a 2D axisymmetric simulation of disruption in OPERA is imposed on the 3-D model in ANSYS to obtain the eddy currents and Lorentz forces. A static and dynamic stress pass is then run and the stresses are computed. A 1/r correction is applied in the ANSYS script to account for the difference in vector potential formulation of OPERA axisymmetric vs. ANSYS

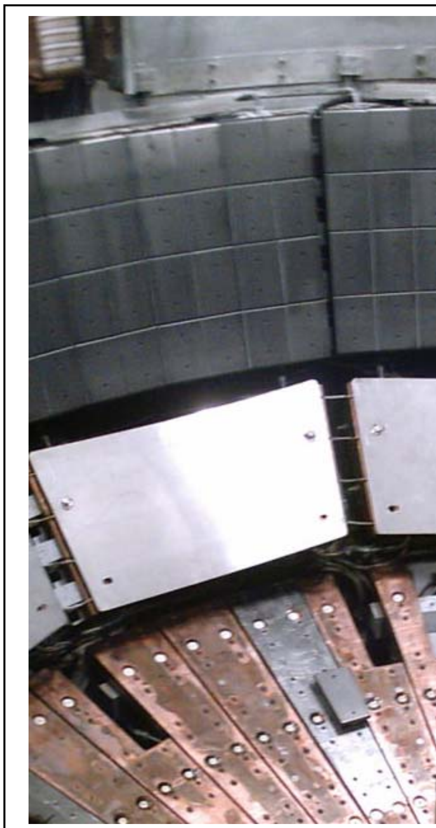

Figure 3.3-1 Photograph of the NSTX Passive Plates (October 2009)

3D solution. The opera solution includes poloidal background field that has been maximized for the component location. A. Brooks 1/r toroidal field is added by ANSYS script

The solid models of the vessel, umbrella structure, port extensions and support legs are imported from Pro-E. The model retains all the complex 3-D geometry but the port extensions, legs and the vessel are merged together to form one solid. The umbrella structure is a separate solid. This model is meshed with 8 node bricks in workbench and the mesh is carried into ANSYS classic. To get around the DOF compatibility issues, the mesh is rebuilt in ANSYS classic, retaining the number of nodes and elements and the connectivity. A vector potential gradient is then applied on this model to see if the model works. Eddy currents and Lorentz forces obtained agreed with intuition. An approximate model of the passive plates, in agreement with the 2-D model used in OPERA, is modeled in ANSYS. This is tied to the vessel using constraint equations. The degree of freedom coupled is Volt during the E-mag run and Displacement during the structural run. Figure 3.3-2 depicts the NSTX disruption analysis at the mid-plane for a 2 Ma Ip disruption.

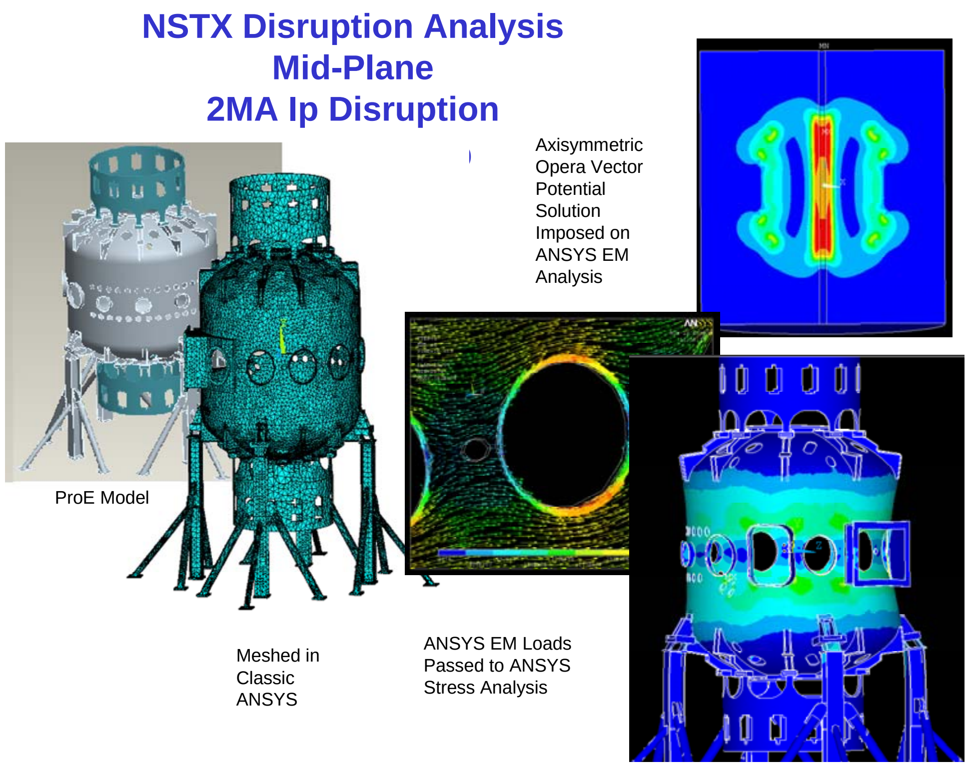

Figure 0-2 Passive Plate Disruption Analyses Process

The analysis uses a vector potential solution. Grad A is B:

$$\mathbf{B} = \nabla \times \mathbf{A}.$$

Vector potentials obtained from OPERA are arranged in 80x80 tabular form so that they can be fed into ANSYS. The first 11 tables are considered for the study and these tables are spaced 0.5 ms apart. Macros are developed that read these values into ANSYS. The meshes in OPERA and ANSYS are dissimilar, but since ANSYS interpolates the tables between two adjacent indices, proper indexing of the coordinates yields a reasonable approximation of the Vector Potentials. The element type used was SOLID 97 and the material properties used are that of Stainless Steel except for the passive plates which are made up of copper. This model is then solved for eddy currents and Lorentz forces. Figure 0-3 shows the relationships between Vector Potential (A) and the Field (B).

$$B_x = \frac{\partial A_z}{\partial y} - \frac{\partial A_y}{\partial z}$$

$$B_y = \frac{\partial A_x}{\partial z} - \frac{\partial A_z}{\partial x}$$

$$B_z = \frac{\partial A_y}{\partial x} - \frac{\partial A_x}{\partial y}$$

Figure 0-3 Relation between Vector Potential (A) and Field (B)

The model is then converted into a structural model by switching the SOLID 97s into SOLID 45s. 11 load steps, 5ms apart are written for the stress pass. Forces are read from the earlier E-mag results fie using LDREAD command and both the Static and Dynamic analyses are performed. A 0.5% damping factor is used in the dynamic run.

The maximum stress obtained during the static analysis (ignoring the sharp corners) is 1600 Mpa and that from the dynamic analysis is 290 Mpa. Four nodes are picked in the model to compute the DLFs and the stresses seem to have reduced by a factor of 0.18-0.23. Figure 3.3-4 shows the vessel disruption stresses.

Vessel Disruption Stresses

(We apologize for the tilted vessel It just artistic license – It is not falling over)

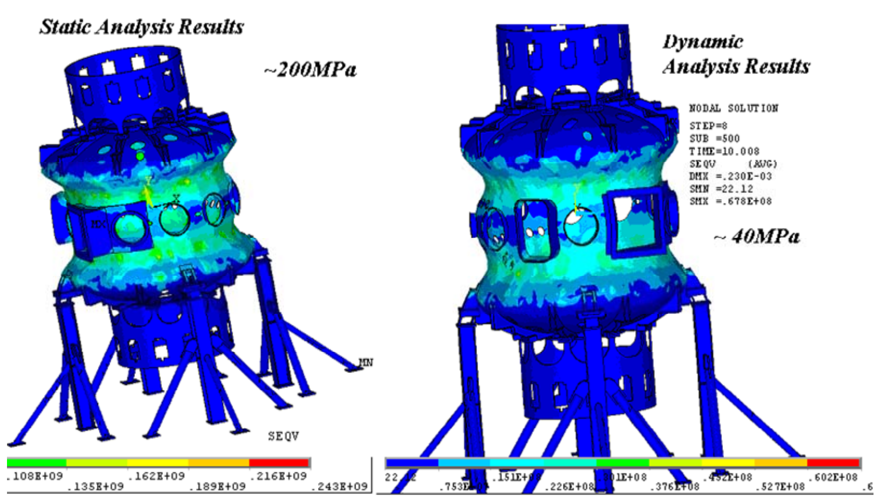

Figure 0-4 Vessel Disruption Stresses

The method employed uses the vector potential solution from an axisymmetric OPERA run and applies it to a mode complex model of the vessel and passive plates. In order to ensure the solution is in geometric registration with the passive plates, the coordinates that were used in the OPERA analysis were used to generate the passive plate mesh. Figure 3.3-5 shows the passive plate disruption eddy currents and stresses. Table 3.3-1 shows the passive plate and outboard divertor coordinates.

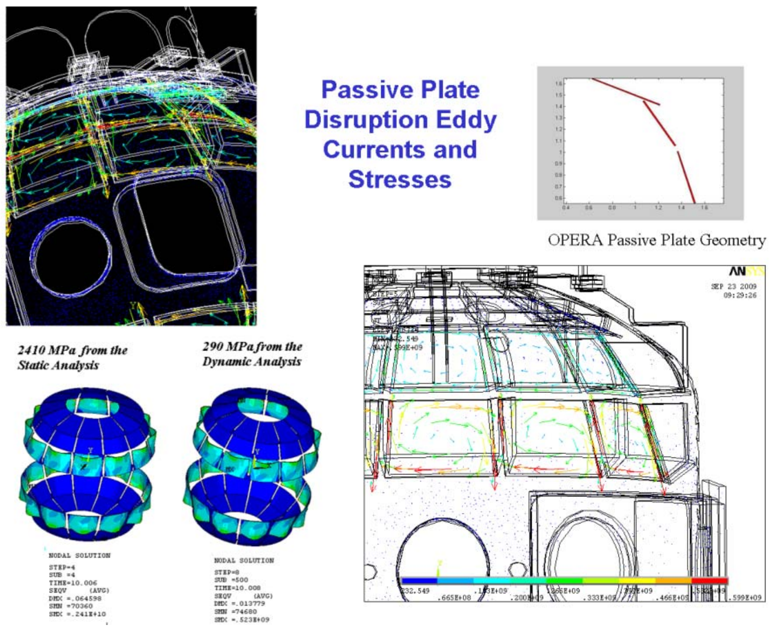

Figure 0-5 Passive Plate Disruption Eddy Currents and Stresses

Table 3.3-1 Passive Plate and Outboard Divertor Coordinates

Primary Passive Plate Coordinates	Secondary Passive Plate Coordinates	Outboard Divertor Coordinates
X=1.3600 Y=1.0056	X=1.0640 Y=1.4447	x=0.6208 y=1.6390
X=1.5092 Y=0.5530	X=1.3399 Y=1.0543	x=1.2056 y=1.4092
X=1.5213 Y=0.5569	X=1.3503 Y=1.0617	x=1.2149 y=1.4185
X=1.3720 Y=1.0095	X=1.0744 Y=1.4520	X=1.0744 Y=1.4520

Results from these analyses show that:

- The Dynamic Load Factors are found to less than 0.25
- The stresses are under acceptable limit.
- Macros developed here have been used for other models to simulate disruption stresses.
- This method (of imposing Vector Potentials) circumvents the modeling of air and other complexities involving complex 3-D geometry.
- The disruption scenario studied here is just the Outboard Diverter disruption. The other two scenarios : Primary Passive Plate and Secondary Passive Plate will be studied.

- All the high stress modes of vibration might not have been picked up by the dynamic analysis because of memory limitations of PC
- CAD model of the Passive Plates has been obtained, de-featured, meshed and is in the process of being analyzed
- All the high stress modes of vibration might not have been picked up by the dynamic analysis because of memory limitations of PC
- CAD model of the Passive Plates has been obtained, de-featured, meshed and is in the process of being analyzed

Figure 3.3-6 shows the meshed detail model. As a cross check of the results, The vertical Bdot in the outer area of the vessel near the mid plane was compared with the results reported for the High Harmonic Fast Wave (HHFW) discussed in section 2.1. The passive plate analysis yielded a vertical field HHFW analyses yielded 280 Tesla/sec. Both were for 2 Mamp 1 millisecond disruptions. The HHFW analysis was for a simple linear rampdown in plasma current. The passive plate analysis is for a more complex simulation of a the disruption at the divertor disruption. **Error! Reference source not found.** Figure 3.3-7 shows the passive plate attachment details. depicts the constraint equations that stitch the passive plate structure to the vessel.

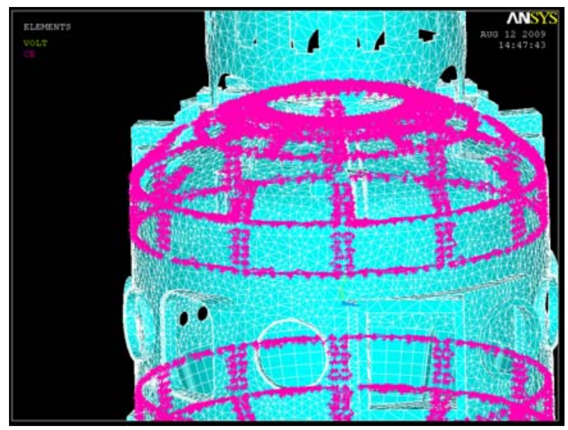

Figure 3.3-6 Constraint Equations

Results of the passive plate analysis show no significant non-cyclic symmetry resulting from the distribution of differing ports at the equatorial plane. The approach used is to perform a detailed analysis of only a 60 degree sector of the vessel, divertor, and passive plates to allow an adequately detailed modeling of the actual mounting hardware. Figure 3.3-7 shows field-time plots along with field transient calculations. These have been compared with the original OPERA disruption simulation, and with the HHFW antenna discussed in section 6.1. The results are close enough to justify the assumptions made in this analysis of the passive plates.

3.4. Imposing the Background Fields

The following produce a 1/R field in a cylindrical volume:
It uses Az=-.5*BR*log(r^2). It's not necessary to nrotate the nodes into a cylindrical system if that conflict with other BC's.

Per Art Brooks, the following also works using: Az=-.5*BR*log(x^2+y^2). Figure shows the background field equations.

```
/prep7
et,1,97,0
mp,murx,1,1.
!
cylind,.5,1.5,-1,1,0,90
esize,.1
vmesh,all
d,all,ax,0.
d,all,ay,0.
!
! apply 1/R field using magnetic vector potential thru body
!
BR=1. ! Telsa-meters
!NI=BR*.5e7
*get,nmax,node,,num,max
*do,i,1,nmax
xx=nx(i)
yy=ny(i)
d,i,az,-.5*BR*log(xx*xx+yy*yy)
*enddo
!
fini
/solu
solve
fini
/post1
plvect,b,,,,vect,,on
```

Figure 3.3-8 Background Toroidal Field Equations

Similar but more complex macros have been developed by Art Brooks to superimpose appropriate vector potential distributions to add poloidal background fields. This allows addition of background fields specific to the component location.

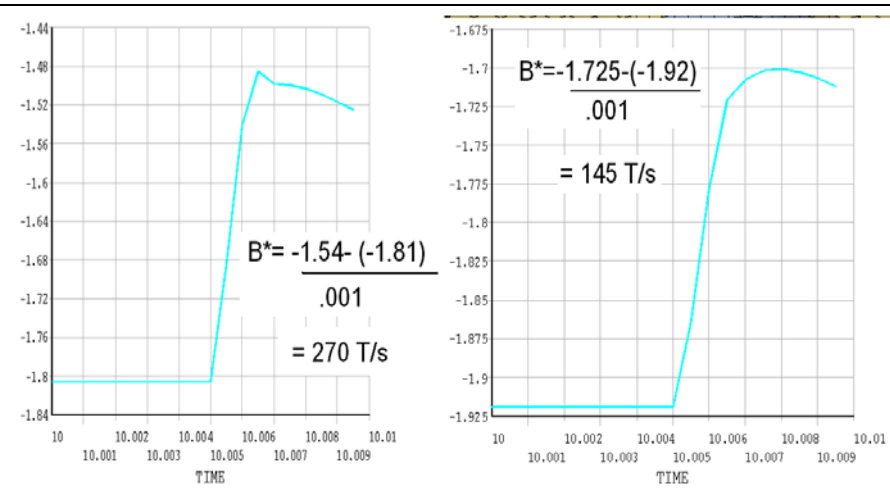

Figure 3.4-7 Field-Time Plots Along With Field Transient Calculations

3.5 Analysis of the Detailed ProE model of the Passive Plates
3.5.1 Analysis with of Ron Hatcher's Primary Passive Plate File

As of November 9 2009, the ProE model of the mounting hardware was available. From this a 30 degree ProE model was meshed and then reflected to fit vessel 60 degree sector model. The vessel was added to model current sharing. Reflection was done to allow precise CP command coupling.

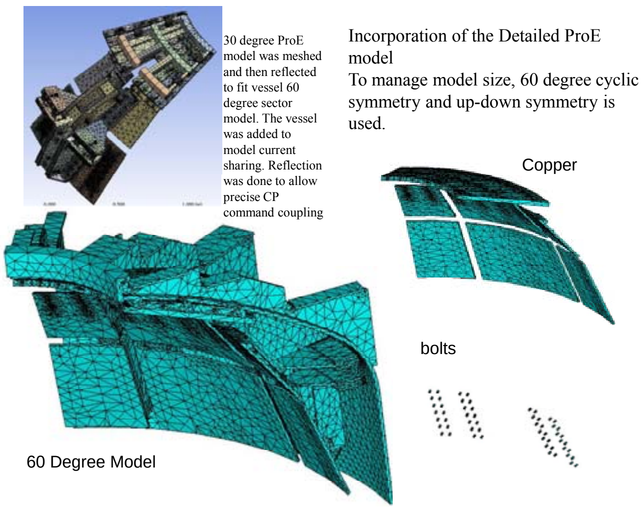

Figure 3.5-1 The ProE model and its Conversion to a meshed ANSYS cyclic Symmetry Model

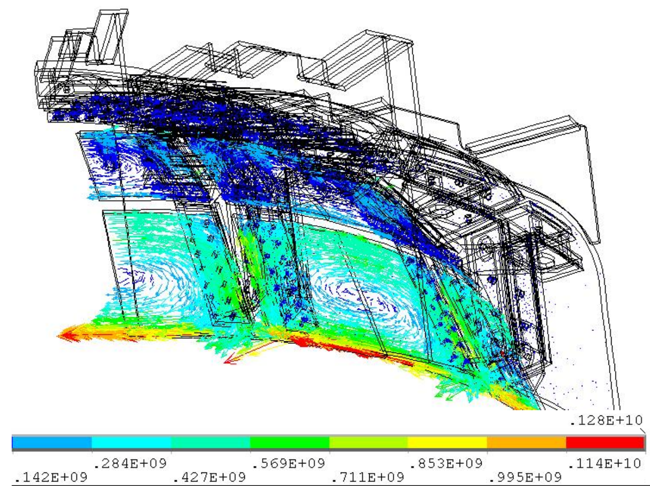

Figure 3.5-2 Eddy Currents in the Detailed Model

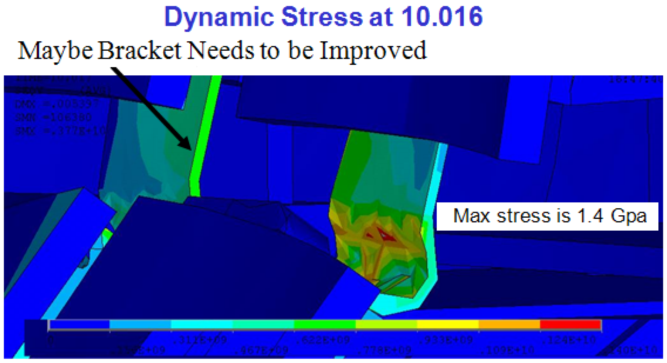

Figure 3.5-3

In an email, Larry Dudek stated that "The high stress areas look like they are in the poloidal jumpers which are no longer used. They were probably removed when the toroidal straps were cut off. There are also some gussets at the end of the brackets which are not in your models. John Mitchell should be able to help you update the models to reflect the as-built condition."

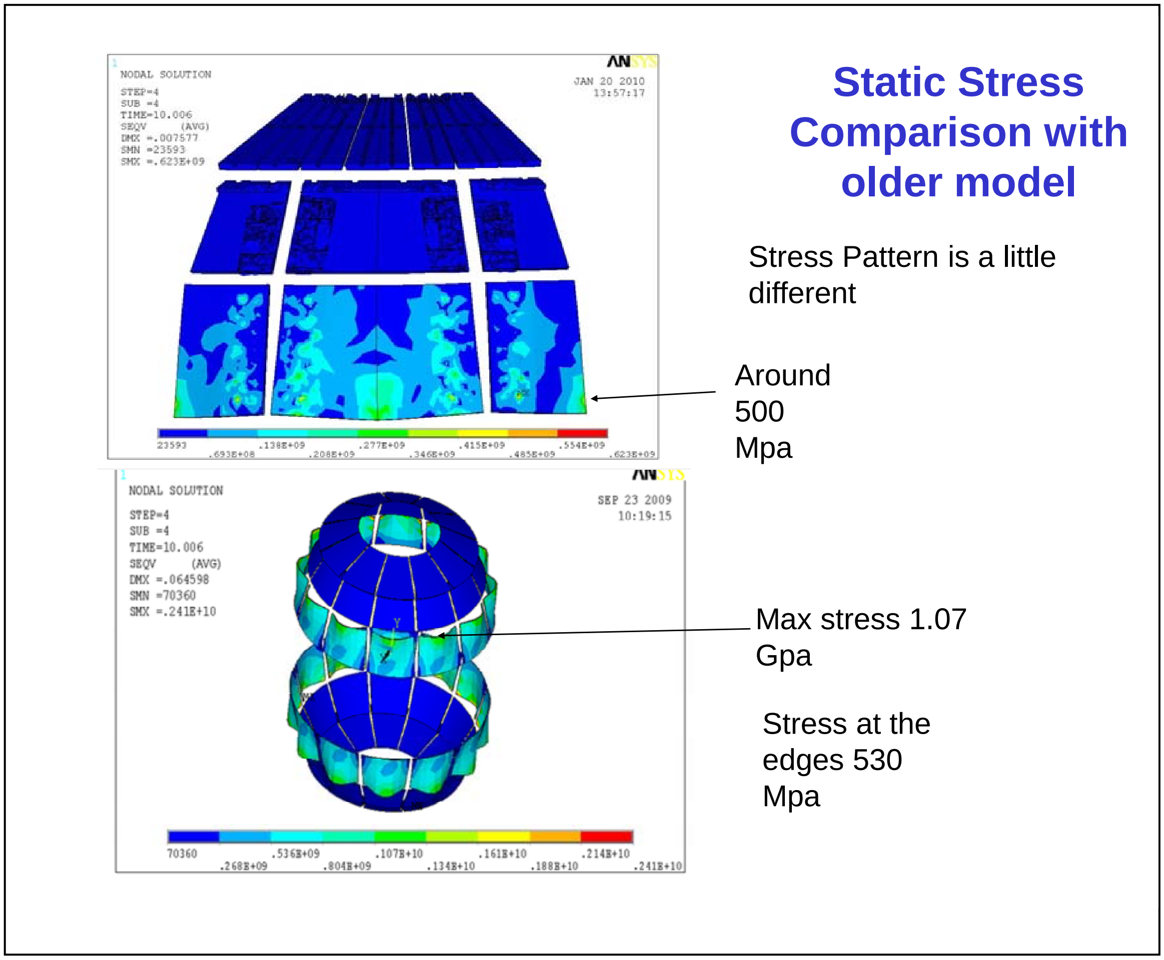

3.5.2 Analysis of the VDE Plasma 1 to 5

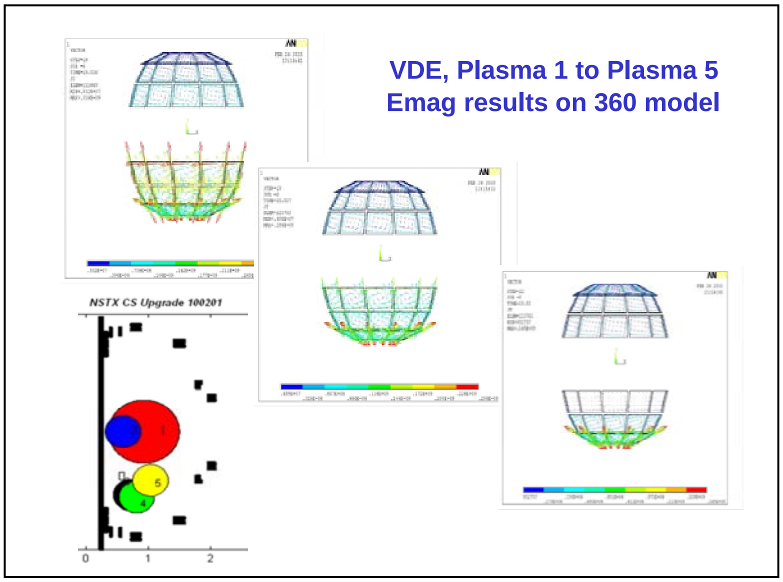

In this analysis early in 2010, the GRD spec for the VDE was run by Ron Hatcher. The GRD did not include a current quench after translation to the secondary passive plate/ lower divertor area. Discussions of whether this was adequately conservative resulted. For a very fast VDE, the currents induced in the vessel wall will appear the same as for a mid-plane disruption, because the change in flux before and after the disruption results from the change between a mid-plane plasma and no plasma - with some complicated reversals of currents during the translation. Consequently the mid-plane disruption was expected to adequately model the quench even for a VDE. The VDE currents for just the translation were simulated. For the FDR, slow VDE's with a current quench near the secondary passive plates and lower divertor are planned.

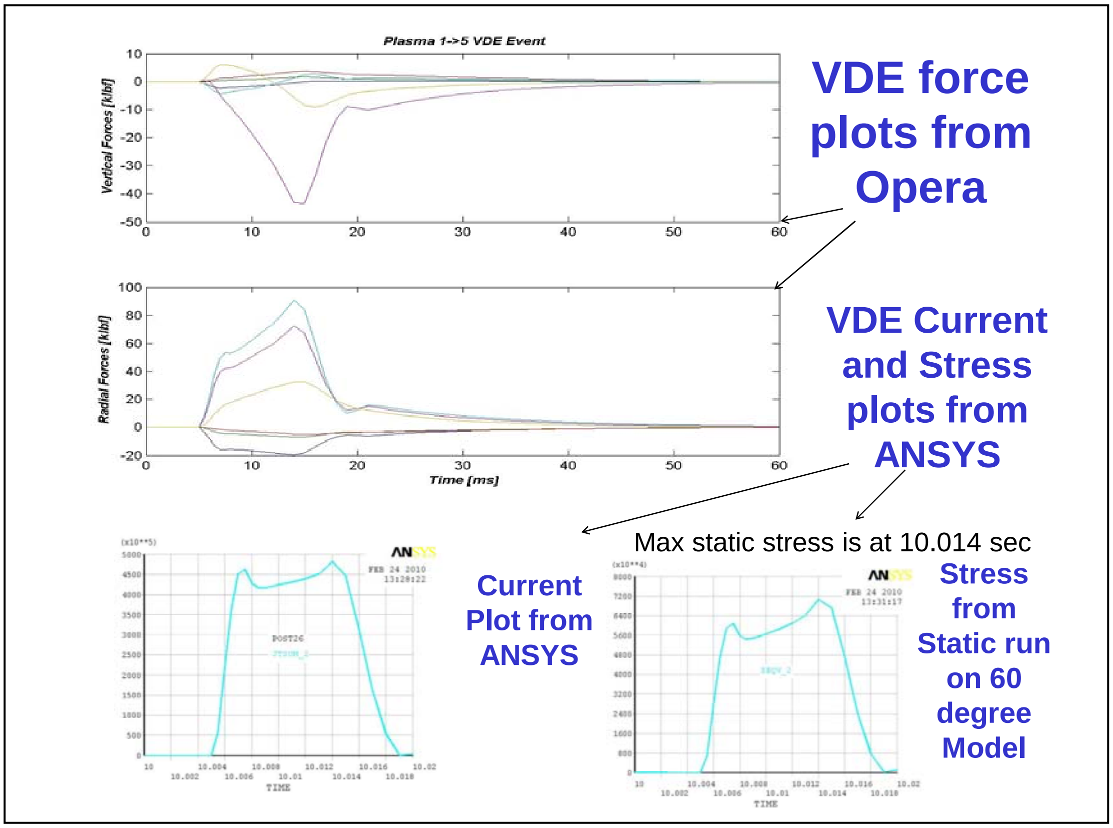

Passive Plate Disruption Analyses With Halo Currents

Electromagnetic Model as of July 15th 2010. The secondary passive plates are not yet included

Passive Plate and Divertor Mounting Hardware Stress

Estimate of 5/8 bolt shear stress

4. Vacuum Vessel & Support Structure (WBS 1.1.2)

4.1.Overview

The vacuum vessel is a major component in many individual analyses because it is the major support structure for most of the outboard components of NSTX. The vessel supports the passive plates for which disruption loads are the major loading. The vessel participates in the electromagnetic response to the disruption, and is included in the disruption analysis discussed in Section 3. The vessel provides in-plane support of the TF outer legs at the umbrella structure. The vessel also provides the support for OOP loads on the TF outer legs via connections through low stiffness truss links just above the upper and below the lower head intersection with the cylindrical part of the shell. The vessel is included in the analysis of the TF outer legs. The global model includes a model of the vessel and attempts to bring all the loading together and addresses bake-out, operating temperatures and Lorentz Loads. In section 6, the effect of the neutral beam bellows vacuum loads is considered. As–builts are being gathered and evaluated.

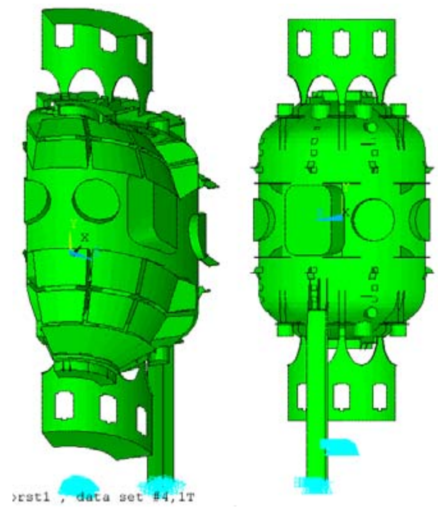

Figure 4.1-1 H.M. Fan's Original Quarter Symmetry
Plates

The vessel is out of round by the following:

- Most locations are round to within .13"
- Near ports, it is out of rouund to about .75"
- The vessel is made of 2 arcs(~179 deg each) and there are 2 flats , on the weld seems

Many of the as-built attachment details are being measured and detailed with the hope that many will not require upgrade. Analysis efforts began with the quarter symmetry model prepared by H.M. Fan, Figure 4.1-1. Models are more recently meshed from the ProE solid model.

Figure 4.1-1 shows the vessel response to the disruption shown in Section 3.1. **Error! Reference source not found.** shows the global model results.

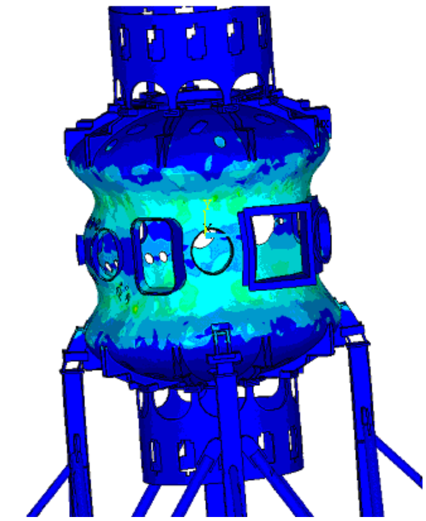

Figure 4.1-1 Vessel Response to a Disruption

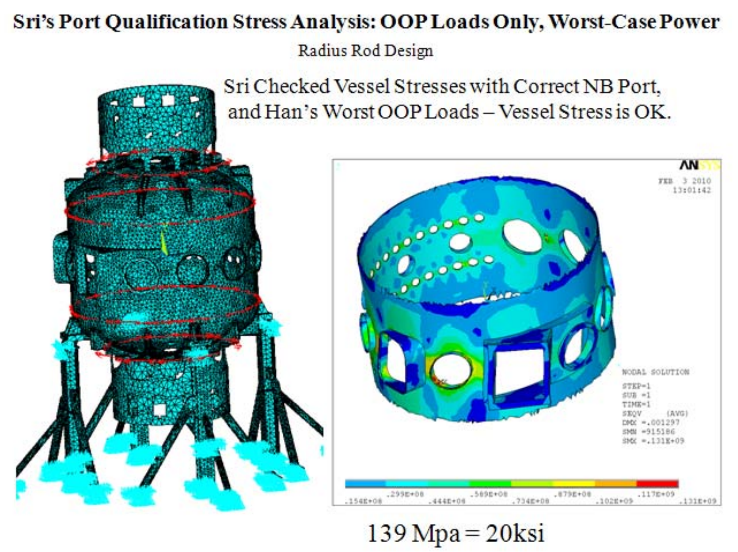

Vessel Stress Due to TF Coil Out-of-Plane (OOP) Loading

4.2 Port L stress analysis

Presented is an update of the Port L stress analysis presentation, including two new analyses: with the 4" port hole at Port J filled; and with the 4" port hole filled and the Port J/K cap frame thickness increased from 5/8" to 3/4". A summary table with the stress results for all the analyses is shown on the last slide.

From the table, filling the 4" hole reduces the peak stress at Port L by ~ 1 ksi, and increasing the cap wall thickness reduces the peak stress another ~ 1 ksi. To meet the Design Criteria maximum allowable of 23 ksi with the pressure (~ 6 ksi) and disruption stresses (~6 ksi) superimposed, the peak stress must be reduced by ~ 10 ksi. Adding the 1/2" thick backing reinforcements at L and J should help (next analysis), but in last Wednesday's project meeting,

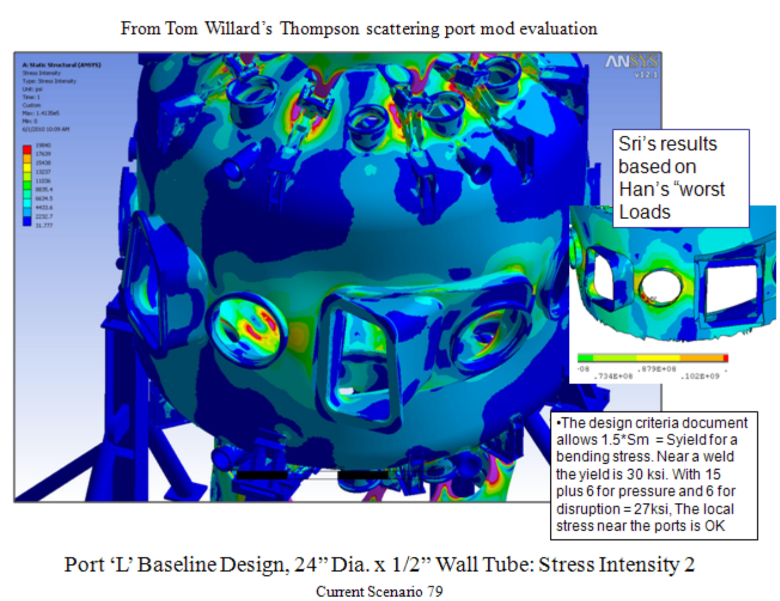

Figure 4.2-1

Peter suggested reducing the cap cut-out in the vessel wall, and Tim seemed to think that reducing the opening was possible. After viewing these results, maybe we should together to discuss reducing the opening, and other reinforcement options (i.e., gusseting the cap).

The peak stress reported in these analyses is a bending stress. The design criteria document allows 1.5*sm for a bending stress. The yield of the vessel plate material is 45 ksi. Near a weld heat effected zone it would be closer to 30 ksi. (annealed 304). With Sm =2/3 yield the bending allowable would be 1.5*2/3*30ksi=30ksi. As long as the welds are full penetration, and the welds are penetrant inspected as well as visually inspected, the weld allowable is the same as the base metal. The high stress location is small and the more strict welding requirements could be limited to this area. So with 23+6+6 = 35ksi and an allowable of 30 ksi, only a modest reinforcement is needed.

These allowables take credit for the ductility of the 304 material. If there are diagnostics near this high stress location that can't be realigned easily, it might be necessary to add stiffeners.

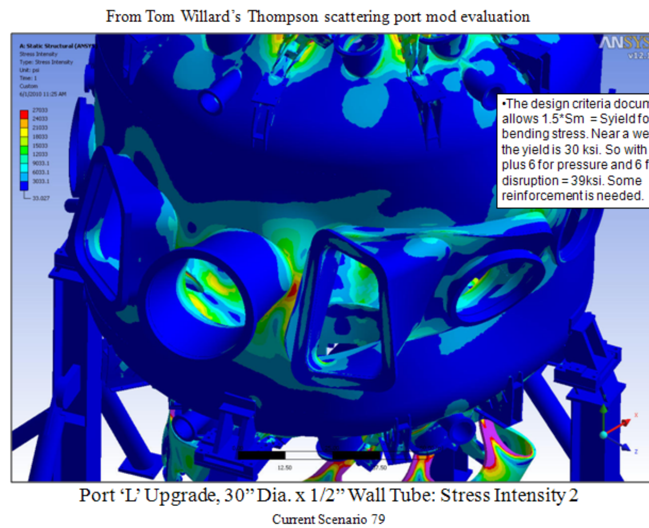

Figure 4.2-2

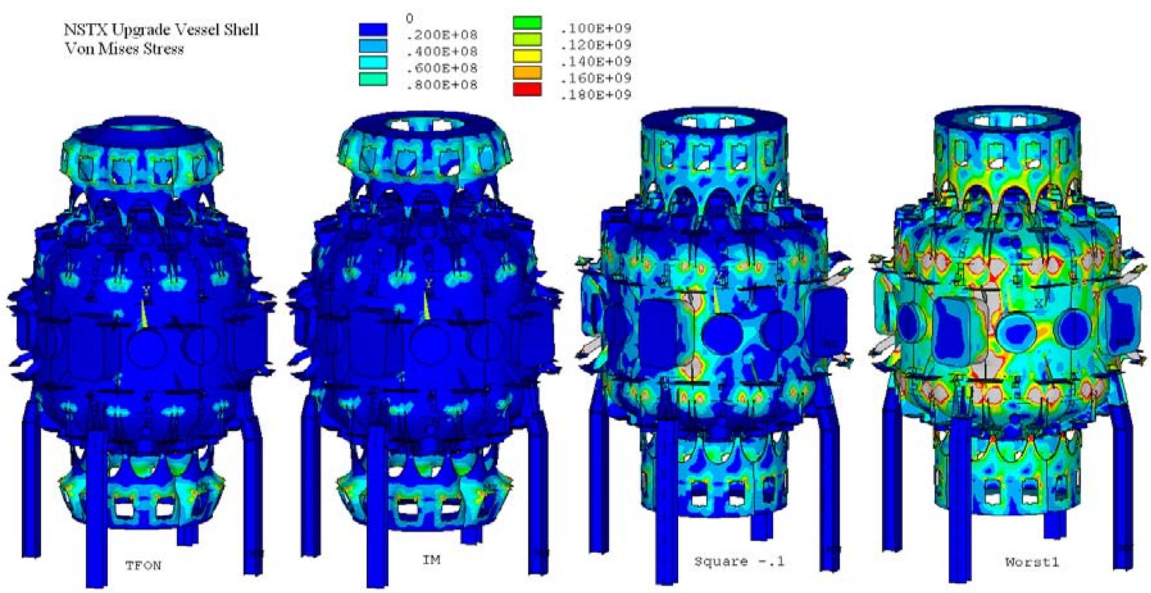

Figure 4.1-2 Early Global Model Vacuum Vessel Results

4.3 Vessel Outer Leg Connection

The main beam gusset plates are 1.5 inches thick . Visually scaling the welds, they are about 2 inches long and maybe 3/8 fillets. Figure 4.1-3 show pictures of the Bay B C gusset plates. Figure 4.2-2 shows the ANSYS models of these gusset plates. There are 3 on each outside edge and 3 inside- maybe more on the underside. The he weld size is estimated as 3/8 inch, These weld sizes will be measured during machine down times and analyzed and qualified during preliminary and final designs.

Figure 4.1-3 Bay B C Gusset Plate

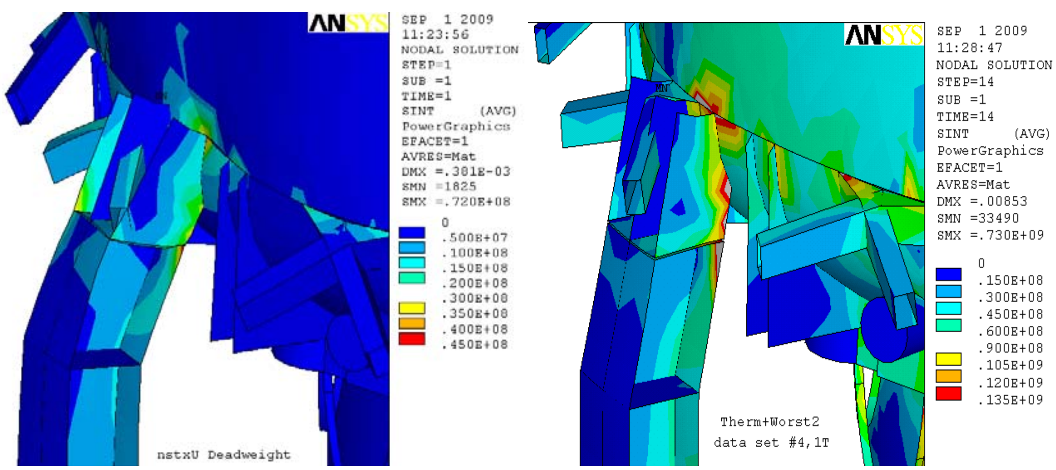

Figure 4.1-4 ANSYS Models of the Bay B C Gusset Plates

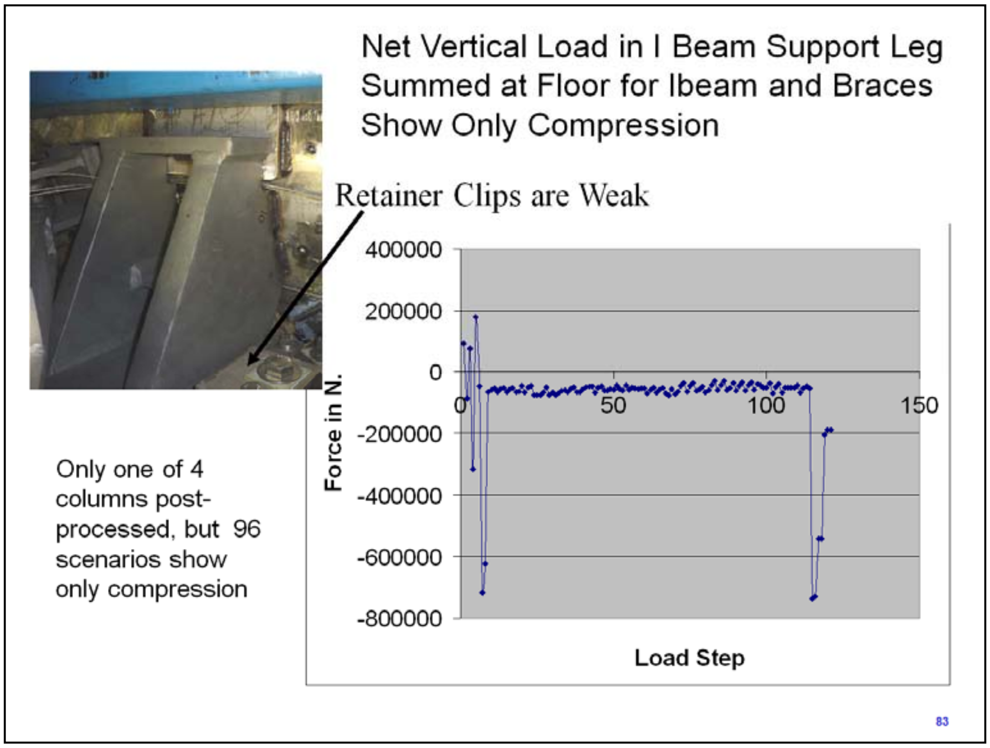
Net Vertical Load in I Beam Support Leg Summed at Floor for Ibeam and Braces Show Only Compression
Retainer Clips are Weak
Only one of 4 columns post-processed, but 96 scenarios show only compression
400000
200000
0
-200000
-400000
-600000
-800000
0
50
100
150
Force in N.
Load Step
83

4.4 Upper Lid/Diaphragm/Cover/Flex

4.4.1 Lid/Diaphragm/Cover/Flex Stress

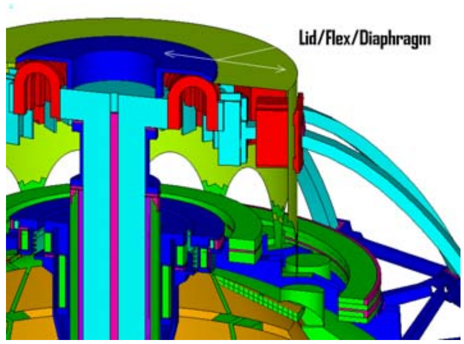

Figure 4.4-1 Global Model Segment

A flex plate or cover or "lid" is intended as the structure that extends from a connection to the TF central column flags to the outboard edge of the umbrella structure. Functionally the lid or flex plate replaces the gear tooth connection presently used in NSTX. The lid or flex plate, like the gear tooth assembly must transmit the global machine torque, while allowing thermal growth. The details shown here are only concepts in the drawings currently, but a simple representation of the plate is included in the global model (Figure 4.4.1-1). The flex plate must allow the relative motions of the central column which is fixed vertically at the lower end by connections to the pedestal and to the lower TF flag extensions. The upper connections between the outer rim of the umbrella structure and the TF flags must allow the full vertical expansion of the central column. This is 9 mm at the elevation of the connection. The lid/flex plate is intended to bend and absorb the vertical motions elastically. Bending stresses develop at the ID and OD of the plate which produce prying moments at the bolt circles.


Figure 4.4-3 Bruce Paul's Model of the Lid/Flex

The torsional moment for design of the lid/flex/Diaphragm bolting and the TF steps or keys is 0.3MN-m for the lower lid (Figure 4.4.2-1) and 0.25 MN-m for the upper flex (Figure 4.4.2-1). This is the torque being transmitted from the centerstack TF to the outer rim of the umbrella structure. These may vary a bit as better models of the bellows, TF OOP support, and umbrella structure are developed, so it would be wise to put some margin in the design. The prying moment at the bolt circles is 6300 N-m per meter of perimeter. The prying moment can probably be reduced by reducing the assumed thickness of the 5/8 in thick lid.

Figure 4.4.1 and Figure 4.4-5 show the several views of the Upper Flex Plate Diaphragm.

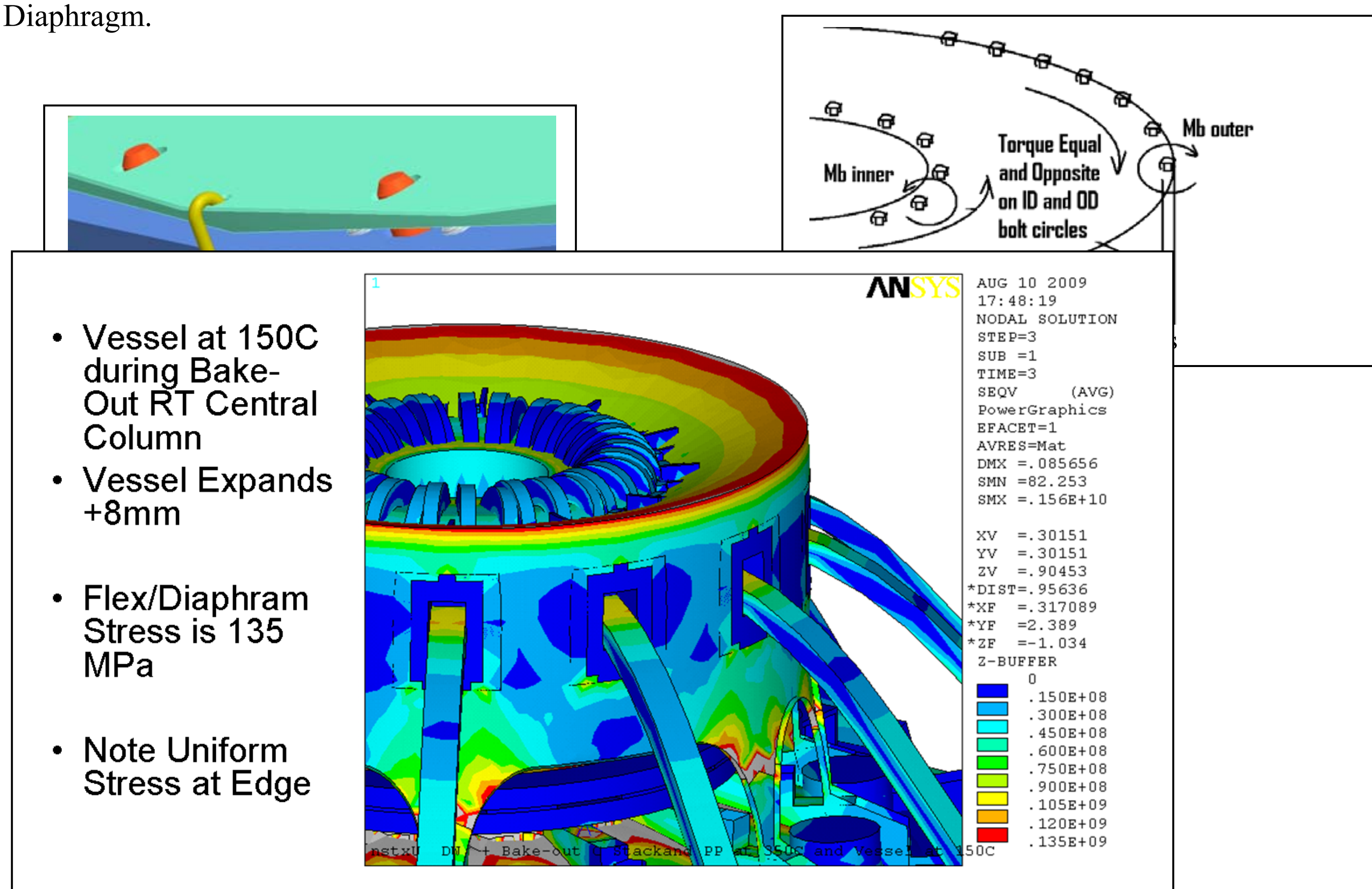

Figure 4.4-5 Flex Plate/ Diaphragm at 15C Bake-Out

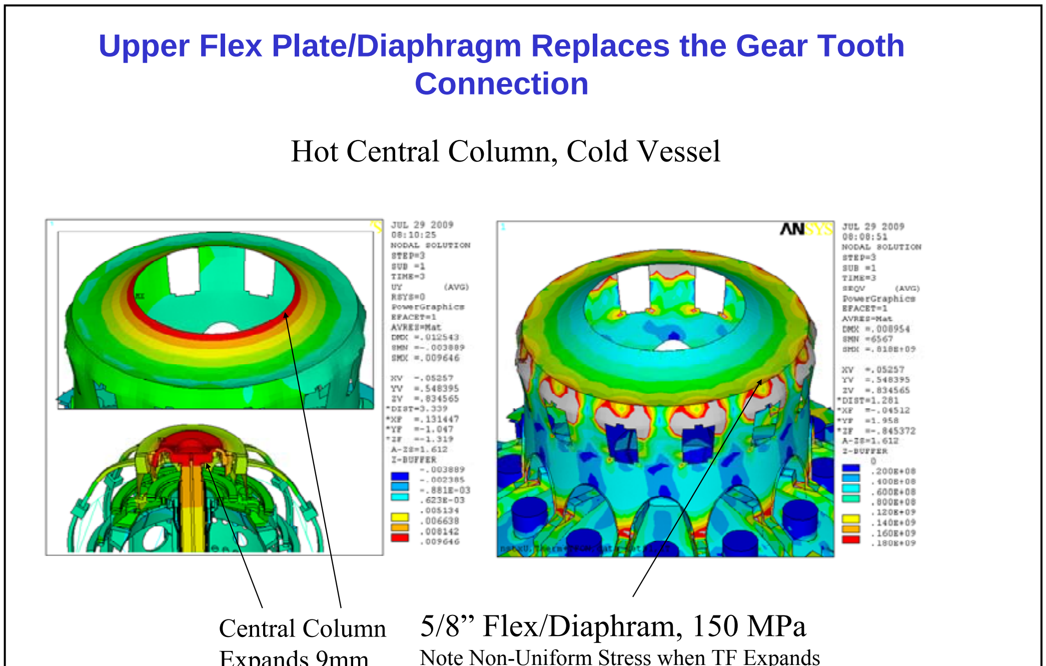

Figure 4.1-6 Upper Flex Plate Diaphragm Hot Central Column, Cold Vessel

The prying moments or Mb inner and outer(in Figure 2) are the bending stress multiplied by the plate section modulus or on a per perimeter length basis, the moment is the stress times t^2/6. At the outboard bolt circle, the stress is about 150 MPa (Figures 4 and 5) and the moment is 150 MPa *(5/8/39.37)^2/6 = 6300 N-m/m. If there were bolts every 20cm then the prying moment would be 6300*.2 = 1260 N-m and if the distance from the bolt centerline to the edge of the plate were 10 cm, the bolt load would be 12600 N or 3000 lbs. In the global model, the inner edge is pinned, due to a plate element to solid transition. It will probably be a bolted connection, for design purposes, the inner flex can be considered as having 150 MPa bending as well as the outer diameter of the flex.

4.4.2 Lid/Diaphragm/Cover/Flex Stress Torsional shear loading on the Lid bolt circles and the TF steps, Pockets or Keys

The torsional load from the lid/flex/diaphragm is transmitted to the mechanisms that engage the torsional load from the TF inner leg. In the present design the TF flags are staggered to engage a G-10 ring that is then bolted to the flex/lid. The keyed connection of the G-10 ring appears to have a larger capacity to carry torque than the bolt circle. Maybe shear keys or pins should be added here as well

To calculate the torsional moment being transmitted across the lid/flex, the torsional shear stress in the solid element portion of the model is post-processed using the ANSYS time history post-processor, Post26. All thermal cases and the 96 scenarios shear stress results are then used to compute the moment within post 26. The moment is then plotted.

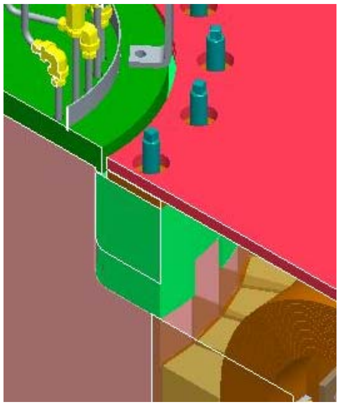

Figure 4.4.2-1 Stepped Feature

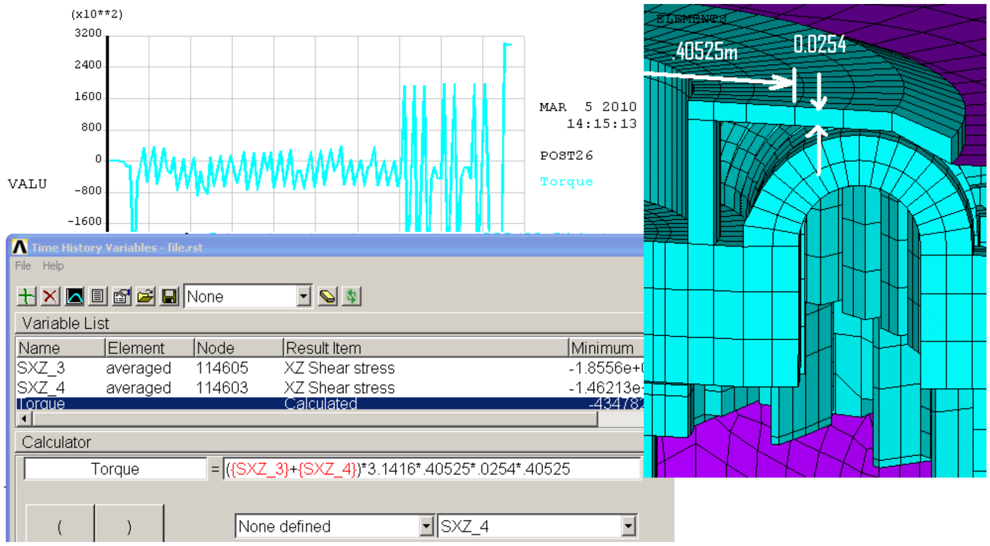

Figure 4.4.2-2 Torque on Upper Lid/Flex - About .2 MN-m

As a sanity check on the torque: For Scenario 79 the total OOP load on one upper half of a TF outer leg - mid plane to aluminum block is 127000N = 28550 lbs. Take out 5kips for the knuckle clevis or 23550lbs This is split between the aluminum block and shear in the TF outer leg mid-plane or 11775 lbs at each end. At the aluminum block, some goes into the lid. and some goes to the legs. - assume half goes to the lid or about 5900lbs to the lid then the moment is 12*5900/.2248*1.1= .34 MN-m.

The lower lid or flex plate needs to be removable to allow installation of the bus bars, coolant leads, and instrumentation. The lower lid was modeled with a series of holes to allow the services to pass. Circular holes have been modeled because the actual hole geometry to allow the power/coolant/instrumentation have not been sized and layed out.

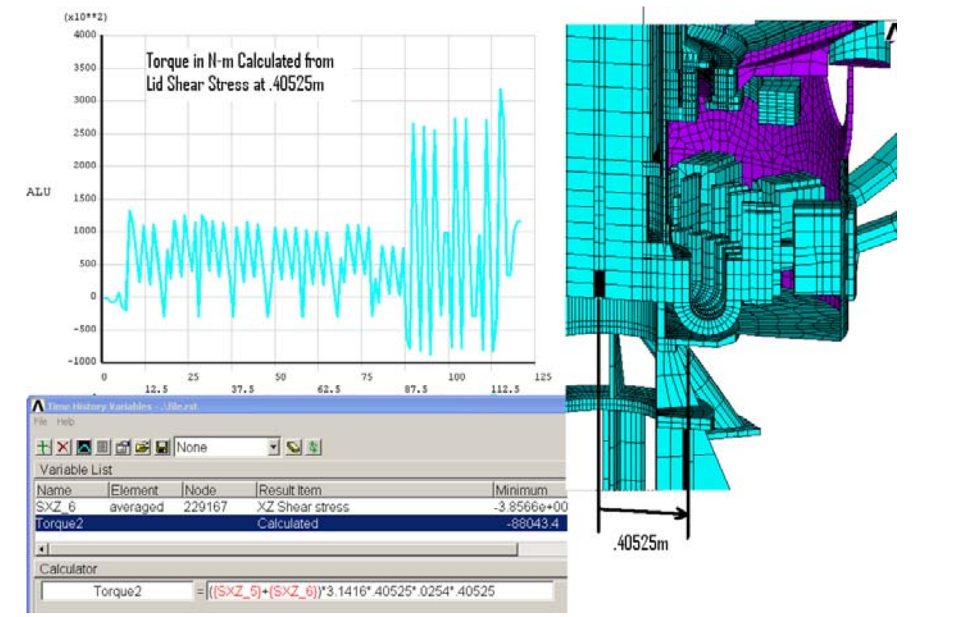

Figure 4.4.2-3 Torque on Lower Lid/Flex

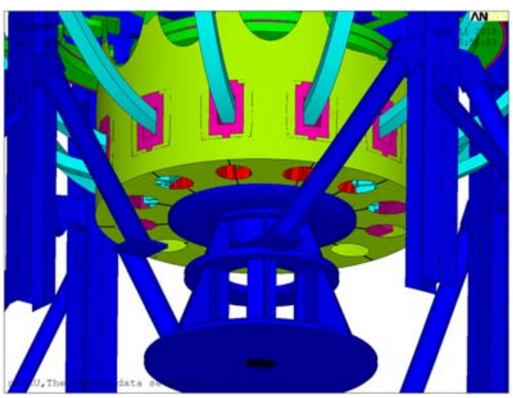
Figure 4.4.2-5

The torsional moment for design of the lid/flex/diaphragm bolting and the TF steps or keys is 0.28MN-m for the lower lid – With Holes -Only slightly less than without.

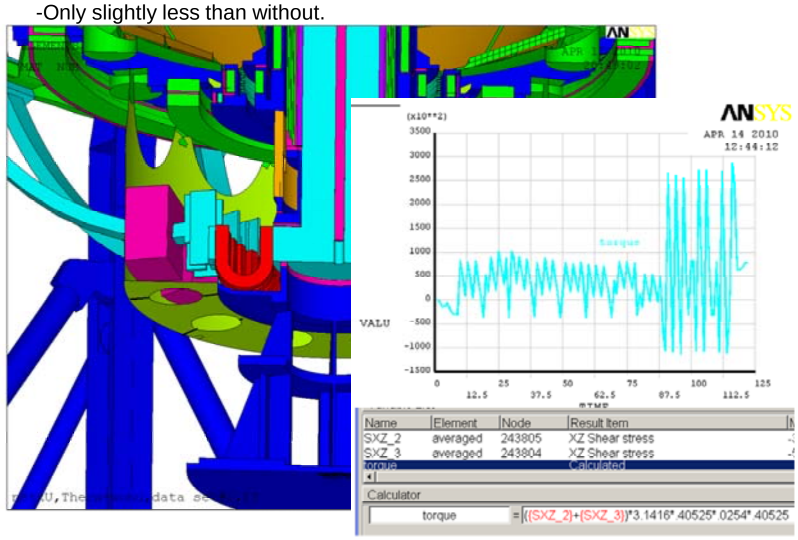

Figure 4.4.2-4Torque on Lower Lid/Flex -With Access Holes

The torsional moment for design of the lid/flex/Diaphragm bolting and the TF steps or keys is 0.3MN-m for the lower lid (Figure 7) and 0.25 MN-m for the upper flex (Figure 8). This is the torque being transmitted from the centerstack TF to the outer rim of the umbrella structure. These may vary a bit as better models of the bellows, TF OOP support, and umbrella structure are developed, so it would be wise to put some margin in the design.

The prying moment at the bolt circles is 6300 N-m per meter of perimeter. The prying moment can probably be reduced by reducing the assumed thickness of the 5/8 in thick lid.

A flex plate or cover or "lid" is intended as the structure that extends from a connection to the TF central column flags to the outboard edge of the umbrella structure. These details are only concepts in the drawings currently, but a simple representation of the plate is included in the global model (Figure 1). The flex plate must allow the relative motions of the central column which is fixed vertically at the lower end by connections to the pedestal and to the lower TF flag extensions. The upper connections between the outer rim of the umbrella structure and the TF flags must allow the full vertical expansion of the central column. This is 9 mm at the elevation of the connection. The lid/flex plate is intended to bend and absorb the vertical motions elastically. Bending stresses develop at the ID and OD of the plate which produce prying moments at the bolt circles.

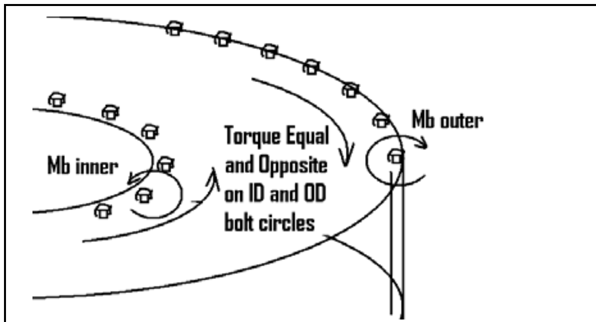

Figure 2 Torques and Moments


Figure 3 Bruce Paul's Model of the Lid/Flex Region

The prying moments or Mb inner and outer(in Figure 2) are the bending stress multiplied by the plate section modulus or on a per perimeter length basis, the moment is the stress times t^2/6

At the outboard bolt circle, the stress is about 150 MPa (Figures 4 and 5) and the moment is 150 MPa *(5/8/39.37)^2/6 = 6300 N-m/m. If there were bolts every 20cm then the prying moment would be 6300*.2 = 1260 N-m and if the distance from the bolt centerline to the edge of the plate were 10 cm, the bolt load would be 12600 N or 3000 lbs. In the global model, the inner edge is pinned, due to a plate element to solid transition. It will probably be a bolted connection, for design purposes, the inner flex can be considered as having 150 MPa bending as well as the outer diameter of the flex.

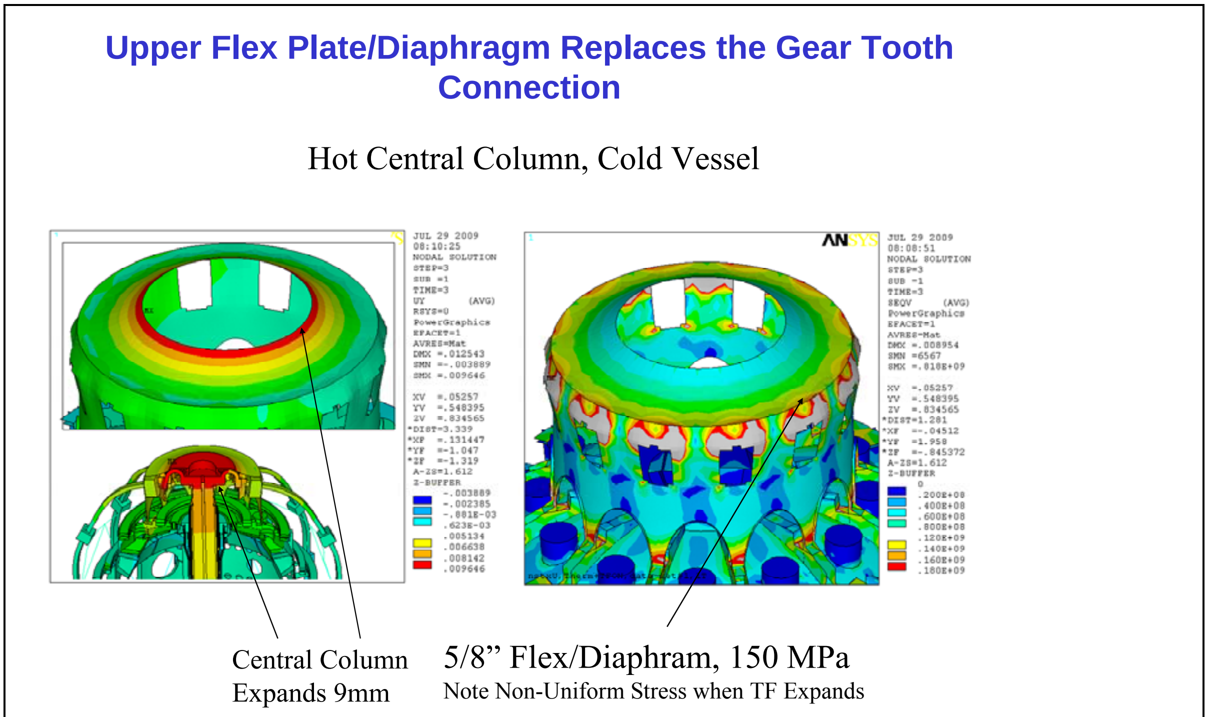

Figure 4 CDR Description of the Lid/Flex, Showing Vertical Displacement due to Centerstack Temp rise

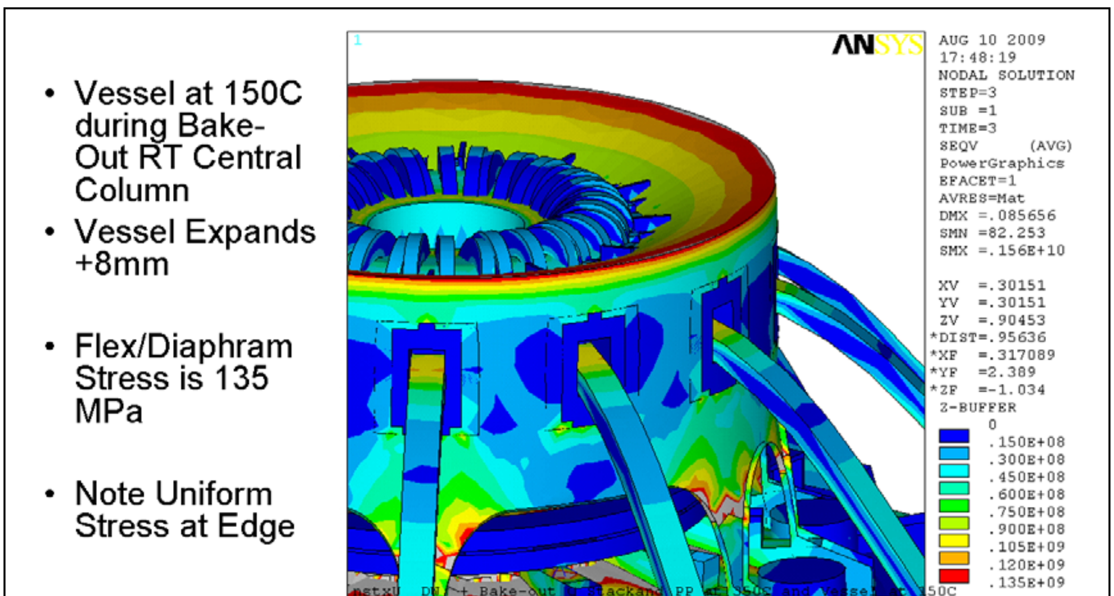

Figure 5 CDR Description of the Lid/Flex, Showing Vertical Displacement due to Vessel bake-out

Lid/Flex/Diaphragm Stresses with Access Ports

The torsional load from the lid/flex/diaphragm is transmitted to the mechanisms that engage the torsional reactions at the central column

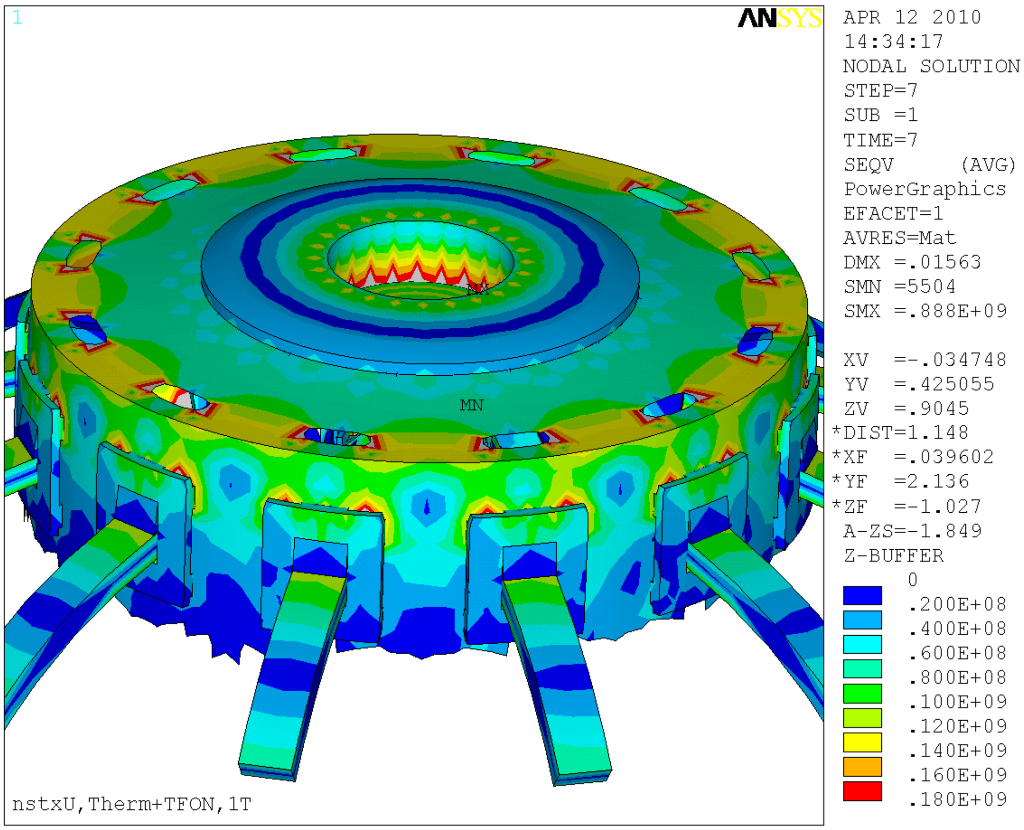

Figure 4.1-7 Upper Lid/Flex Plate With Access Holes Hot Central Column, Cold Vessel

Figure 4.4.2-6 Segment of the lower Lid/Flex

4.5 Umbrella Structure

The Umbrella structure appears in a number of models. It is one of the major support structures for the outer legs, and is a component of the global torque shell. One area of

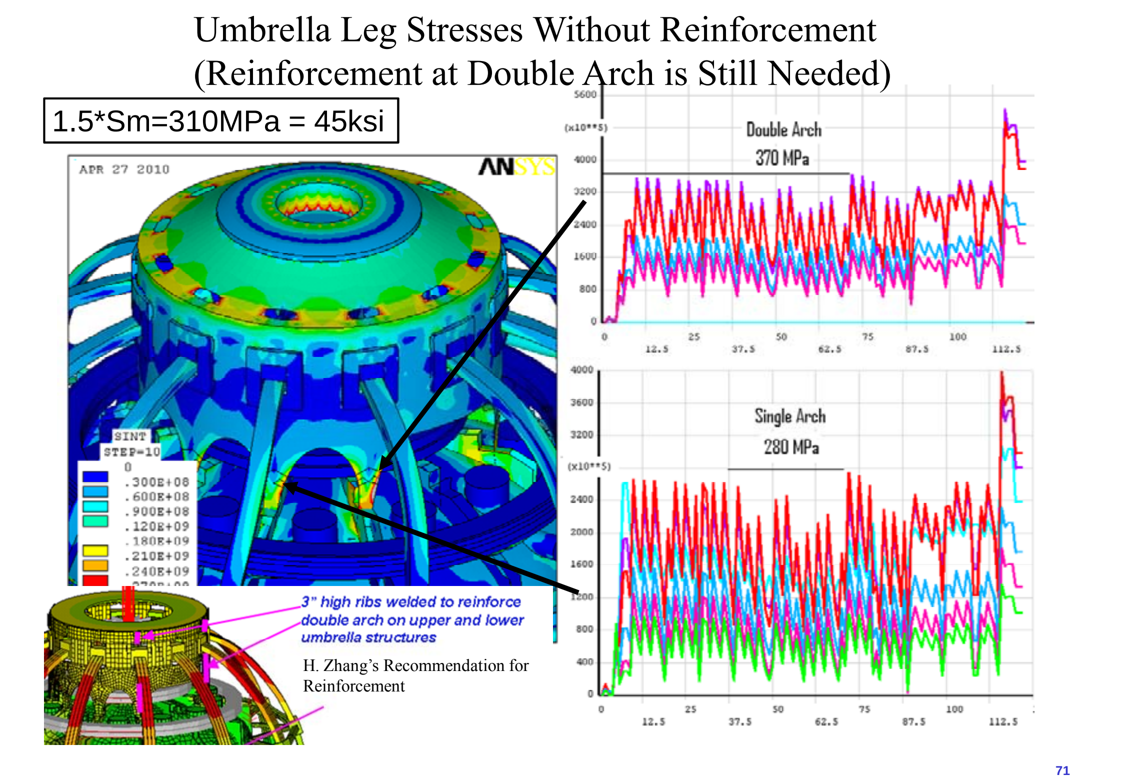

Figure 4.5-1 Need for Umbrella Structure Reinforcement

concern throughout the CDR and PDR is the support legs that form the arches. The arches are needed for access to instrumentation, diagnostics and power leads. These also may be needed to connect/disconnect the TF flex connections. The arch and support legs have been considered in a number of analyses. Evaluation of the TF outer leg support provisions have included evaluations of the umbrella legs. A number of reinforcement concepts have been suggested based on the maximum power supply loading in the design point. At the PDR, the legs have been analyzed for the 96 load cases, and have been found marginally acceptable except the legs framing the double arch. The loading on the umbrella structure comes mainly from the loads imposed by the

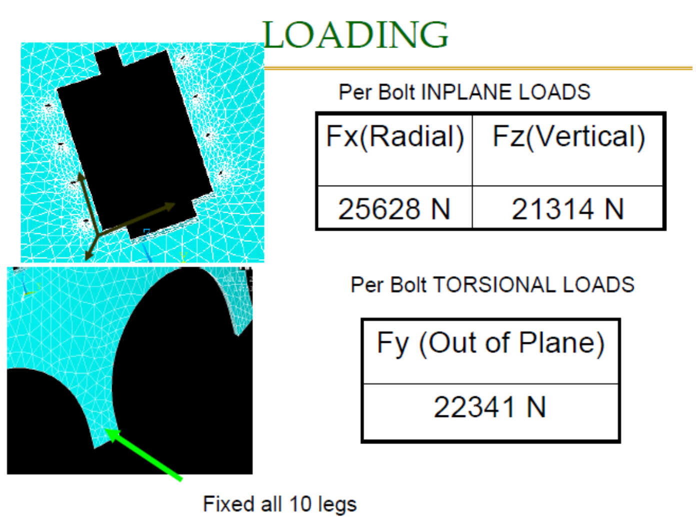

Figure 0-1 Umbrella Structure Loading

TF outer legs through the aluminum blocks that clamp the outer legs. The aluminum blocks are connected to the umbrella structure by eight 3/4 bolts. This connection must take in-plane loads from the constant tension D behavior of the outer legs as well as the out-of-plane(OOP) loads from the TF coil interaction with the poloidal field coils.

The figures shown here are from an early analysis of the TF outer leg loads on the aluminum block and bolting. The conclusion of this analysis is that there are some modest reinforcements needed to improve the capacity of the aluminum block bolting to take the TF tension. Loads were applied on the bolt hole locations in the umbrella structure. Out-of plane were applied as shear loads. Further analysis of the umbrella loads are presented in Section 0. Figure 0-1 depicts the umbrella structure loading. Figure 4.5-5 shows the results of the aluminum block analysis. Figure 0-4 shows a view inside

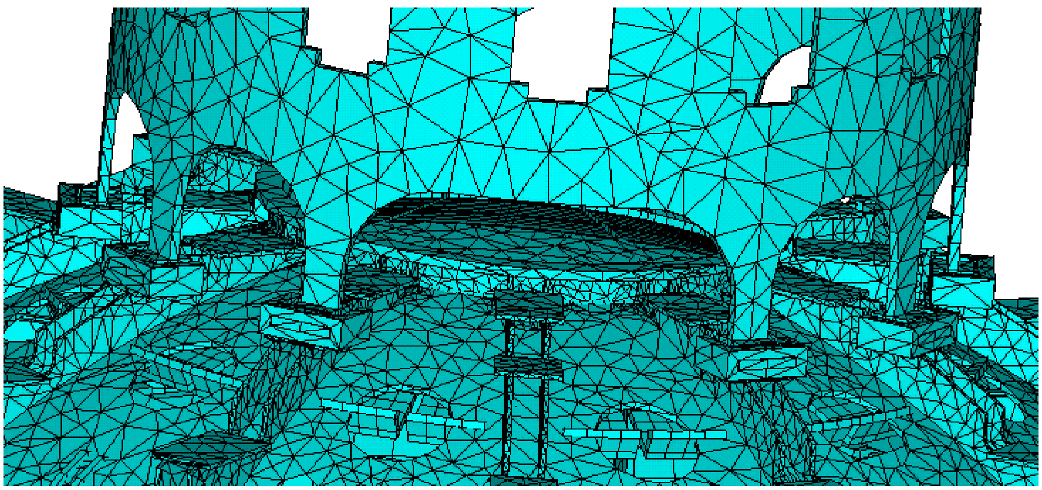

Figure 0-2 FEA Model of the Umbrella Structure Showing Large Span Arch

the umbrella structure. Plates will be added to distribute bolt loads into the shell more effectively. Figure 0-3 shows a view outside the umbrella structure. Figure 0-2 depicts a FEA model of the umbrella structure and shows a large span arch. Figure 4.6.2-10 depicts the Umbrella Structure response to In-Plane Loads from the TF Outer Legs.

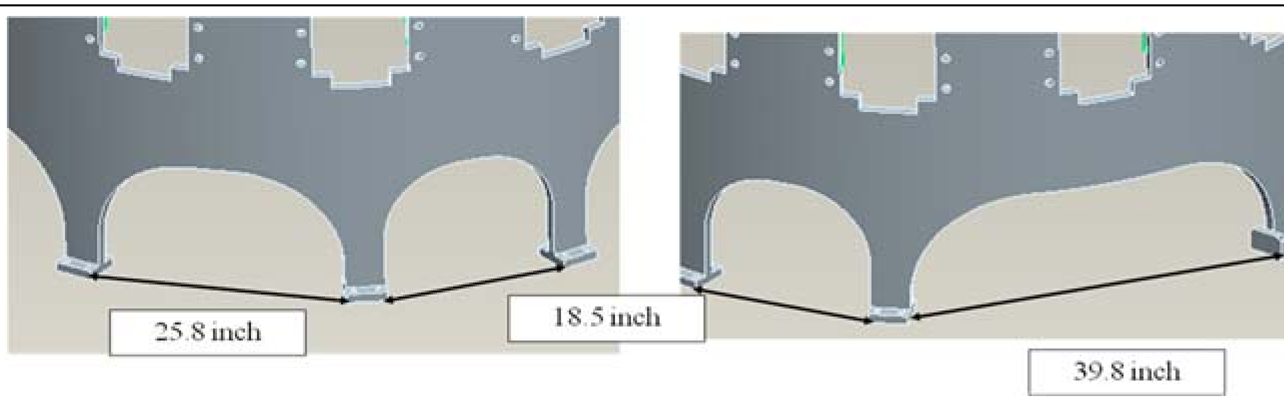

4.5.1 Aluminum Block Connection of the TF to the Umbrella Structure

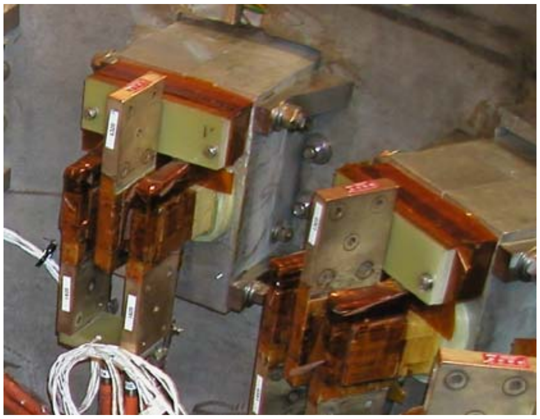

Figure 0-4 View Inside Umbrella Structure

Figure 0-3 View from Outside the Umbrella Structure

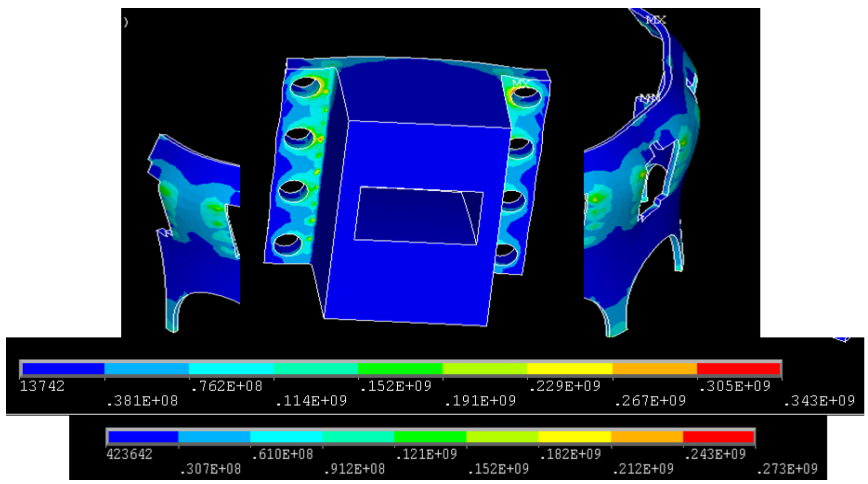

Figure 4.5-5 Aluminum Block Analysis Results

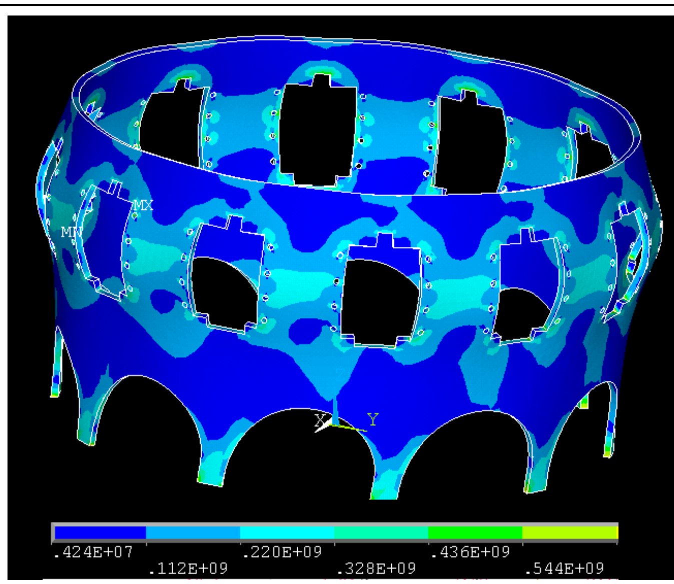

Figure 0-6 Umbrella Structure Response to In-Plane

4.5.2 Umbrella Structure Support Feet

The umbrella support feet are mounted on sliding blocks that attach to the vessel head rib weldment. These must transfer the OOP loading from the TF outer legs as well as vertical loads. The sliding feature is intended to allow the unrestrained growth of the vessel during bake-out. In the present design, the foot is held to the weldment with four bolts that connect through the welded plate and are loaded in shear by the OOP loading. The sliding feet assembly will be replaced with stronger components. The base of the slider will have lips to capture the welded plate to takes the shear off the bolts.

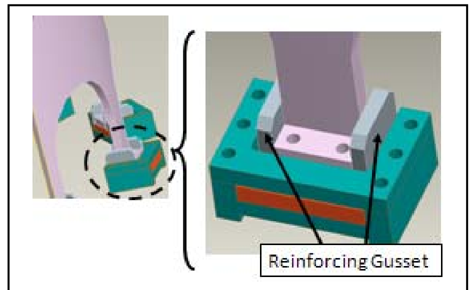

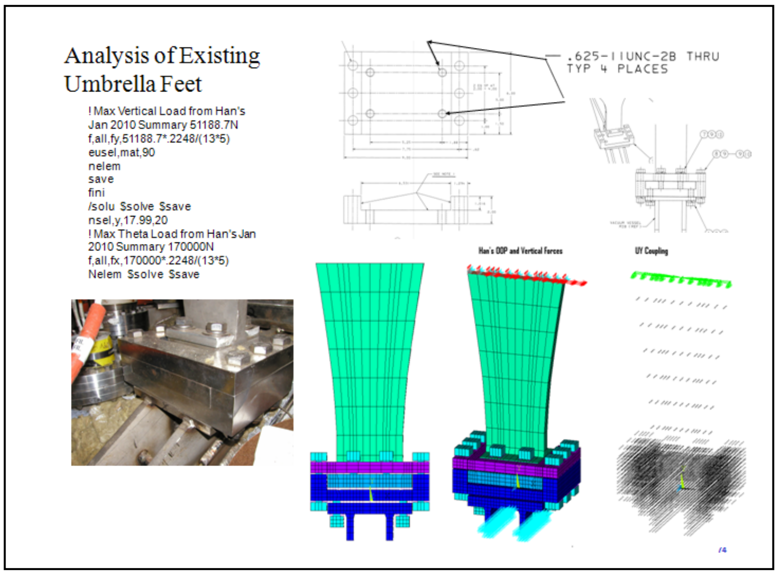

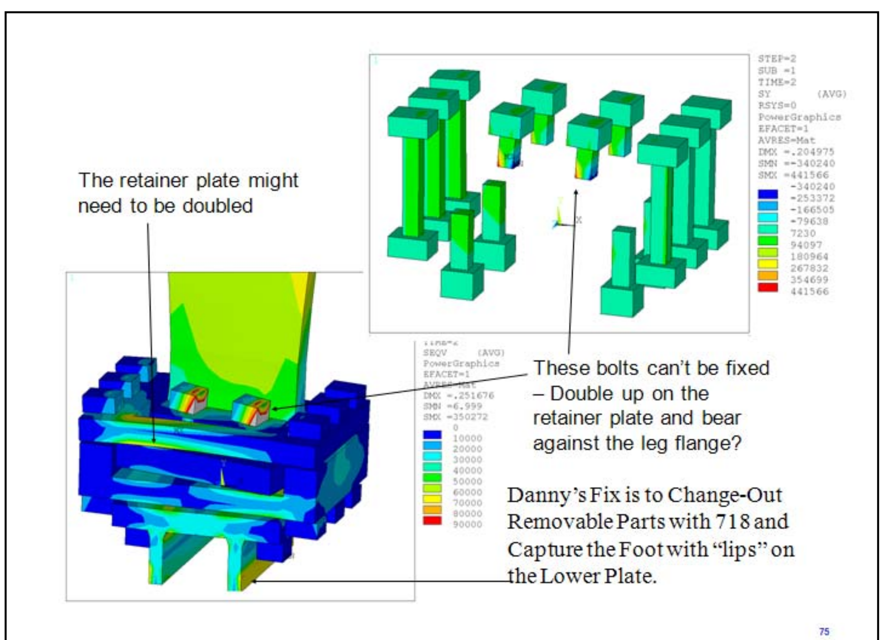

4.6 Support Ribs on the Dished Head

The ribs that stiffen the dome or dished head of the vessel and form the PF and umbrella structure supports, were cut to the nominal head profile. During assembly, this was found to produce a poor fit to the actual profile of the spun dished heads. This was picked up in a non-conformance report which was dispositioned by H.M. Fan. The repair was a series of tabs welded the rib and head that bridged the gap. Bruce Paul made the solid model based on the non-conformance report. This was meshed and used to analyze the welds and PF support brackets. Loading is from PF1c, PF2 and PF3 and the umbrella loads The weld detail is substantial and the weld and dished head stresses are less than 96 MPa, or 13 ksi. which is acceptable for the weld and the head. It is hard to imagine that the weld and tab details used for the rib connection can be qualified for fatigue loading. Some of these local high stress points are candidates for in-service inspection. One such point is shown in 4.5-5.

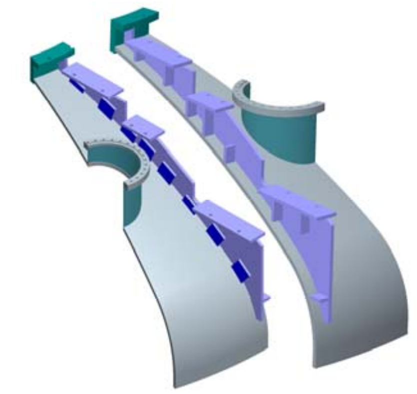

Figure 4.6-1

Design Point PF Forces
Applied to the Upper Dome/Rib Model

Fz(lbf)	PF1cU	PF2U	PF3U	PF3L	PF2L	PF1cL
Min	-30125	-67757	-148839	-31442	-42996	-68673
Worst Case Min	-168089	-194414	-303940	-246951	-192144	-143125
Max	68673	42996	100954	148839	54525	30125
Worst Case Max	143125	192144	246951	303940	194414	168089

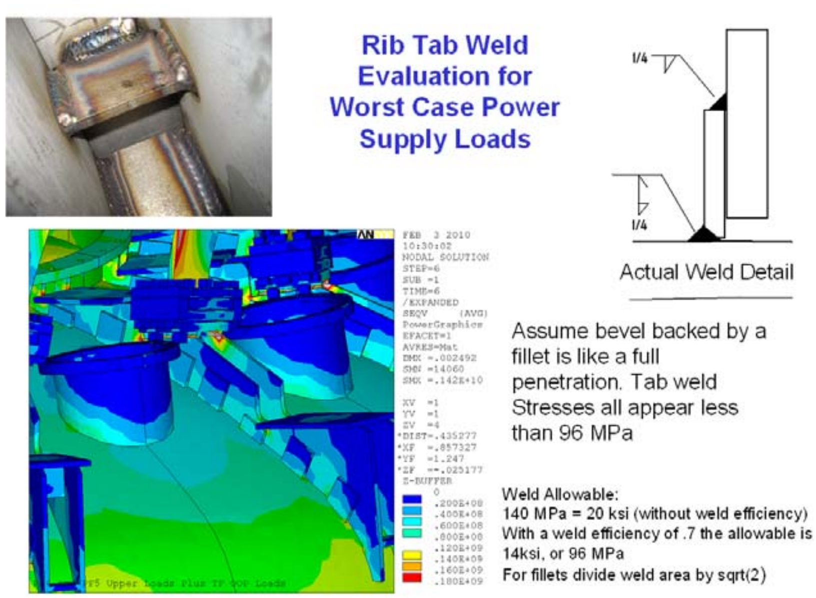

Figure 4.6-3

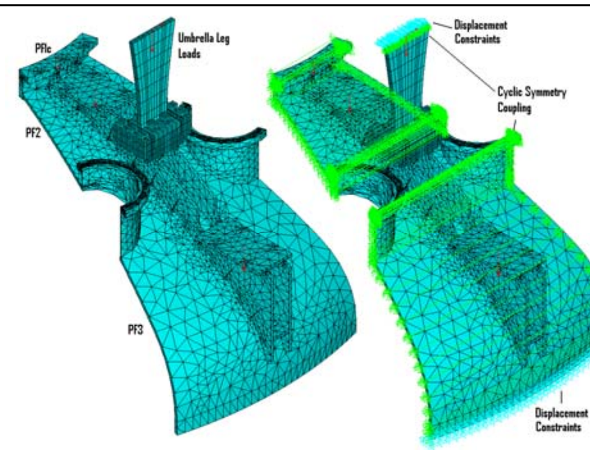

Figure 4.6-2 "Dome" model with ribs showing cyclic symmetry coupling.

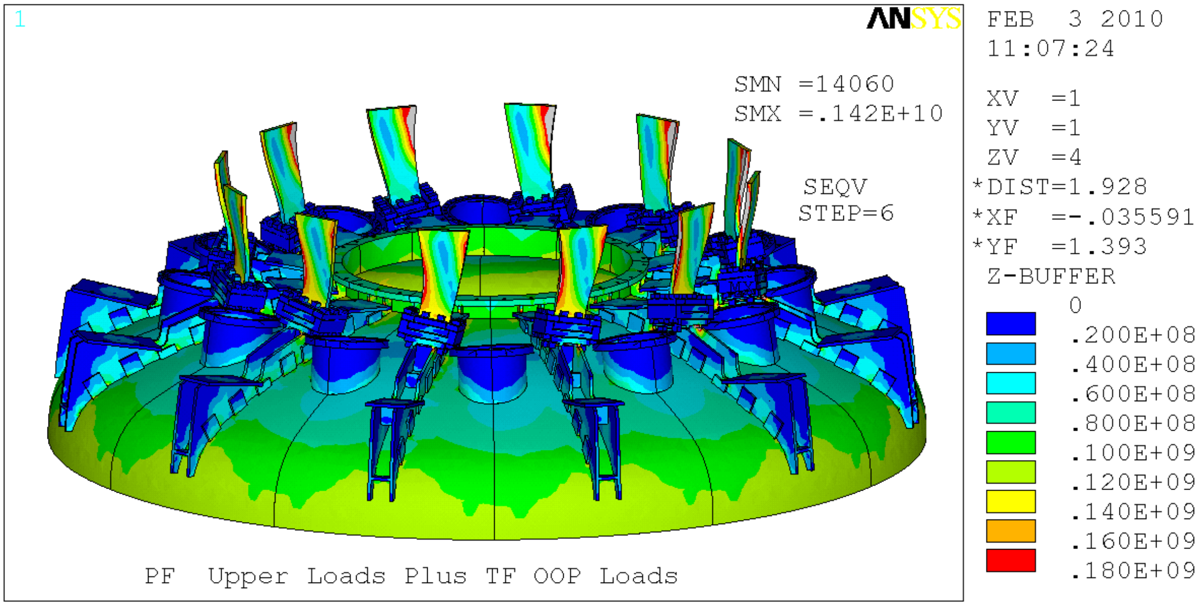

Figure 4.6-4

```
/title,PF 1,2,3 Worst Power Supply
 Loads Plus TF OOP Loads
bf,all,temp,20
f,985,fz,-168089/12/.2248      !PF1c
f,402,fz,-194414/11/.2248      !PF2
f,4588,fz,-100000    !Umb Foot
f,4588,fy,60000
f,1237,fz,-303940/11/.2248     !PF3
solve
```

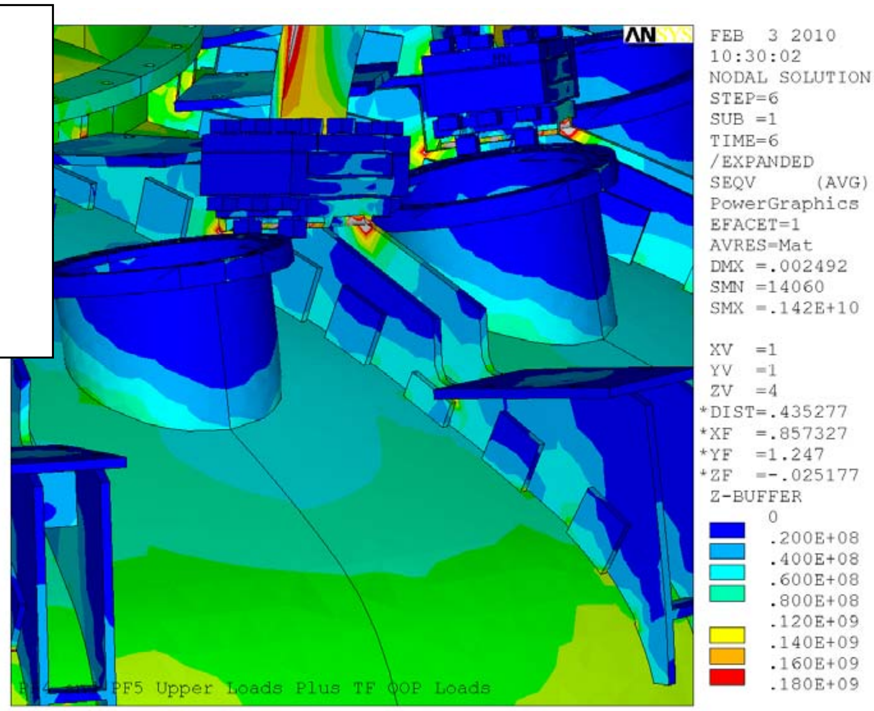

Figure 4.6-5 Stresses at the Vessel Ribs. There are some local peaks that are candidates for in-service inspection.

4.7 Center Stack

There are a number of concerns to address in the design of the centerstack casing. It supports the inner PF's – PF1a, and b. This is discussed in Section 1.3.3.3 . It supports the plasma facing components – tiles and backing plates for the central column and for the inner upper and lower divertor. Consequently it is exposed to the heat loads from these components. Current is run vertically through the casing to heat it during bake-out to 350 degrees C. Operationally, early estimates were that the casing could go to 500C or higher. This posed a problem for the support of the inner PF coils and local stresses in the and the halo current loads Figure 4.7-1 shows the upper end of the casing showing PF1a,and B, and PF1c which sit on the outboard side of the bellows and is supported by the vessel.

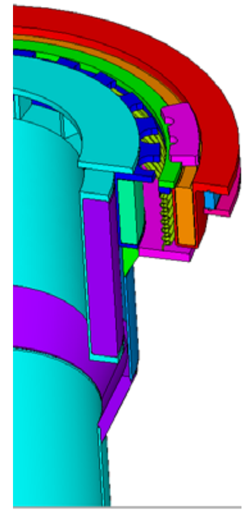

Figure 4.7-1 Centerstack Casing and Upper Inner PF's

4.7.1 Centerstack Casing Thermal Loads

Heat balance calculations in Section 3.1 quantify the temperatures that result from plasma. Figure 0 shows the center stack casing dimensions. Figure 0-7 shows the casing stress estimate with the case at 500C peak operating temperature, and the PF support area maintained at 100C.

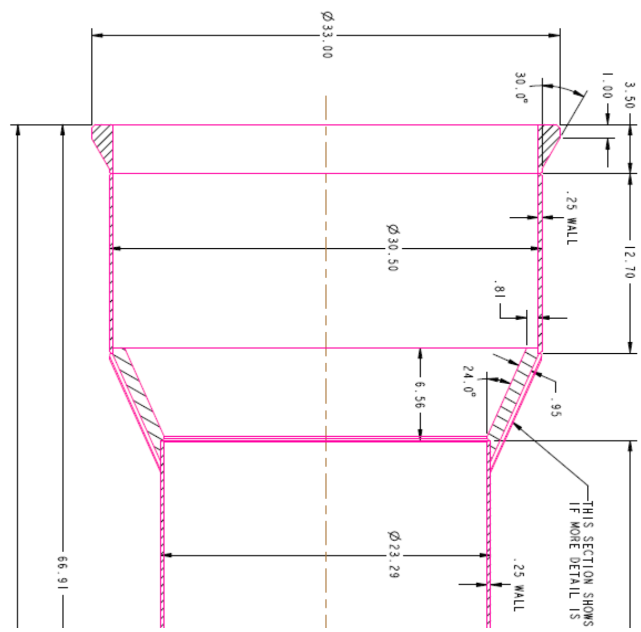

Figure 0 Center Stack Casing Dimensions

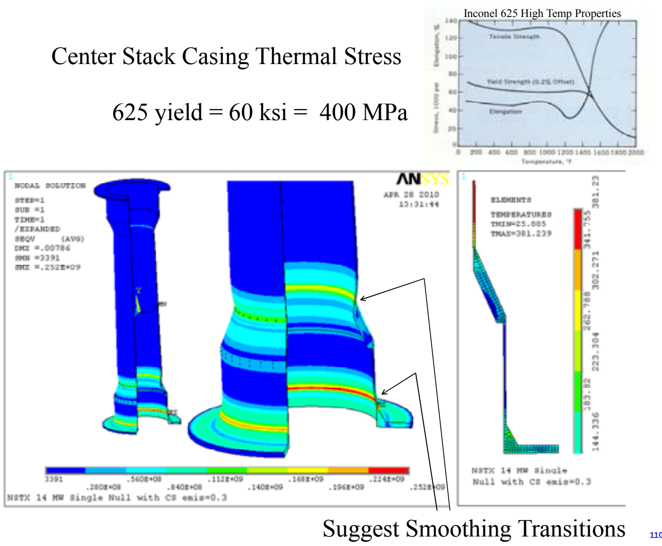

Figure 4.7.1-8 CSC Thermal Stress 252 MPa Max (Art Brooks Stress Pass based on temperatures from his heat balance calculations with a more gradual thermal gradient that assumed at right

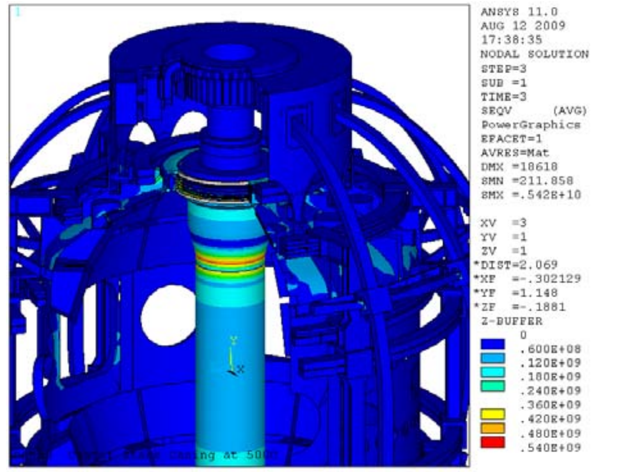

Figure 0-7 Casing Stress Estimate for the 500 Degree CSC from the Global model

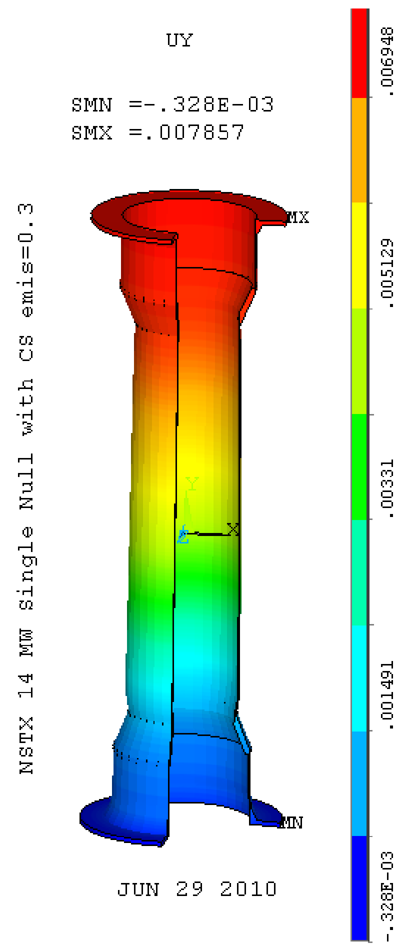

Figure Vertical Displacement of the Centerstack Casing for the calculated operating heat loads

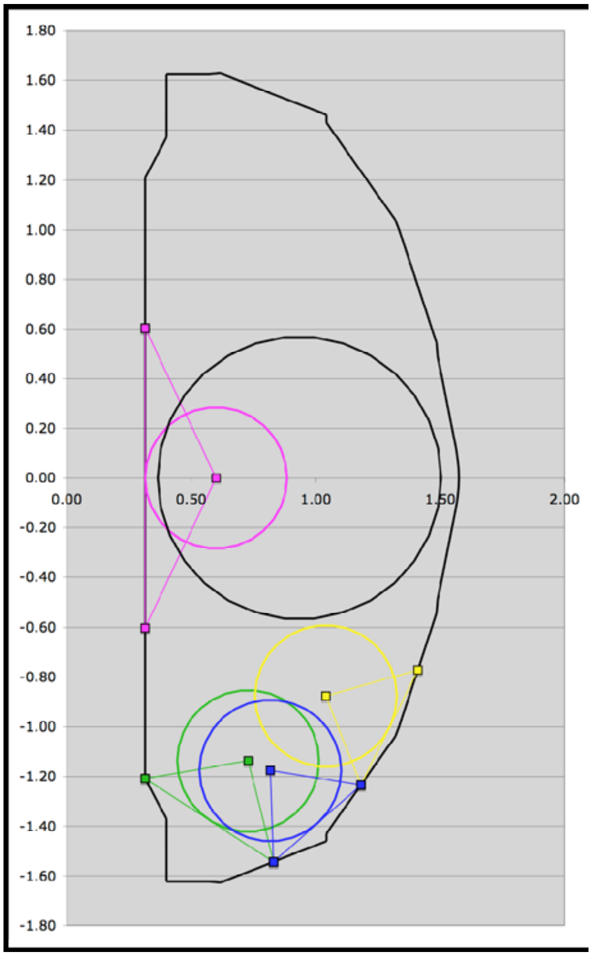

Figure 0-9 GRD Disruption Diagram

4.7.2 Centerstack Casing Halo Loads

From the NSTX_CSU-RQMT-GRD rev. 0 10 March 30, 2009**:** "A peak poloidal halo current up to 10% of the maximum plasma current prior to the disruption, with a toroidal peaking factor of 2:1; that is, the toroidal dependence of the halo current is [1 + cos (ϕ - ϕ_0)], for all toroidal phase angles ϕ_0 from 0 to 2*π. Halo current entry/exit locations shall assume a separation of 1.0m with vertical displacement + or - 0.25m about the midplane Location of Disrupting Plasmas & Halo Current Entry/Exit Points. See Figure 0-9 below.

.

Current and field directions (referring to Figure 0-9) shall be as follows:

- Plasma current Ip into the page (counter-clockwise in the toroidal direction,viewed from above)
- Halo current exits plasma and enters the structure at the entry point, exits the structure and re-enters the plasma at the exit point (counter-clockwise poloidal current, in the view of the Figure 0-9)
- Toroidal field into the page (clockwise in the toroidal direction, viewed from above)

Table 6-1 below shows the disruption and halo current analysis procedure and results.

Table 6-1 Disruption and Halo Current Analysis Procedure and Results

Halo Current	n.a.	20%=	35%=	35%=	35%=
		400kA	700kA	700kA	700kA
Halo Current Entry point (r,z)	n.a.	0.3148m	0.3148m	0.8302m	1.1813m
		0.6041m	-1.2081m	-1.5441m.	-1.2348m
Halo Current Exit point (r,z)	n.a.	0.3148m	0.8302m	1.1813m	1.4105m
		0.6041m	-1.5441m	-1.2348m	-0.7713m

Sri Avasarala and Ron Hatcher's disruption analyses were used to provide a vector potential "environment" for a model of the center stack casing. Sri has developed a procedure which starts with Ron Hatcher's OPERA disruption simulation, and transfers the axisymmetric vector potential results into a 3 D model of the vessel and passive plates. With modest changes any of the internal components can be evaluated with this procedure. A model of the center stack casing was input to Sri's electromagnetic analysis. The results are shown in Figure 0-11 and Figure 4.6.2-10.

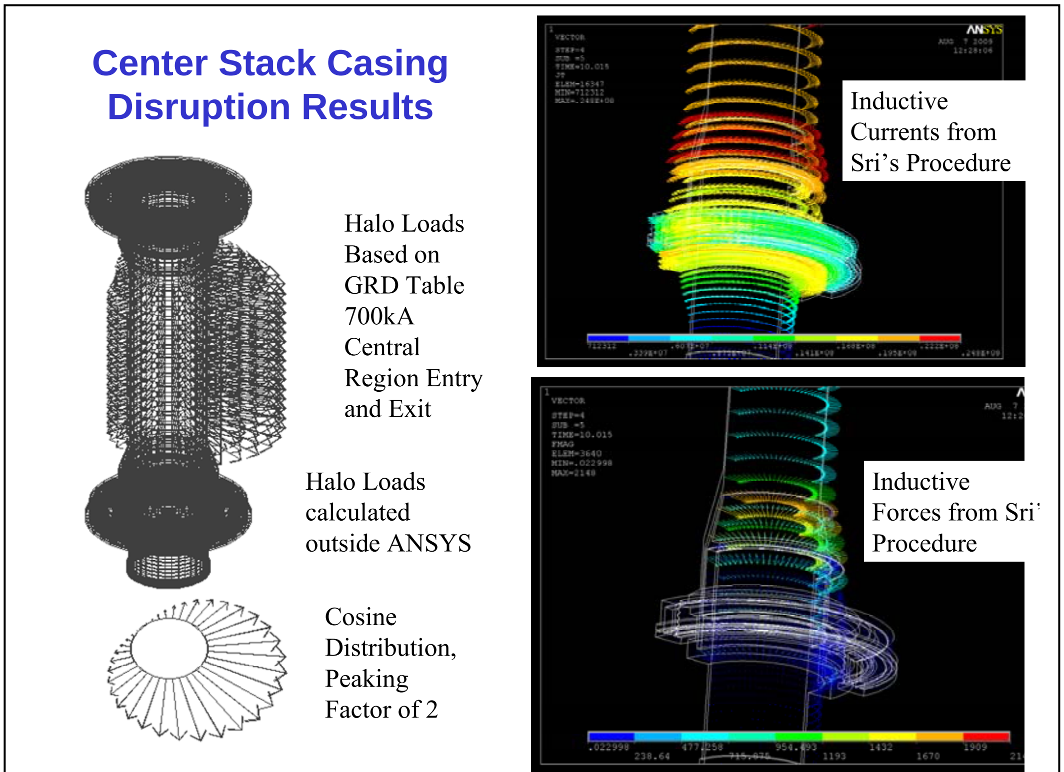

Figure 0-11 Center Stack Casing Disruption Results

Lorentz loads from these current entry and exit points were calculated assuming a peaking factor of 2. At present, only the equatorial plane halo current distribution has been evaluated. The acceptability of the results depends on the Dynamic Load Factor. Static str4uctural analysis produces unacceptable results. Dynamic analysis

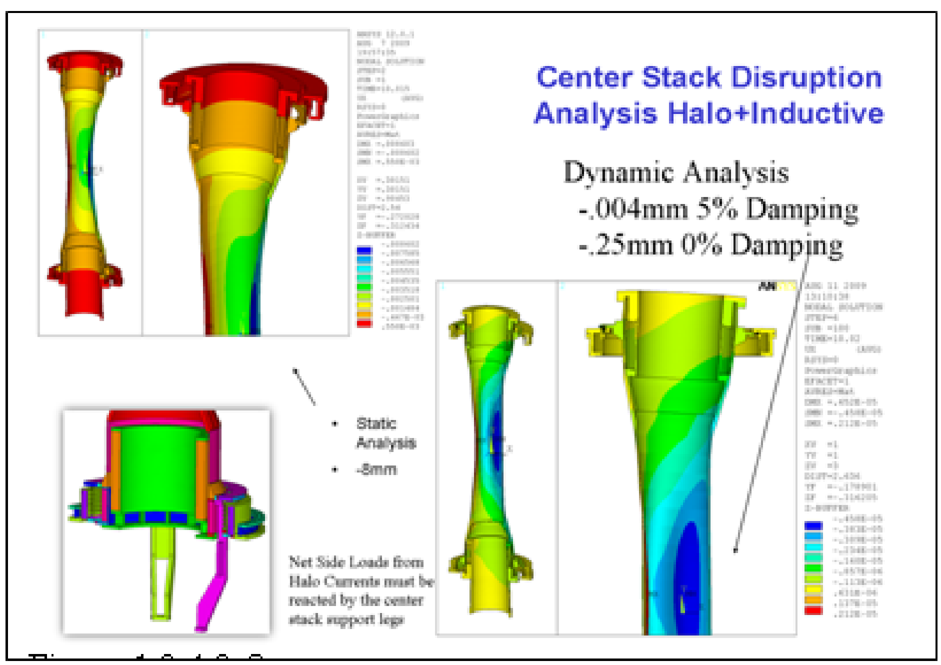

Figure 4.6.2-10 Center Stack Disruption Analysis (Halo + Inductive)

produced manageable results, with further evaluation of the net loads action on the support legs and bellow, needing qualification. **Error! Reference source not found.** provides yield data for Inconel 625.

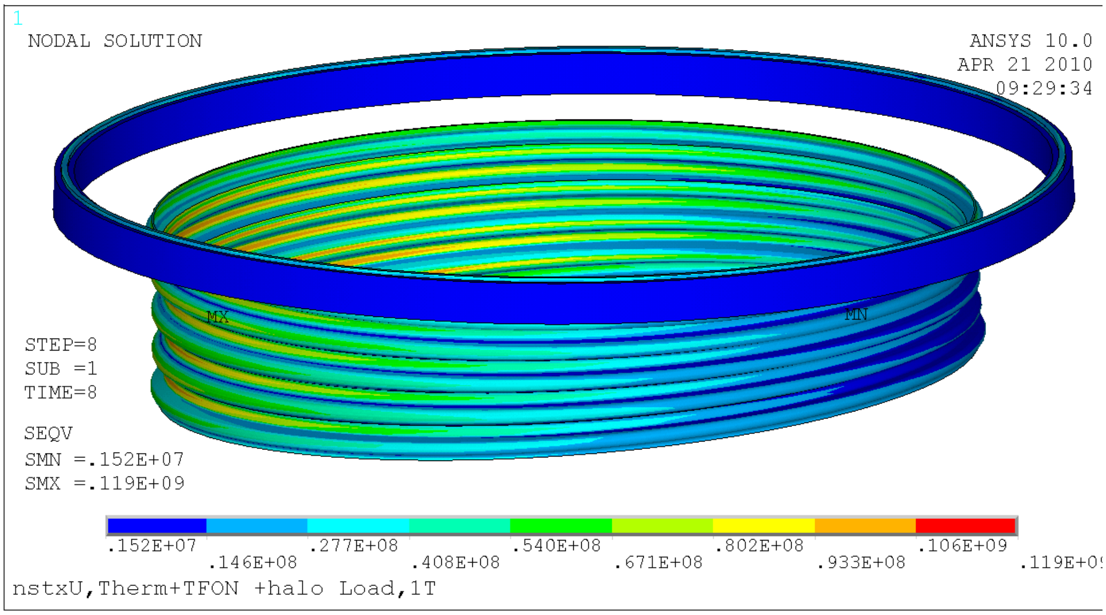

Bellows Stress with Halo Loads Applied in the Global Model

INCONEL 625

Test Temperature, °F(°C)	Ultimate Tensile Strength, ksi (MPa)	Yield Strength at 0.2% offset,ksi (MPa)	Elongation in 2" percent
Room	138.8 (957)	72.0 (496)	38
200	133.3 (919)	67.3 (464)	41
400	129.4 (892)	62.2 (429)	44
600	125.6 (866)	59.5 (410)	45
800	122.2 (843)	59.2 (408)	45
1000	119.9 (827)	58.8 (405)	46
1200	119.6 (825)	57.0 (393)	47

Table 0-2 Yield Data for Inconel 625

5. Magnet Systems (WBS 1.1.3)

5.1. Coil Builds

The latest coil builds are included inn the design point spreadsheet available on the NSTX engineering website. The builds tabulated here are from an early equilibrium flexibility based on "squareness" that was published by J. Menard. These builds were used in the global model described in Section 2. Table 5.1-1 shows the PF coil builds. Figure 5.1-1shows two views of the PF coils. Figure 5.1-2 shows the coil builds for the TF Coils.

Table 5.1-1 PF Coil Builds

#			r	z	dr	dz	nx	nz
1	CS		.2344	.0021	.01	4.3419	2	20
2	CS		.2461	.0067	.01	4.2803	2	20
3	CS		.2577	.0022	.01	4.2538	2	20
4	CS		.2693	-.0021	.01	4.1745	2	20
5	PF1aU	28	.3239	1.5906	.0413	.3265	4	4
6	PF1bU	10	.4142	1.8252	.042	.1206	4	4
7	PF1cU	10	.56	1.8252	.042	.1206	4	4
8	PF2U	14	.7992	1.8526	.1627	.068	4	4
9	PF2U	14	.7992	1.9335	.1627	.068	4	4
10	PF3U	7	1.4829	1.5696	.1631	.034	4	4
11	PF3U	8	1.4945	1.5356	.1864	.034	4	4
12	PF3U	7	1.4829	1.6505	.1631	.034	4	4
13	PF3U	8	1.4945	1.6165	.1864	.034	4	4
14	PF4U		1.795	.8711	.0922	.034	4	4
15	PF4U		1.8065	.9051	.1153	.034	4	4
16	PF4U		1.7946	.8072	.0915	.068	4	4
17	PF4L		1.795	-.8711	.0922	.034	4	4
18	PF4L		1.8065	-.9051	.1153	.034	4	4
19	Pf4L		1.7946	-.8072	.0915	.068	4	4
20	PF5U	12	2.0118	.6489	.1359	.0685	4	4
21	PF5U	12	2.0118	.5751	.1359	.0685	4	4
22	PF5L	12	2.0118	-.6489	.1359	.0685	4	4
23	PF5L	12	2.0118	-.5751	.1359	.0685	4	4
24	PF3L	7	1.4829	-1.5696	.1631	.034	4	4
25	PF3L	8	1.4945	-1.5356	.1864	.034	4	4
26	PF3L	7	1.4829	-1.6505	.1631	.034	4	4
27	PF3L	8	1.4945	-1.6165	.1864	.034	4	4
28	PF2L	14	.7992	-1.8526	.1627	.068	4	4
29	PF2L	14	.7992	-1.9335	.1627	.068	4	4
30	PF1cL	10	.56	-1.8252	.042	.1206	4	4
31	PF1bL	10	.4142	-1.8252	.042	.1206	4	4
32	PF1aL	28	.3239	-1.5906	.0413	.3265	4	4
33	Ip		.9344	0	.5696	1	6	8

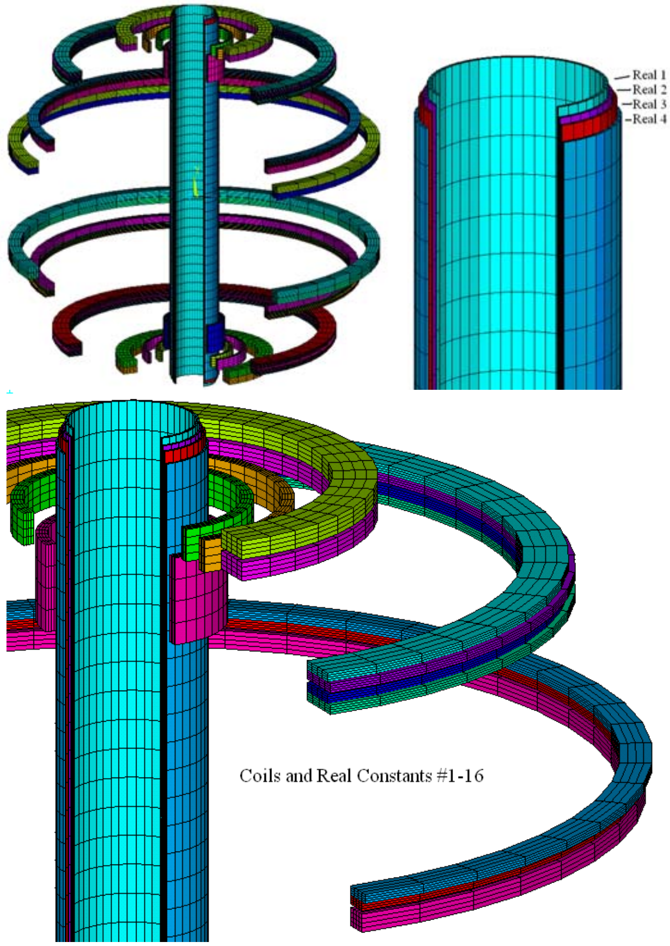

Figure 5.1-1 Two Views of the PF Coil s

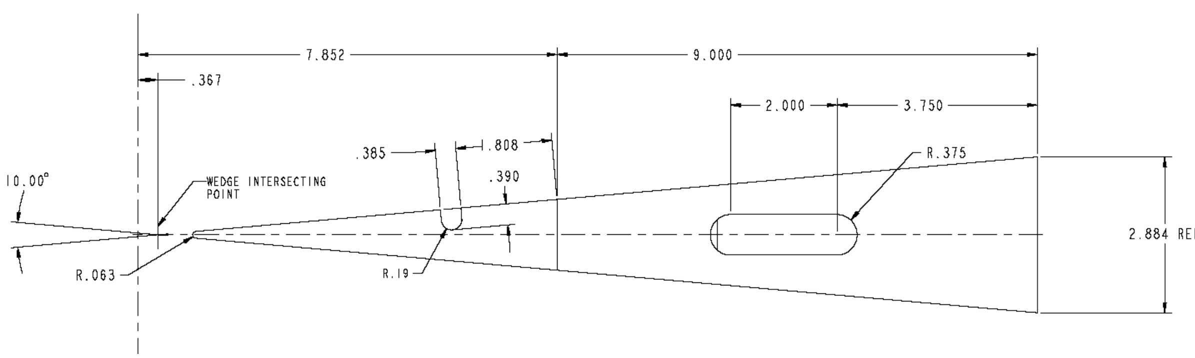

Figure 5.1-2 TF Coil Builds (Including Flag)

5.2. PF Currents

The latest design poiint on the NSTX engineering website includes 96 current scenarios. Table 5.2-1 is included because it is consistent with the coil build table above.

Table 5.2-1 PF Scenario Currents In Mat

Coil #	**TFON**	**IM**	**-0.1**	**-0.05**	**0**	**0.05**	**0.1**	**Worst 1**	**Worst 2**	**Worst3**	**Worst4**	**Worst5**
Step	**2**	**3**	**4**	**5**	**6**	**7**	**8**	**9**	**10**	**11**	**12**	**13**
	Nst1	**Nst2**	**Nst3**	**Nst4**	**Nst5**	**Nst6**	**Nst7**	**Nsw3**	**Nsw4**	**Nsw5**	**Nsw6**	**Nsw7**
1	0	5.88	.000	.000	.000	.000	.000	-5.88	5.88	5.88	-1.47	-1.47
2	0	5.808	.000	.000	.000	.000	.000	-5.808	5.808	5.808	-5.808	-1.452
3	0	5.76	.000	.000	.000	.000	.000	-5.76	5.76	5.76	-5.76	-1.92
4	0	5.664	.000	.000	.000	.000	.000	-5.664	5.664	5.664	-5.664	-1.416
5	0	0	7.172	7.196	7.234	7.348	7.452	0.784	0.784	0.784	0.784	0.784
6	0	0	-5.650	-4.763	-3.628	-2.331	-.946	0.12	0.12	0.12	0.12	0.12
7	0	0	-4.922	-4.014	-2.936	-1.755	-.517	0.2	0.2	0.2	0.2	0.2
8	0	0	4.484	4.307	3.941	3.401	2.772	0.168	0.168	0.168	0.168	0.168
9	0	0	4.484	4.307	3.941	3.401	2.772	0.168	0.168	0.168	0.168	0.168
10	0	0	-1.058	-1.426	-1.655	-1.720	-1.690	-0.112	-0.112	-0.112	-0.112	-0.112
11	0	0	-1.058	-1.426	-1.655	-1.720	-1.690	-0.128	-0.128	-0.128	-0.128	-0.128
12	0	0	-1.058	-1.426	-1.655	-1.720	-1.690	-0.112	-0.112	-0.112	-0.112	-0.112
13	0	0	-1.058	-1.426	-1.655	-1.720	-1.690	-0.128	-0.128	-0.128	-0.128	-0.128
14	0	0	-2.388	-1.183	-.206	.488	.923	-0.08	-0.08	-0.08	-0.08	-0.08
15	0	0	-2.388	-1.183	-.206	.488	.923	-0.1	-0.1	-0.1	-0.1	-0.1
16	0	0	-2.388	-1.183	-.206	.488	.923	-0.16	-0.16	-0.16	-0.16	-0.16
17	0	0	-2.388	-1.183	-.206	.488	.923	-0.08	-0.08	-0.08	-0.08	-0.08
18	0	0	-2.388	-1.183	-.206	.488	.923	-0.1	-0.1	-0.1	-0.1	-0.1
19	0	0	-2.388	-1.183	-.206	.488	.923	-0.16	-0.16	-0.16	-0.16	-0.16
20	0	0	-3.374	-4.340	-5.139	-5.771	-6.210	-0.384	-0.384	-0.384	-0.384	-0.384
21	0	0	-3.374	-4.340	-5.139	-5.771	-6.210	-0.384	-0.384	-0.384	-0.384	-0.384
22	0	0	-3.374	-4.340	-5.139	-5.771	-6.210	-0.384	-0.384	-0.384	-0.384	-0.384
23	0	0	-3.374	-4.340	-5.139	-5.771	-6.210	-0.384	-0.384	-0.384	-0.384	-0.384
24	0	0	-1.058	-1.426	-1.655	-1.720	-1.690	-0.112	-0.112	-0.112	-0.112	-0.112
25	0	0	-1.058	-1.426	-1.655	-1.720	-1.690	-0.128	-0.128	-0.128	-0.128	-0.128
26	0	0	-1.058	-1.426	-1.655	-1.720	-1.690	-0.112	-0.112	-0.112	-0.112	-0.112
27	0	0	-1.058	-1.426	-1.655	-1.720	-1.690	-0.128	-0.032	-0.128	-0.128	-0.128
28	0	0	4.484	4.307	3.941	3.401	2.772	0.168	0.168	0.168	0.168	0.168
29	0	0	4.484	4.307	3.941	3.401	2.772	0.168	0.168	0.168	0.168	0.168
30	0	0	-4.922	-4.014	-2.936	-1.755	-.517	0.2	0.2	0.2	0.2	0.2
31	0	0	-5.650	-4.763	-3.628	-2.331	-.946	0.12	0.12	0.12	0.12	0.12
32	0	0	7.172	7.196	7.234	7.348	7.452	0.784	0.784	0.784	0.784	0.784
33	0	0	2.000	2.000	2.000	2.000	2.000	2	2	2	2	2

5.3. Lorentz Force Plots – TF and TF+OH

The peak toroidal field from the load files used in the global model is 4.9T. The peak field from the electromagnetic current diffusion model is 4.2T. They used different TF inner leg dimensions from different design point published throughout the CDR2009. below provides the TF current specification L/R decay. Figure 5.3-2 shows the Lorentz Forces Due Only to the Toroidal Field. .Figure 5.3-2 shows the Total Field Plots – These are fields due only to the Toroidal Field Coil Current. Figure 5.3-1 shows Fields at the TF Joints from a Biot Savart Analysis. Figure 5.3-3 shows typical TF out-of-plane loads. Figure 5.3- shows other typical TF out-of-plane loads (Note that the TF Inplane is Included at Left at a Different Scale).

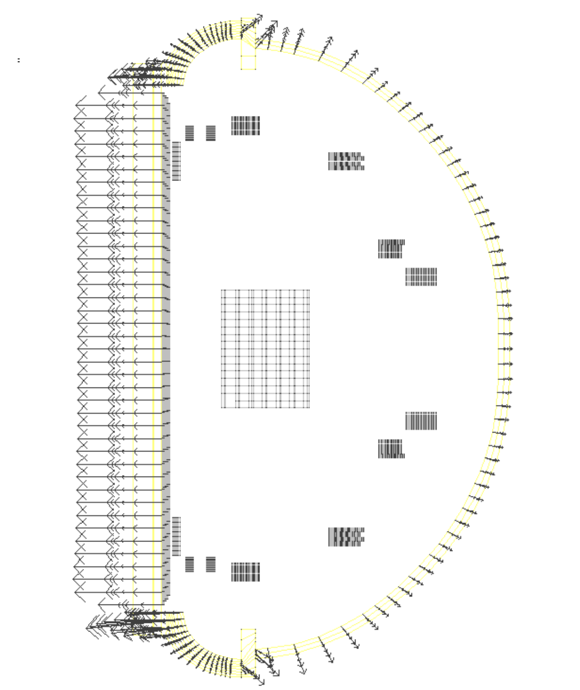

Figure 5.3-2 TFON, or Lorentz Forces Due Only to the Toroidal Field Coil

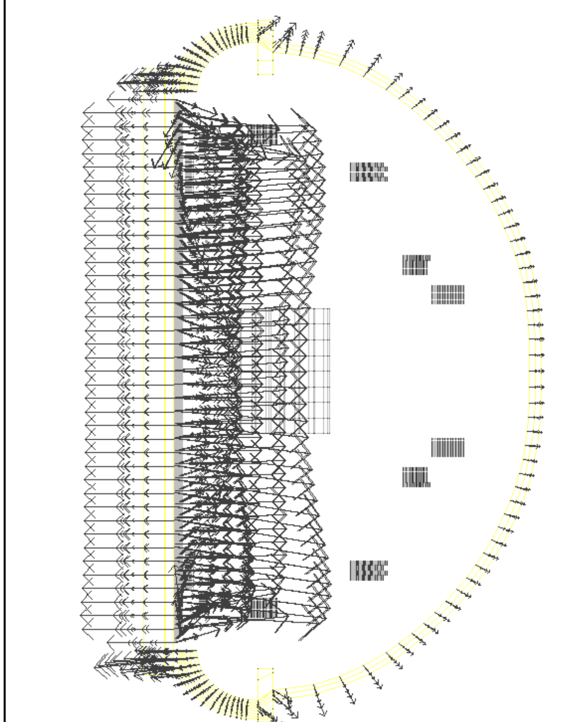

Figure 5.3-1 Lorentz Nodal Forces for the Initial Magnetization or Precharge Time Point

5.3.2 ANSYS NSTX TF Current Profile Input

```
!    NSTX Normal Pulse
NumSteps=29
tfbscale=1.0
t1= .1   $ i1= 0
t2= .2  $ i2= 0
t3= 1.952   $ i3= 15690.906*tfbscale
t4= 2.072   $ i4= 38658.746*tfbscale
t5= 2.192   $ i5= 58169.054*tfbscale
t6= 2.312   $ i6= 74742.32*tfbscale
t7= 2.432   $ i7= 88820.681*tfbscale
t8= 2.552   $ i8= 100779.71*tfbscale
t9= 2.672   $ i9= 110938.46*tfbscale
t10= 2.792   $ i10= 119567.93*tfbscale
t11= 2.912   $ i11= 126898.33*tfbscale
t12= 3.032   $ i12= 129777.84*tfbscale
t13= 4.0   $ i13= 129777.84*tfbscale
t14= 5.0     $ i14= 129777.84*tfbscale
t15= 6.0   $ i15= 129777.84*tfbscale
t16= 7.0   $ i16= 129777.84*tfbscale
t17= 8.0   $ i17= 129777.84*tfbscale
t18= 9.0   $ i18= 129777.84*tfbscale
t19= 9.512   $ i19= 129777.84*tfbscale
t20= 9.632   $ i20= 91022.609*tfbscale
t21= 9.752   $ i21= 58895.183*tfbscale
t22= 9.872   $ i22= 32262.092*tfbscale
t23= 9.992   $ i23= 10183.711*tfbscale
t24= 10.136   $ i24= 0
t25= 15.0   $ i25= 0
t26= 20.0   $ i26= 0
t27= 30.0   $ i27= 0
t28= 40.0   $ i28= 0
t29= 1000.0   $ i29= 0
```

```
!    NSTX Faulted Pulse
NumSteps=51
t1= .1   $ i1= 0
t2= .2   $ i2= 0
t3= 1.952   $ i3= 15690.906
t4= 2.072   $ i4= 38658.746
t5= 2.192   $ i5= 58169.054
t6= 2.312   $ i6= 74742.32
t7= 2.432   $ i7= 88820.681
t8= 2.552   $ i8= 100779.71
t9= 2.672   $ i9= 110938.46
t10= 2.792   $ i10= 119567.93
t11= 2.912   $ i11= 126898.33
t12= 3.032   $ i12= 129777.84
t13= 4.00   $ i13= 129777.84
t14= 5.00   $ i14= 129777.84
t15= 6.00   $ i15= 129777.84
t16= 7.00   $ i16= 129777.84
t17= 8.00   $ i17= 129777.84
t18= 9.512   $ i18= 129777.84
t19= 9.632   $ i19= 113132.22
t20= 9.752   $ i20= 98621.613
t21= 9.872   $ i21= 85972.17
t22= 9.992   $ i22= 74945.174
t23= 10.136   $ i23= 63563.326
t24= 10.256   $ i24= 55410.543
t25= 10.376   $ i25= 48303.454
t26= 10.496   $ i26= 42107.938
t27= 10.616   $ i27= 36707.073
t28= 10.736   $ i28= 31998.937
t29= 10.856   $ i29= 27894.677
t30= 10.976   $ i30= 24316.839
t31= 11.096   $ i31= 21197.903
t32= 11.216   $ i32= 18479.01
t33= 11.336   $ i33= 16108.848
t34= 11.456   $ i34= 14042.689
t35= 11.576   $ i35= 12241.54
t36= 11.696   $ i36= 10671.411
t37= 11.816   $ i37= 9302.6701
t38= 11.936   $ i38= 8109.4875
t39= 12.056   $ i39= 7069.3453
t40= 12.176   $ i40= 6162.6142
t41= 12.296   $ i41= 5372.1826
t42= 12.416   $ i42= 4683.1337
t43= 12.536   $ i43= 4082.4638
t44= 12.656   $ i44= 3558.8372
t45= 12.776   $ i45= 3102.3723
t46= 12.896   $ i46= 2704.4546
t47= 13.016   $ i47= 2357.5748
t48= 15.0   $ i48= 1000
t49= 20.0   $ i49= 100
t50= 40.0   $ i50= 0.0
t51= 1000.0   $ i51= 0.0
```

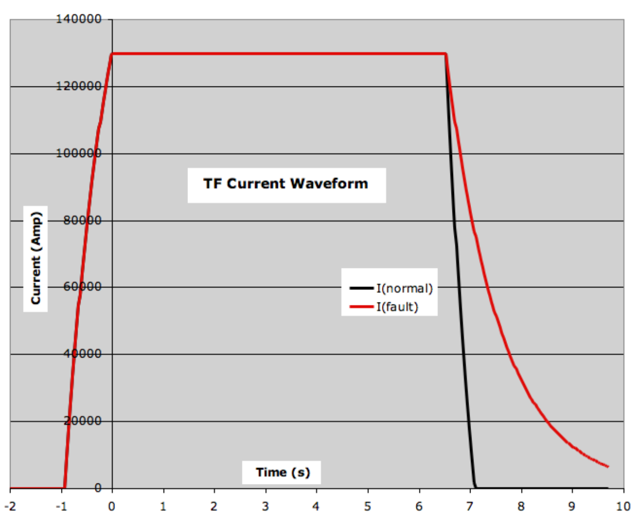

Figure NSTX Normal Operation Waveform from the June 2010 Design Point

5.3.3 Toroidal Field Plots

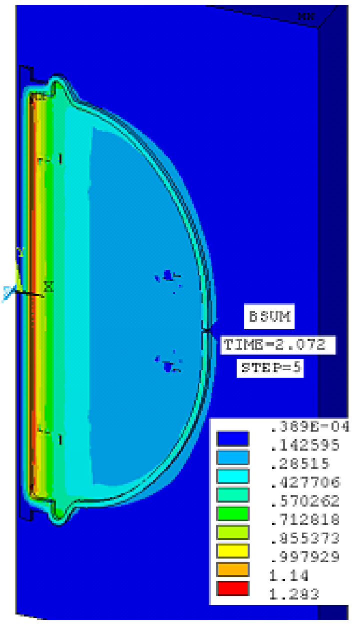

Figure 5.3-3 - Total Field Plots – These are fields due only to the Toroidal Field Coil Current, from P Titus Current Diffusion Analysis.

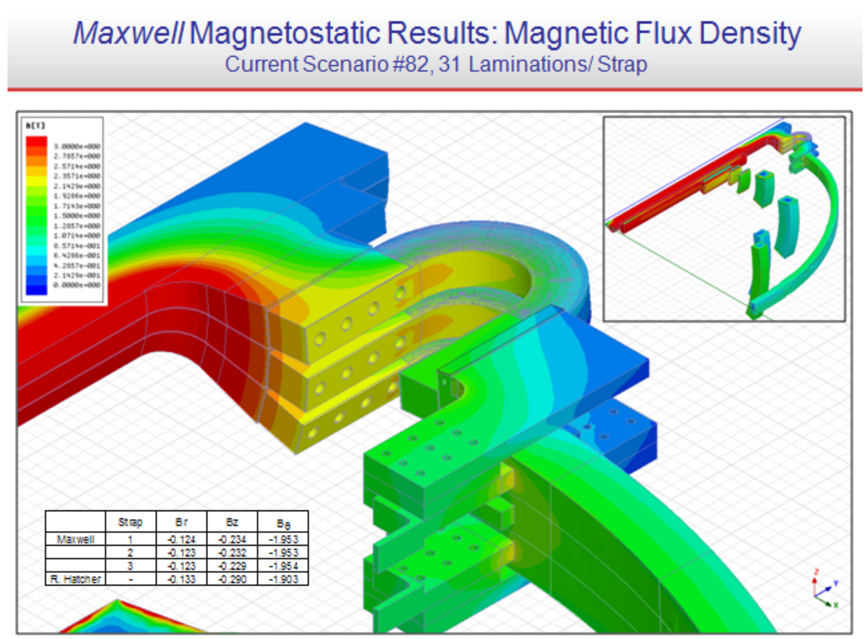

	Strap	Br	Bz	Bθ
Maxwell	1	-0.124	-0.234	-1.953
	2	-0.123	-0.232	-1.953
	3	-0.123	-0.229	-1.954
R. Hatcher	-	-0.133	-0.290	-1.903

Figure 5.3-4 Total Field from T. Willard's Flex Analysis

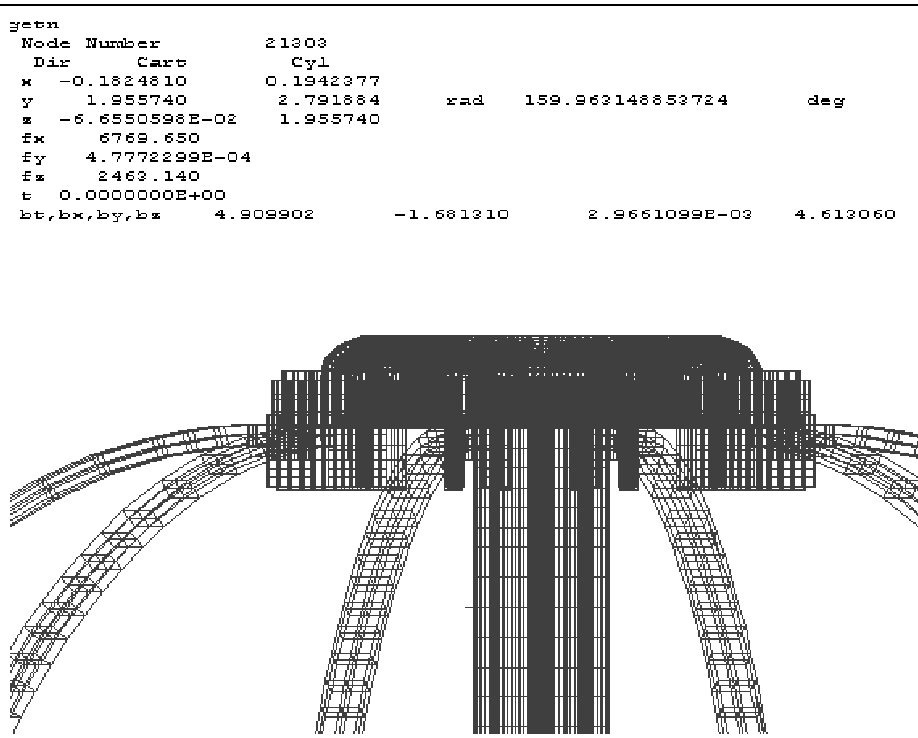

Figure 5.3-5 - Fields at the TF Joints, from a Biot Savart Analysis

5.3.4 TF Out-of-Plane Loads

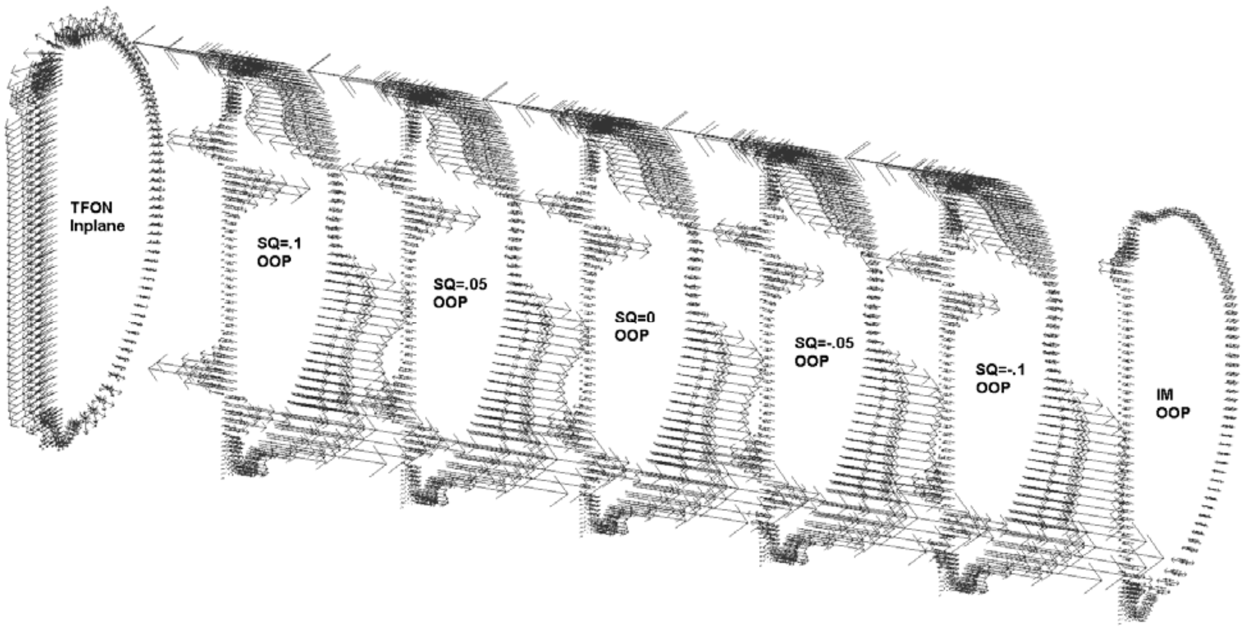

Figure 5.3.4-1 Typical TF Out-of-Plane Loads

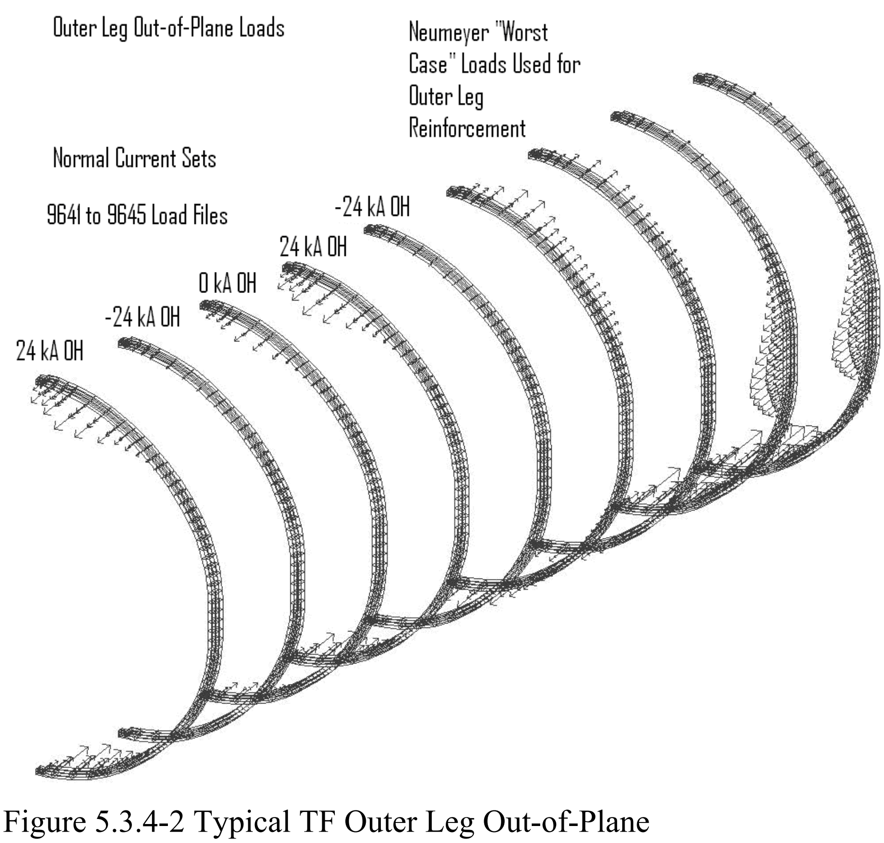

Figure 5.3.4-2 Typical TF Outer Leg Out-of-Plane

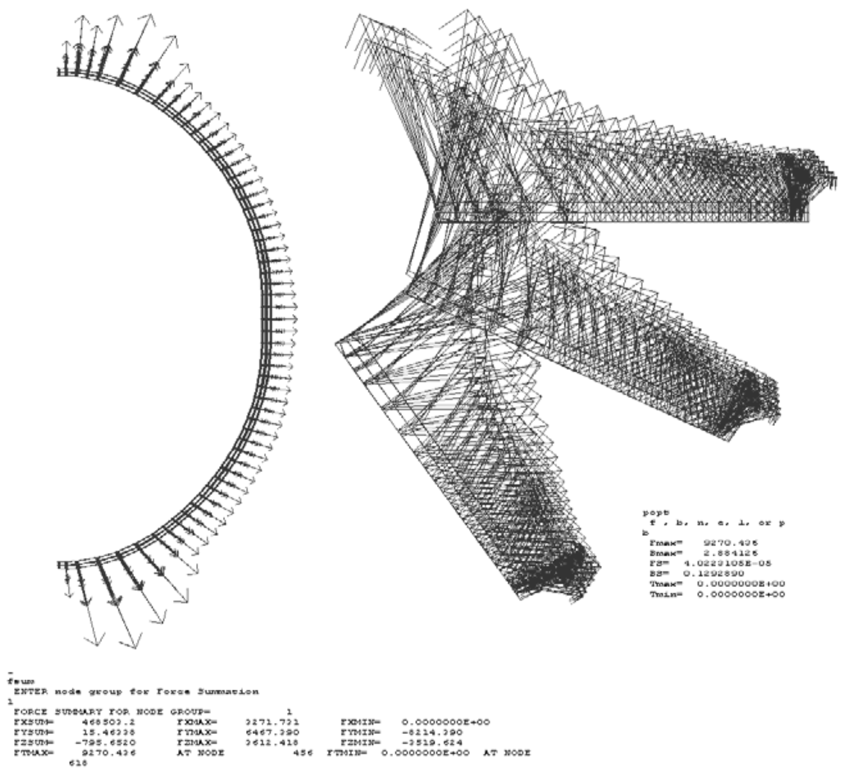

Figure 5.3.4-3 TFON Outer Leg Loading. The net outward load is 468503N=105000 lbs

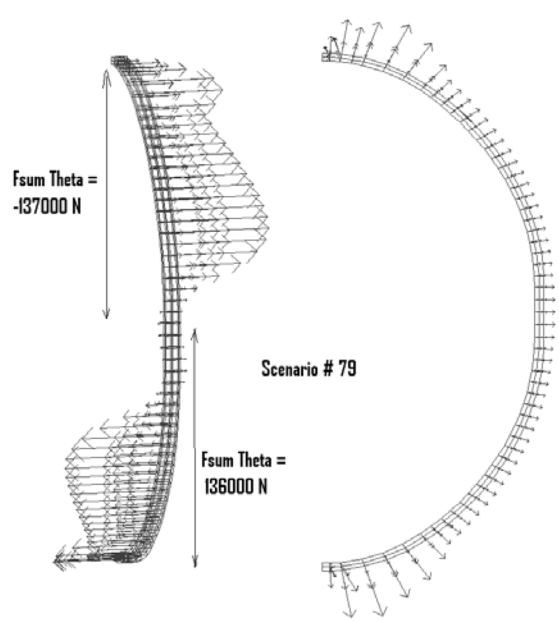

Figure 5.3.4-4 OOP Forces for Scenario #79 Summed from the joint flags out. From the aluminum blocks out the sum is 127000 N for the upper half.

5.3.5 Poloidal Field Plots

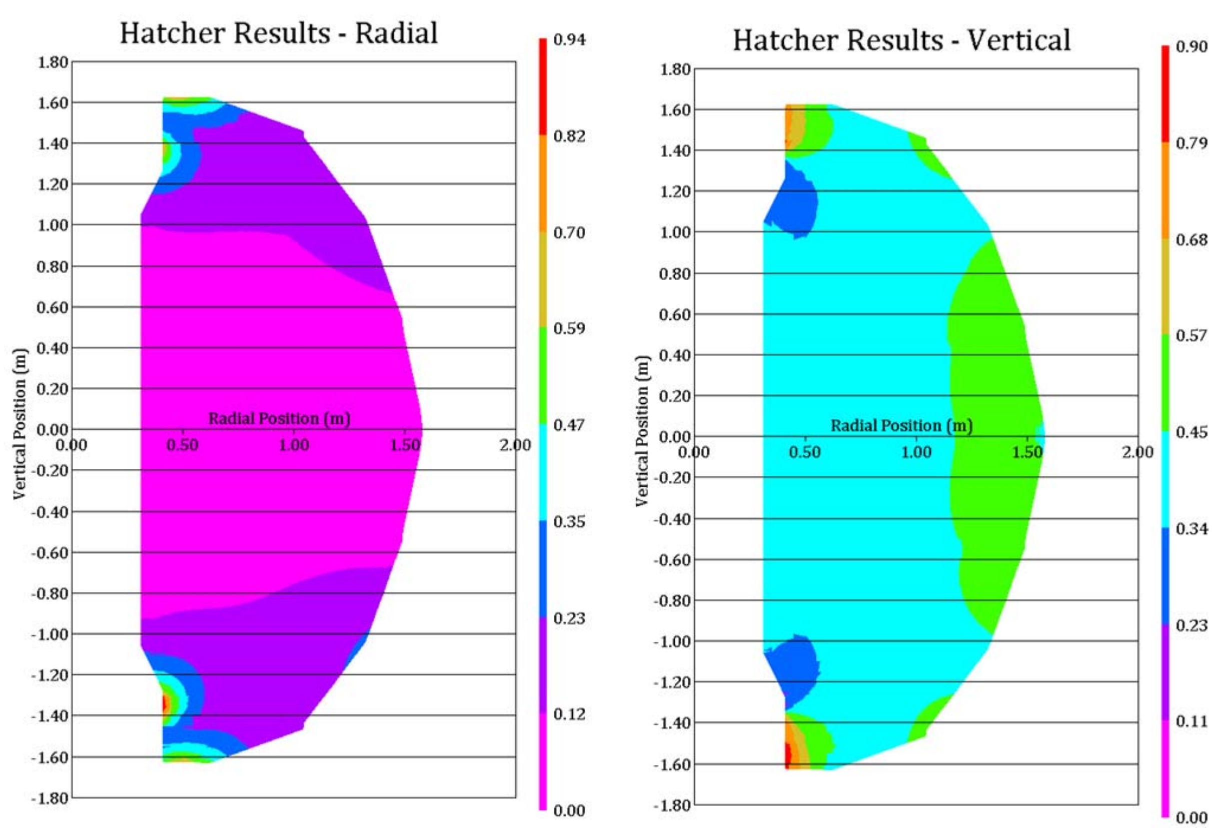

Figure 5.3.5-1 Maximum

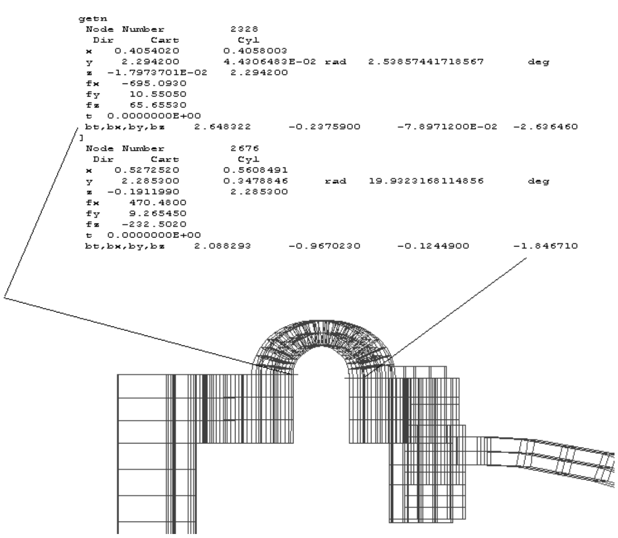

Figure 5.3.5-2 Flex Joint Fields, 9905 Load Case

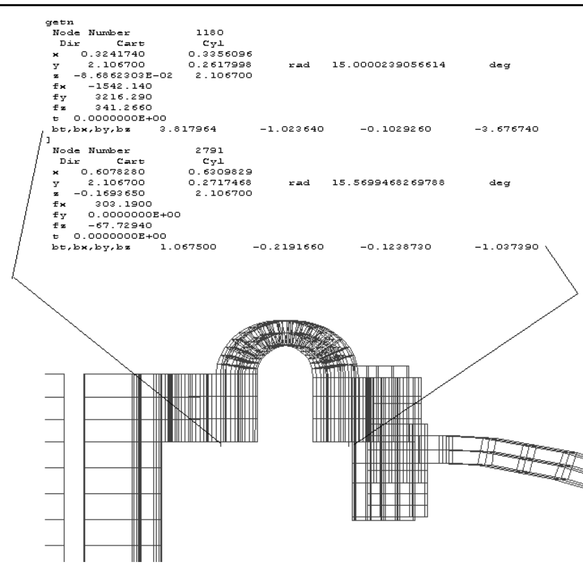

Figure 5.3.5-3 Flex Joint Fields, 9905 Load Case

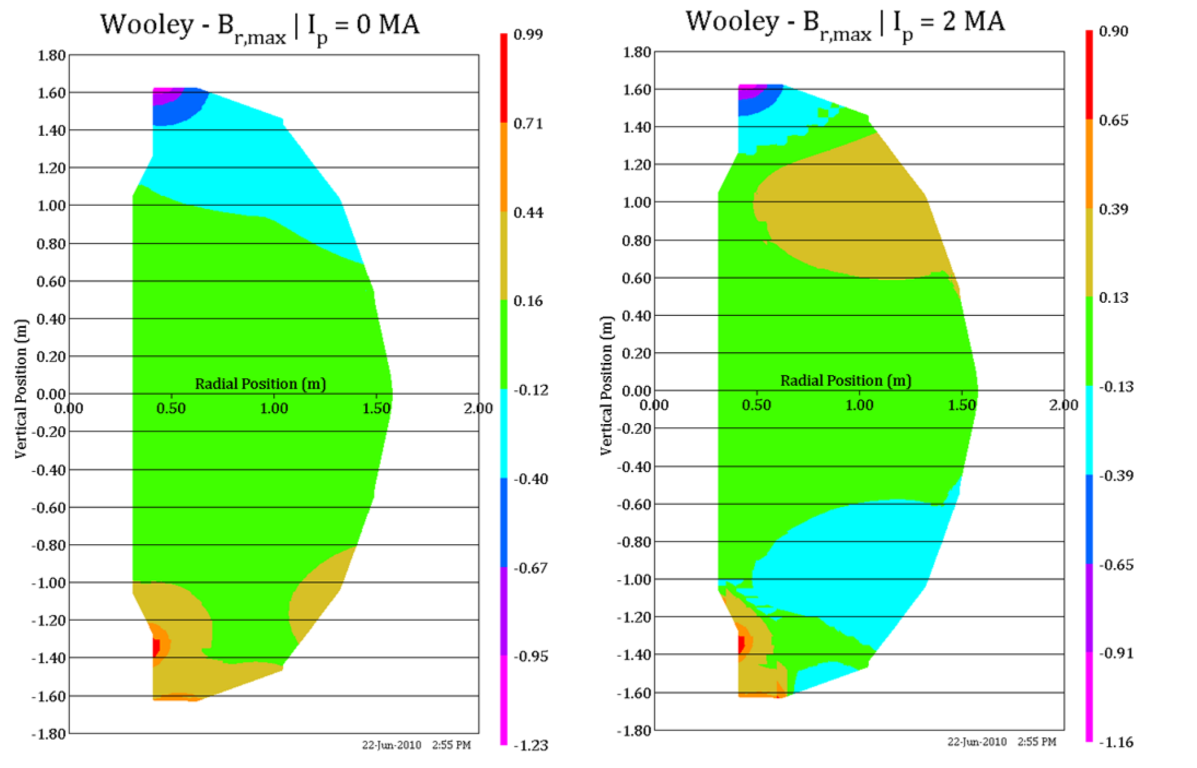

Value of the maximum absolute value of the Poloidal field for the 96 scenarios)

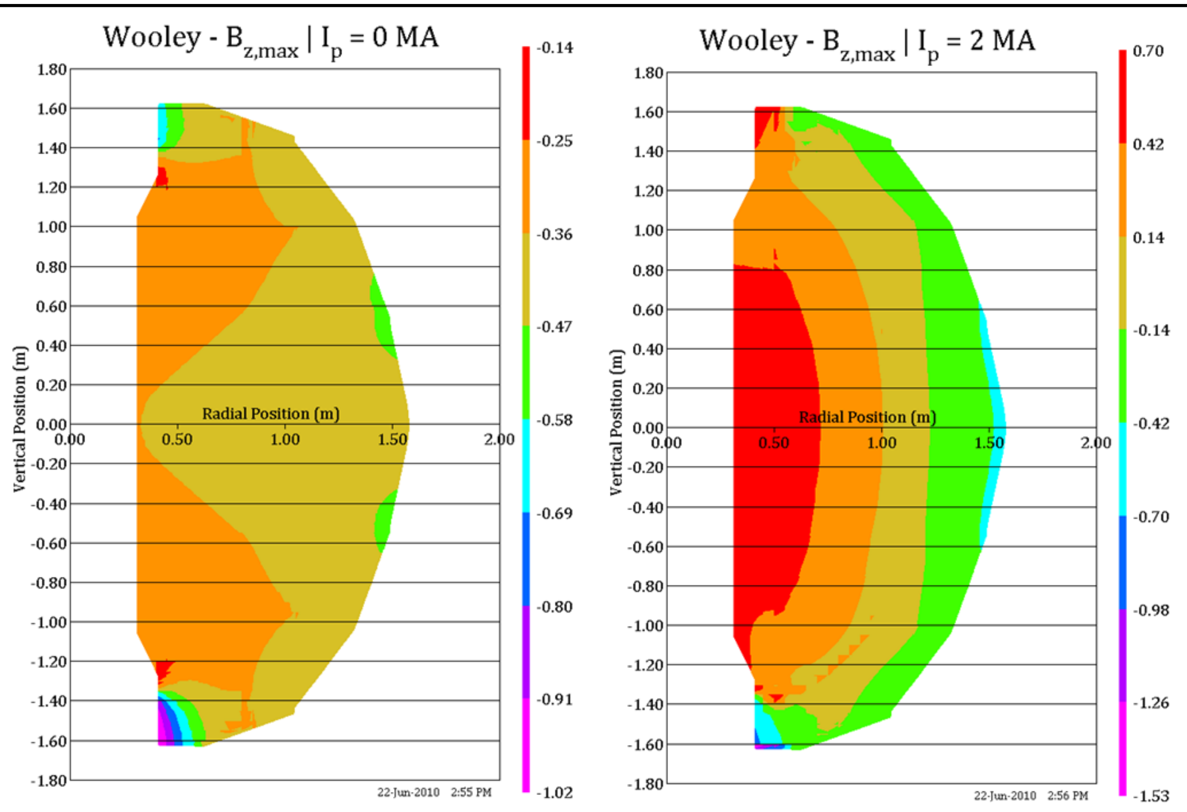

Maximum of the 96 scenarios

5.4 Toroidal Field Coils

The TF inner leg is sized mainly based on the inertial cooling requirements and not on stress limits. At the equatorial plane, the stress is modest – only 40 to 50 Mpa. This provides a conservative stress in the copper including ample allowance for the cooling holes, but minimal wedge pressure to augment the shear capacity. Figure 0-1 shows the inner leg equatorial plane results from the electomagnetic thermal model. Figure 0-2 shows the inner leg equatorial plane results from the global model.

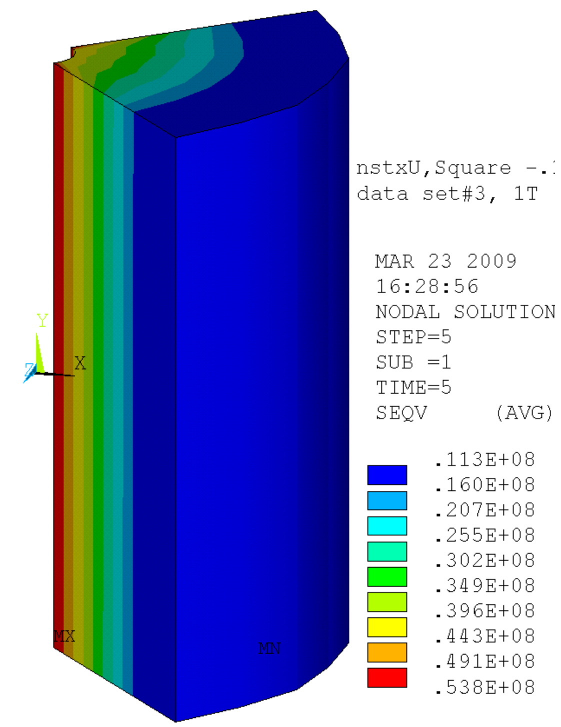

Figure 0-2 Stress Results from the Global Model

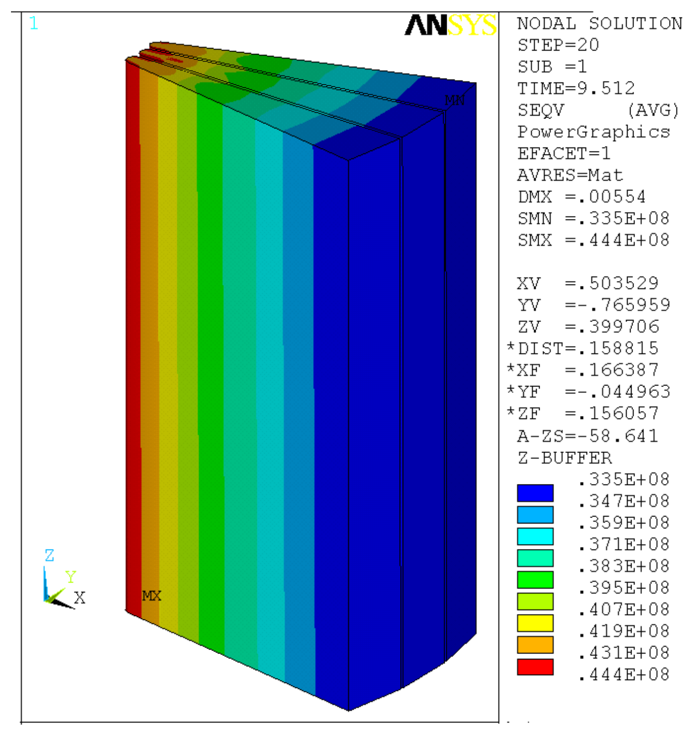

Figure 0-1 Stress Results from the Electromagnetic-Thermal Model

5.4.1. Coupled Electromagnic-Thermal Analysis

The objective of this analysis is to calculate the temperature and stresses during TF coil ramp up, flat top and ramp down (Fig. 1). PF field is not considered. This analysis is based on the coupled field electromagnetic and thermal analysis for a simple model by P. Titus [1], [2]. This was continued by Han Zhang, adding more detail to the TF model and flex region, and considering the cooldown between shots. The distribution of current in TF coil depends on the resistance, inductance and contact pressure in the contact area. Coil temperature reaches highest at the end of the pulse, i.e., 10.136s (having begun at 2 seconds for a total duration of about 8 seconds and a flat top of 7 seconds) for normal operation (see Figure 5.4.1-1).

Maximum temperature is 117ºC, at the inner side of TF flex/arch and inner TF leg. Comparing with C. Neumeyer's result (101 ºC temperature rise [3]), this analysis with current diffusion effect, results in a little higher temperature. The expected design limit for the TF inner leg epoxy system is 100C. This is appropriate for CTD 101K, but the full capacity of the system is only achieved with a primer that is applied immediately to the copper after abrasive blast and solvent cleaning. Primers are more susceptible to temperatures around 100C. As of August 2010, an acceptable primer has not been found. The target temperature limit is 100C. At present temperatures are slightly above this, and teh project is looking for options to gain the few degrees needed. The max outer coil temperature is 47 ºC at the end of pulse. But the temperature at the end of the coil can reach 65 ºC because it connects to the arch which has higher temperature.

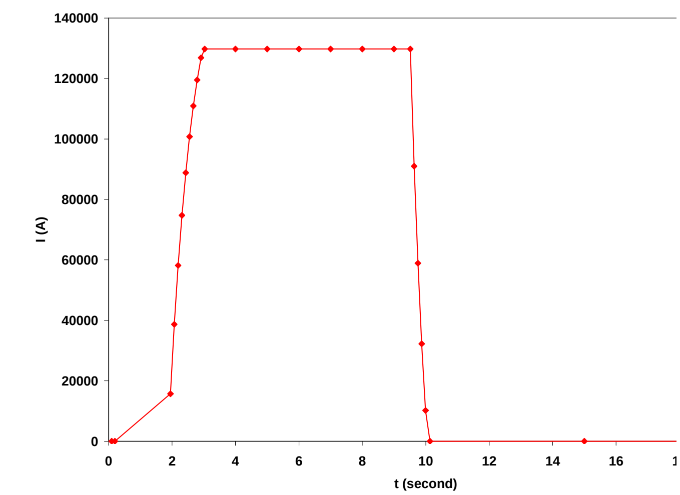

Figure 0.1-1 NSTX Normal Operation Waveform

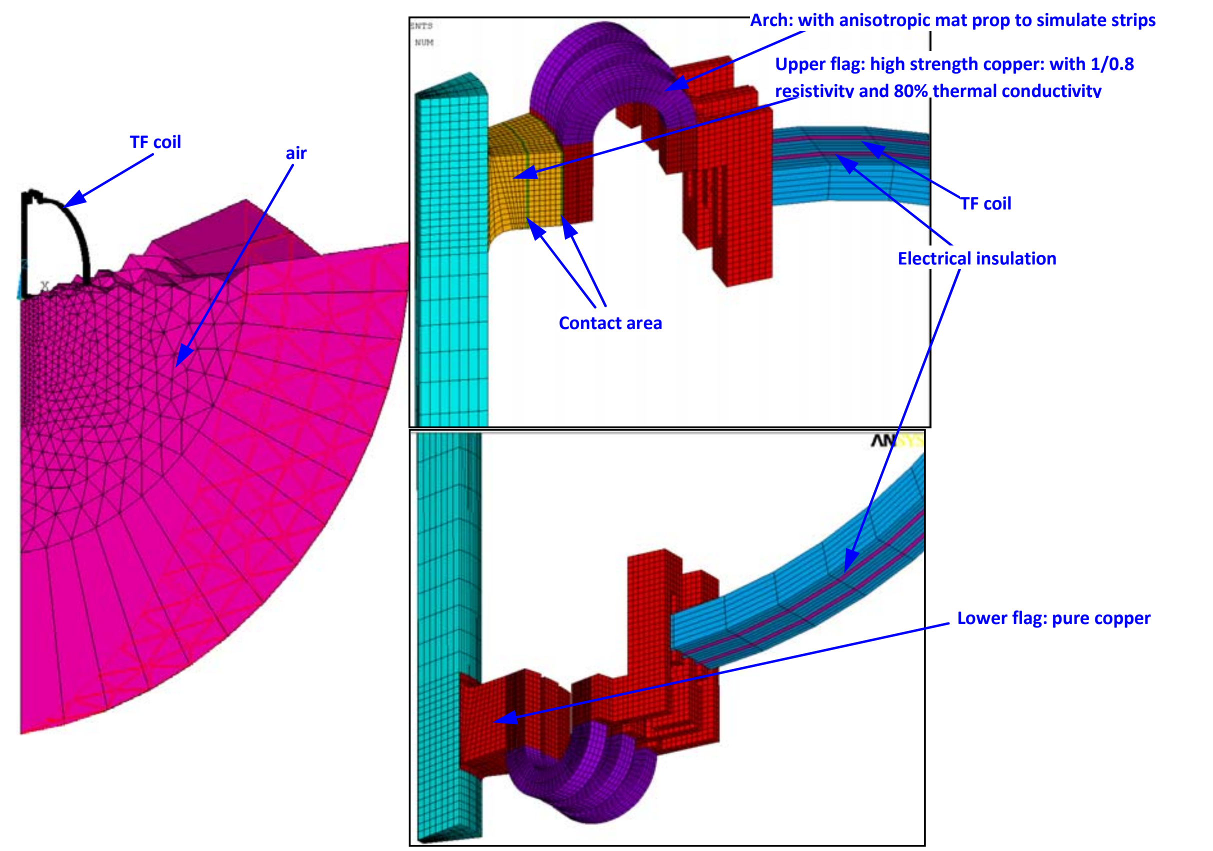

Figure 0.1-2 Model of TF Flex/Arch

In this model, the arch is modeled by two solid pieces. But in reality, they are made of many straps. So the arches in this model have anisotropic material properties (mechanical properties are based on the local structure model results of T. Willard [4]), Current density, magnetic flux density and temperature from this analysis have been provided to T. Willard for his detailed simulation of the joint (see Figure 0.1-).

Using high strength copper (80% IACS) in the flag extension increases the temperature only by < 1ºC. Thus high strength copper can be used if required to increase the pressure of joint bolt insert over the capacity of pure copper.

The central beam has maximal hoop tension stress of 72.7MPa at 9.512s (i.e. the end of flat top) and 58.5MPa at 10.136s (i.e. the end of pulse), similar to Titus's result [2]. But there is another even higher hoop stress point of 95.5MPa at 9.512s, at the connection between central beam and flag, which is due to the L-shape connection part between the arch and TF outer leg.

Toroidal field contours have been provided for use in other calculations—in particular the background field in the antenna calculation.

Structural response at the joint has been included for comparison with more detailed modeling of the joint by T. Willard [4].

5.4.1.1 Electromagnetic Current Diffusion Analysis Method

TF conductors are wide with respect to their toroidal thickness, somewhat like bitter plate coils used in FIRE or C-Mod. Current densities will distribute non-uniformly in the conductor section. The analysis described here is a transient thermal, coupled field analysis. An electromagnetic model (Figure 5.4.1-7) is used to calculate the current diffusion effect and transfer the generated heat and Lorenz force to thermal and structural model. The thermal and structural model calculates the temperature, displacement, thermal stress, contact pressure at contact areas, and then transfer these data back to electromagnetic model (Figure 0-3). The materials have temperature dependent material properties, including electrical resistivity, thermal conductivity, specific heat, coefficients of thermal expansion. The arches have anisotropic resistivity and thermal conductivity to simulate the straps. Because the arch is made of many straps and not a solid copper, it becomes

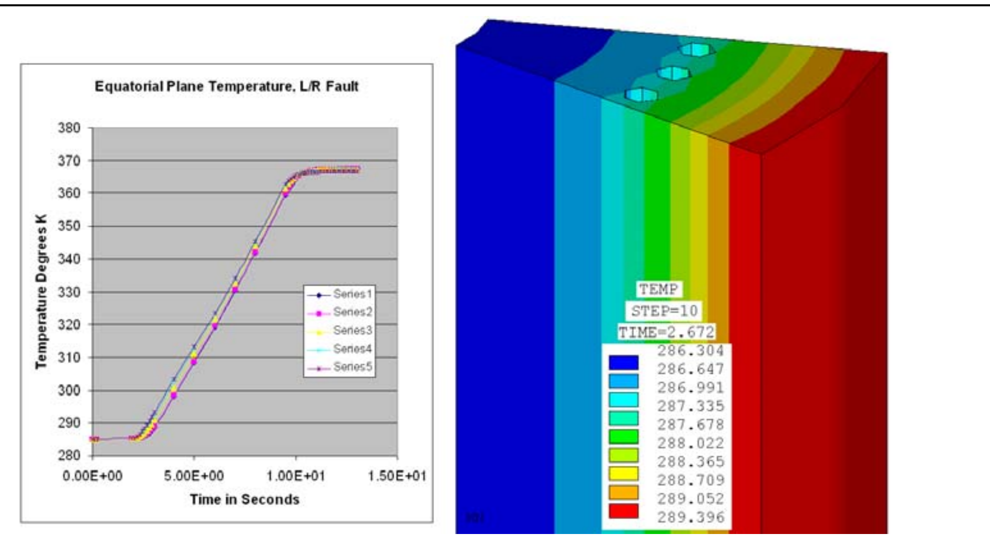

Figure 0-3 Equatorial Plane Time History. The contour plot is early in the transient showing effects of current diffusion. The end average temperature is 367.15, Ref [6],[7]

much more compliant. The modulus of the arch is based on the results of T. Willard [4]. The upper flag uses high strength copper which has 1/0.8 resistivity and 80% thermal conductivity of pure copper. In next section, the results show that using high-strength copper or pure copper doesn't have much difference. The lower flag uses pure copper. In the electromagnetic model, the contact regions have pressure dependent resistivity and the data are from Table 1 of R. Woolley [5].

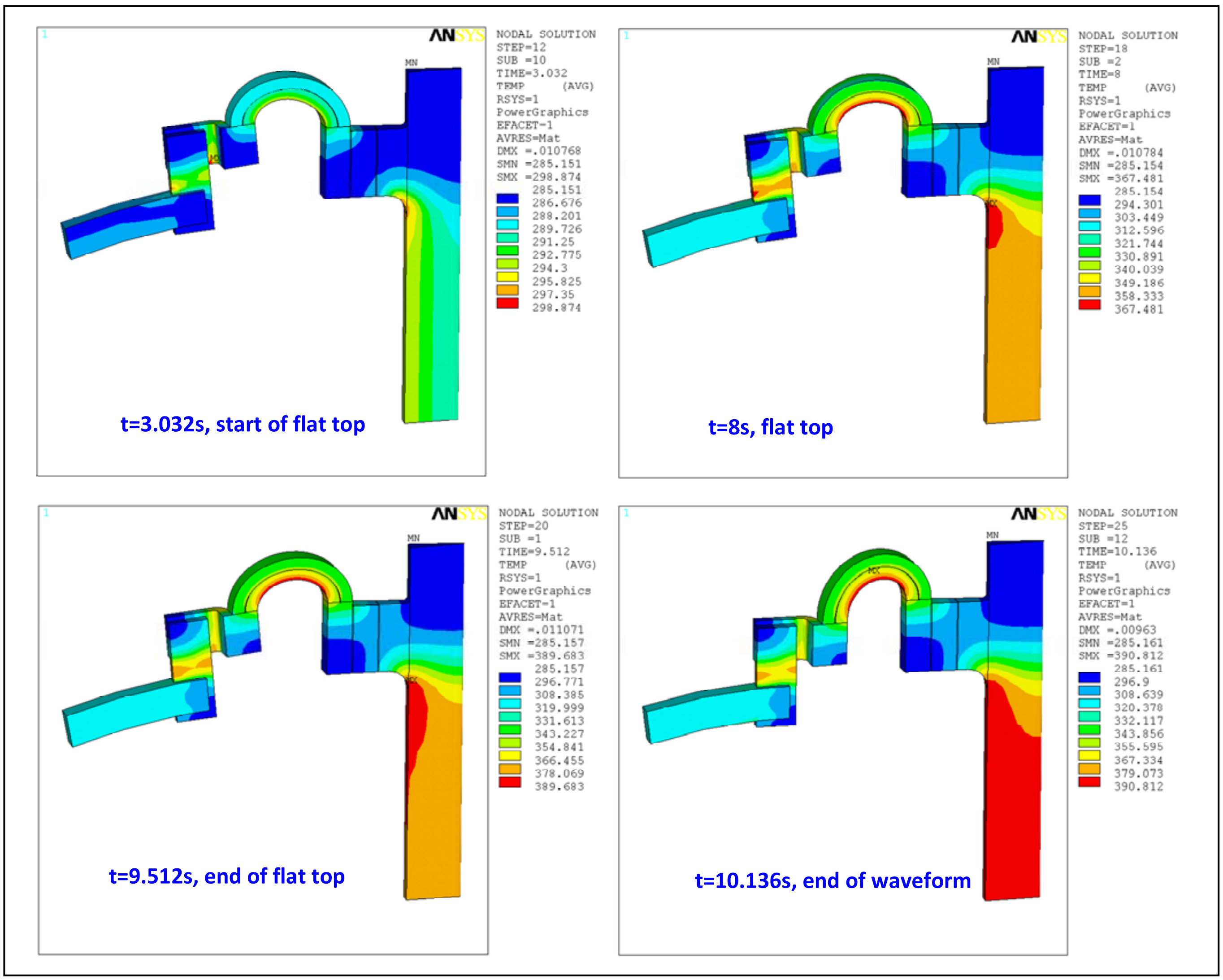

Thermal Results for the Coupled-Electromagnetic Diffusion Analysis

Figure 5.4.1.2-1 Temperature from Coupled Electromagnetic Thermal Analysis Compared with Resistive Simulation of Current flow by Tom Willard

**The delta T for Han is 388-280 = 108 C
The Delta T for Tom is 135.71-20 = 115.7C**

5.4.1.2 TF Thermal Results Including Cooldown.

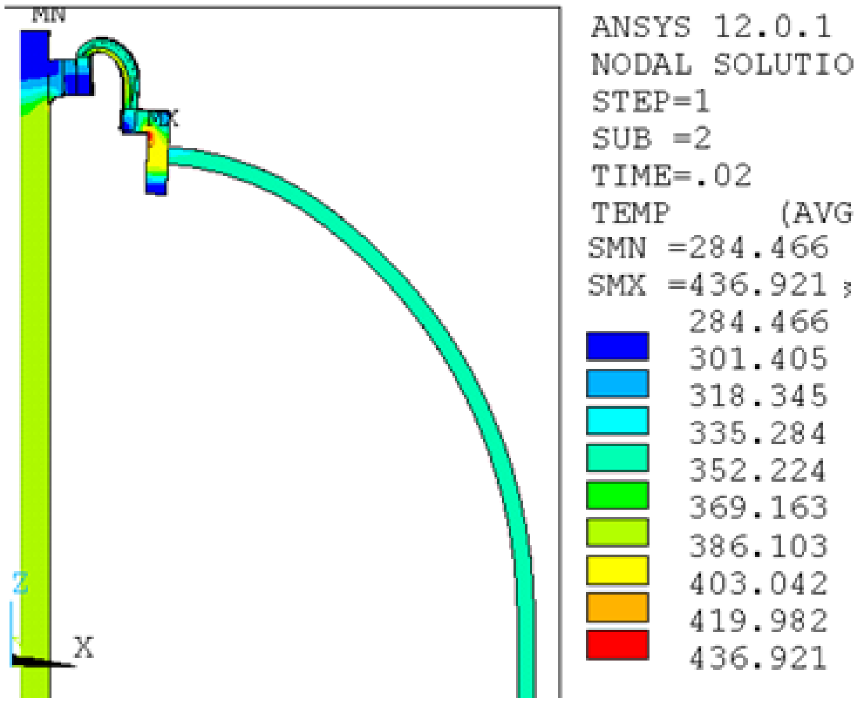

Figure 5.4.1.2-2

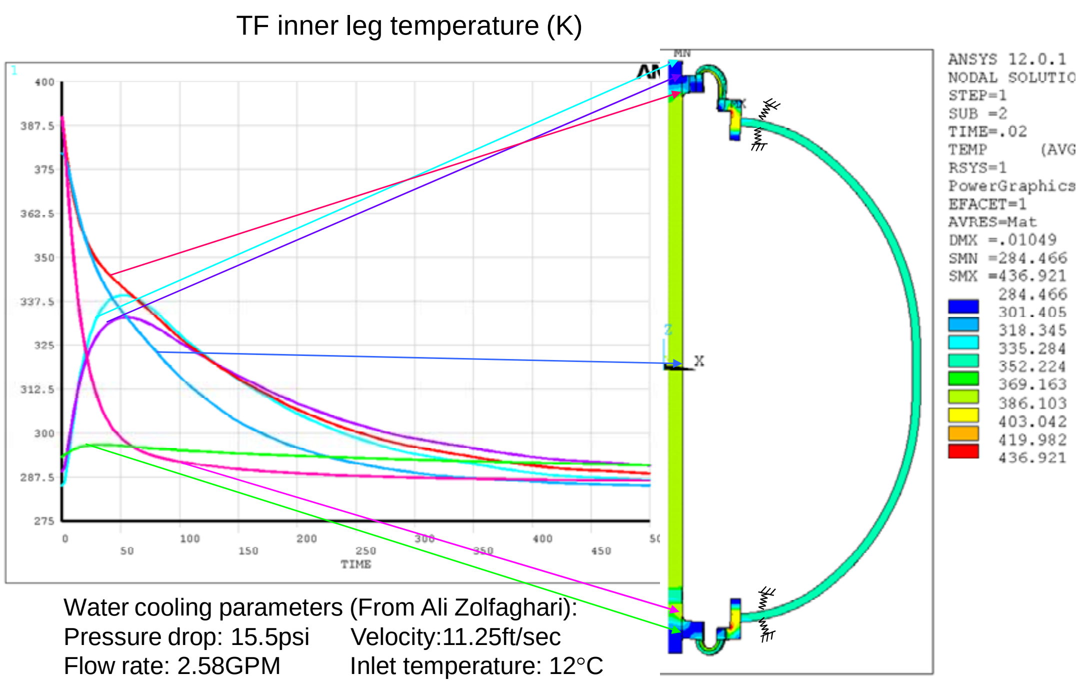

Figure 5.4.1.2-3

Cooldown Thermal Strains

Thermal gradients around the coolant hole will cause strains and stresses that potentially could cause de-lamination of the inner leg insulation near the coolant hole. This will have to be addressed in the FDR by adjusting the cooling procedure - to match the cooldown time to the OH, or by putting in Kapton or other predictable parting plane.

Figure 5.4.1.2-4 Difference in temperature across the inner leg conductor during cooling

Cyanate Ester has about 50 MPa tensile capacity - not 100 MPa

Figure 5.4.1.2-6 Temperature and Von Mises Stress Contours During the Cooldown Process

Figure 5.4.1.2-7 Temperature and Hoop Stress Contours During the Cooldown Process

Resolving the Peak Temperature in the TF Inner leg to flag connection

5.4.1 Structural Pass after the Electromagnetic/Thermal Analysis

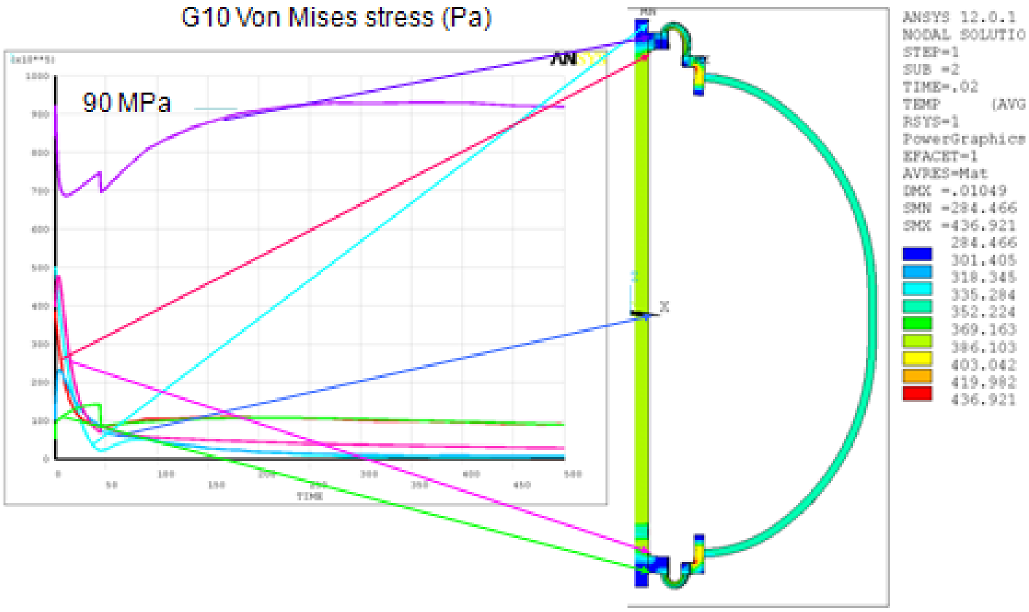

Figure 5.4.1.2-6

In Figures 5.4.1.2-7, and 8 there is a difference between available thermal stress calculations that is being investigated. . The offset in the joints may introduce some bending and teh spike in the corner may be physical. It doesn't appear in the joint model.

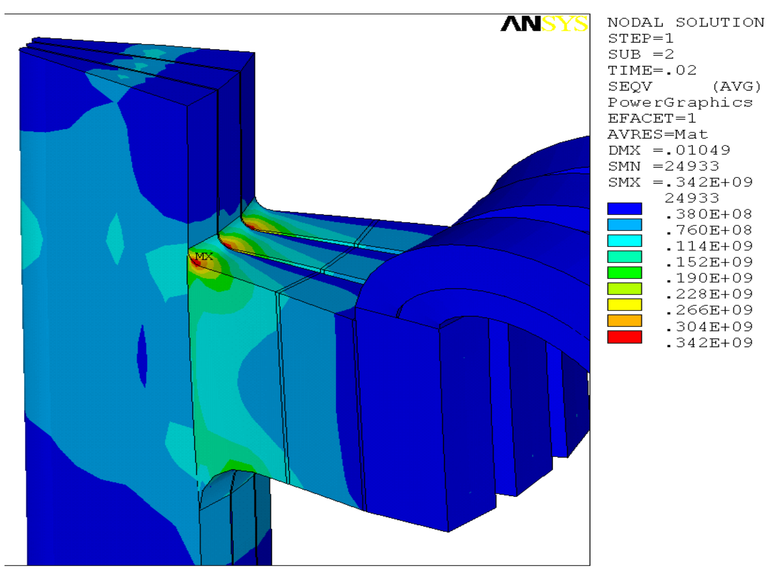

Figure 5.4.1.2-7 TF Coil thermal stress

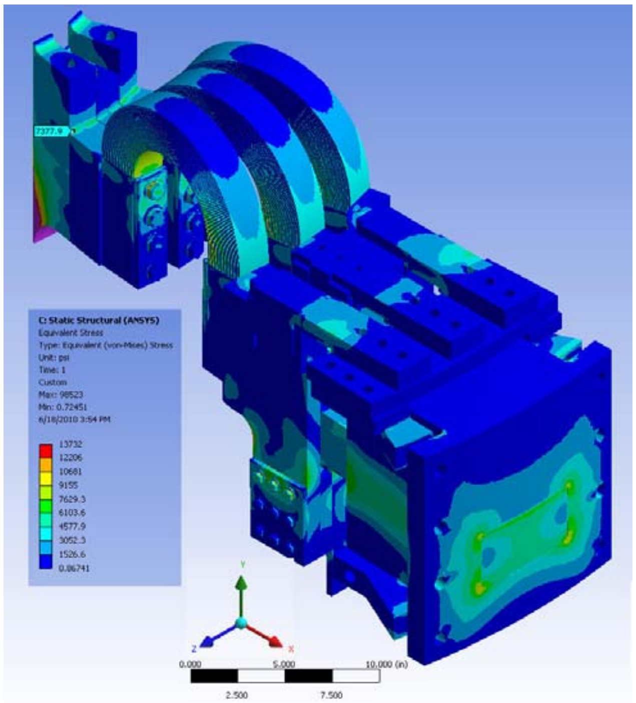

Figure 5.4.1.2-8

Extended Hub Structural Pass

Figure 5.4.1-4 shows the structural pass forces, constraints, and temperatures. Figure 5.4.1-4 shows the inner TF leg stress time history with no thermal stress. Figure 0-6 shows the inner leg Von Mises stress time history with thermal stresses - The higher stress at the end of the pulse results from the restraint of center stack thermal expansion by a stiff modeling of the joint loop. This for the Nominal TF Current Profile. Figure 5.4.1-5 shows the Inner Leg Von Mises Stress Time History – With Thermal Stress.

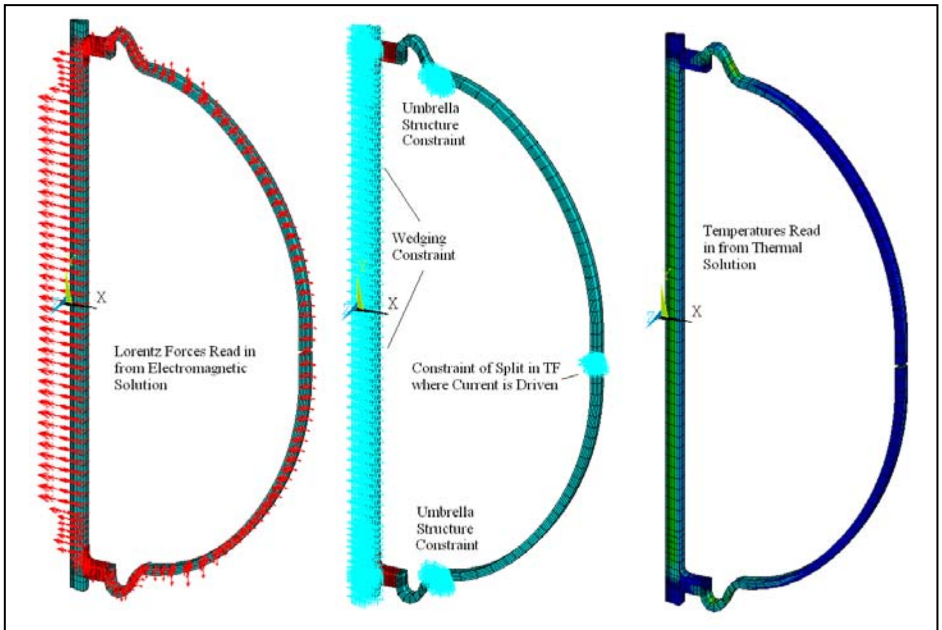

Figure 5.4.1-4 Structural Pass Forces, Constraints, and Temperatures

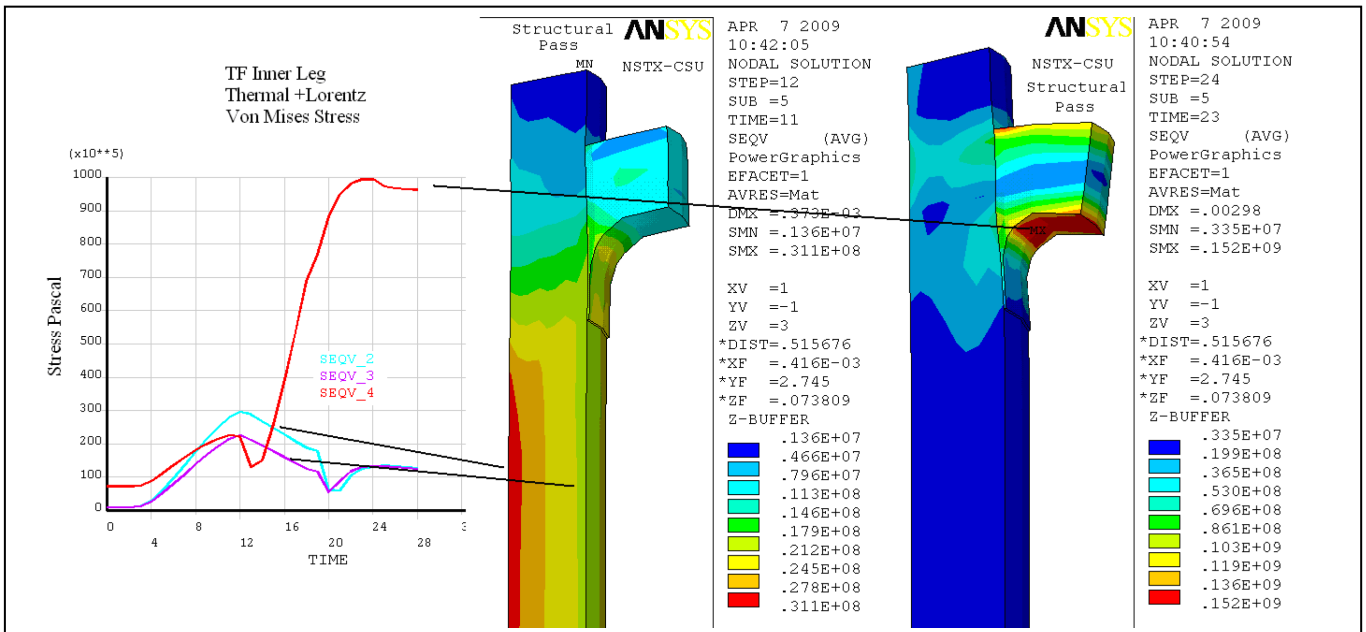

Figure 5.4.1-5 Inner Leg Von Mises Stress Time History – With Thermal Stress

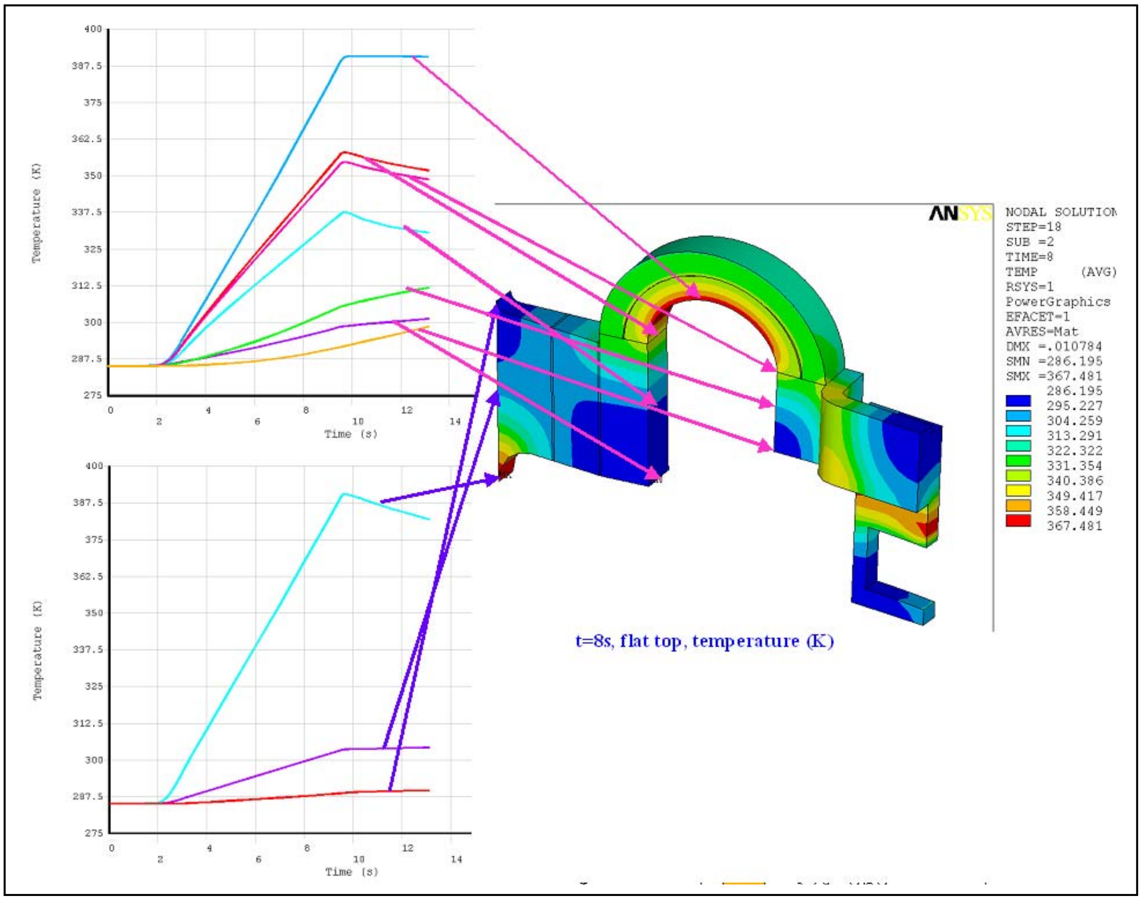
Temperature (K)
Time (s)
NODAL SOLUTION
STEP=18
SUB =2
TIME=8
TEMP (AVG)
RSYS=1
PowerGraphics
EFACET=1
AVRES=Mat
DMX =.010784
SMN =286.195
SMX =367.481
t=8s, flat top, temperature (K)

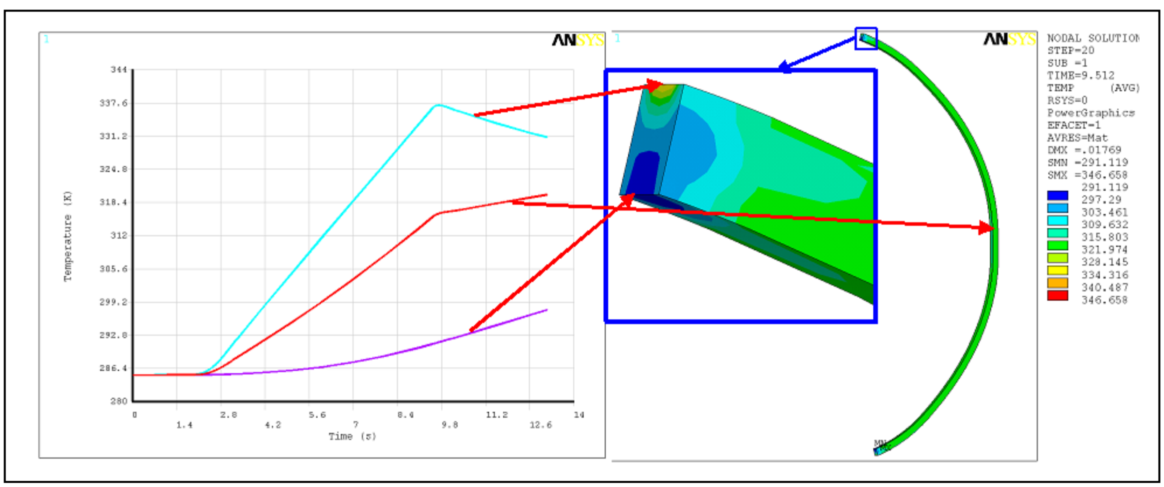
Temperature (K)
Time (s)
NODAL SOLUTION
STEP=20
SUB =1
TIME=9.512
TEMP (AVG)
RSYS=0
PowerGraphics
EFACET=1
AVRES=Mat
DMX =.01769
SMN =291.119
SMX =346.658

Figure 5.4.1-7 Displacements from the Electromagnetic Current Diffusion Model - Inner Leg Temperature, L/R Fault

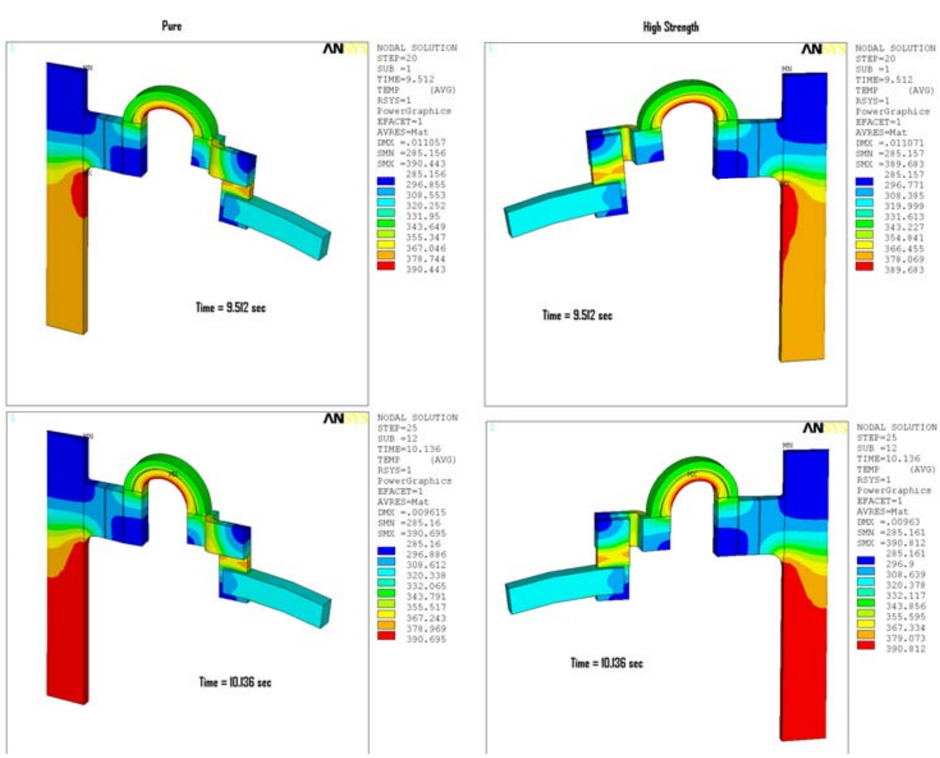

5.4.4 Joint Option Studies

5.4.4.1 Concept Options

The demountable inner leg of the spherical tokamak is a key feature which is also very challenging [2]. The current density is quite high and adequate contact pressure must be maintained at the joint under all conditions of electromagnetic loading. Currents, fields, and forces are quite high and in some cases bidirectional. The TF inner leg assembly experiences substantial axial thermal which has to be accommodated by the radial limbs without causing high stresses or moments which would spoil the contact pressure at the joint. The area is quite congested and access to fasteners is difficult. The radial limbs must make up for fabrication tolerances on the inner legs and assembly tolerances on the outer legs.

In order to develop a robust solution for the NSTX center stack upgrade four concepts had been independently developed and were competitively evaluated. the assessment as shown in Figure 5.4-10.

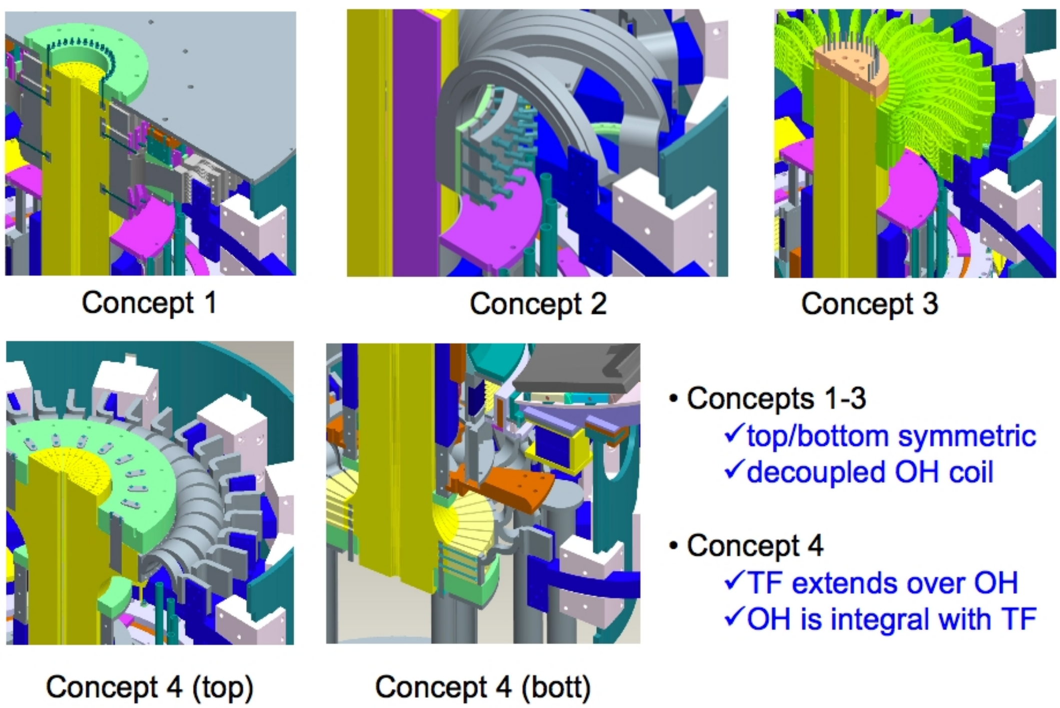

Figure 0-8 TF Center Stack Options

Concepts 1-3 are basically different than 4 since the TF inner legs do not include any extensions at the ends so that the OH coil can be separately manufactured and installed/removed repeatedly. In concept 4, radial extensions would be e-beam welded to the wedge shaped turns yielding the advantage of jointing at a greater radius (lower field, greater surface area) but the disadvantage of the fabrication of the TF and OH being linked, and the OH coil being trapped.

The essential features of the joint concepts are:

- Concept 1: Bolted joint with inserts, constant tension shaped radial, flexibility both in-plane & out-of-plane, torque transmitted to lid
- Concept 2: Jacking ring joint connection, flexibility in-plane, self-supported against torque
- Concept 3: Jacking ring joint connection, constant tension shaped radial, flexibility in-plane, self-supported against torque
- Concept 4: e-beam welded extensions, bolted joints with inserts, flexibility in-plane, torque transmitted to lid

Concept 4 was chosen for the conceptual and preliminary design efforts (See Figure 0-9).

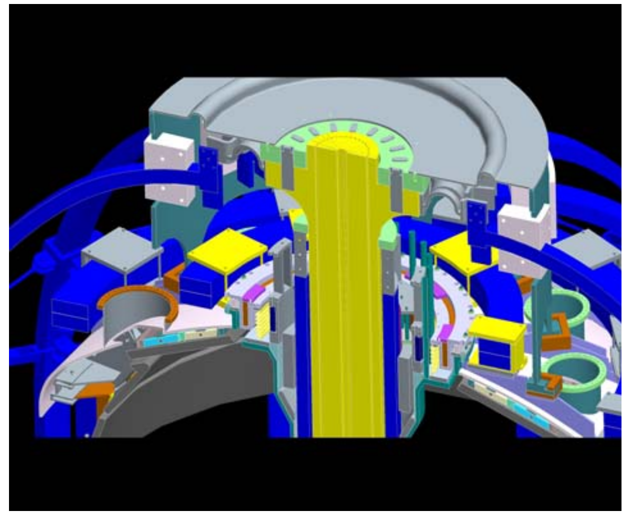

Figure 0-9 Concept 4 - Extended Hub Concept

5.4.4.2 TF Joint Qualification and Model

5.4.4.2.1. TF Joint Qualification Boundary Conditions

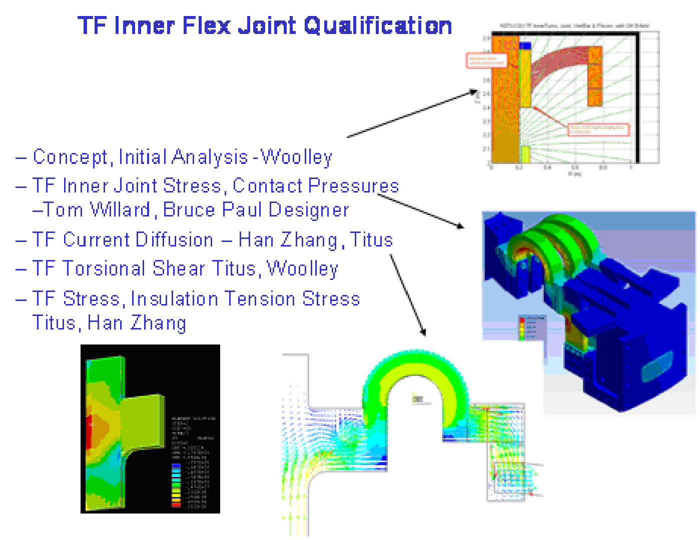

Figure 0.4.2-1 TF Inner Joint Qualification

The TF joint is part of the larger NSTX structural system and has many interfaces. The outer flags are attached to the umbrella structure aluminum blocks which in turn are supported by the vessel umbrella structure and are loaded by the TF outer leg loads. The connection at the centerstack assembly sees the 8 mm vertical thermal growth of the joule heated TF inner leg. The inner and outer attachment points of the joint are held in toroidal registration by the upper and lower diaphragms described and analyzed in Section 0. Figure 5.4-12 shows the TF Inner Flex Joint qualification. Figure 5.4-13 shows the details of this joint. Figure 5.4-14 shows the results of the analyses of the TF Inner Flex Joint. Figure 5.4-15 shows the maximum vertical field at the TF straps. Figure 5.4-16 shows the toroidal displacements at the Flex Joint.

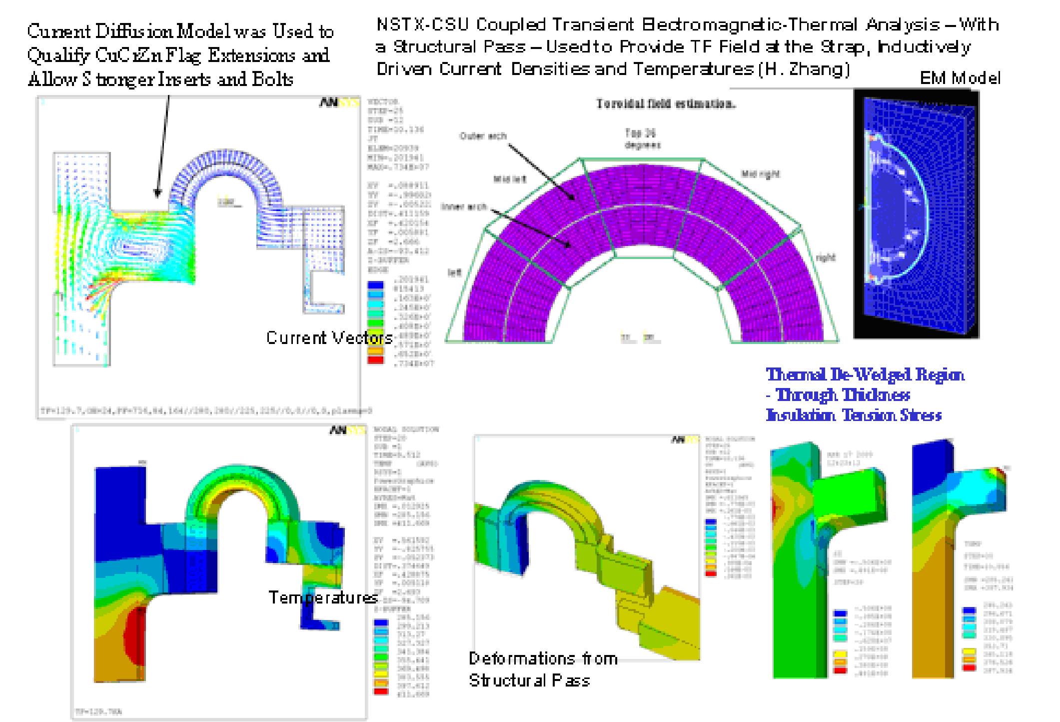

Figure 0-10 TF Inner Flex Joint Analyses

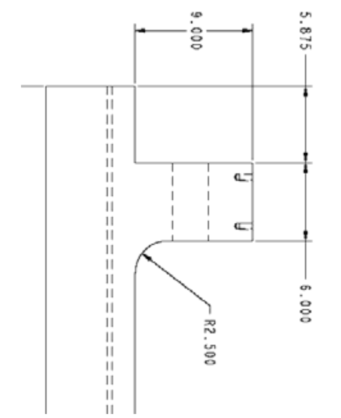

Figure 0-11 Details of the TF Inner Flag Extension

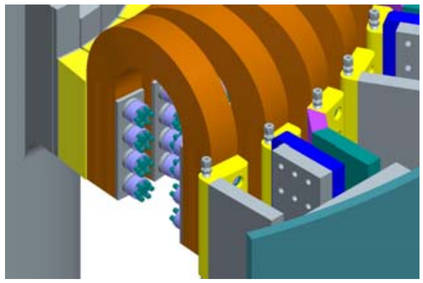

Figure 5.4.4.2.2-1

5.4.4.2.2. TF Joint Local Model

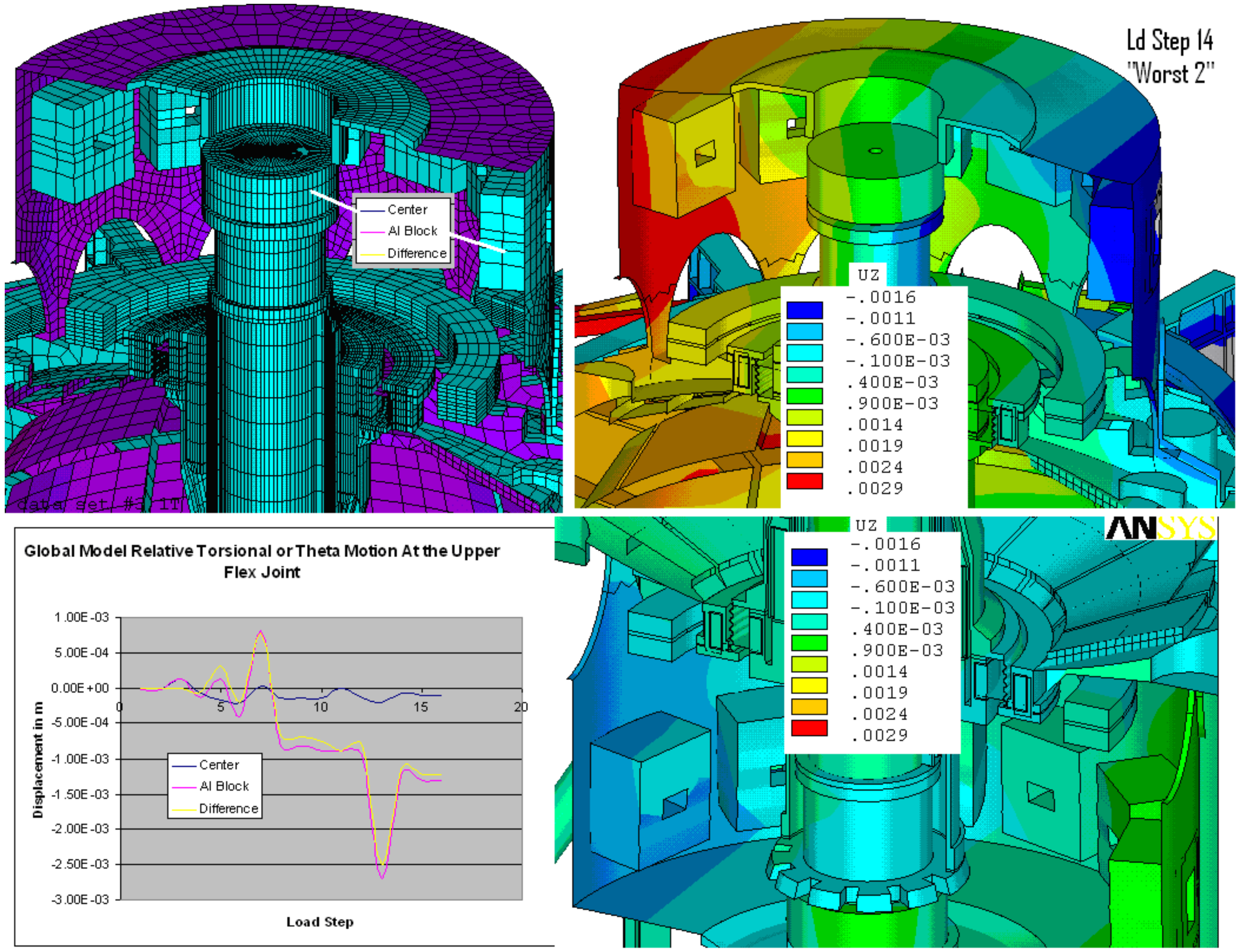

Figure 0-12 Toroidal Displacements at the Flex Joint

A complete treatment of this analysis may be found on the NSTX Centerstack Upgrade Engineering Web page and is documented in ref [4]. Figure 5.4-17 is a model of the TF joint. Mesh density is fairly high throughout but the innermost and outermost straps have a higher mesh density.

The objectives of this analysis of the NSTX Upgrade TF Flex Strap and TF Bundle Stub design were:

- To determine if the design is adequate to meet the requirements specified in the NSTX Structural Design Criteria, specifically, if the flex strap lamination stresses and the copper lead extension thread stresses meet the requirements for fatigue, yield, and buckling, under worst-case/ power supply-limit load conditions: 130,000 amps/ strap, 0.3 T poloidal field, and 1.0 T toroidal field; and

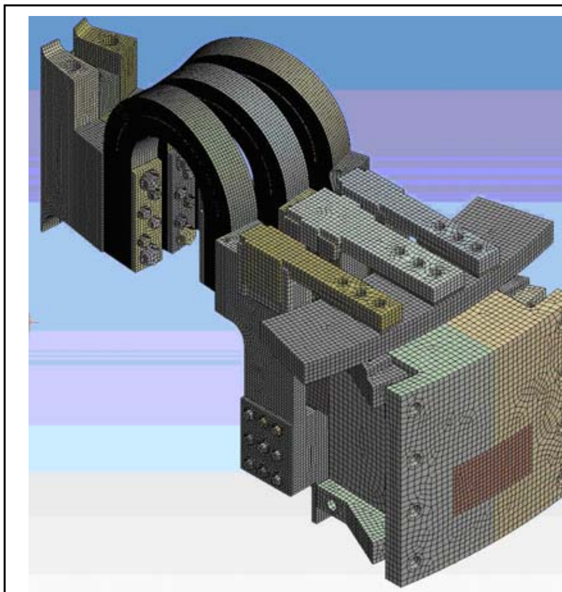

Figure 0.4.2.2-1 TF Joint Model

- To verify that the local contact pressure in the bolted electrical joints is a minimum of 1500 psi, sufficient to maintain the joint contact electrical conductance above the design goal, based on the current-design development tests, of 1.0E06 siemens/in^2.

At the CDR, the loads were computed by hand from simple estimates. For the PDR analysis, the fields and Lorentz forces were computed from a MAXWELL simulation. The advantage of MAXWELL over doing all analysis in ANSYS is that MAXWELL can map a low mesh density emag result to a fine ANSYS structural model. One of the field plots from this analysis is included in the field plot section of this analysis. The results of the ANSYS multiphysics finite element analysis - electric, transient thermal, magnetostatic, and static structural are shown in Figure 5.4-18. These results show that:

- The maximum equivalent stress in the laminations is 27.5 ksi, which is 25.5 ksi below the fatigue allowable for the full-hard C15100 copper-zirconium strip;
- The maximum equivalent stress in the copper threads is 29.1 ksi, which is 32.9 ksi below the fatigue allowable for the full-hard C18150 copper-chromium-zirconium plate;
- The minimum average contact pressure is >6500 psi, and the minimum local contact pressure is >2500 psi, which is 1000 psi above the design goal; and
- The lamination minimum linear buckling load multiplier factor (LMF) is > 58, which is approximately 10x the minimum allowable specified in the NSTX Design Criteria document.

Table 0-1 shows a design operating point comparison between the present and upgrade designs.

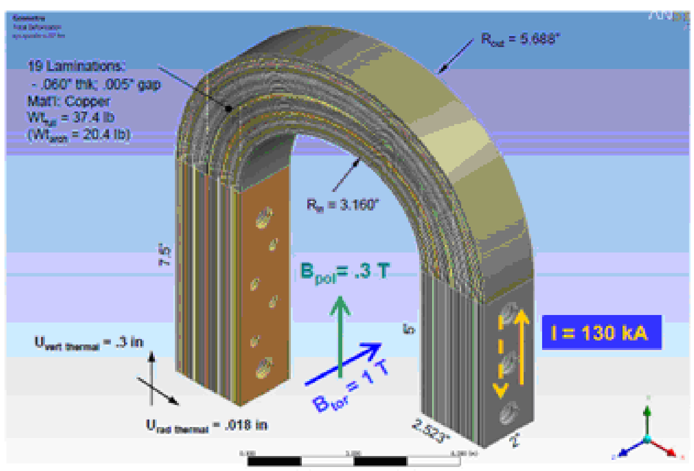

Figure 0-13 ANSYS Multiphysics Finite Element Analysis

Table 0-1 Design Operating Point Comparison

Table 2.1 - Design Operating Point Comparison				
Design	Total Current (A)	Maximum TF (Tesla)	Maximum PF (Tesla)	On-Time Pulse Duration (sec)
Current	72,000	0.6	0.1	0.5
Upgrade	130,000	1.0	0.3	7.0

5.4.4.2.3. Joint Mechanical Parameters Comparison

A comparison of the mechanical parameters of the TF lead-extension bolted joint designs is shown in Table 0-2. From this table, it is clear that the upgrade design is much more robust.

Table 0-2 Comparison of the Joint Mechanical Parameters

Table 2.2 - Joint Mechanical Parameters Comparison							
Design	Joint Contact Area (in^2)	Total Bolt Force (lbf)	Average Initial Contact Pressure (psi)	Minimum Operating Local Contact Pressure (psi)	Calculated In-Plane Mating Torque (in-lbf)	Max. TF In-Plane Separating Torque (in-lbf)	Lift-off Torque Margin
Current	3.382	20,000	5,914	0	12,500	17,500	-0.29
Upgrade	12.739	94,000	7,379	~2500	90,875	30,143	2.01

The joint is located further from the CS winding, so the joint contact area is much wider. It is also taller, so the contact area is approximately 4x larger. The number of bolts/ joint has increased, and there is a mix of 3/8 and 5/8 bolts, with the 5/8 bolts located furthest from the bolt centroid. The lead-extension material has been changed to a high strength copper alloy C18150 copper-chromium-zirconium, so that the bolt pretension is limited by the strength of the bolts and not the shear strength of the copper threads. All of this results in a nearly 5x increase in total bolt force, a 50% increase in initial contact pressure, and a large positive lift-off torque margin. Since there is no lift-off, the local contact pressure never falls below a minimum value, determined in the ANSYS analysis below to be > 2500 psi.

5.4.4.2.4. Joint Electrical/ Thermal Parameters Comparison

A comparison of the electrical and thermal parameters of the joints is shown in Table 2.3. Though the total current is higher in the upgrade design, the current density is only 1/2 the density in the current design. The initial (closed joint) electrical resistance and heat generated in both designs is small, as is the estimated temperature rise across the joints, assuming no thermal capacitance.

Table 0-3 Joint Electrical/Thermal Parameters Comparison

Design	Current Density (A/in^2)	Initial Electrical Resistance (W)	Heat Generated I^2R (W)	Thermal Power Density (W/in^2)	Initial Thermal Resistance (W/C)	Zero-Heat Capacity Temperature Rise (C)
Current	**21,289**	**1.48E-07**	**7.66E+02**	**2.27E+02**	**1.18E-02**	**9.1**
Upgrade	**10,205**	**3.93E-08**	**6.63E+02**	**5.21E+01**	**3.14E-03**	**2.1**

5.4.4.2.5. Static Bolt Strengths and Insert Pull-Out Loads Comparison

A comparison of the static bolt strengths and insert pull-out loads of the two joint designs is shown in Table 0-4. From the table, it can be seen that the shear strength of the C10700 copper threads in the current design limits the 3/8 bolt pretension to below the maximum allowable bolt load. When the estimated 2000 lbf operational cyclic load is considered, the allowable bolt pretension is reduced to only 5000 lbf: a 2000 lbf reduction due to the cyclic load, and a 3000 lbf reduction due to the reduced shear strength of the copper for fatigue at 60,000 cycles.

Table 0-4 Static Bolt Strength and Insert Pull-Out Comparison

Table IV - Static Bolt Strength and Insert Pull-Out Load Comparison

Design	Bolt Size	Qty/ Joint	Bolt Mat'l	Bolt Yield Strength (psi)	Bolt NSTX D.C. Allowable (psi)	Tensile Stress Area (in^2)	Max Bolt Load	Tap-Lok Insert Outer Thread	Insert Length (in)	Effective Shear Area (in^2)	Copper Alloy	Yield Strength (psi)	Shear Strength (psi)	Insert Pull-out Load (lbf)
Current	3/8-16	4	Inconel 718	185,000	138,750	0.0775	10,753	9/16-16	0.562	0.4864	C10700	36,000	20,772	10,104
Upgrade	3/8-16	4	Inconel 718	185,000	138,750	0.0775	10,753	9/16-16	0.687	0.608	C18150	75,000	43,275	26,311
	5/8-11	2				0.226	31,358	25/32-11	1.125	1.61				120,750

The upgrade design uses high strength C18150 copper-chromium-zirconium, with more than twice the shear strength of the C10700 copper, for the lead-extensions,. Also, because the extensions are longer, a longer 3/8 insert is used, with a larger shear area. This results in the copper thread strength being greater than the bolt tensile strength, so the maximum allowable bolt pretension is limited by the strength of the bolt. The bolt reactions from the ANSYS analysis below indicate that the cyclic load is small (10-15% of the bolt pretension), so can be reduced to nearly zero with the use of Belleville washers. To maximize the contact pressure and lift-off margin, without exceeding the maximum allowable bolt loads, the following bolt pretensions were chosen for the upgrade design: 10,000 lbf for the 3/8 bolts; and 27,000 lbf for the 5/8 bolts.

5.4.4.2.6. TF Joint Comparison Summary

In summary, joint pitting damage in the current design occurs with TF fields > .45 T, in lift-off areas predicted by an ANSYS direct-coupled model and verified by in-situ measurements of joint resistivity. No pitting damage occurs in joints further from the plasma that do not lift-off. Bolt pretension, limited to 5000 lbf due to the low shear fatigue strength of the copper threads, is not sufficient to prevent lift-off, given the long lever arm of the TF Radial Flag.

The upgrade flex strap design reduces the lever arm length, minimizing the prying torque. The more robust design , with bolt pretensions limited by the strength of the bolts, also increases the mating torque, resulting in a large positive lift-off margin. A description of the ANSYS multiphysics analysis, used to determine the stresses in the laminations and the minimum local contact pressure in the joints, follows.

Figure 0-14 shows the static structural analyses results of the von Mises stress. Figure 0-15 shows the static structural analysis results of the TF Bundle Stub Bolted Joint. Figure 0-16 shows that the inner-most lamination stress increases only about 7% with the addition of the 2.5mm torsional displacement: 22899 psi vs 21445 psi. Figure 0-17 shows outer-most lamination model with the 2.5mm OOP displacement added to the Emag loads and thermal displacements, the stress increased by only 3% (21827 psi vs 21178 psi). This shouldn't be a problem if we use C15000 copper or better.

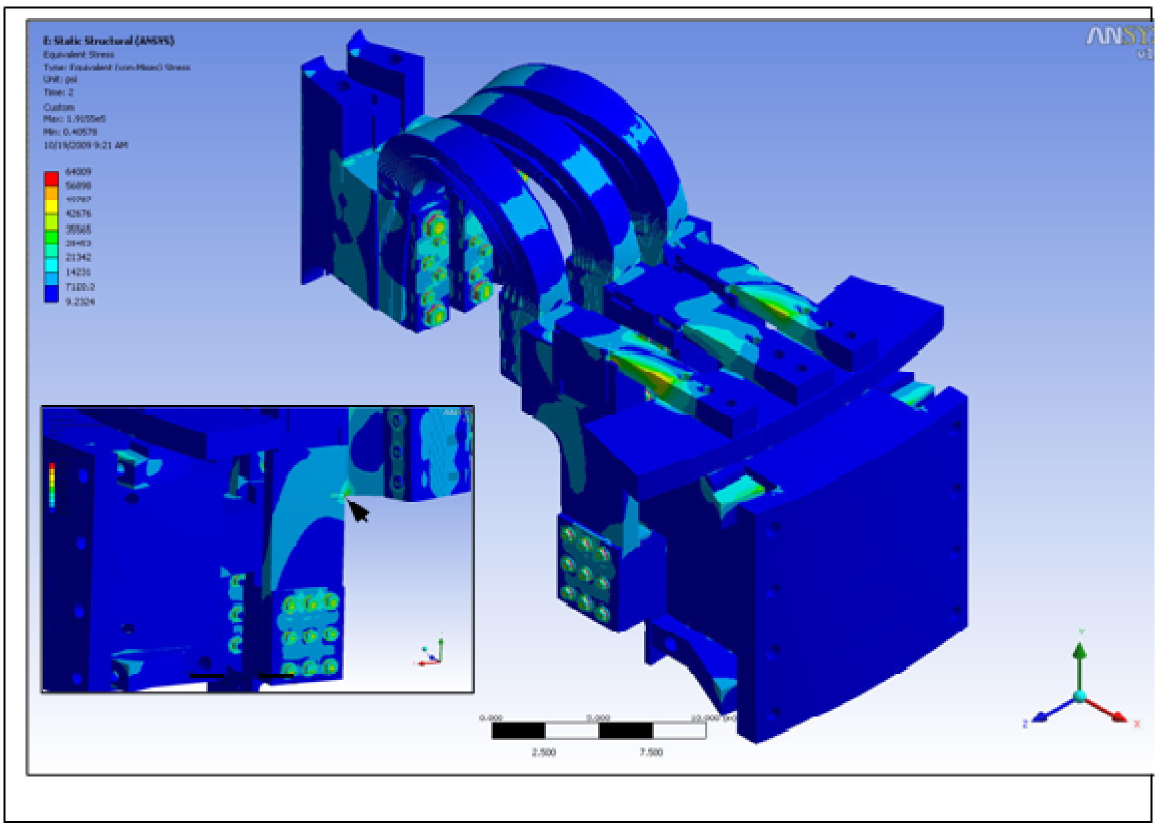

Figure 0-14 Static Structural Analysis Results: von Mises Stress

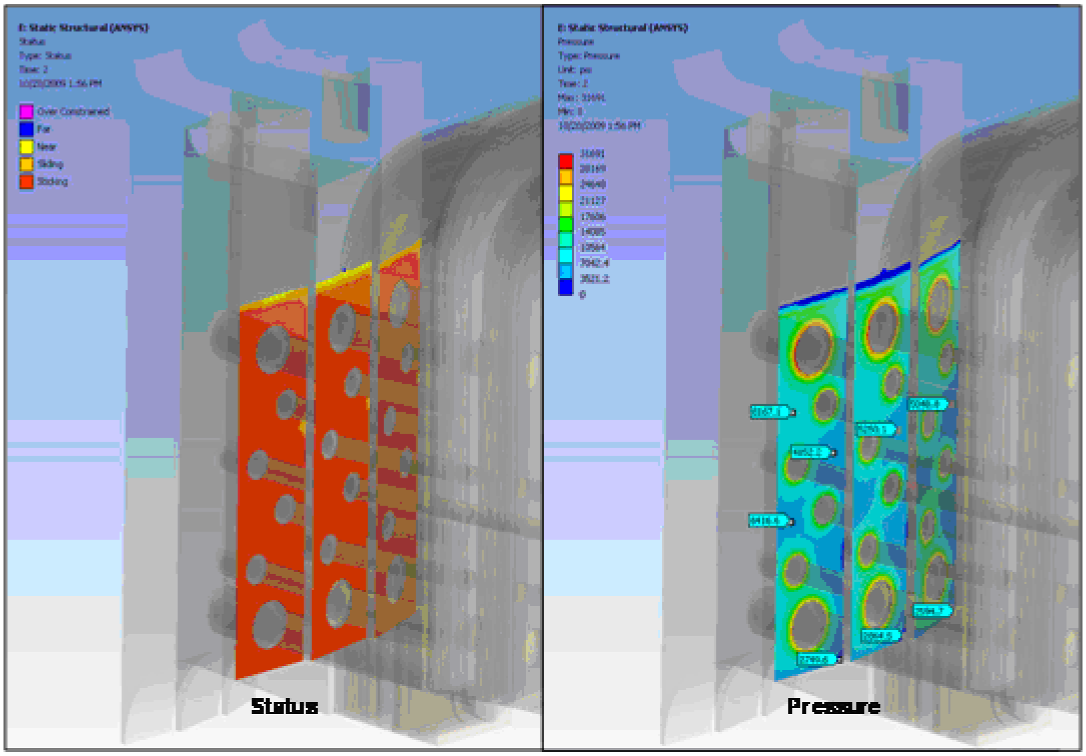

Figure 0-15 Static Structural Analysis Results: TF Bundle Stub Bolted Joint

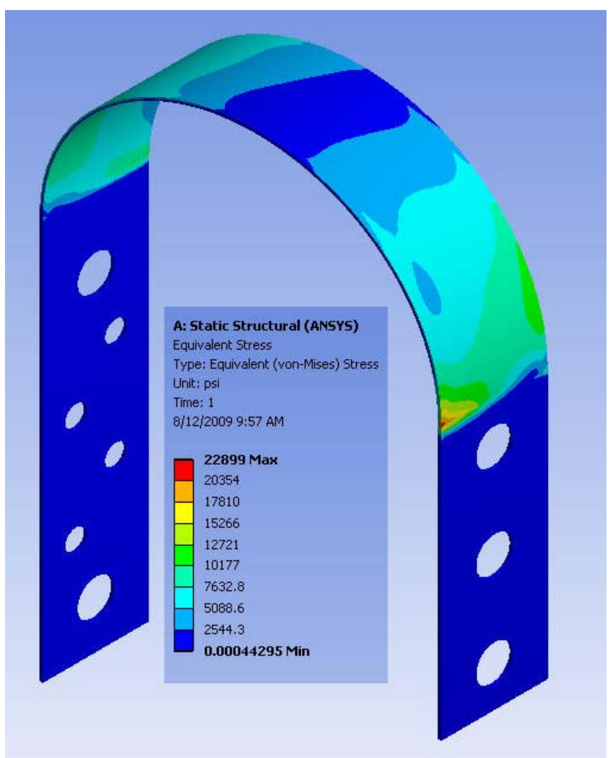

Figure 0-16 Inner-Most Lamination Model

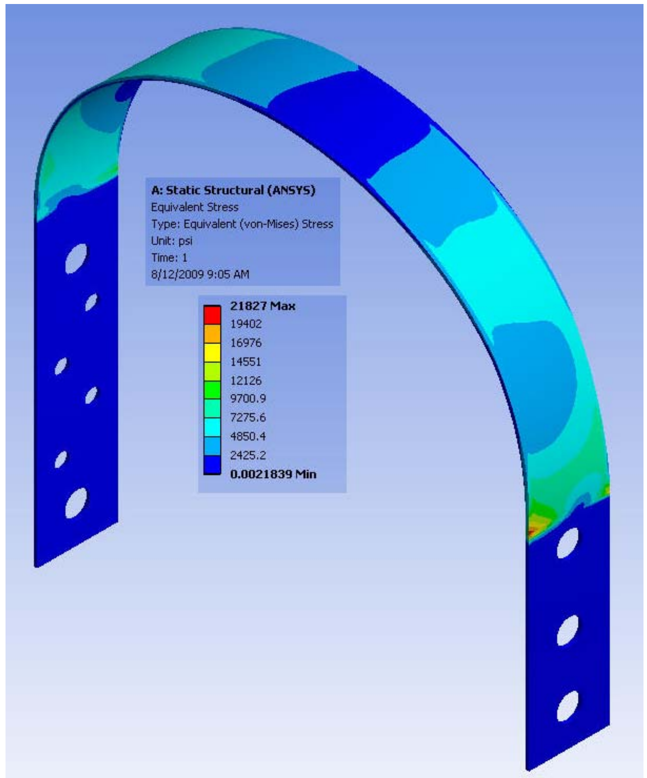

Figure 0-17 Outer-Most Lamination Model

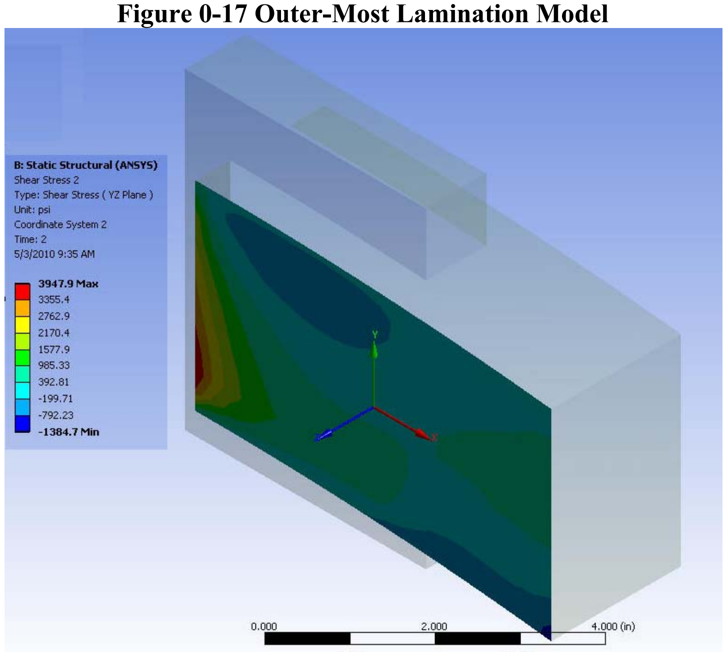

Figure 0-18 TF Stub Torsional Shear

Strap Solder/Braze Bond

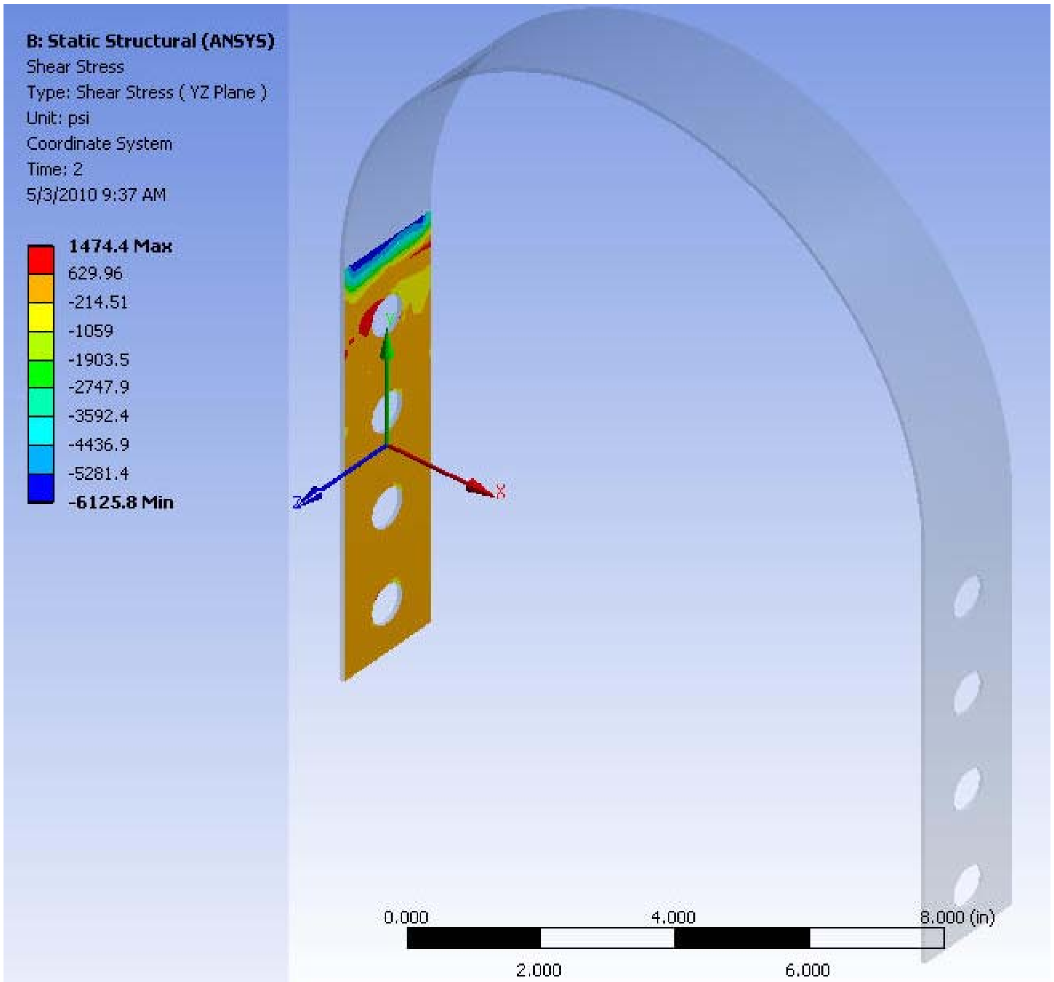

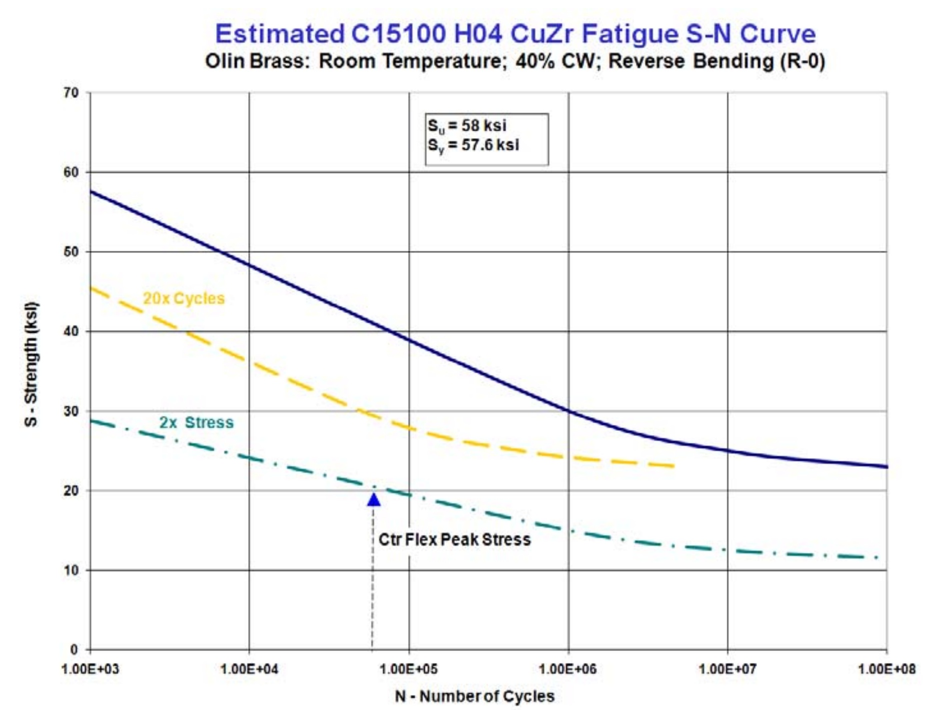

Copper-Zircalloy SN Curve And Flex Peak Stress

The 718 bolts have been tensioned via the super nuts to .9*yield. The criteria requires the bolts to have a stress limited to 2/3 * yield for applied loads - exclusive of the preload. A higher stress is allowed for the preload.

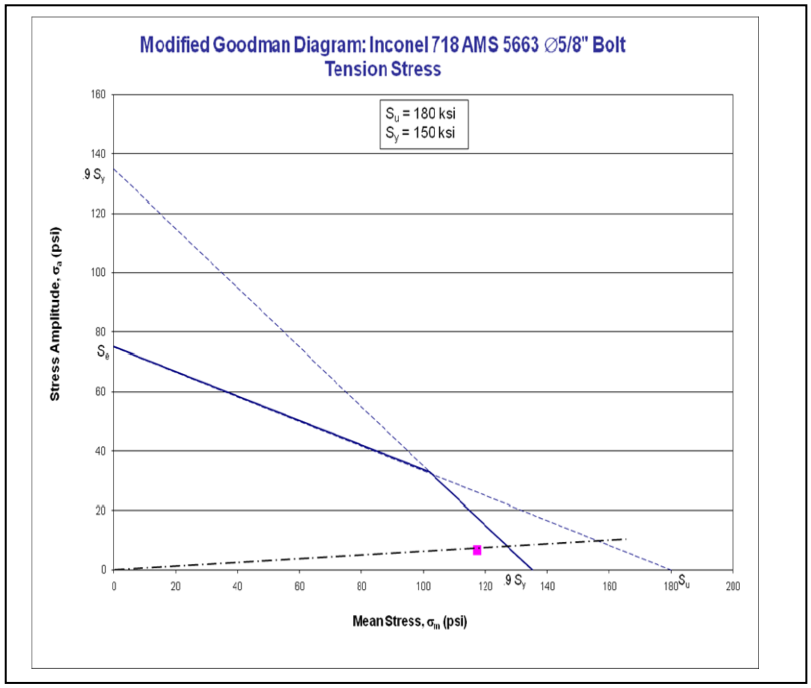

5.4.5. Global Torques

Out-of-Plane loading can be calculated as a general function of the 13 independent PF currents and current streams in the TF coil geometry [8]. This allows certain out-of-plane torques to be included in the design point calculations. Figure 0-19 shows the net TF system outer leg torque equations. Figure 0-20shows the net upper half TF system torque equations.

$$\left[\frac{\text{Net TF System OuterLeg Torque}}{1\,\text{N-m}}\right] = 6315.4\left(\frac{n_{\text{PF1AU}}^{\text{turns}}}{120}\right)\left[\frac{I_{\text{PF1AU}} - I_{\text{PF1AL}}}{1\,\text{kA}}\right] + 20167.5\left(\frac{n_{\text{PF1BU}}^{\text{turns}}}{180}\right)\left[\frac{I_{\text{PF1BU}} - I_{\text{PF1BL}}}{1\,\text{kA}}\right] + 36655.0\left(\frac{n_{\text{PF1CU}}^{\text{turns}}}{180}\right)\left[\frac{I_{\text{PF1CU}} - I_{\text{PF1CL}}}{1\,\text{kA}}\right] + 12478.3\left[\frac{I_{\text{PF2U}} - I_{\text{PF2L}}}{1\,\text{kA}}\right] + 14566.9\left[\frac{I_{\text{PF3U}} - I_{\text{PF3L}}}{1\,\text{kA}}\right]$$

Figure 0-19 Net TF System Outer Leg Torque Equations

$$\left[\frac{\text{Net Upper Half TF System Torque}}{1\,\text{N-m}}\right] = 13563.1\left[\frac{I_{\text{OH}}}{1\,\text{kA}}\right] + 4240.0\left(\frac{n_{\text{PF1AU}}^{\text{turns}}}{120}\right)\left[\frac{I_{\text{PF1AU}} + I_{\text{PF1AL}}}{1\,\text{kA}}\right] + 8892.5\left(\frac{n_{\text{PF1BU}}^{\text{turns}}}{180}\right)\left[\frac{I_{\text{PF1BU}} + I_{\text{PF1BL}}}{1\,\text{kA}}\right] + 16750.0\left(\frac{n_{\text{PF1CU}}^{\text{turns}}}{180}\right)\left[\frac{I_{\text{PF1CU}} + I_{\text{PF1CL}}}{1\,\text{kA}}\right] + 5197.5\left[\frac{I_{\text{PF2U}} + I_{\text{PF2L}}}{1\,\text{kA}}\right] + 21915.7\left[\frac{I_{\text{PF3U}} + I_{\text{PF3L}}}{1\,\text{kA}}\right] + 56813.9\left[\frac{I_{\text{PF4}}}{1\,\text{kA}}\right] + 118636.5\left[\frac{I_{\text{PF5U}}}{1\,\text{kA}}\right] + 713308.9\left[\frac{I_{\text{plasma}}}{1\,\text{MA}}\right]$$

Figure 0-20 Net Upper Half TF System Torque Equations

5.4.6 TF Inner Leg Torsional Shear

5.4.6.1.Global Model Results

Out-of-Plane (OOP) loads on a toroidal field (TF) coil system result from the cross product of the poloidal field and toroidal field coil current. Support of OOP loads is statically in-determinant, requiring an understanding of the flexibility of the outboard structures and the inboard stiffness of the central column. For NSTX CSU, this is accomplished in the global model. For the worst PF loads considered in the global model, the peak torsional shear stress is 20 MPa – just below the allowable of 21.7 MPa.

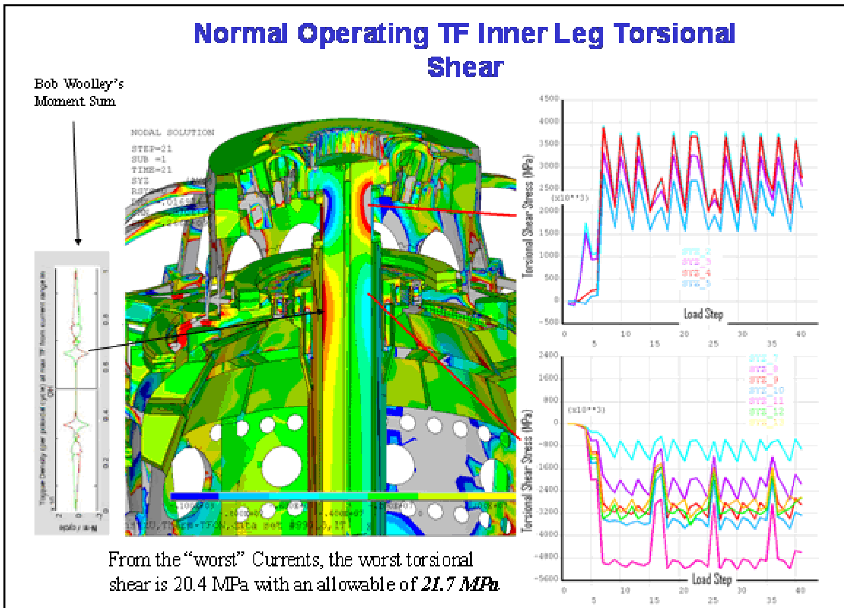

Figure 0-22 Global Model Inner Leg Torsional Shear

Figure 0-22 shows the global model inner leg torsional shear. also shows the global model inner leg

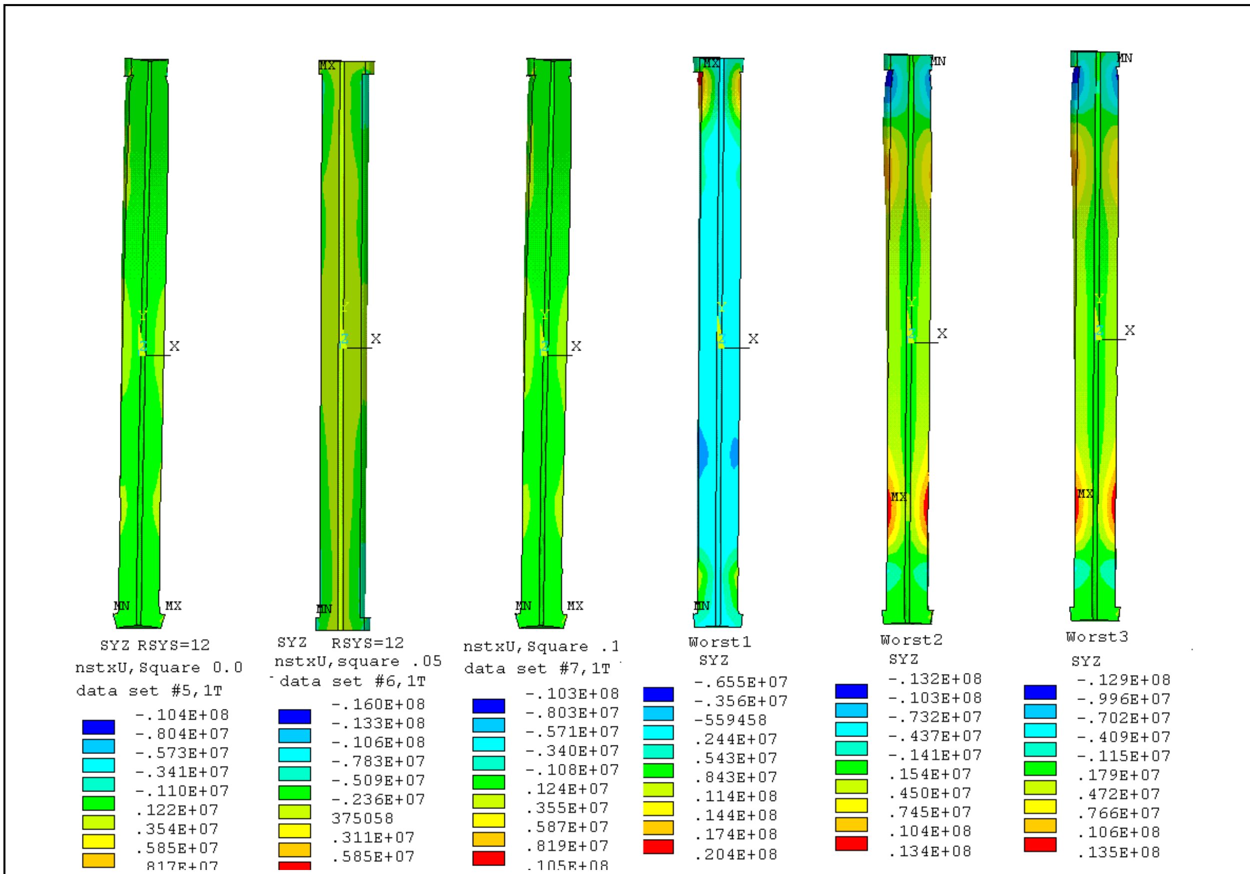

Figure 0-21 Global Model Inner Leg Torsional Shear – Worst Case PF Loads

torsional shear with the worst case PF Loads. Figure 0-23 shows a more detailed view of the global model inner leg torsional shear.

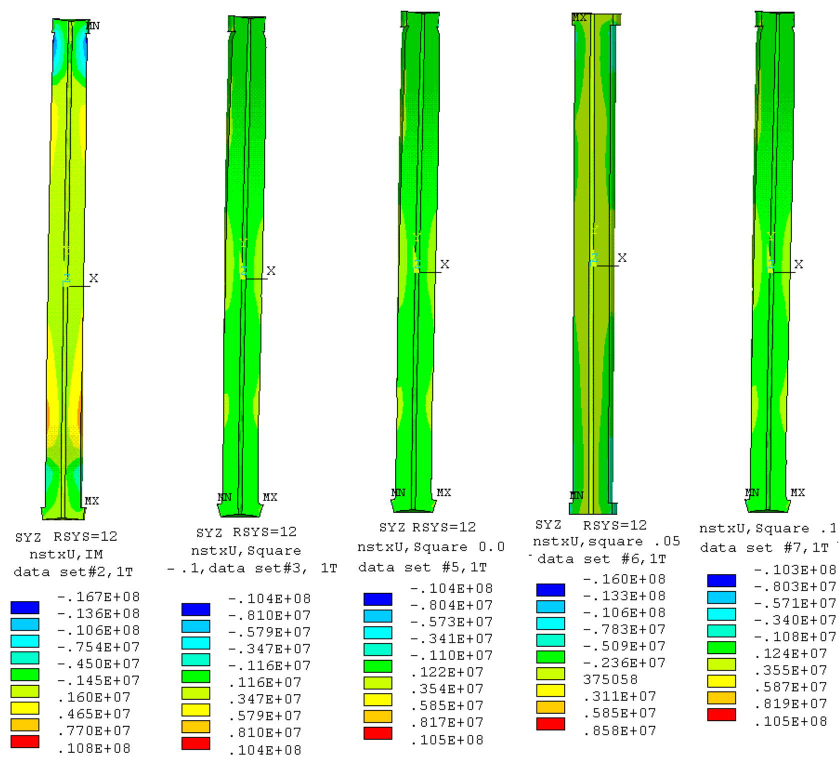

Figure 0-23 Another View of the Global Model Inner Leg Torsional Shear

Additional discussions of torsional shear may be found in Bob Woolley's calculation NSTX-CALC-132-003-00 which provides moment calculations which are useful to find the maximums in the NSTX Design Point spreadsheet. His summation of the outer leg moment is directly useful in evaluations of the up-down asymmetric case that Han Zhang is running in the diamond truss/tangential - radius rod calculations. (Section 5.4.4.2)

5.4.6.2.Simplified Analysis

A simplified method for calculating OOP shear stresses and their distributions, suitable for systems codes, is described here. The TF coil system and structure is modeled as a toroidal shell The poloidal field is calculated at the shell using axisymmetric current loops and an elliptic integral solution. OOP Lorentz forces are computed by crossing the TF current with the poloidal field. The torsional stiffness of segments of the TF shell is computed, adjusting shear modulus and thickness to simulate the stiffnesses of the tokamak. In practice the global finite element model is used as a guide in selecting the shell properties. This kind of approach can be implemented in the Design Point.

Figure 0-25 shows a simplified Toroidal Field Coil shell model. OOP loads are computed from the TF current and PF currents using an elliptical integral solution for the PF fields. TF OOP loads are assumed to be applied to a toroidal shell – with varying thickness to simulate more complex OOP structures. Shear deformations are accumulated to a split in the shell, then a moment is applied to align the split. Figure 0-24shows the NSTX TF shell model. Figure 0-26 shows a comparison of Woolley's global FEA and a Simple Shell Analyses.

Figure 0-27 shows torsional shear for IM and some equilibria. Figure 0-28 shows the out-of-plane force density along the TF center line starting with outboard equatorial plane. Figure 0-30 shows the distribution of the poloidal field magnitude plotted around the perimeter of the TF coil, Figure 0-31, is a plot of the poloidal field vectors at the TF coils. Figure 0-32 shows the torsional shear stress in the TF coil or "shell" plotted on the TF cross section. Figure 0-33 shows Out-of-Plane Displacements of the TF Coil and "Shell.

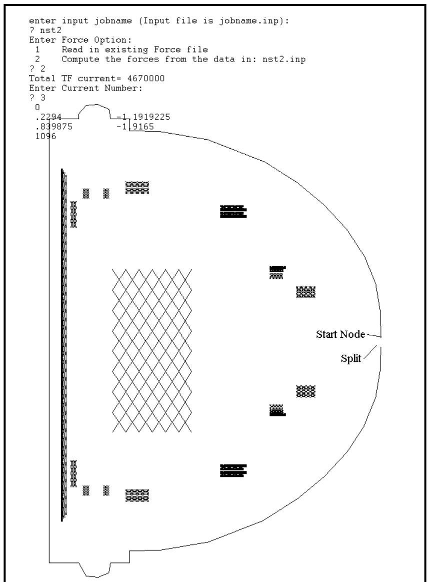

Figure 0-24 NSTX Shell Model

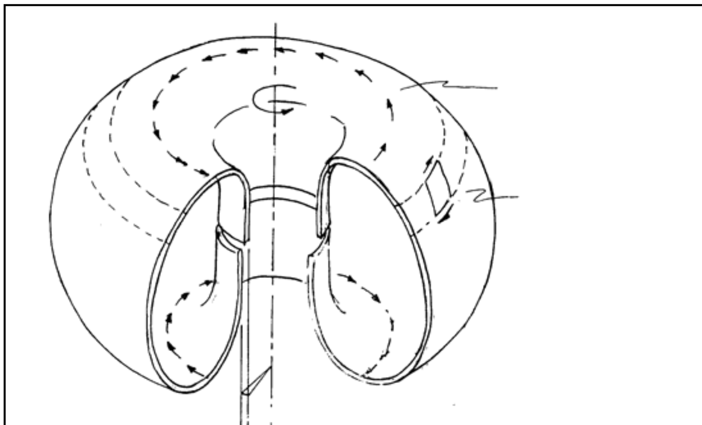

Figure 0-25 Simple Toroidal Field Coil Shell Model

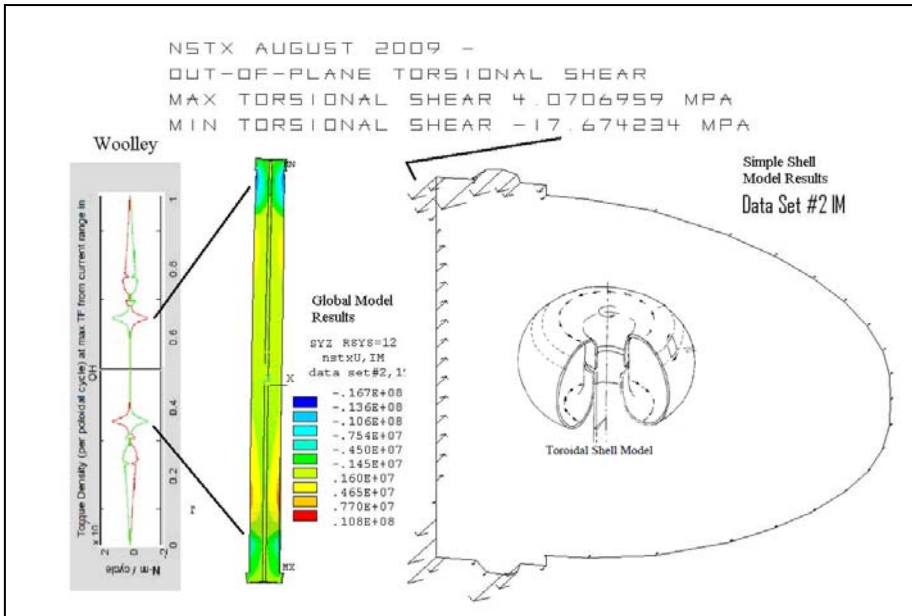

Figure 0-26 Comparison of Woolley, Global

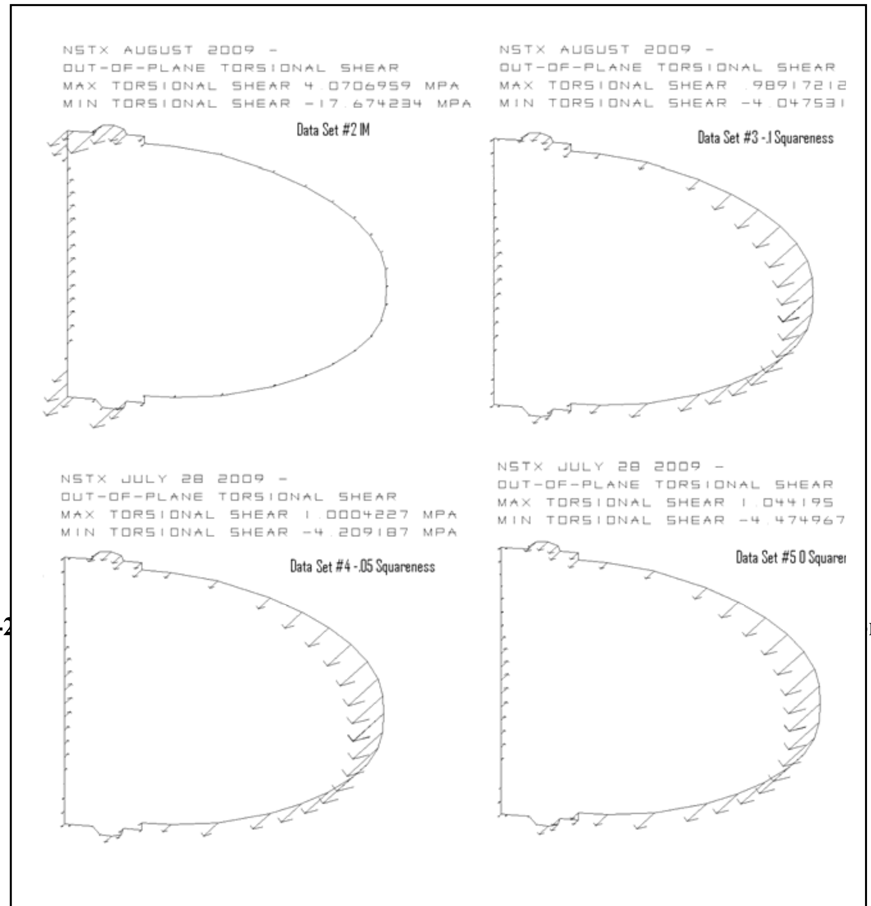

Figure 0-2 ... rial Plane

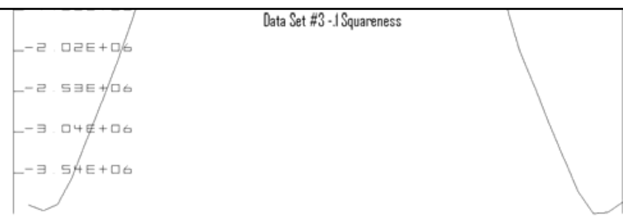

Figure 0-29 OOP Torsional Shear Stress Along the TF CL Starting from the Outboard Equitorial Plane

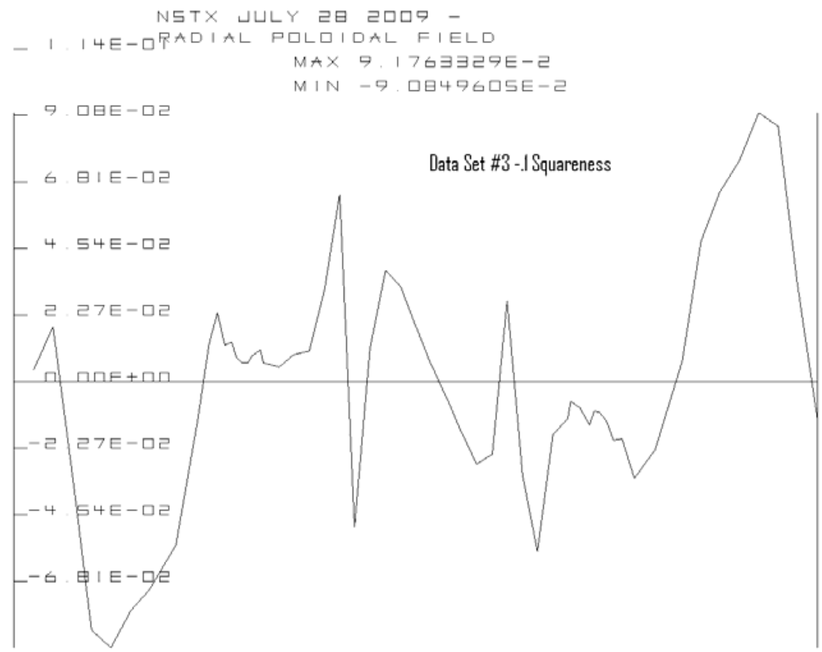

Figure 0-30 Radial Poloidal Field, Plotted Along the Perimeter of the TF Coil

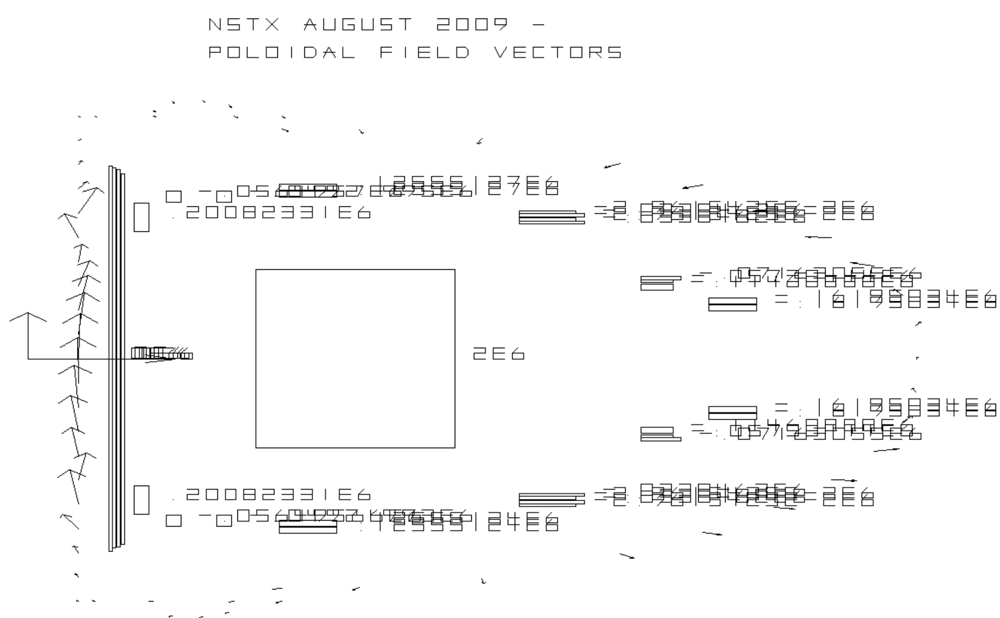

Figure 0-31 Poloidal Field Vectors

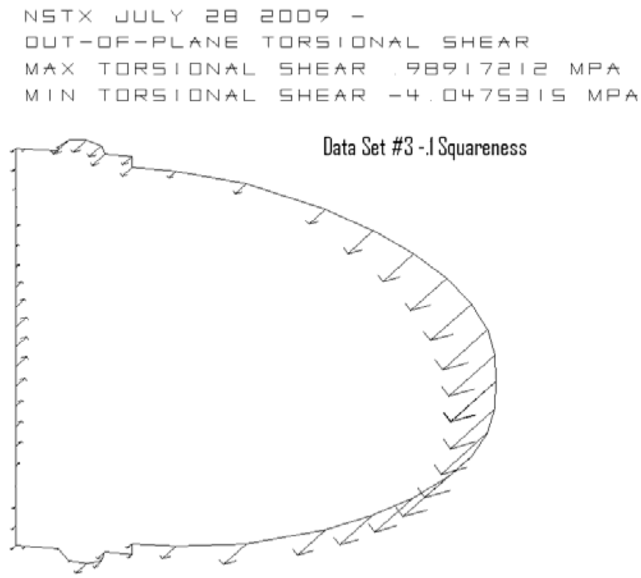

Figure 0-32– Torsional shear Stress plotted along the TF Perimeter

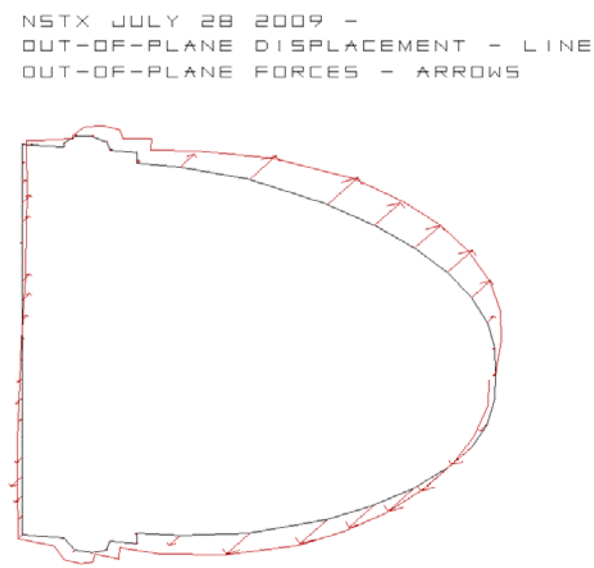

Figure 0-33 - Out-of-Plane Displacements of the TF Coil and "Shell Effect of De-Wedged Area in the TF Corner

Electromagnetic current diffusion causes a concentration in current density in the corner of the TF. A thermal differential results that results in a tensile thermal stress (Figure 0-34). This occurs at the ID of the TF column, where the torsional shear is a minimum. In order to provide some additional assurance that de-lamination will not propagate into regions of the TF that must sustain shear, overwraps of tensioned glass tape are being considered.

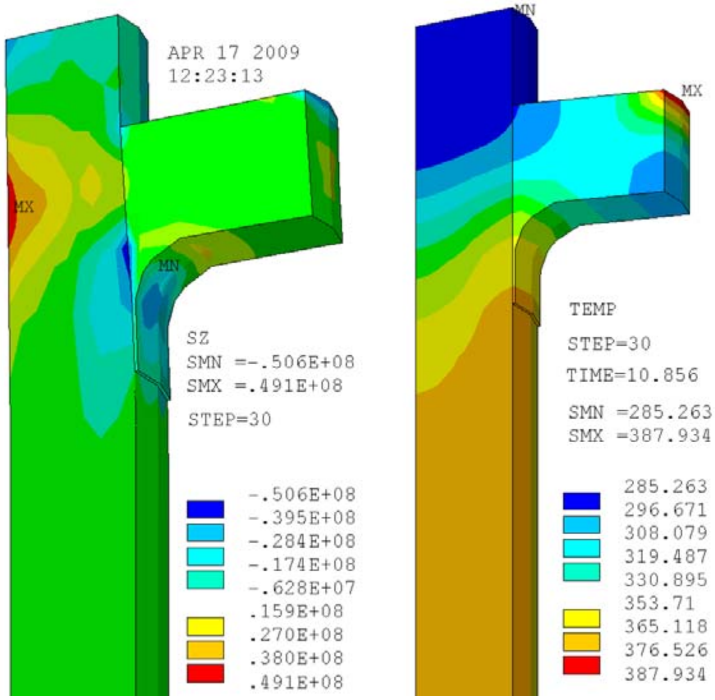

Figure 0-34 Effect of De-Wedged Area in the TF Corner

The occurrence of tensile stresses at the ID of the TF coil, where the currents turn the corner will be addressed by tension winding epoxy glass around the vertical extension of the TF leg.

5.4.6.3.**TF Outer Leg Reinforcement**
5.4.6.4.**Is TF Outer Leg Reinforcement Needed?**

To understand the necessity of reinforcing the outer TF coils, H. Zhang, D. Mangra, and P. Titus ran models with no OOP support. The bending stress for the 50 scenarios analyzed is 200 MPa. This alone is not a problem. The shear stress in the turn-to-turn insulation (Han's analysis) is too high at 37 MPa.

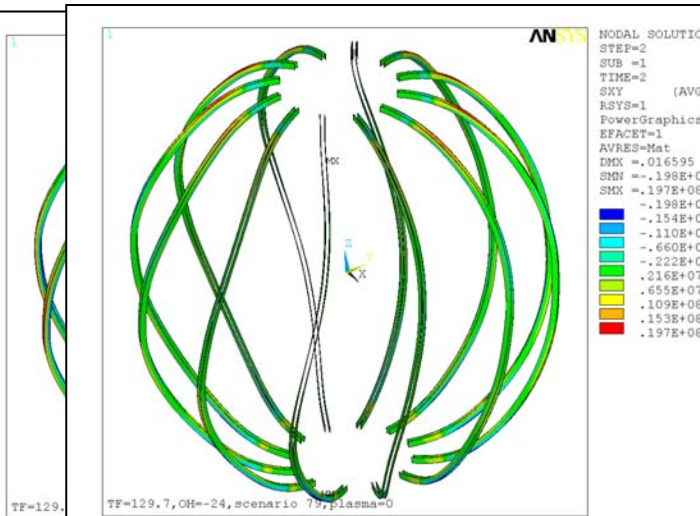

Han's ... sulation. 37 Mpa is too high for
the in...

Han's Analysis of the Shear Stress in the Turn to Turn Insulation. 19.7 Mpa is marginal for the insulation bond stress.

OOP Displacement, - No Outer Leg OOP Support

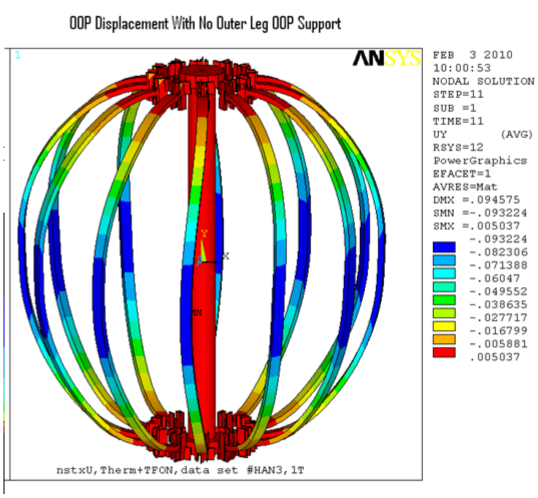

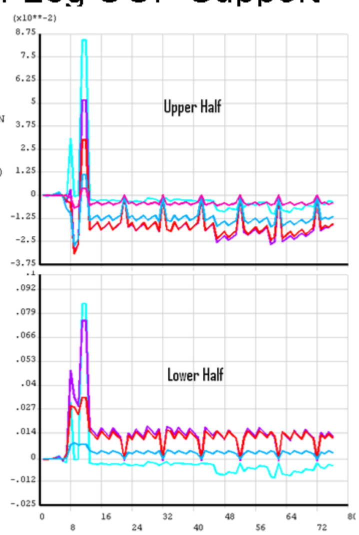

Titus Global Model Results

No ring and no radius rods

Han Zhang's Results:

Scenario 49: Utheta=18.9mm (0.744")
Scenario 79: Utheta=17mm (2/3")
Scenario 82: Utheta=13.6mm (0.535")

Scenario 79: shear of epoxy between coil turns is 37.3MPa (5408 psi). Epoxy shear allowable is 21.7MPa (3146 psi).

TF outer leg OOP Lorenz force (about 1/3 of power limit condition)

Scenario 49: 99KN
Scenario 79: 106KN
Scenario 82: 102KN

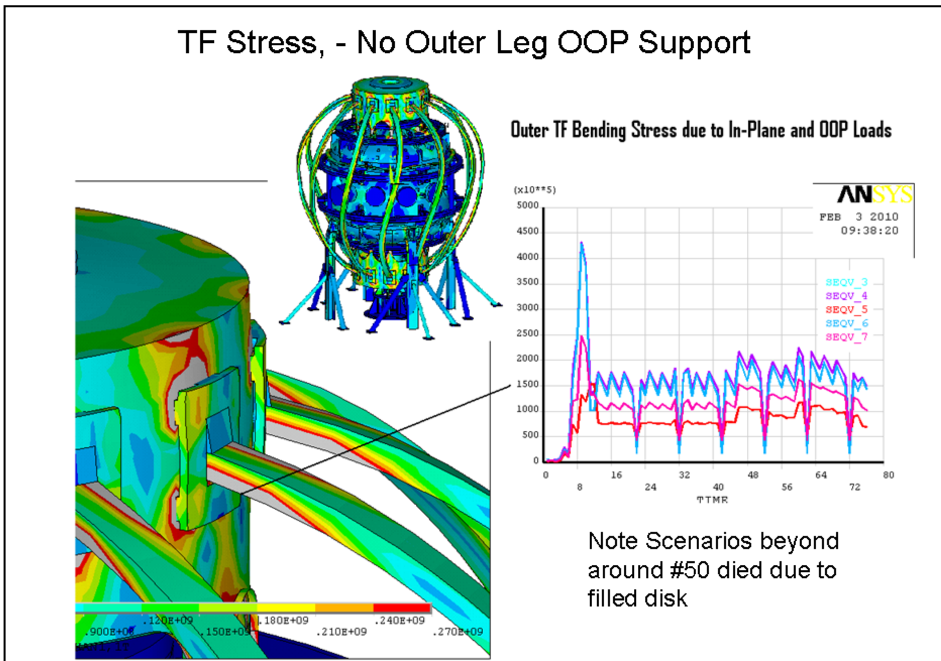

The bending stress for the 50 scenarios analyzed is 200 MPa

TF Outer Leg Reinforcement

The upgrade of NSTX CSU will increase the TF current to 130KA. Upon TF self field and poloidal field, TF outer leg will have in-plane (i.e. in the plane of TF outer leg) force and out-of-plans (OOP) (i.e. perpendicular to the plane of TF outer leg) force. The existing support structure of TF outer leg is the umbrella structure and the existing turnbuckle trusses. Upgrade loads scale by the current squared for in-plane loads and by the increase in poloidal field or plasma current for OOP loads. One TF outer leg is to be replaced. All other existing TF outer legs are to be reused for the upgrade. A significant part of the preliminary design effort has been to provide added support for the TF outer legs while introducing minimal changes to the hardware - particularly hardware that is difficult to access for replacement or reinforcement.

NSTX-CALC-132-01 by H. Zhang, analyzed the TF outer leg reinforcement. The objective of this analysis was to study what kind of additional support structure is needed take some of the in-plane and out-of-plane (OOP) force of TF outer leg. From previous analysis, with the worst case PF currents, the umbrella structure will have very high stress of >1GPa (145 ksi). The umbrella structure has a cylindrical shape and radial load should not be a problem. However, the blocks are bolted to the umbrella structure and must take the radial load. Vertical load will be transferred to vacuum vessel. OOP load will cause the rotation of umbrella structure and produce high stress on the arches. So it is necessary to add additional support structure to take some OOP load and so as to reduce the load to umbrella structure. Figure 0-35 shows the NSTX machine. Figure 0-36 shows the out-of-plane or toroidal displacements of the outer TF legs supported by the continuous diamond truss system.

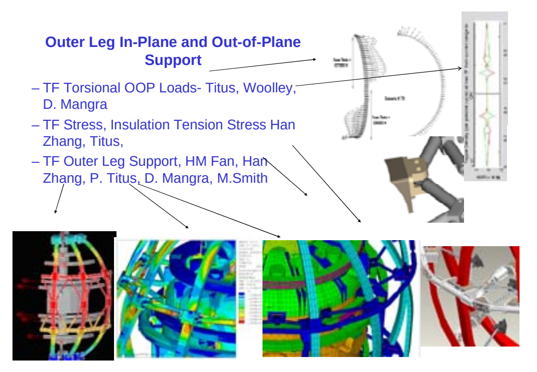

Figure 5.4.6.5 TF In-Plane and Out-of-Plane Support

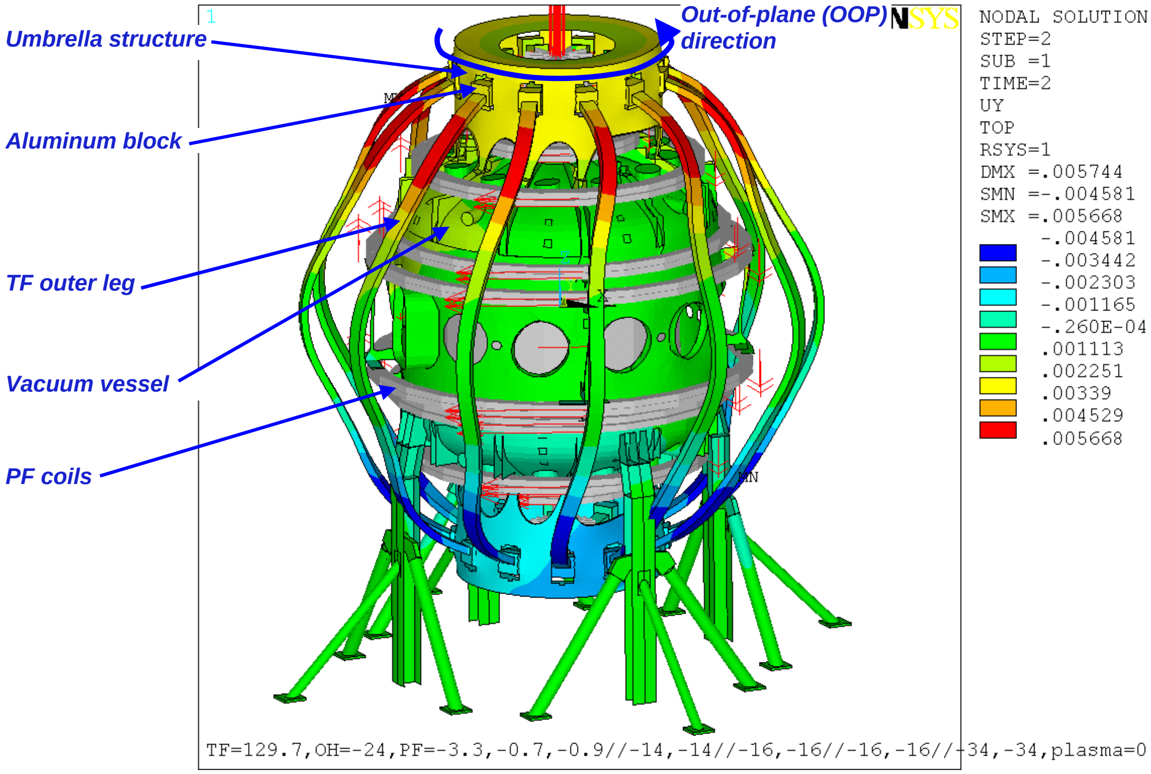

Figure 0-35 Leg Support System Major Components of the NSTX Machine

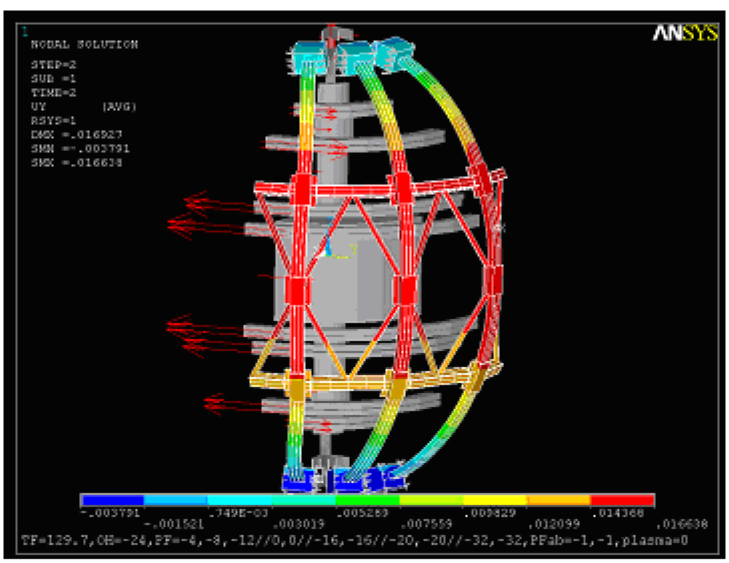

Figure 0-36 .-. Out-of-plane or Toroidal Displacements of the outer TF legs supported by the Continuous Diamond Truss System

The first idea is to add a stainless steel ring to take in-plane expansion and tie bar connected to vacuum vessel to transfer the load to vacuum vessel. But the tie bar will constraint the TF coil due to vacuum vessel bake out.

The second idea is to use stainless steel ring and diamond truss and there is no link to vacuum vessel. However, the space is quite limited and only a few of diamond truss can be added. The non-uniformly distributed diamond truss will cause the non-axisymmetric coil deformation and high stress points in the coil.

The third idea is to use ring and tangential (or radius) rods. They occupy the space of existing turn buckle and not affected by the vacuum vessel bake out. They can transfer the OOP load to vacuum vessel and effective on both symmetric and asymmetric PF currents.

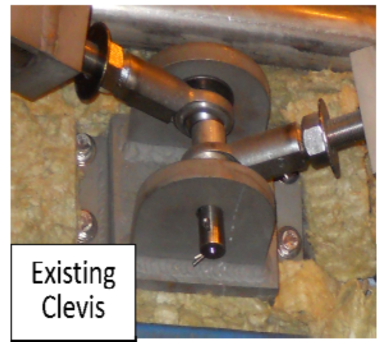

Designs Must Keep Loads on Clevis Attachment at Vessel Knuckle Less than 5 kips (22kN) or 8 kips (35 kN) with Bolt Upgrade, and Limit TF Outer Leg Insulation Shear

Existing TF Prepreg
CTD 12P

2/3 of 24 = **16 MPa (Static)**
C2~.44
Fatigue Capacity was set at 16 Mpa by Prototype QualificationTest

Held by 6
3/8 screws

52

For the PDR, A no-modification-to-the-vessel-attachment design was chosen.

Table 0-5 shows the stress result based on criteria document. The stresses in TF outer legs are almost within allowable (See **Error! Reference source not found.**). The highest stress is at the connection between TF coil and ring. Extending the case as shown in Figure 0-37 may help to reduce it, but this requires further analysis. The stress in the ring is a maximum of 30 ksi for symmetric and maximum of 32.5 ksi for asymmetric current. For symmetric current, max load in radius rod is 18.4 klbs and min load is 4.5 klbs. For asymmetric current, max load in radius rods is 20.3 klbs and min load is 4 klbs. Max load in the ring (in the middle of the ring where connects to radius rod): 86 KN or 19.3klbs for the asymmetric PF current, and 80 KN or 18 klbs for the symmetric PF current.

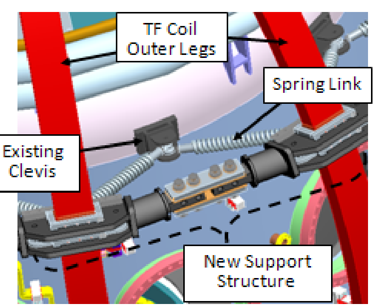

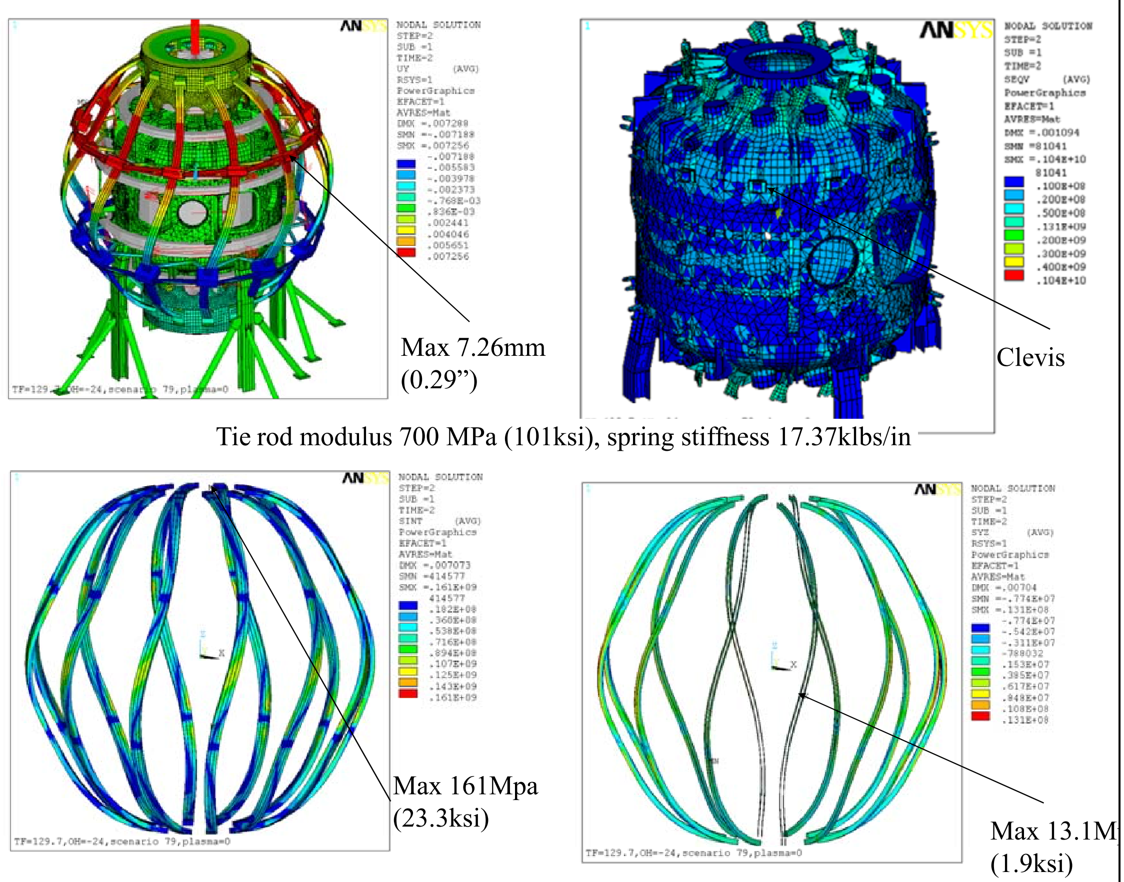

Table 0-5 Stress Evaluation Based on the Criteria Document

	Max Tresca (Mpa) [1]	Allowable (Mpa) [1]	Von Mises stress from analysis (Mpa)
TF outer leg at Al. block	173	156	109 (symm) 107 (asym)
TF outer leg at ring	173	156	147 (symm) 158 (asym)
vessel at Al. block	183	183	313 (symm) 329 (asym)
vessel arch	183	183	289 (symm) 273 (asym)
vessel at radius rod support structure	160	160	139 (symm) 144 (asym)

Note: In this table, "symm" indicated the result is upon up-down symmetric PF currents and "asym" means up-down asymmetric PF currents.

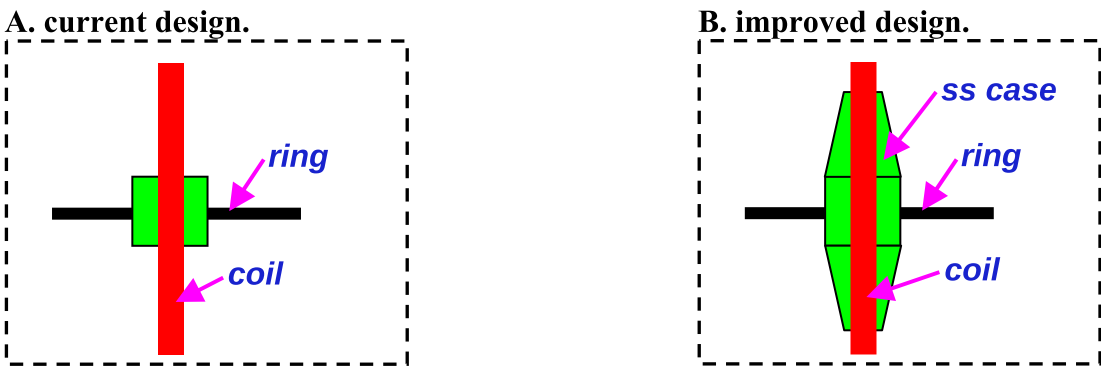

Figure 0-37 Design of Stainless Steel Case

The vessel stress at the aluminum block is too high. It is mainly because the direct coupling of nodes of Al. block and umbrella structure so as to cause element discontinuity. This should be further analyzed by a detailed model. Stress in vessel arch area is too high and requires reinforcement in that area. Vessel stress at radius rod support area is within allowable.

In these analyses, rings were added to reduce the pull-out (in-plane) loads at the umbrella structure (Figure 0-38). Various trusses (including tie bars, diamond bracing, and tangential rods) were tried reduce out-of-plane loads from the outer TF legs. Since the machine is already crowded, interference was a severe problem limiting the addition of trusses. Although we don't want to transfer more load to vacuum vessel, up-down asymmetric currents and resulting net twist required an attachment to the vessel. Tangential radius rods can take the net twist and also provided adequate OOP support for symmetric case. Tangential radius rods use the existing territory of turn buckle and there is enough room for them. Loads in the tangential radius rods allow attachment to the vessel with only modest modification and local stress of 20ksi. Vessel stresses in the umbrella structure and equatorial plane port region are acceptable or require only modest modification.

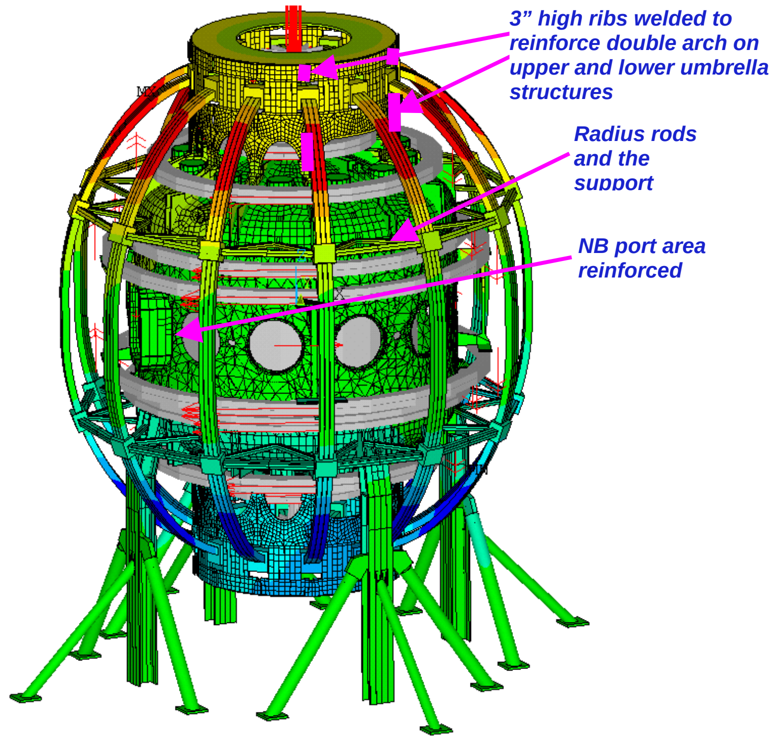

Figure 0-38 NSTX Machine with Reinforcements

The vessel stress at the aluminum block is too high. It is mainly because the direct coupling of nodes of Al. block and umbrella structure so as to cause element discontinuity. This should be further analyzed by a detailed model. Stress in vessel arch area is too high and requires reinforcement in that area (Figure 0-39). Vessel stress at radius rod support area is within allowable (Figure 0-40). The Tangential Radius Rod concept supports OOP loads, uses territory that is already used by the TF Support Truss, and allows radial growth during bake-out.

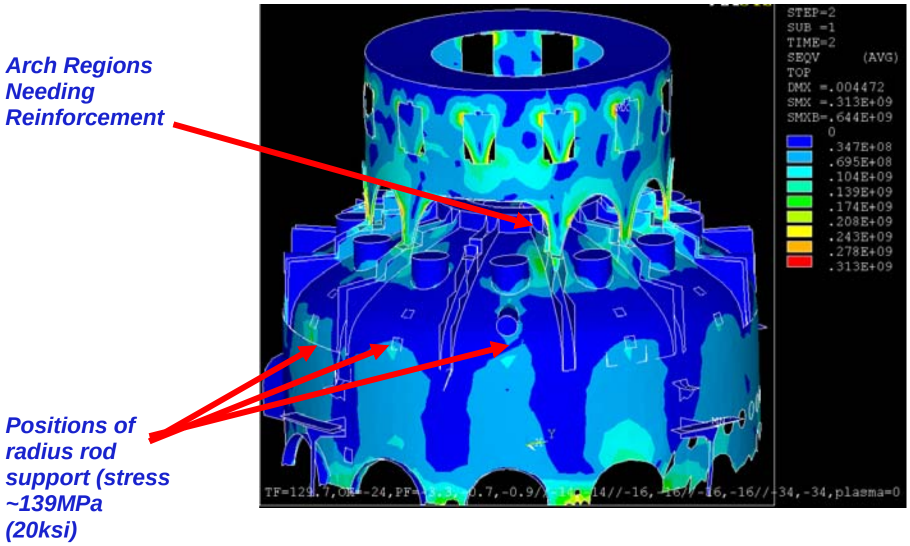

Figure 0-39 Vessel Stresses with Tangential Radius Rods

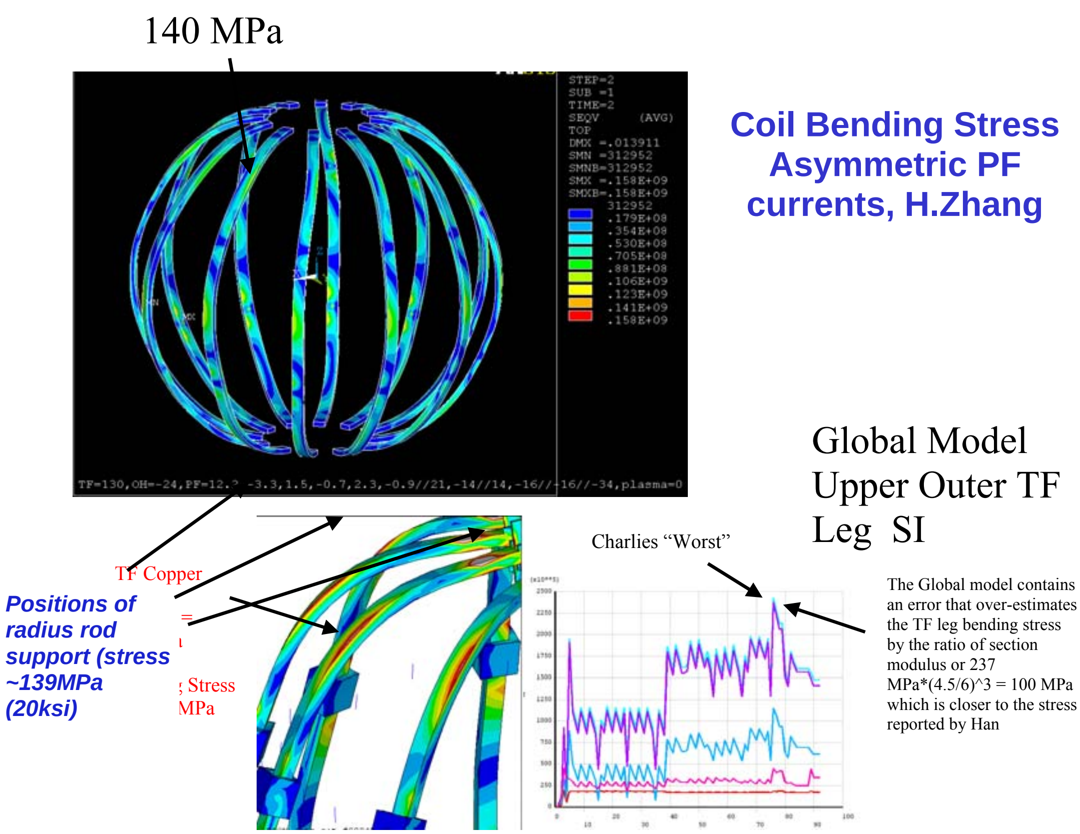

Figure 0-40 Outer Leg Stress with Tangential Radius Rods

5.4.6.4 TF Outer Leg Bond Shear

The existing outer legs will be qualified for the higher loads – as mitigated with the addition of the support rings and truss springs. Bending stresses have been qualified in section 5.4.6.3. Bending related shear stresses must be sustained with a turn to turn bond in the existing coils. The outer leg is made up from 3 turns of copper, each of which is 2 inches thick. The global model TF outer leg contains a dimensional error that over estimates the bending stress and the shear stress - the Toroidal Width of the TF Outer Leg Should Be 6 inches. Stresses would scale as the section modulus or by d^3. The mid-plane shear was plotted in the figure, and this actually is in the middle of one of the 3 conductors so the global model overestimates the shear in a couple of ways. However even with these errors, the shear stress for a range of normal scenarios is 6.25 MPa with a shear alowable that may be as high as 21.7 MPa (See Figure 0-41). Further evaluation will be required to address the worst case loads that have been used to qualify the bending stress.

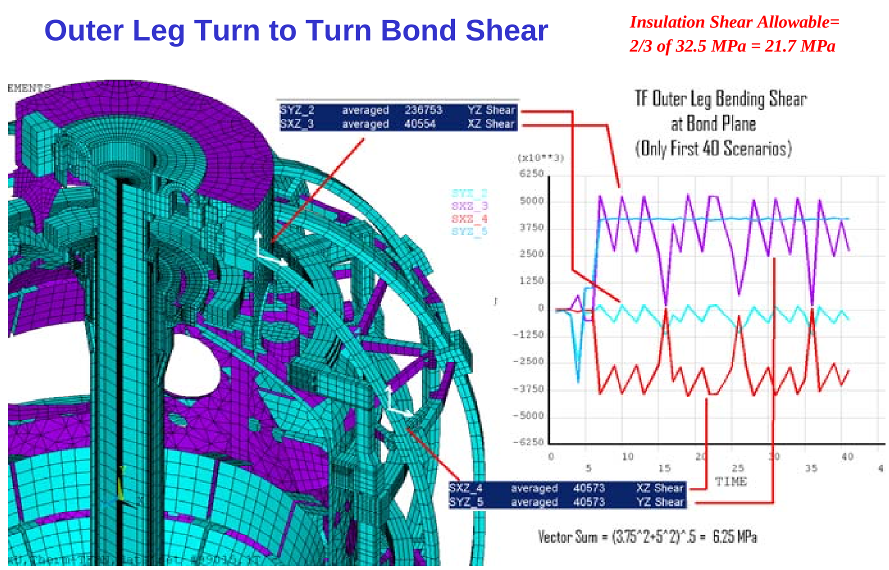

Figure 0-41 Global Model Bending Related Shear

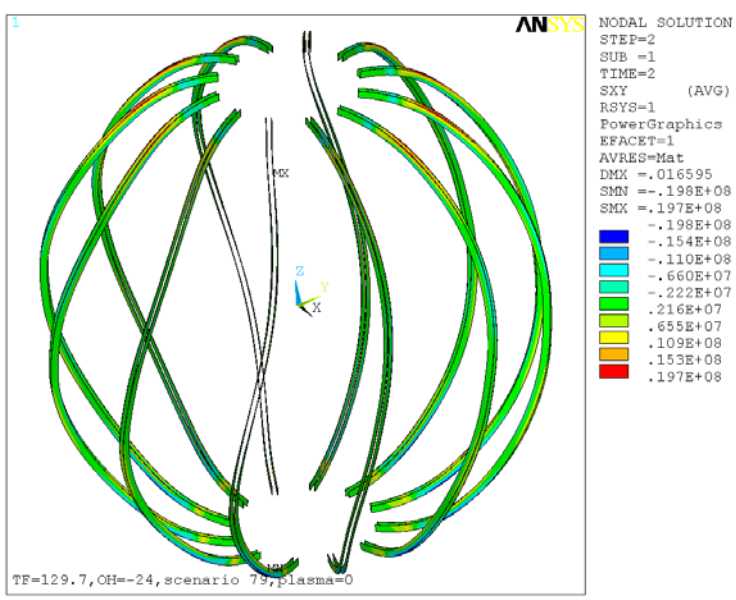

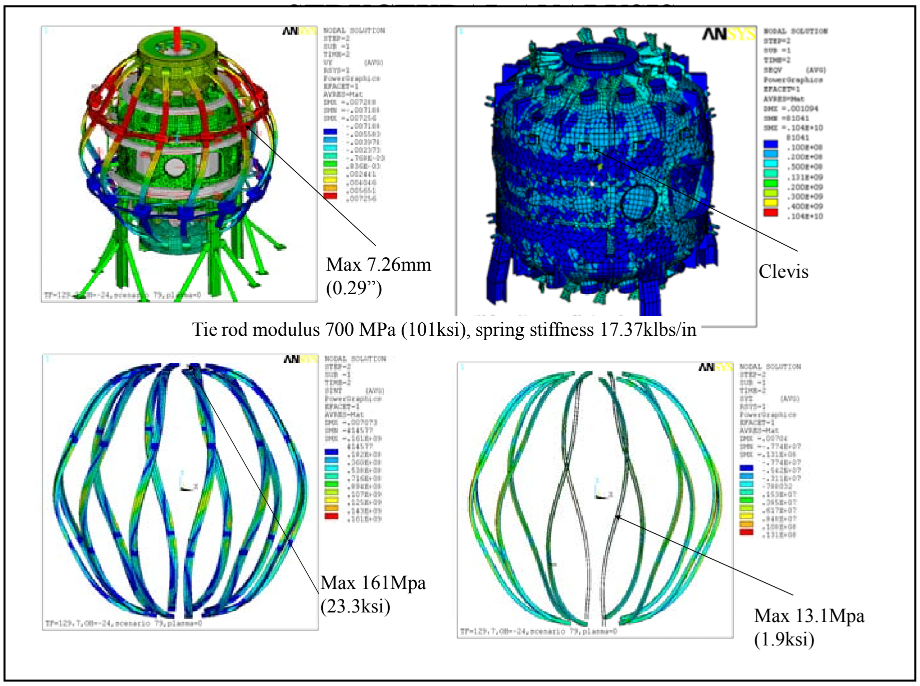

Self Loads

The attractive force between the three conductors of the outer leg adds little to the compressive force on the insulation. This was evaluated with a representation of the three outer leg TF conductors with parallel current. Estimates based on Han Zhang's model and the analysis described, indicate about 1 MPa of insulation compression due to the self load in the outer leg The shear strength imposed by the out of plane loading will have to satisfy the bond strength of the epoxy without the aid of significant compression.

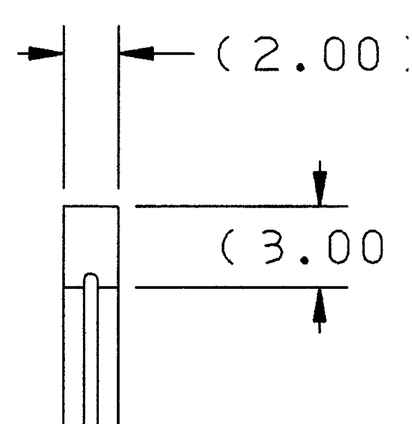

Outer Leg Single Turn Cross Section. Three of these make up the outer leg

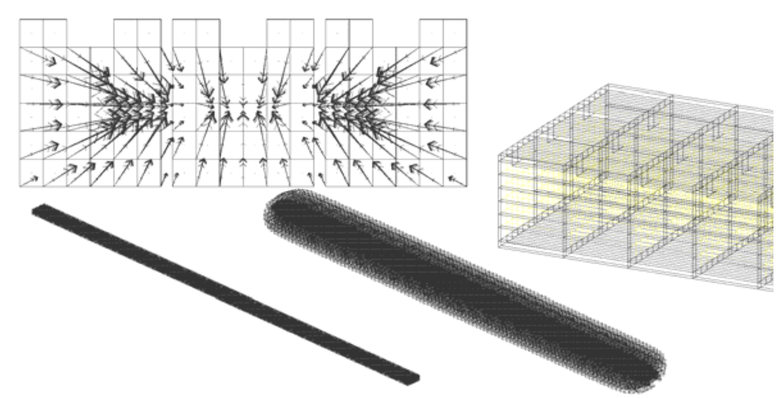

Biot Savart Model of the TF Outer Leg Self Fields.

The PDR design for the outer leg reinforcement is based on a soft spring that limits the loads on the clevis attached to the vessel knuckle. The spring is not so soft that it allows unacceptable shear stresses in the legs.

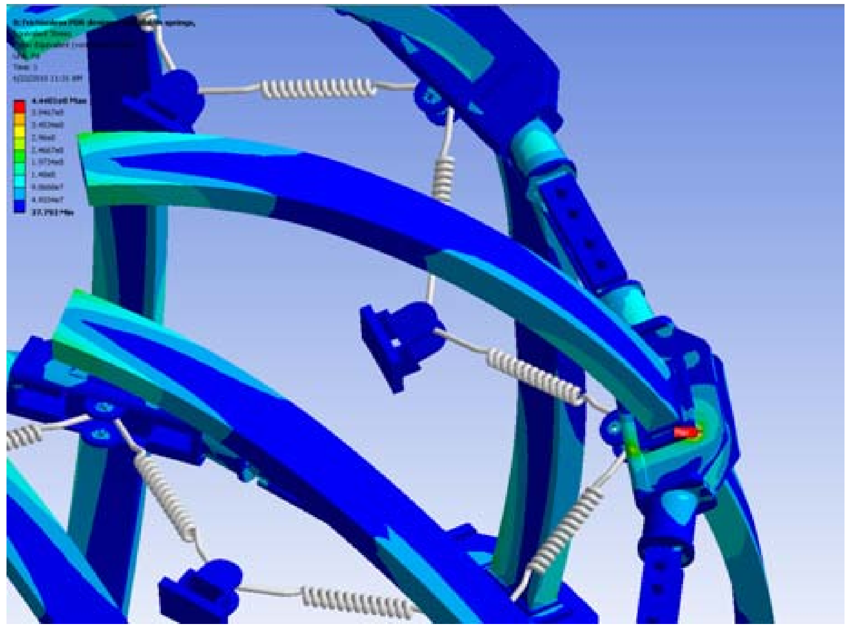

Bracket Design/Analysis by D. Mangra, Mark Smith, P. Rogoff

TF Outer Leg Ring Loads and Connection Details

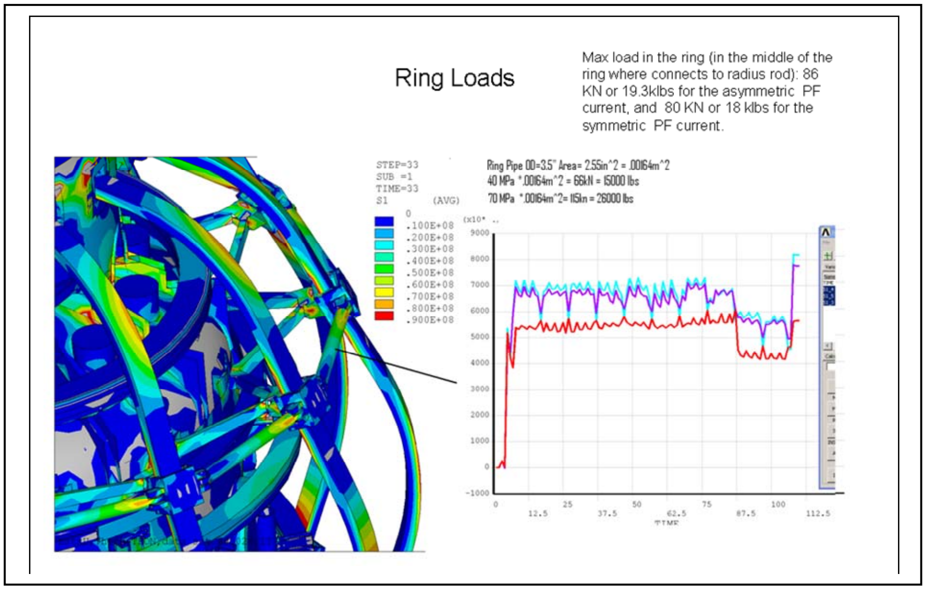

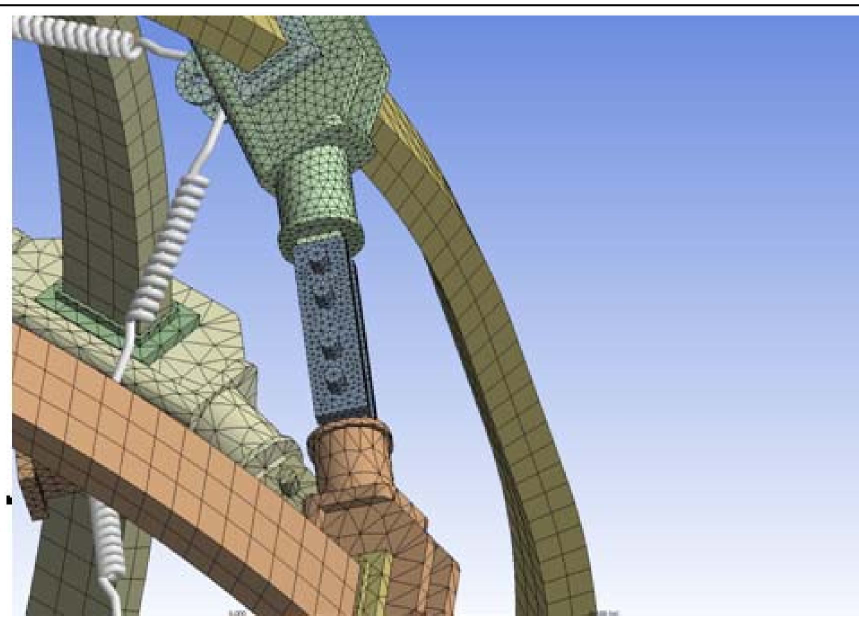

Bracket Analysis by D. Mangra, Mark Smith, P. Rogoff

5.4.6.5 Bake-Out TF Stresses

Bake-out causes the vessel to expand, loading the clevis in compression. The soft springs introduce minimal shear and no tension in the 3/8 Clevis screws. clevis pin results in average stress of 40MPa. Max coil stress is 106MPa (15.4ksi). TF coil bending stress is 106 MPa in Han Zhang's analysis which has the PDR

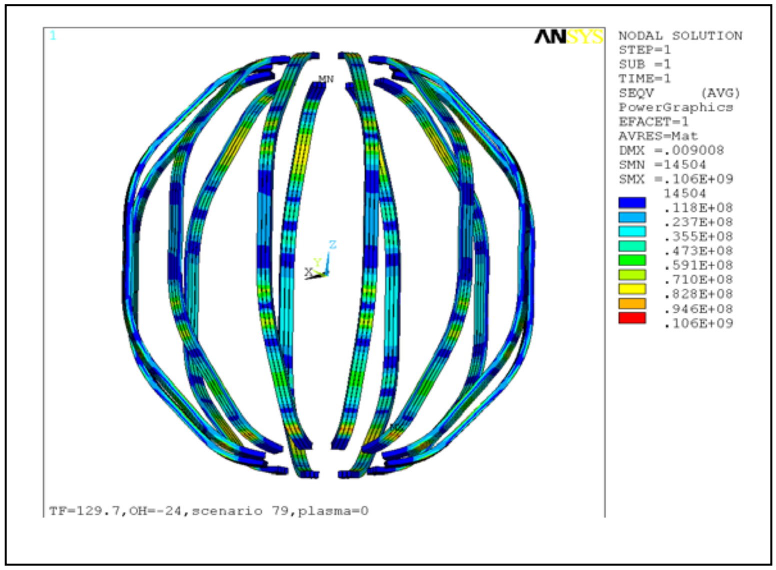

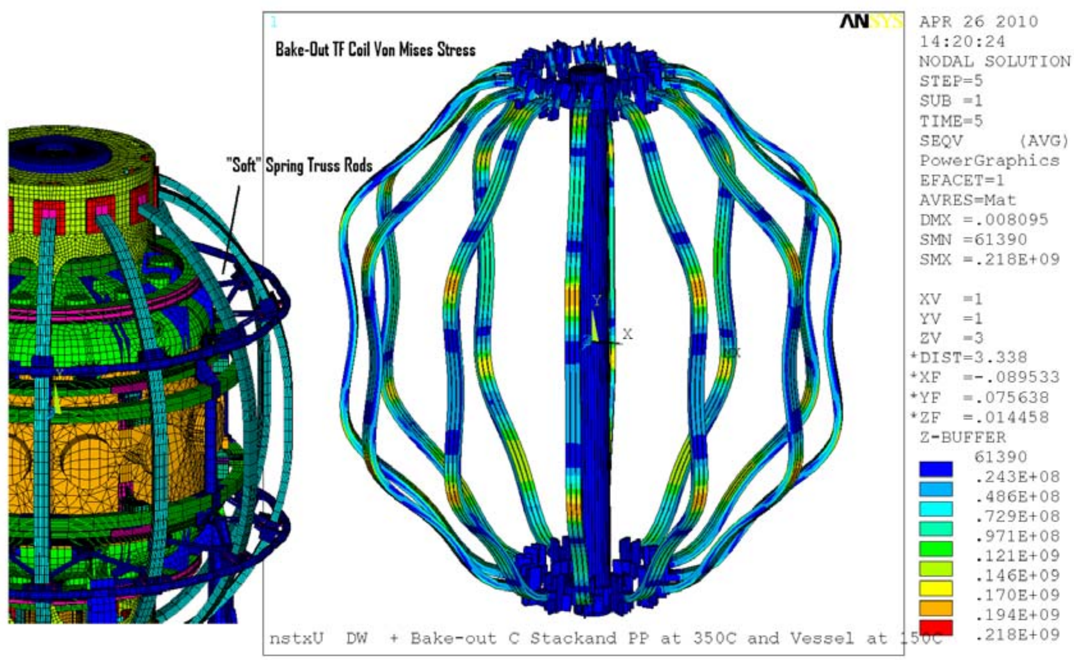

Global Model Bake-Out Bending Stress from Run #24

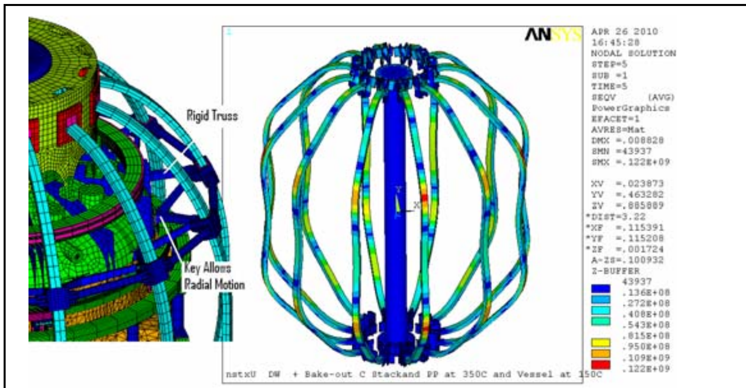

From Run #22

5.4.6.6 TF Upper and Lower "Teeth" Connecting the TF to the Lid/Flex/Diaphram

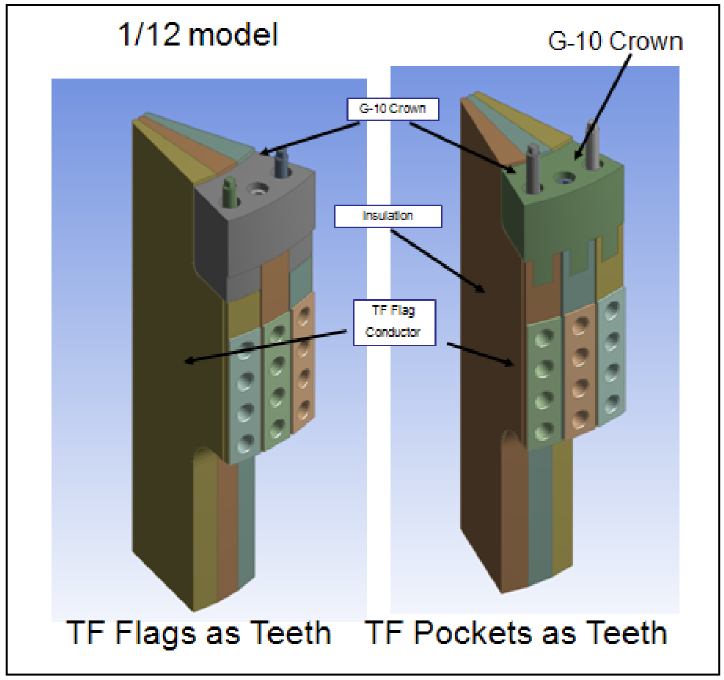

There are two sets of teeth used in the connection between an end of the TF

leg and the lid/or flex. They occur in the G-10 ring or collar shown as green in the figure above and labeled the crown in the figure at upper right. At the bottom of the collar, at the upper end of the TF, the teeth engage the flags of the TF legs. at the upper end of the collar, the teeth engage teeth on the lid.

The torque on the lid is .3MN-m . The radius to the teeth is about .23 m . For the 36 teeth, the load is .3e6/.23/36*.2248 = 8145 lbs. This was rounded up to 9000 lbs.

From Blodgett, the torsional shear is 16*Moment/pi/d^3 = 16*.3e6/pi/(.1934*2)^3 = 26 MPa. The peak torsional shear stress for the 96 scenarios in the global model is 24 MPa. The allowable is 21.7 for the present estimate of the torsional shear stress allowable for CTD 101K . We are a bit above the torsional shear stress allowable based on this calculation.

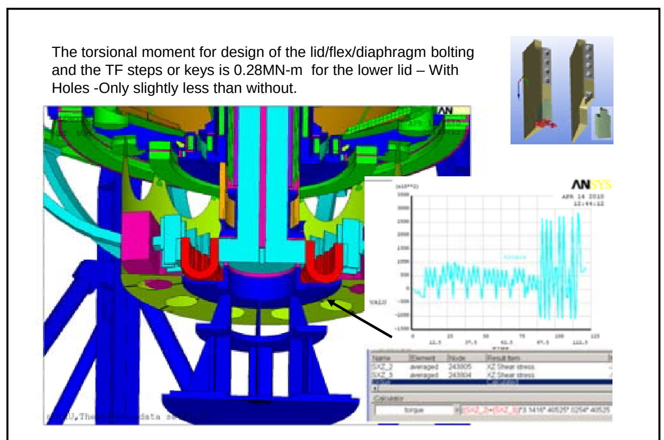

Torque on the lower lid

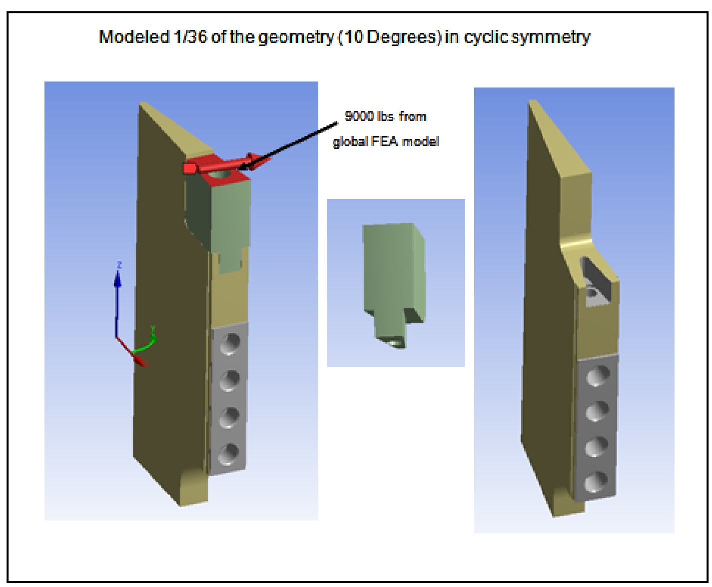

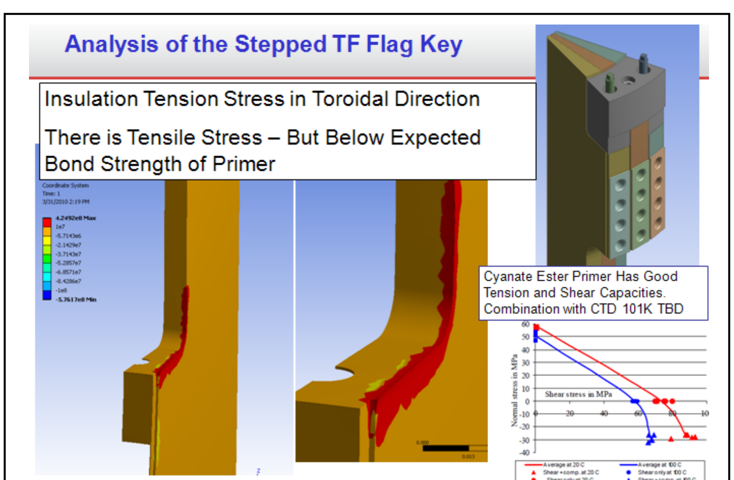

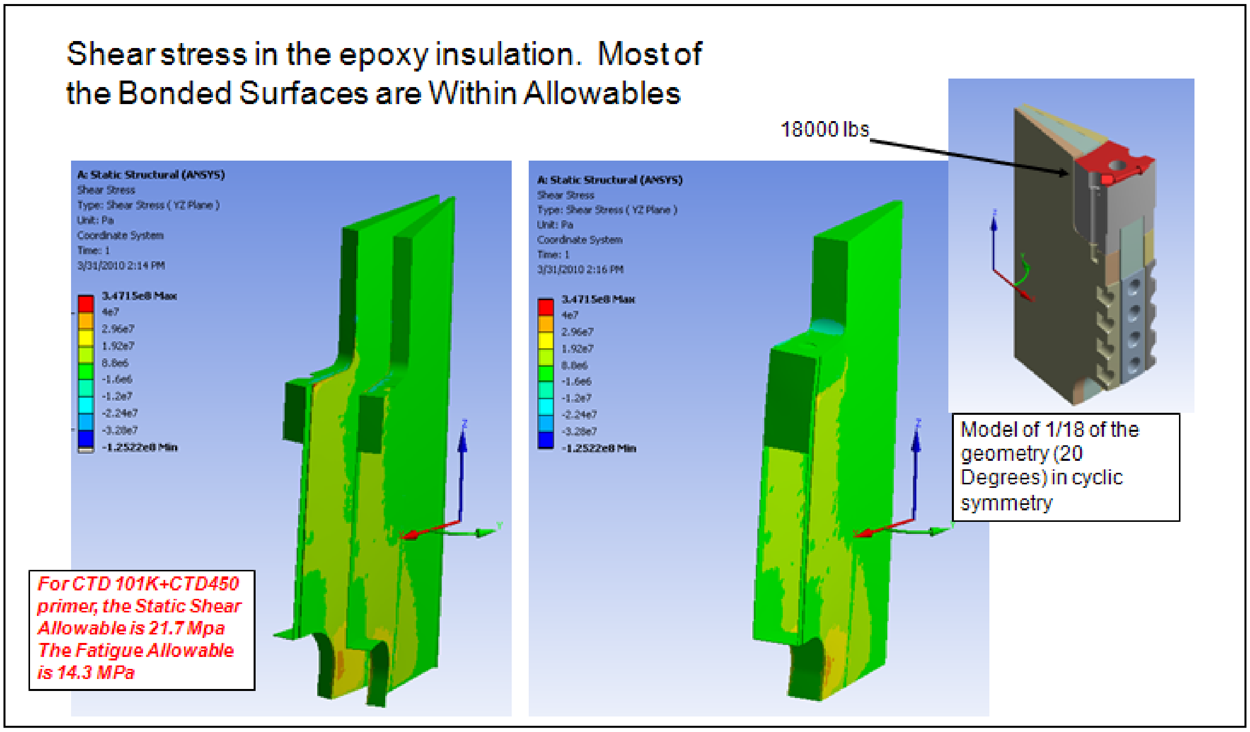
Shear stress in the epoxy insulation. Most of the Bonded Surfaces are Within Allowables
18000 lbs
A: Static Structural (ANSYS)
Shear Stress
Type: Shear Stress (YZ Plane)
Unit: Pa
Coordinate System
Time: 1
3.4715e8 Max
-1.2522e8 Min
Model of 1/18 of the geometry (20 Degrees) in cyclic symmetry
For CTD 101K+CTD450 primer, the Static Shear Allowable is 21.7 Mpa The Fatigue Allowable is 14.3 MPa

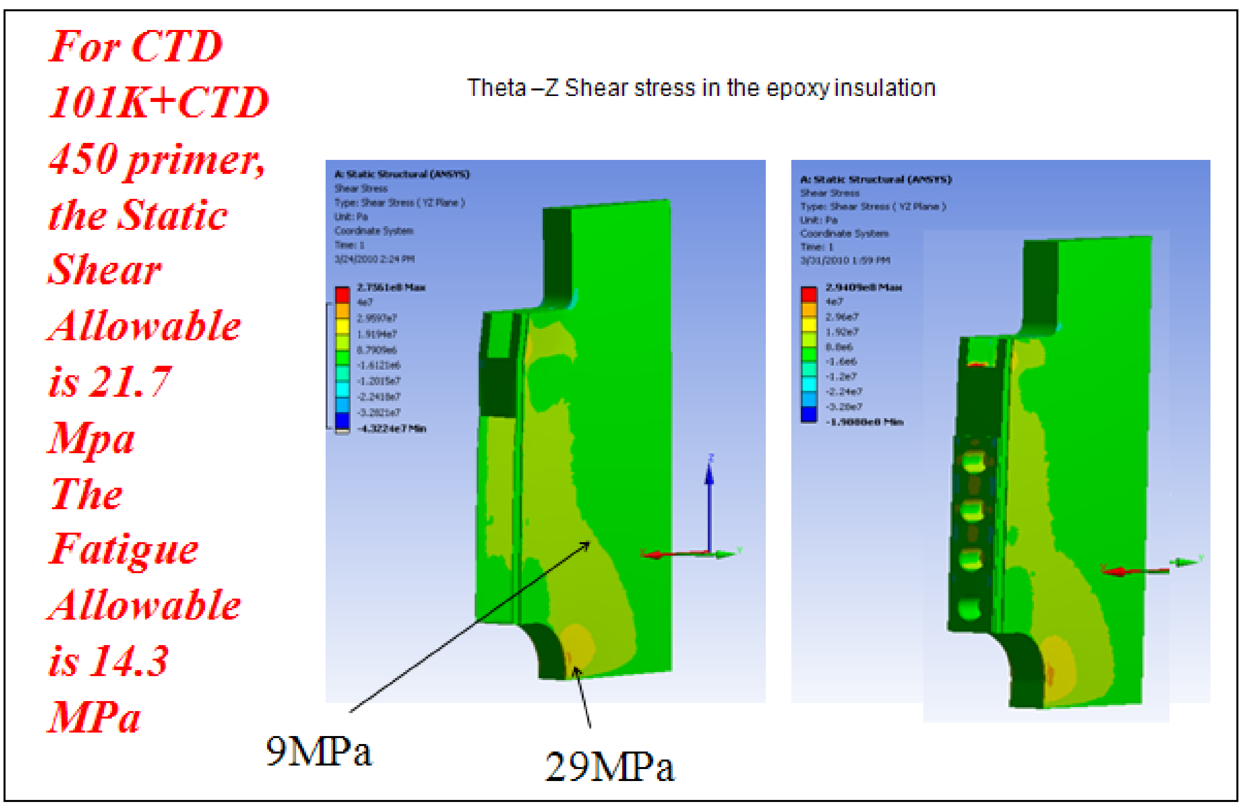
For CTD 101K+CTD 450 primer, the Static Shear Allowable is 21.7 Mpa The Fatigue Allowable is 14.3 MPa
Theta –Z Shear stress in the epoxy insulation
A: Static Structural (ANSYS)
Shear Stress
Type: Shear Stress (YZ Plane)
Unit: Pa
Coordinate System
Time: 1
2.7561e8 Max
-4.3224e7 Min
2.9409e8 Max
-1.9088e8 Min
9MPa
29MPa

Stress Analysis of the G-10 Collar or Crown.

Insulating Material Strengths

	@4	@77	@292 degK
Comp.Strength Normal to Fiber			
G-10CR	749	693	420 Mpa Ref[27]
G-11CR	776	799	461 MPa Ref[27]
Tensile Strength (Warp)			
G-10CR	862	825	415 MPa Ref[27]
G-11CR	872	827	469 MPa Ref[27]
Tensile Strength (Fill)			
G-10CR	496	459	257 MPa Ref[27]
G-11CR	553	580	329 MPa Ref[27]

Large Sstress on G10 crown teeth in both designs

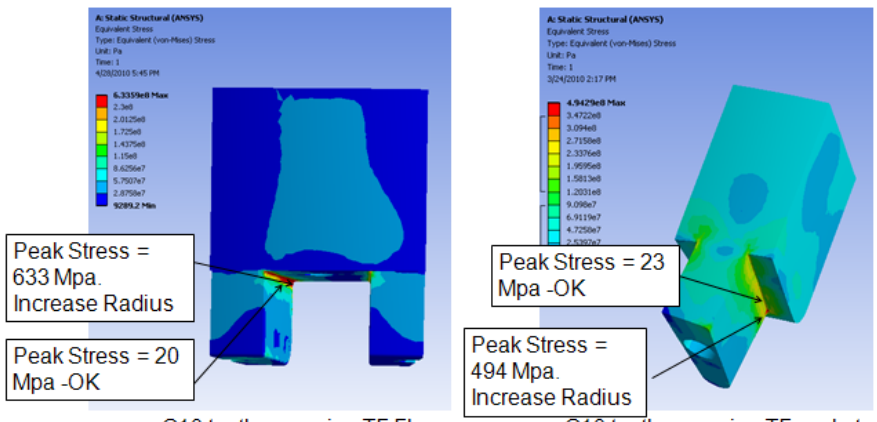

G10 teeth engaging TF Flag G10 tooth engaging TF pocket

Increase Radius, Use 3D weave FRG, or maybe Double Teeth?

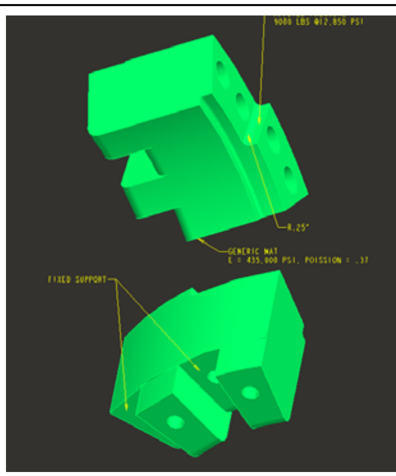

Inner G10 teeth
Load = 9000 lbs
Pressure = 12,850 psi
Radius = .25"
Total load per segment = 18,000 lbs
Generic mat,
Slide 2, E = 2000,000
Slide 3, E = 435,000

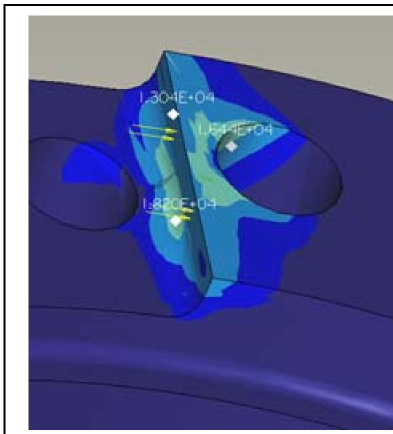

5.4.6.7 Stress at Friction Stir Weld at TF Extension

Aside from the stresses due to the Lorentz Forces

5.4.6.8 TF Flag Extension Flash Shield Detail

The Kapton flash shield addresses flash-over between coil joints, but introduces a geometry that looks initial crack where shear stresses are significant. A proposed stress relief detail is shown at right.

5.4.7.1 OH Analyses in the Centerstack Assembly

The objective of this analysis was to estimate the anticipated stresses in the upgraded NSTX OH coil in various discharge scenarios. Axisymmetric coupled structural /Emag modeling of the OH coil and interaction with PF coils were performed using ANSYS. The OH coil was modeled both as a volume with smeared property and as discrete conductors and insulation volumes. Additionally the maximum stress in the OH coil due to thermal expansion in the TF coils was calculated. This stress results from the fault scenario where the OH coil, which is wound on the TF bundle, fails to energize while TF bundle is energized and expands out thermally.

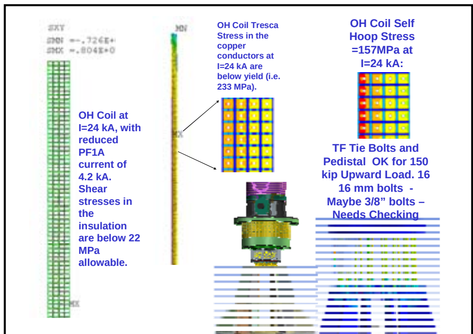

Figure 0-42 Analysis of the OH Coil

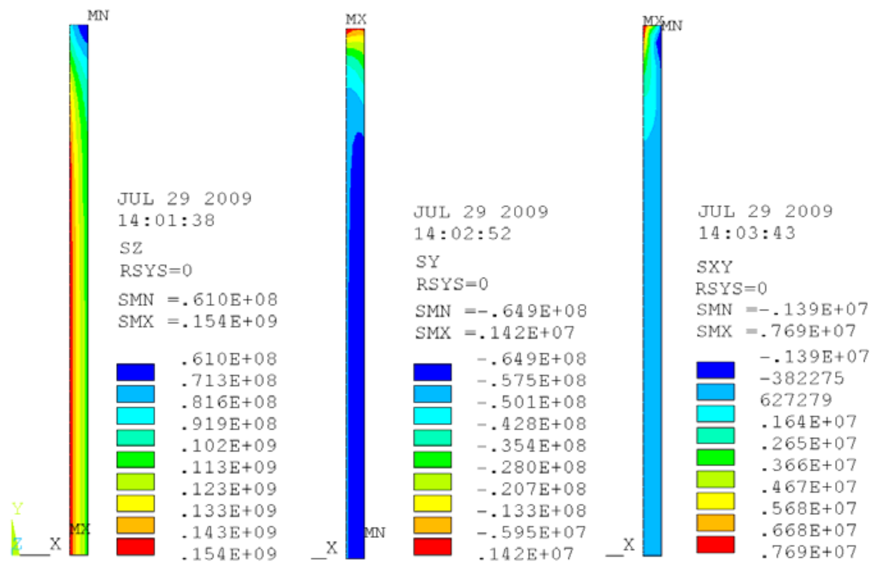

CS Hoop Stress **CS Axial Stress** **CS Shear Stress**

Figure 5.4.7.1-1 "Smeared" - Early Results (CDR level) with only the OH Current

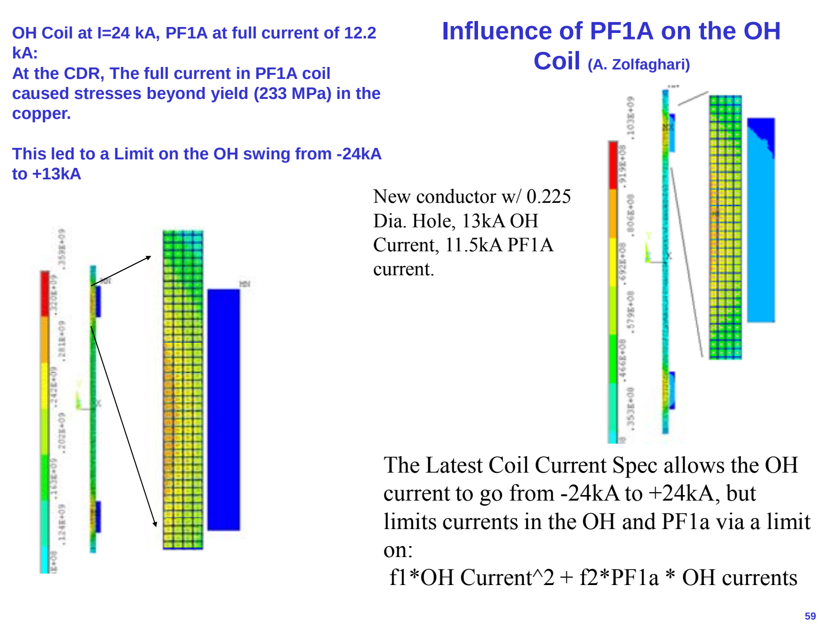

Figure 5.4.7.1-2 Influence of PF1A on the OH Coil

Figure shows the influence of PF1A on the OH coil.

Figure shows the "smeared" results with only the OH current.

Results of the analysis (Figure 0-42) shows that the OH coil can withstand its self hoop stress, shear stress and normal to plane stresses at I=24kA. The analysis also revealed that running the PF1A coil at full 12.2 kA concurrently with the OH coil will cause stresses in the OH conductors beyond yield (233 MPA) in a large fraction of the OH coil cross section inside of PF1A coil. Limiting the OH current swing from +24kA to -13kA will keep this stress below yield. The stress in the OH coil due to hot-OH cold-TF scenario was found to be acceptable but the frictional shear along the length of the TF-OH interface produces unacceptable vertical tension in the OH coil. Mechanical solutions such as low friction interface and removable interface layer as well as electrical solutions in the coil current control system are being considered for this problem. Figure 0-44 represents the CS structure Emag modeling. Tabulated in the figure are the results that show that there is adequate compression in the Belleville spring stack to maintain compressive contact and minimal motion at the lower OH support hardware where the power leads and coolant connections are made. **Error! Reference source not found.** shows the net load on the CS.

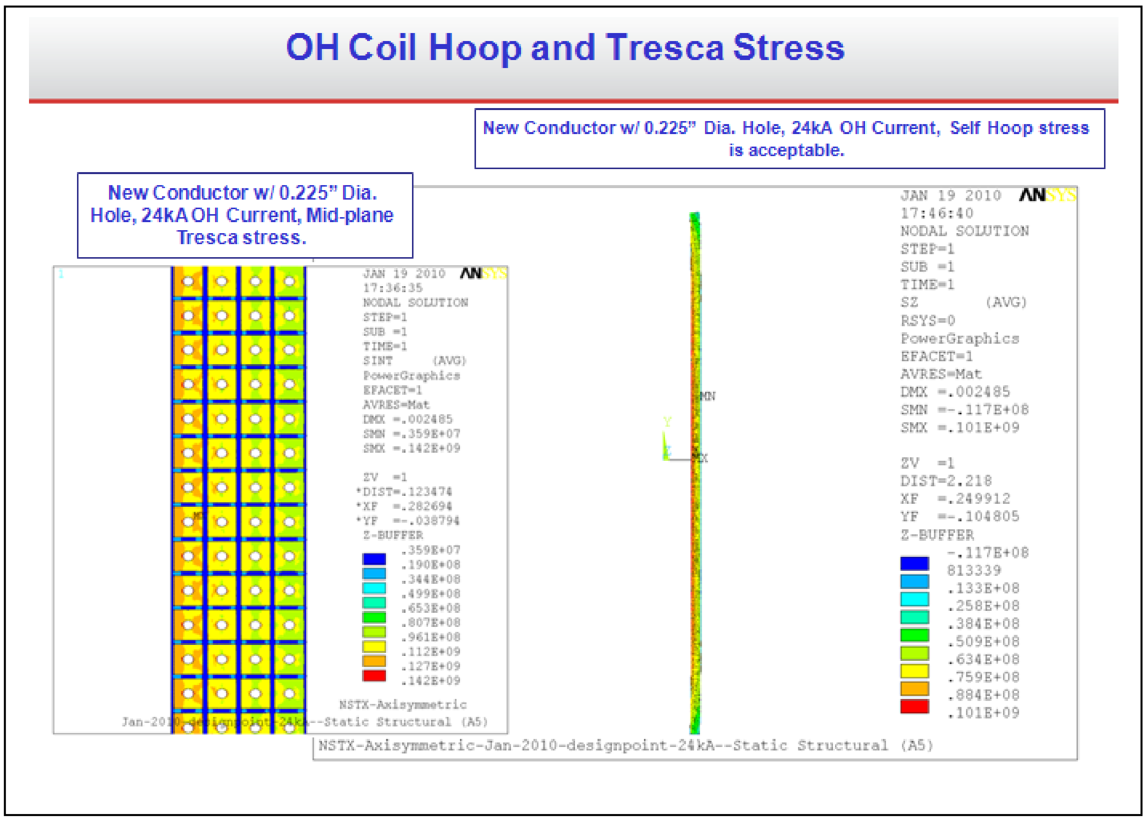

5.4.7.2 OH Preload System

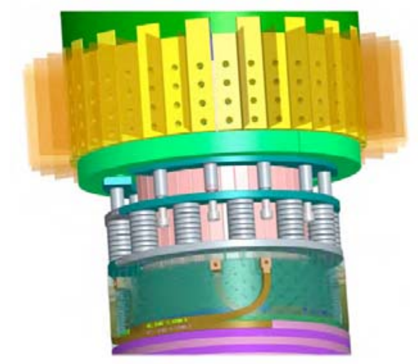

Preload System

The OH coil bears against the bottom flags of the TF inner legs. Relative thermal growth of the OH and TF accumulates at the top of the center stack. An array of Belleville stacks provides preload that is intended to hold the OH assembly down against the lower TF flags. The Belleville stacks must be sized to maintain adequate compression at the bottom end between the coil and TF flags to ensure no relative motion that might disturb the coolant connections or the coax lead assembly in the skirt. Many combinations of coil temperatures and energized states have been considered. The preload system is being optimized to meet the requirements of the design point which has only a 9000 lb max net upward load specified for the OH coil. The system is being designed to resist a 20,000 lb "launching" load to provide some headroom for nominal loads that will be used as a basis for the DCPS set points. The faulted loading is potentially very large - 400,000 lbs. A sacrificial bumper system is being considered to mitigate the effects of the faulted loading.

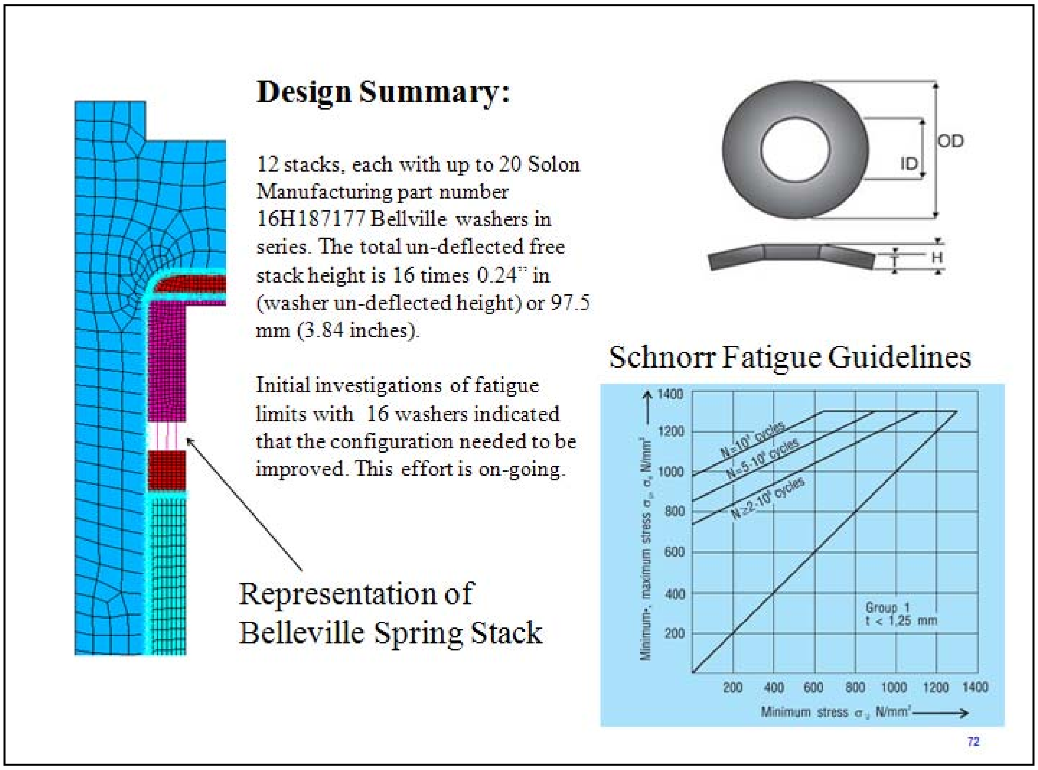

An initial design of the OH Bellville washer stack included 16 Solon 16H187177 washers in series. This was found to result in high stresses that limit the washer fatigue life. A new configuration is being worked on with more washers in order to limit the preload stress on individual washers. The new stack may contain as high as 22 washers. More detail specs have requested on the stainless steel Bellville washers from Solon and Schnorr which will help in final design of the stack.

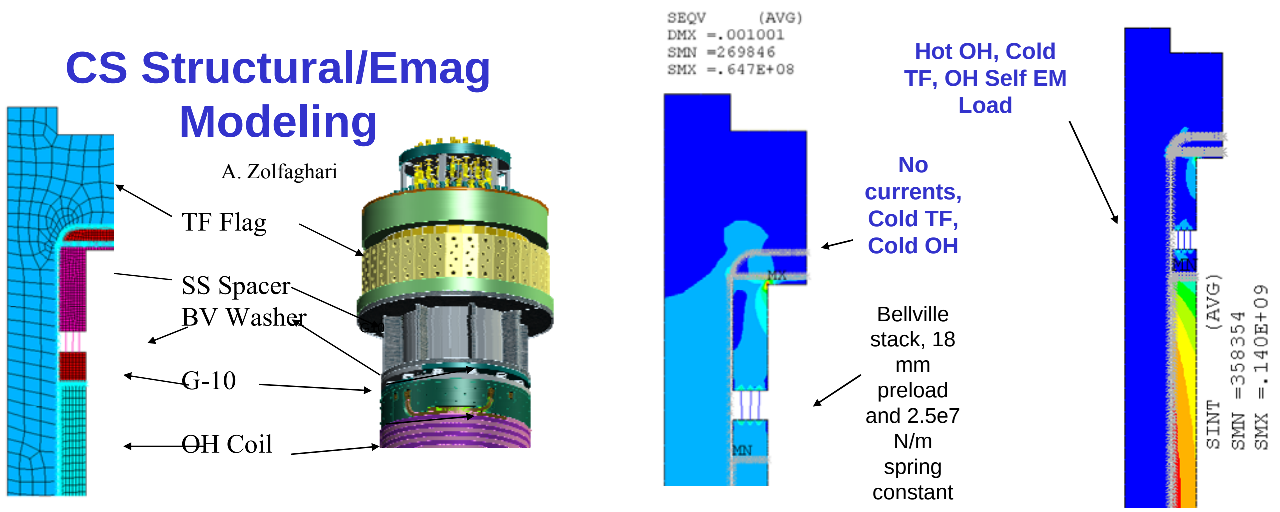

TF Temp.	OH Temp.	TF Current	OH Current	Launch Force	Peak OH Stress	Peak TF Stress	Peak Displacement	OH Lifted?	Case #	Notes
COLD	COLD	OFF	OFF	OFF	7-14 MPA	7-14 MPA	0.6 mm TF	NO	00000	Bellville staff force only
HOT	COLD	ON	OFF	OFF	102-115 MPA	38-51 MPA	8.8 mm TF	NO	10100	TF grows pushing OH laterally
COLD	HOT	OFF	OFF	OFF	10-19 MPA	19-29 MPA	4.6 mm OH	NO	01000	
COLD	HOT	OFF	ON	OFF	125-140 MPA	16-31 MPA	1.6 mm OH	NO	01010	TF was off and OH current was turned on with hoop stress only
COLD	HOT	OFF	ON	ON	123-138 MPA	16-31 MPA	1.9 mm OH	NO	01011	TF was off and OH current was turned on with hoop stress and launch force.
HOT	COLD	ON	ON	ON	117-132 MPA	15-29 MPA	8.2 mm TF	NO	10111	Just in case, OH getting current before heating up
HOT	HOT	ON	ON	ON	110-134 MPA	15-19 MPA	8.3 mm	NO	11111	

Figure 0-44 CS Structure/Emag Modeling

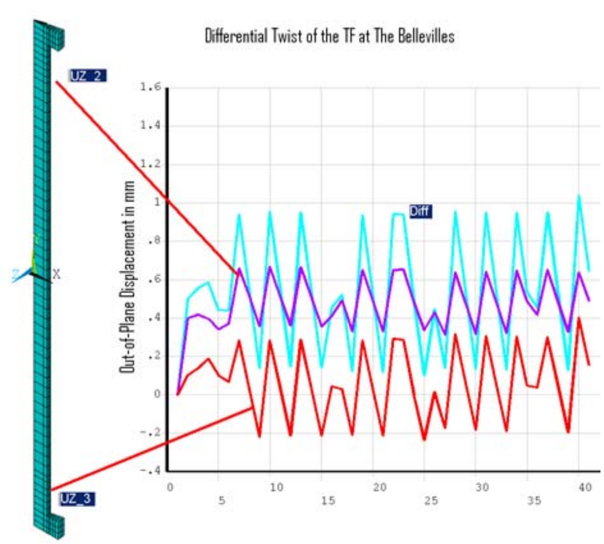

Figure 0-43 Relative Torsional Displacements

Initial sizing was based on the peak Tresca in the conductor. This is interpreted as having a bending stress like distribution with a nearly linear variation across the build of the coil. Figure 0-46 shows some of the analyses that considered these effects. The outcome of these analyses is that that a gap will have to be introduced at the interface. The MAST solution of winding around Teflon impregnated fiberglass strips is being considered. Figure 0-43 shows the relative torsional displacements that must be allowed by the OH Belleville precompression devices. The peak Tresca must pass the bending stress allowable. The average Tresca must also pass the membrane allowable. In Figure 0-47, the Tresca stress across the build of the OH coil is plotted and the average of 168 MPa is above the membrane allowable of 155 MPa. (discussed in section 1.4) During Preliminary Design a bit more capacity was found, with an adjustment in the conductor cross section.

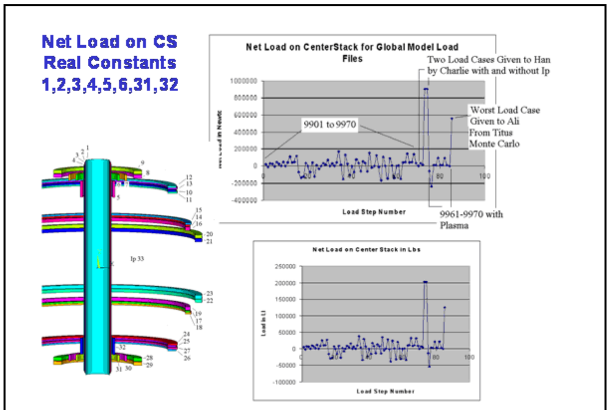

Figure 0-45 – Net Load on CS

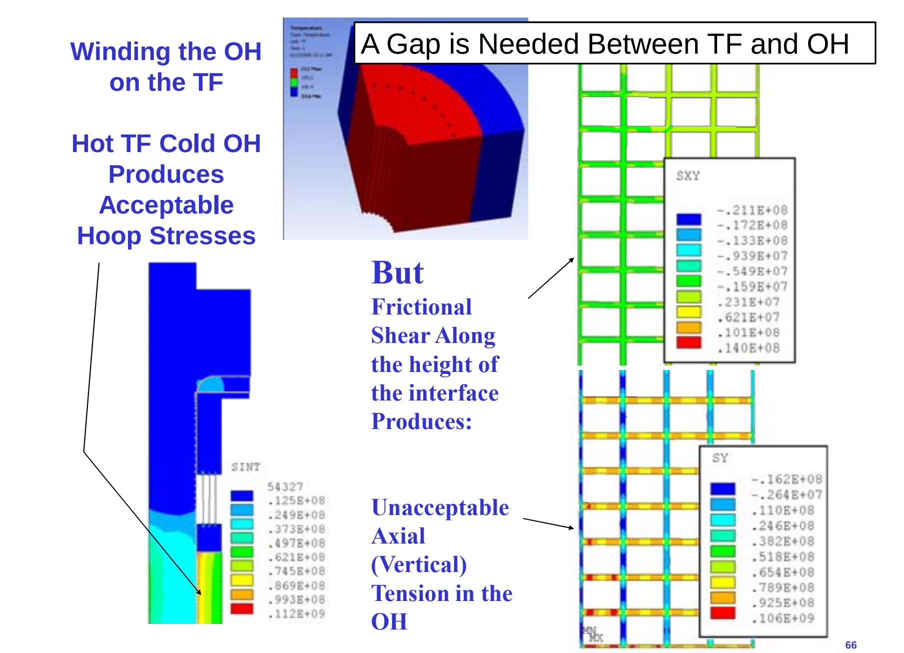

Figure 0-46 Interaction Between the TF and CS

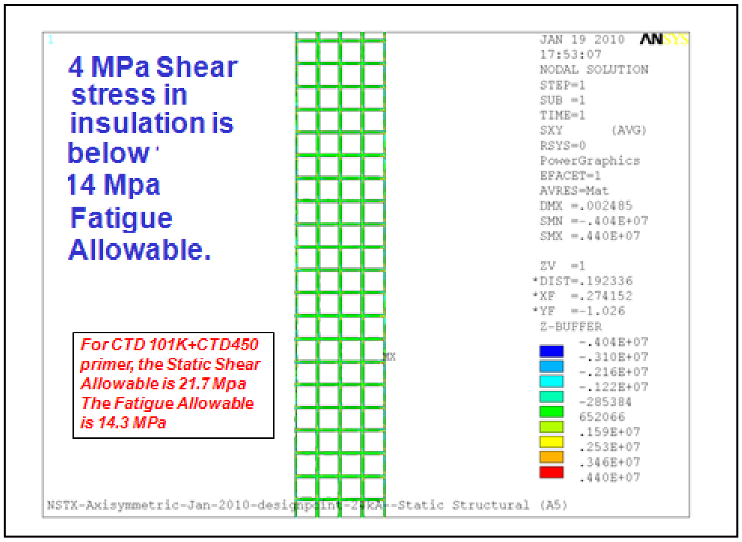

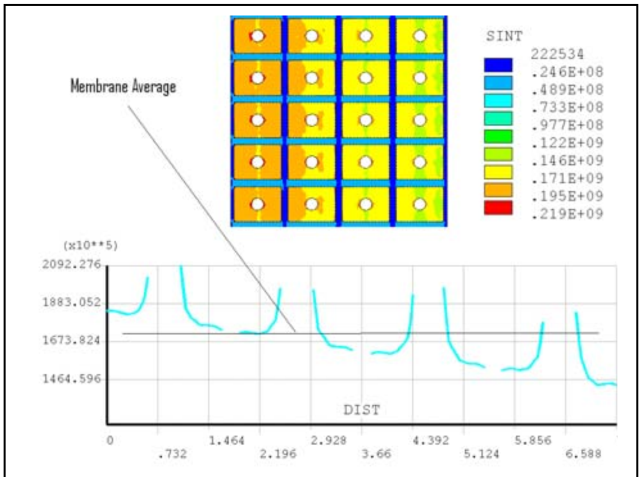

Figure 0-47 – CDR Estimate of Membrane Stress or Average Tresca Across the Radial Build. PDR analyses show adequate margin against thye membrane allowable.

5.4.7.2 OH Conductor Fatigue Evaluation

The OH coil has been sized based on static allowables. Two areas are checked, The peak ID Tresca stress, which must be below 1.5*Sm, and the average stress in the cross section which must be below Sm. NSTX structural criteria, and the GRD require fatigue to be addressed. A couple of possible conductor cross sections are evaluated. Currently the design point is based on a 24 kA conductor with a .175 inch hole. The conductors as currently designed fail the SN based fatigue qualification, but pass a fracture mechanics qualification based on a flaw size less than .5mm^2.

The NSTX criteria document requires either a SN fatigue qualification or a fracture mechanics qualification. The SN qualification requires use of the Tresca to enter the SN curve with factors of safety based on the worst of 2 x Stress or 20 on Life. The Tresca stress for the nominal conductor is shown in figure 1. The peak is 209 MPa. Doubling this to enter the SN curve would indicate no life (Figure 2). The design stress in the OH is well beyond what can be qualified. The alternative is to use fracture mechanics and to implement appropriate NDE on the conductor manufacture to ensure flaw sizes are acceptable for the required life. show the Tresca stresses in the OH conductor. Figure 0-49 shows the typical SN data for Copper.

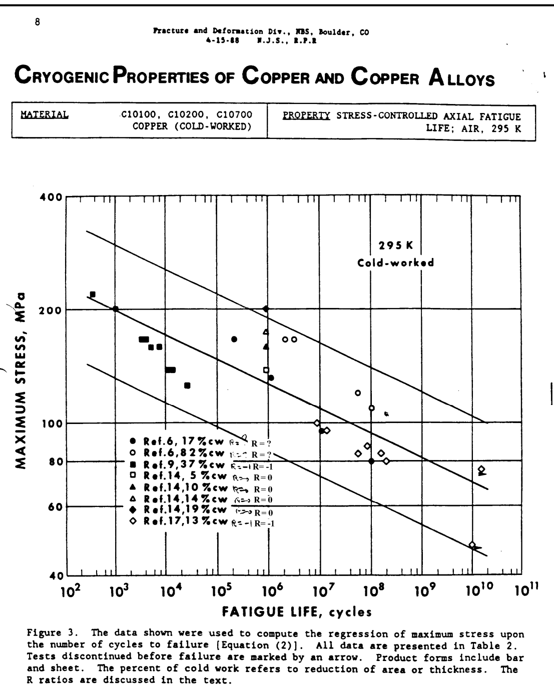

Figure 0-49 - Typical SN data for Copper

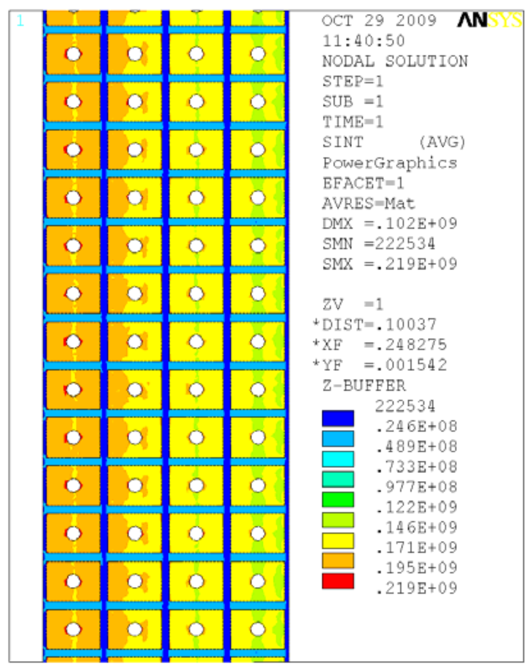

Figure 0-48 - Tresca Stress in the OH Conductor

The basis for the fracture mechanics analysis is summarized in Figure 0-50. This procedure was implemented by Jun Feng to analyze a alternate candidate conductor and the procedure was also used to address the nominal conductor cross section. The following parameters reflect the fracture mechanics information:

- Material
  Hardened copper;
  Paris parameter: C=1.52e-12 m/cycles, m=4.347 ;
  Fracture toughness : $K_{1c} = 150 MPa\sqrt{m}$;
  Walker's coef: 0.8.

- Sample geometry
  Width: 30mm (assumed)
  Thickness: 7.7mm

- Load history
  0 to 149 MPa along axial direction. (Figure 0-51)
  Stress gradient at the hole edge is neglected.

- Crack configuration
  Surface crack at the edge of the hole;
  Initial crack dimension: $0.25mm^2$, $0.5mm^2$;
  Initial aspect ratio: 1.

- Safety factor
  Crack size: 2;

  Fracture toughness: 1.5.

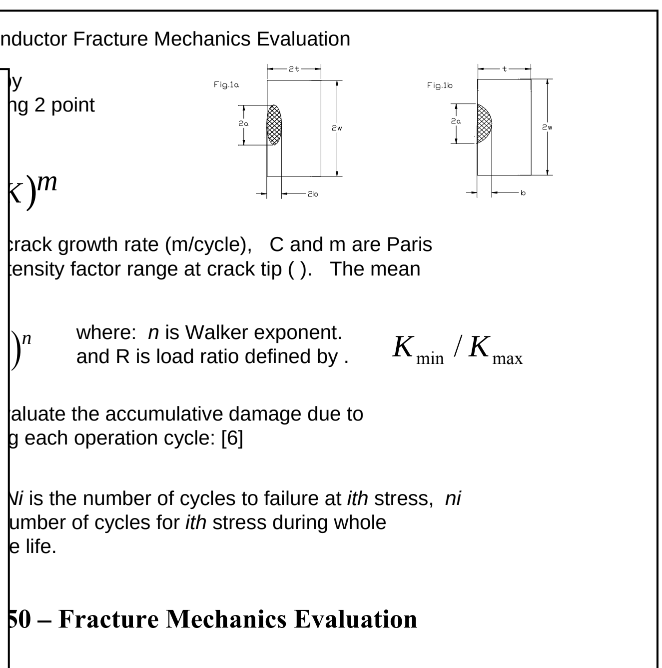

50 – Fracture Mechanics Evaluation

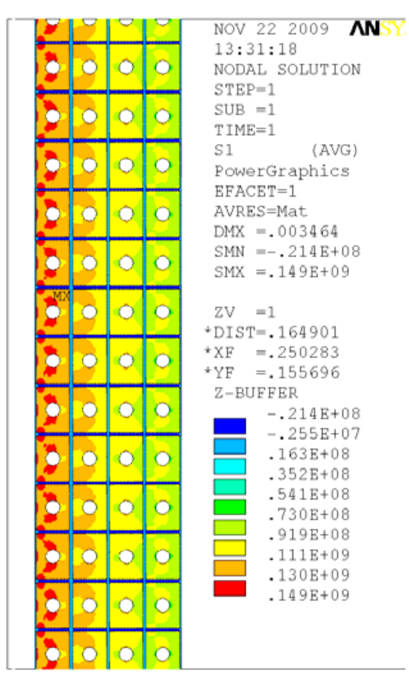

Figure 0-51 - Alternate Conductor Max Principal Stress

Figure 0-52 - Nominal Conductor Max Principal Stress

The results of the fracture crack growth life are shown in Table 0-6.

Table 0-6 Fracture Crack Growth Life

Safety factor	Initial crack size (mm^2)	
	0.25	0.5
Safety Fact Not Applied	701,000	446,000
Safety Factor Applied	446,000	277,000

Titus Calcs (Jun's Program) show:

- 0.5mm^2 crack area;
- 0.707mm crack x 2= .00144 m crack with Safety Factor;
- 145 MPa (Figure 0-51) 201244 cycles
- 175 MPa (**Error! Reference source not found.**) 103416 cycles

This Passes 30,000 cycle (Criteria Doc) Or 60,000 cycles GRD requirement but NDE of conductor will be needed.

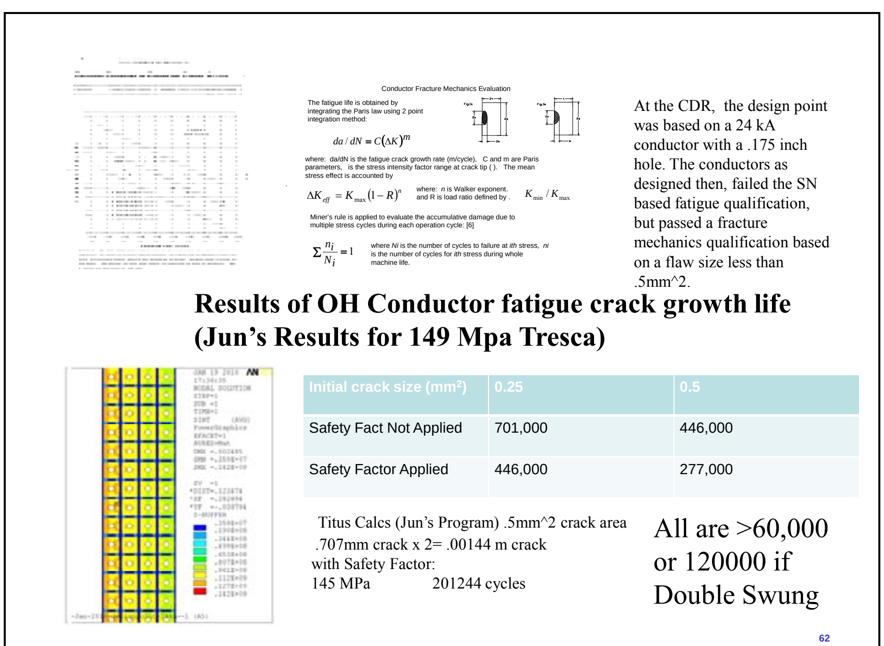

5.4.7.3 OH Coolant Hole Optimization

The objective of this analysis was to estimate the anticipated temperature rise in the OH coil in the upgraded NSTX OH coil during a discharge with 24 kA current and a Tesw of 0.85 seconds. The objective also included estimating the cooling time between OH discharges as a function of pressure drop in the cooling pump. Based on these analyses the coolant channel size was to be optimized in order to keep the maximum temperature of the coil to 100° C. The pump pressure required to keep the cooling time less than 20 minutes were to be estimated.

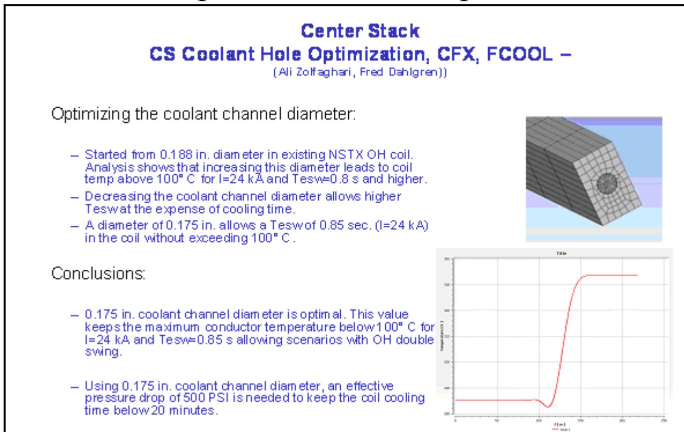

Figure 0-53 Center Stack Coolant Hole Optimization Results Using CFX & FCOOL

The in-house Fcool code and the ANSYS-CFX CFD code were employed to perform the analyses. The results of the analyses showed that a coolant channel diameter of 0.175 in. is optimum in achieving the required Tesw in the coil without exceeding 100° C . The results also show that a 600 PSI pump pressure can provide cooling times less than the 20 minutes required. .

Coolant flow through the OH progresses in a wave that imposes a relatively sharp gradient in temperatures axially along the OH. The thermal differentials may introduce unacceptable stresses in the coil. These will be evaluated during preliminary design. Figure 0-53 shows the results from the CS coolant hole optimization using CFX and FCOOL

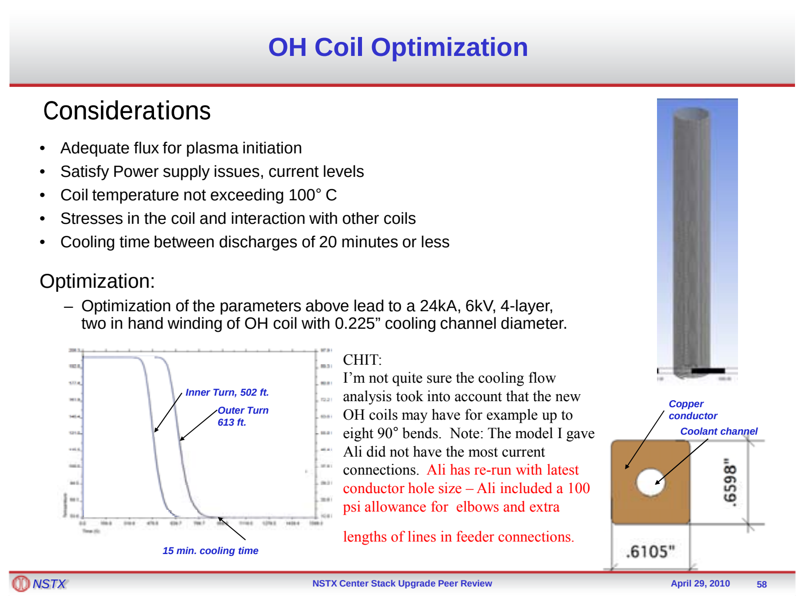

PDR Analysis of the OH Coolant Flow Design

5.4.7.4 Stress Analysis of the Cooldown process.

The four layers of the OH coil have different path lengths depending on their radius. This potentially leads to a non-uniform coil temperature as the cooling waves exit the coil at different times. The thermal stresses that result can cause damage to the insulation. Analysis of this condition yielded over 50 MPa in the turn to turn insulation. Special control of the flow in the four layers will be needed to reduce the thermal gradients at the top of the coil. Design of this flow system and more analysis of the stress state at the top of the coil is planned for the Final Design Activity.

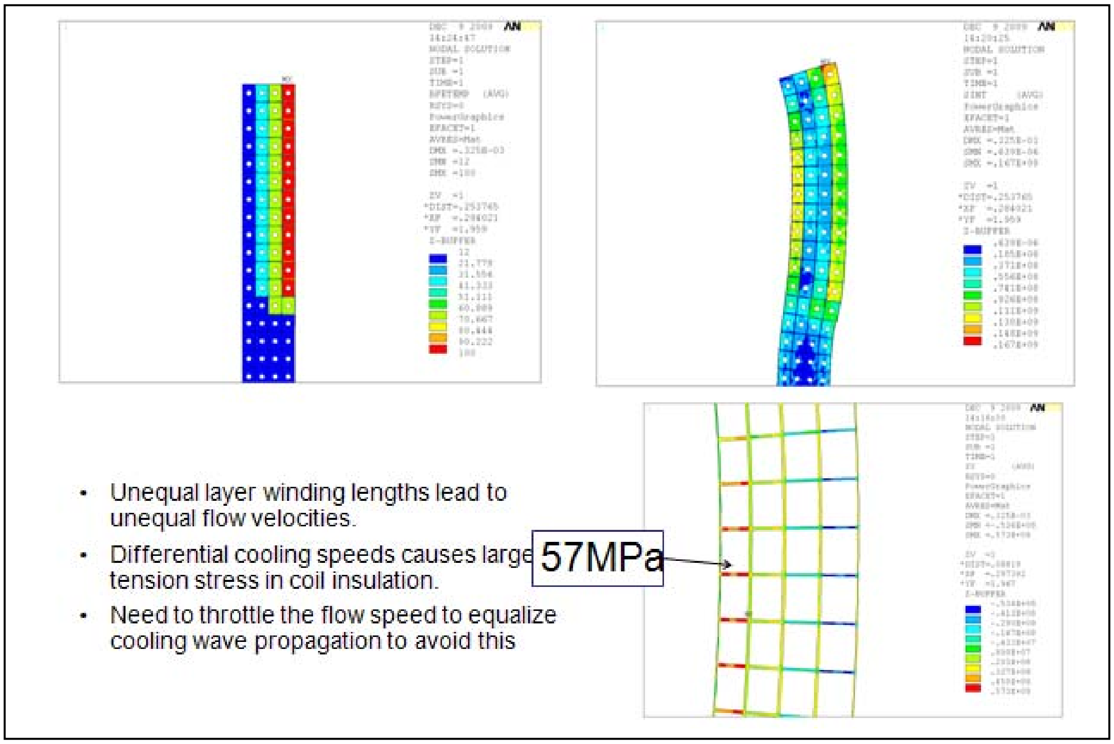

5.4.7.5 OH Cooling Break-Outs

These branches are embedded in a G-10 filler. At the PDR peer review, there was a question regarding the thermal expansion of the leads with respect to the cooler G-10. These are short lengths to accumulate a thermal strain, and they do not carry current and are not loaded by Lorentz forces. With a few layers of Kapton wrap, there should be sufficient compliance. The lap joint at the base of the coolant break-outs does carry current with half the current density of the regular conductor and thus will run cold and produce stresses different than the axisymmetric analysis.

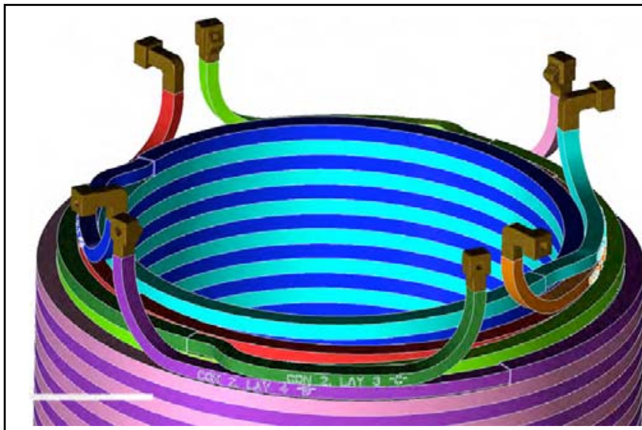

These are actually OH coolant connections that do not carry current .

5.4.7.6 Coax at the bottom of the OH.

The upgrade design repositions the leads to the OH at the bottom of the OH coil, where the coil and connection to the TF inner legs is dimensionally stable Thermal expansions of the coils are upward during operation. The differential motion of TF and OH is accommodated by the Belleville spring stack discussed, in section 5.4.7.2. The conductor connections to the OH coax include some small uncompensated lengths that will be qualified during the final design activities.

5.4.6.8.Inner PF Support Design and Analysis

A structural assessment of the NSTX CSU Inner PF coils (PF1a/1b/1c - Figure 0-54 has been performed based on finite element simulations of the coils and their support structure. A parametric 2D ANSYS EM field model is developed and used to calculate Lorentz forces for each of the 96 equilibria (Menard version F). This also serves as a benchmark for the PPPL force calculation. Nine of these 96 cases produce the largest loads on the subject PF1 coils; faulted conditions are not addressed. The "Worst Case" loads in the design point and in the Monte Carlo Simulation are much larger than is deemed feasible to support with the spaces allotted to the inner PF supports and coolant hardware (Figure 0-55).

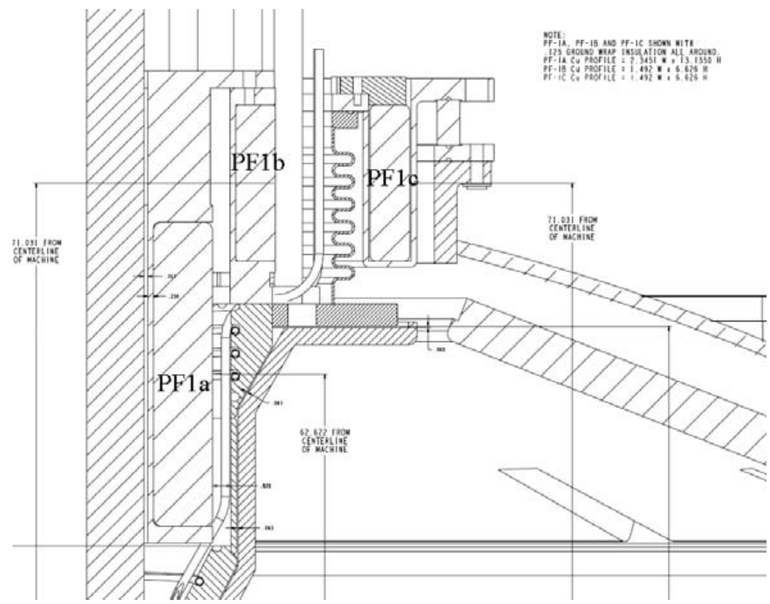

Figure 0-54 Layout of Inner PF Coils

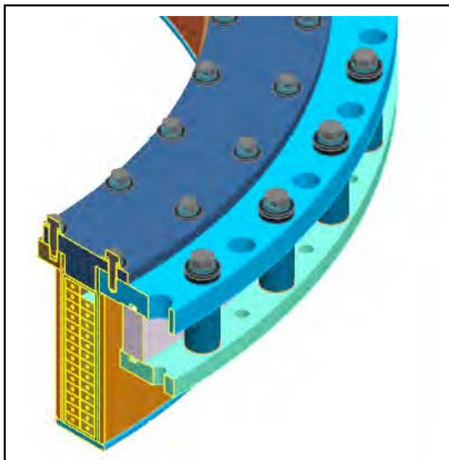

PF1c and the ceramic break showing the viton O rings.

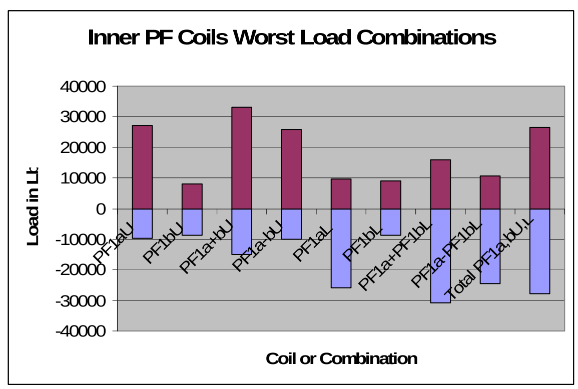

Figure 0-55 Inner PF Coils Worst Load Combinations

The 2D stress analyses indicates that an 80 kip launching force on PF1c requires a more robust hold-down design to stiffen the open coil case. A full cover is recommended over the four hold-down clips design. The 100 kip centering force on PF1a produces some bobbin flange deformations which would benefit from a slight increase in their thickness and/or stiffening gussets. Cu and insulation stresses are generally OK, but would gain some margin with any increases to the structure discussed above.

A 3D stress analysis is used to evaluate the non-axisymmetric structural elements of the support design. The model shows that the PF1a gussets which link the coil bobbin to the PF1b bobbin flange should be thickened and radiused. The net vertical loads which pass down through the three legs to ground produces some large bending stresses which must be addressed with a design/analysis cycle. The PF1c case needs a full cover with ID & OD bolt circles. Figure 0-57 displays the inner PF supports. Figure 0-58 shows the inner PF analysis results.

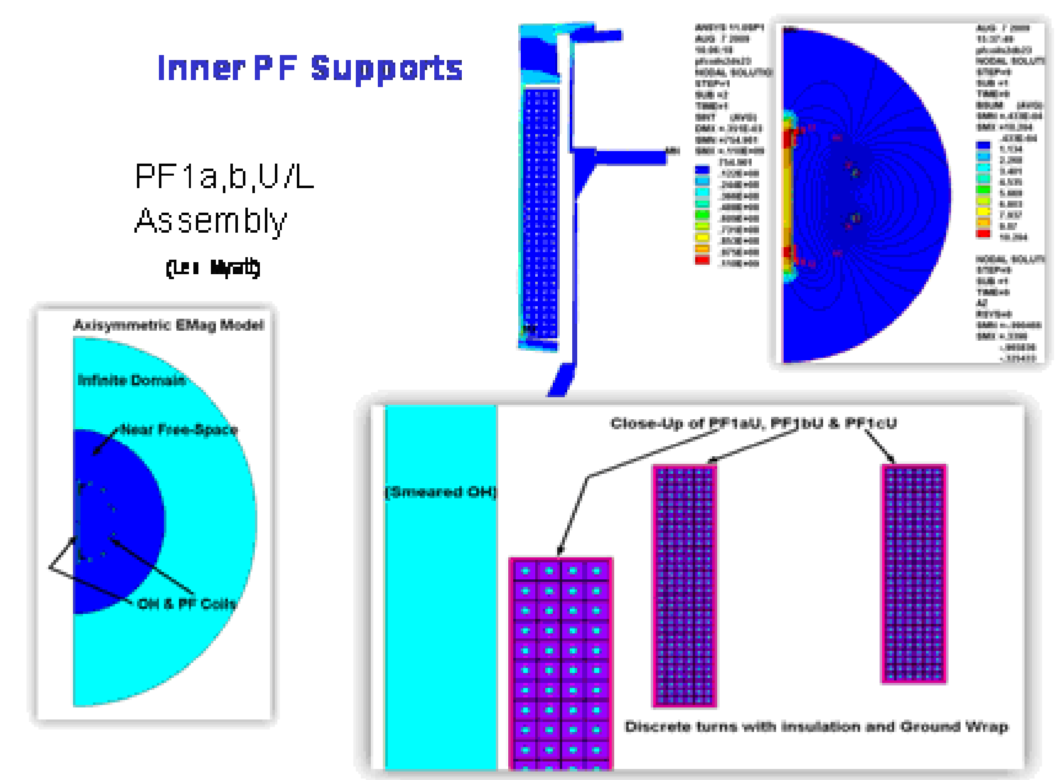

Figure 0-56 Inner PF Support Analysis Models

Figure 0-57 Inner PF Supports

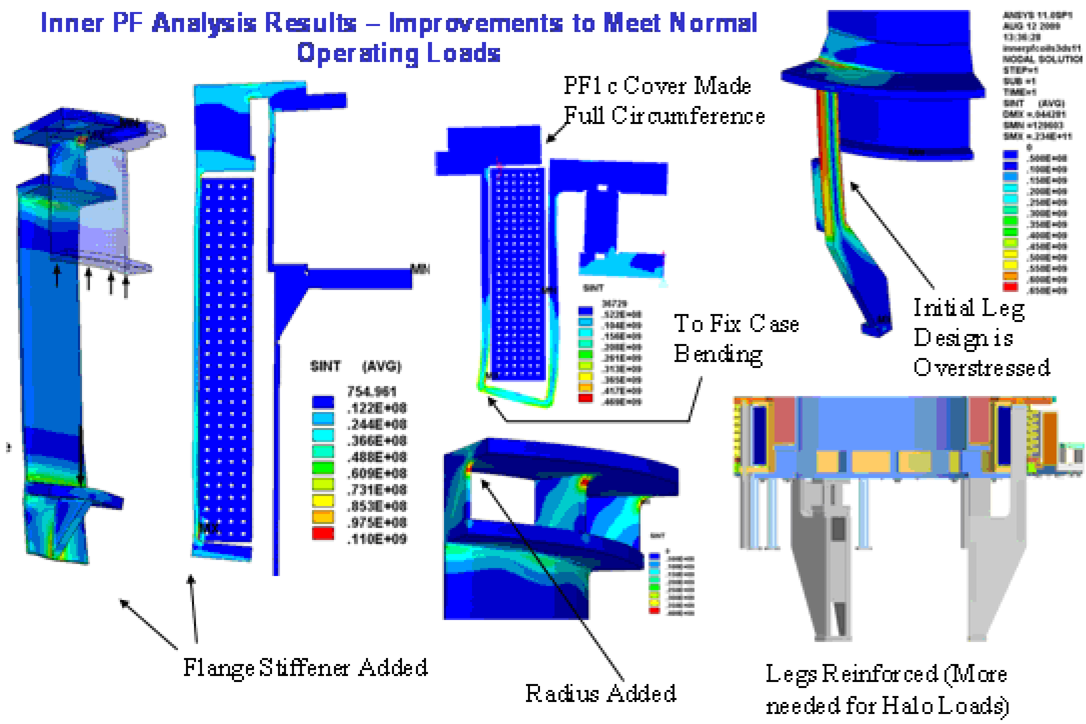

Figure 0-58 Inner PF Analysis Results

Poloidal Field Coil Lateral Stability

The centerstack stability with respect to the rest of the poloidal coil system relies on the stiffness of the Upper and Lower Lid – and some centering system of the OH with respect to the TF. (bumpers in the gap? lateral stiffness of the Belleville spring stacks?) Other stabilities need to be addressed.

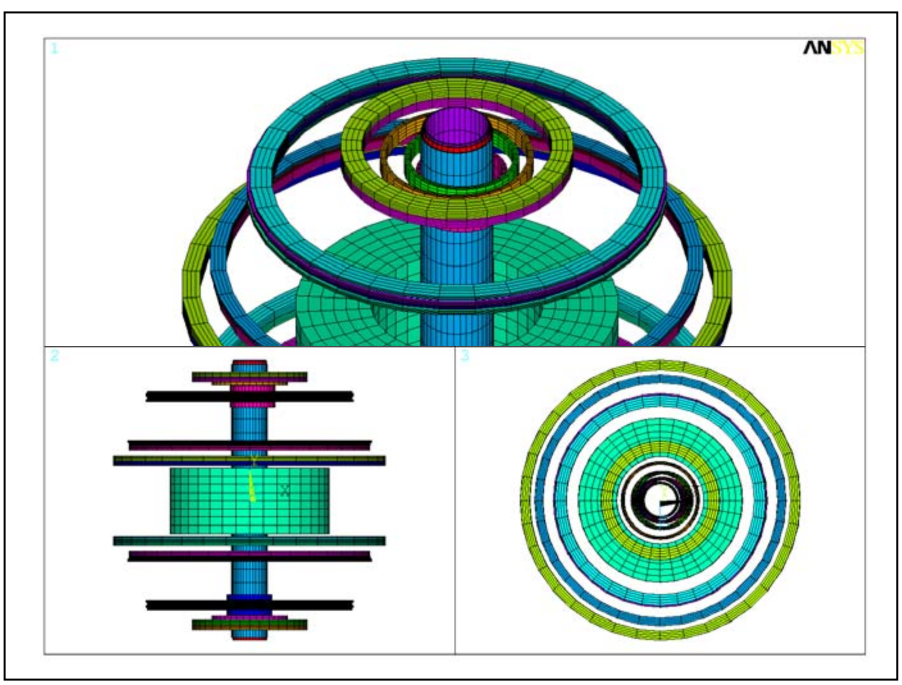

PF1a - OH Lateral Stability

PF1a is supported off the centerstack casing which is stabilized laterally by the bellows/ceramic break assembly. The stiffness of the supports must be sufficient to overcome the magnetic stiffness. To quantify the magnetic stiffness the Lorentz force between the OH and PF1a coils was calculated for different lateral offsets.

Pf1a and Oh coils dimensions and arrangement were used from the latest design point.

Coil	Current (kA)	Turns
OH	24	884
PF1a	18.3	64

The PF1a is moved 2mm and 5mm in the positive Y direction.

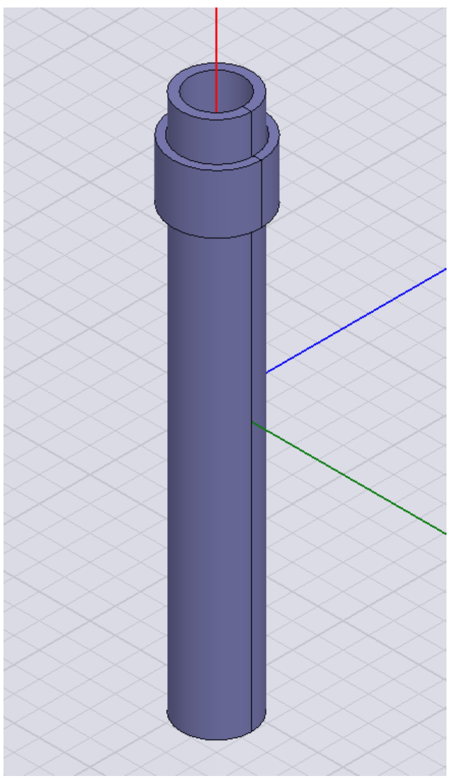

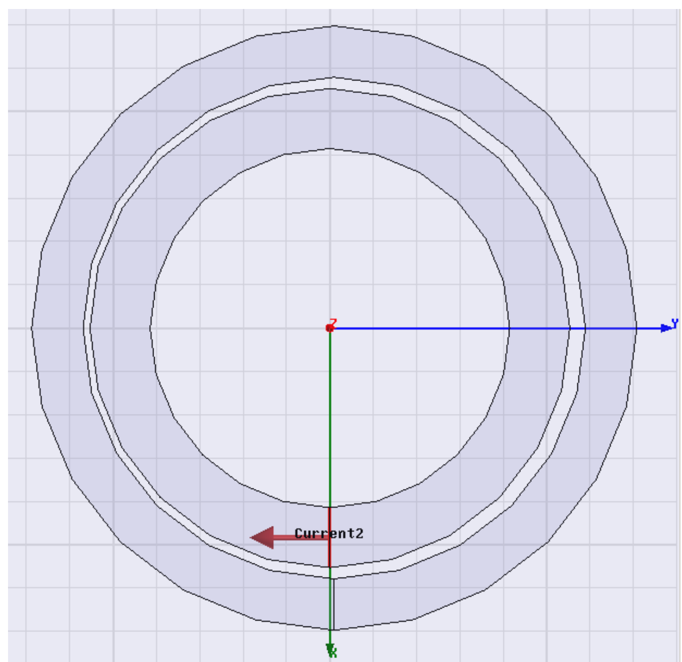

Orientation of currents	PF1a Offset (mm) in +Y direction	Force on PF1a (N) in +Y Direction
Parallel	2	1191
Opposite	2	-1255
Parallel	5	3167
Opposite	5	-3189
Parallel	0	-141
Opposite	0	125

PF1a and b Upper Lead Supports

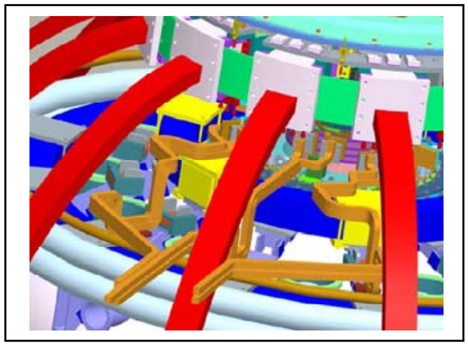

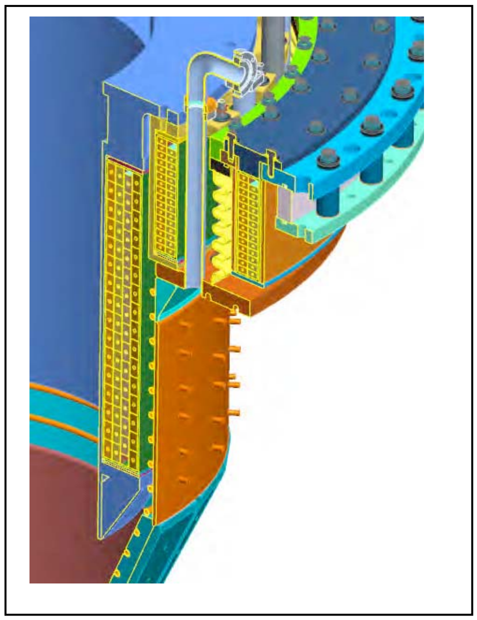

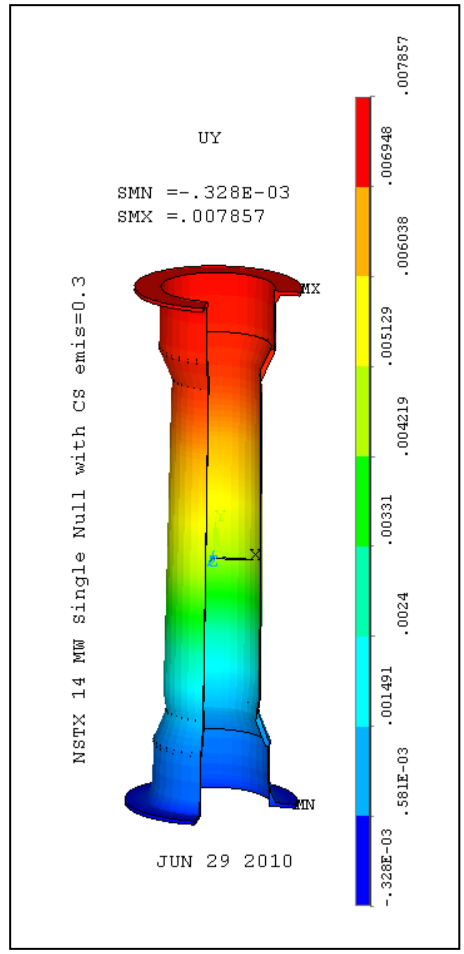

PF 1a and b are supported off the centerstack casing which is subject to thermal expansions excursions that will raise the PF1a and b coils with respect to the top of the vessel. The upper bellows will have to absorb this displacement and still maintain the vacuum boundary and not over stress or load the ceramic break. Also the leads for these PF's will have to be supported to resist the Lorentz loads, but still be flexible enough to allow the thermal growth of the centerstack casing. Art Brooks has calculated the thermal expansion of the casing. This \is shown at right. The design of the PF1a and b leads is similar to the present NSTX OH lead which has the same conflicting requirements of support of the magnetic loads while allowing growth of the OH .

The bellows have been investigated in the global model with an estimated temperature distribution - also derived from Art Brook's work. The global model results are summarized below:

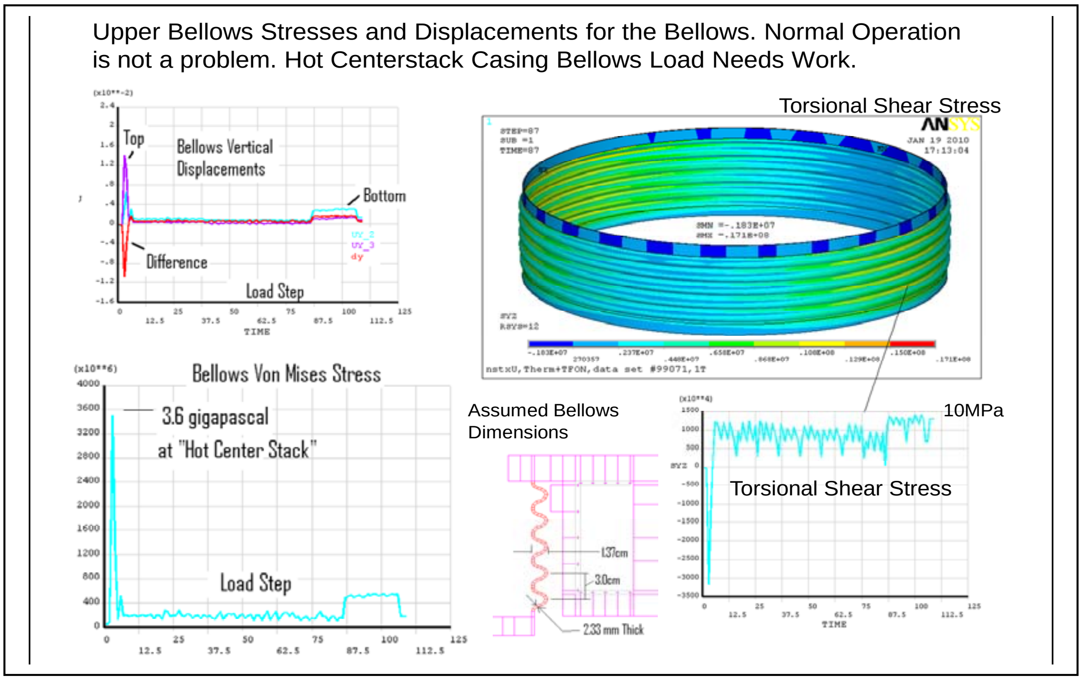

The vertical displacement difference at the bellows of 1.2 cm, is overestimated by the global model simulation. The 3.6 GPa stress report is for a convolution geometry that was subsequently improved.

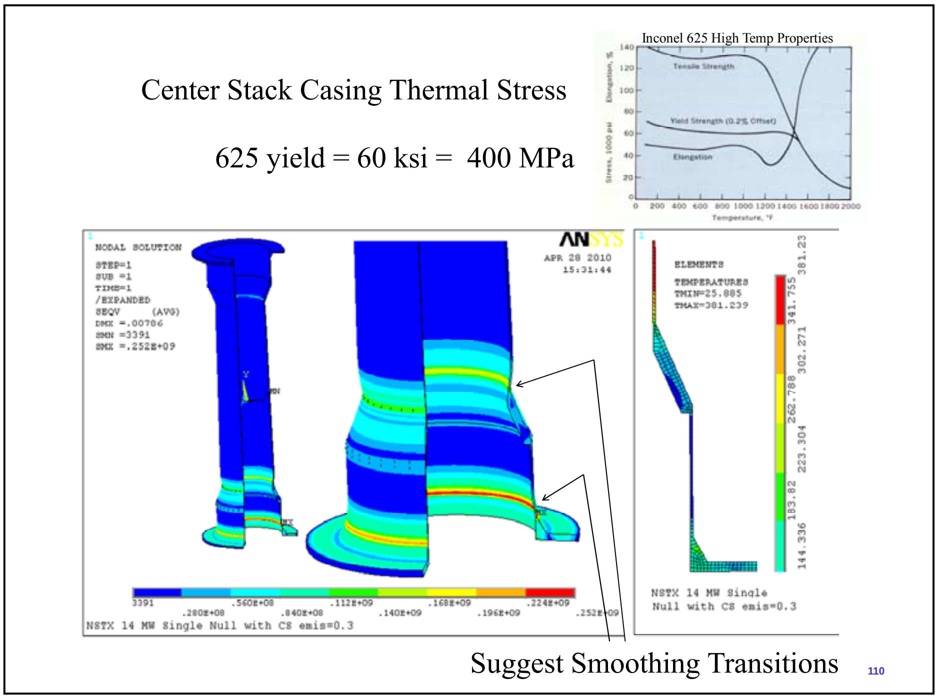
Center Stack Casing Thermal Stress
625 yield = 60 ksi = 400 MPa
Inconel 625 High Temp Properties
Tensile Strength
Yield Strength (0.2% Offset)
Elongation
Temperature, °F
NODAL SOLUTION
STEP=1
SUB =1
TIME=1
/EXPANDED
SEQV (AVG)
DMX =.00706
SMN =3391
SMX =.252E+09
APR 28 2010
15:31:44
ELEMENTS
TEMPERATURES
TMIN=25.885
TMAX=381.239
NSTX 14 MW Single Null with CS emis=0.3
Suggest Smoothing Transitions
110

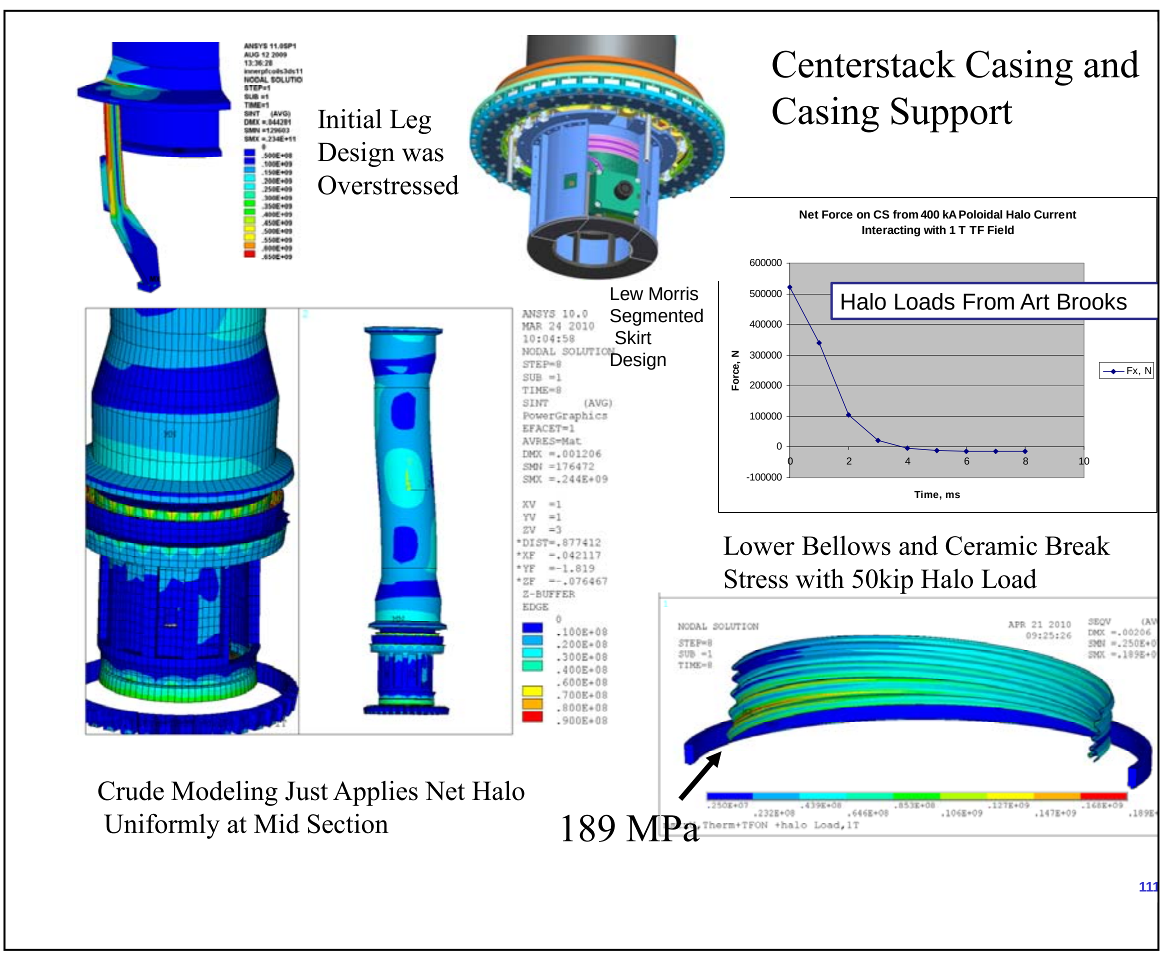
Centerstack Casing and Casing Support
Initial Leg Design was Overstressed
Lew Morris Segmented Skirt Design
Net Force on CS from 400 kA Poloidal Halo Current Interacting with 1 T TF Field
Halo Loads From Art Brooks
Force, N
Time, ms
Fx, N
Lower Bellows and Ceramic Break Stress with 50kip Halo Load
Crude Modeling Just Applies Net Halo Uniformly at Mid Section
189 MPa
111

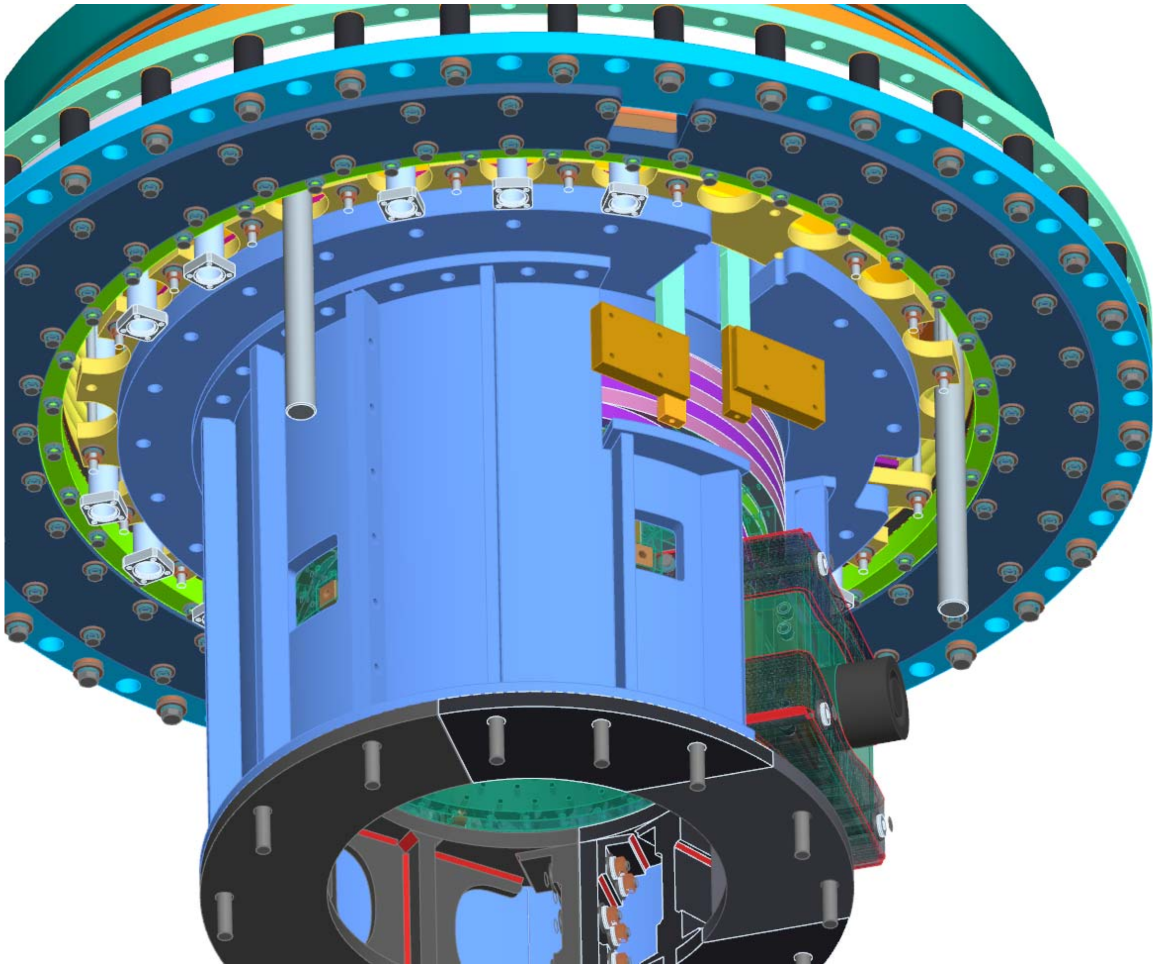

Lower Skirt center stack support

Figure 0-59 Lower Support Skirt Replaces Legs

Differential thermal strains can lead to high bending stresses in the shell structure. However, a more detailed and consistent thermal-stress analysis is required.

5.4.6.9 Pedistal Analysis

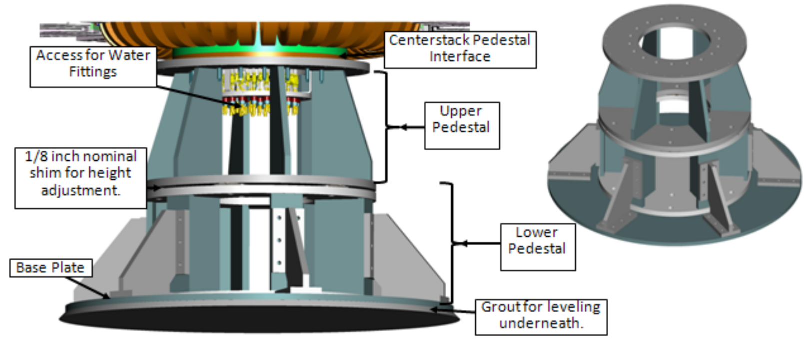

Figure 5.4.6.9-1 Pedistal

The pedistal is the main vertical support for the centerstack. It must allow access to the coolant lines, bus bar connections and instrument lines principally servicing the centerstack. The design chosen for the PDR is torsionally compliant, vertically stiff and strong, and laterally "strong enough". Torsional complience is more a need of the global analysis of the moment transfer from the centerstack to the outer section of the vessel throug multiply redundant or statically in-determinant connections through the TF flags and then to the outer vessel

/lower lid. There is also a torque connection through the pedistal to the ground then to the vessel support legs. Additionally some torque is transferred through the skirt to the centerstack casing then through the bellows to the outer vessel. The design presented at the PDR is the one for which these load paths have been analyzed. Other more torsionally rigid designs have been proposed and may be found attractive during the FDR.

The pedistal contributes to the lateral support of the tokamak during an earthquake. The braced column supports are the main lateral support for the tokamak for this loading. Halo currents can develop net lateral loads that would be transferred throught the skirt to the pedistal. Figure 5.4.6.9-2 shows the pedistal analysis results. The bending stress in the vertical gusset is 130 for the halo + DW loading and 130 MPa for the Normal operating currents +DW.

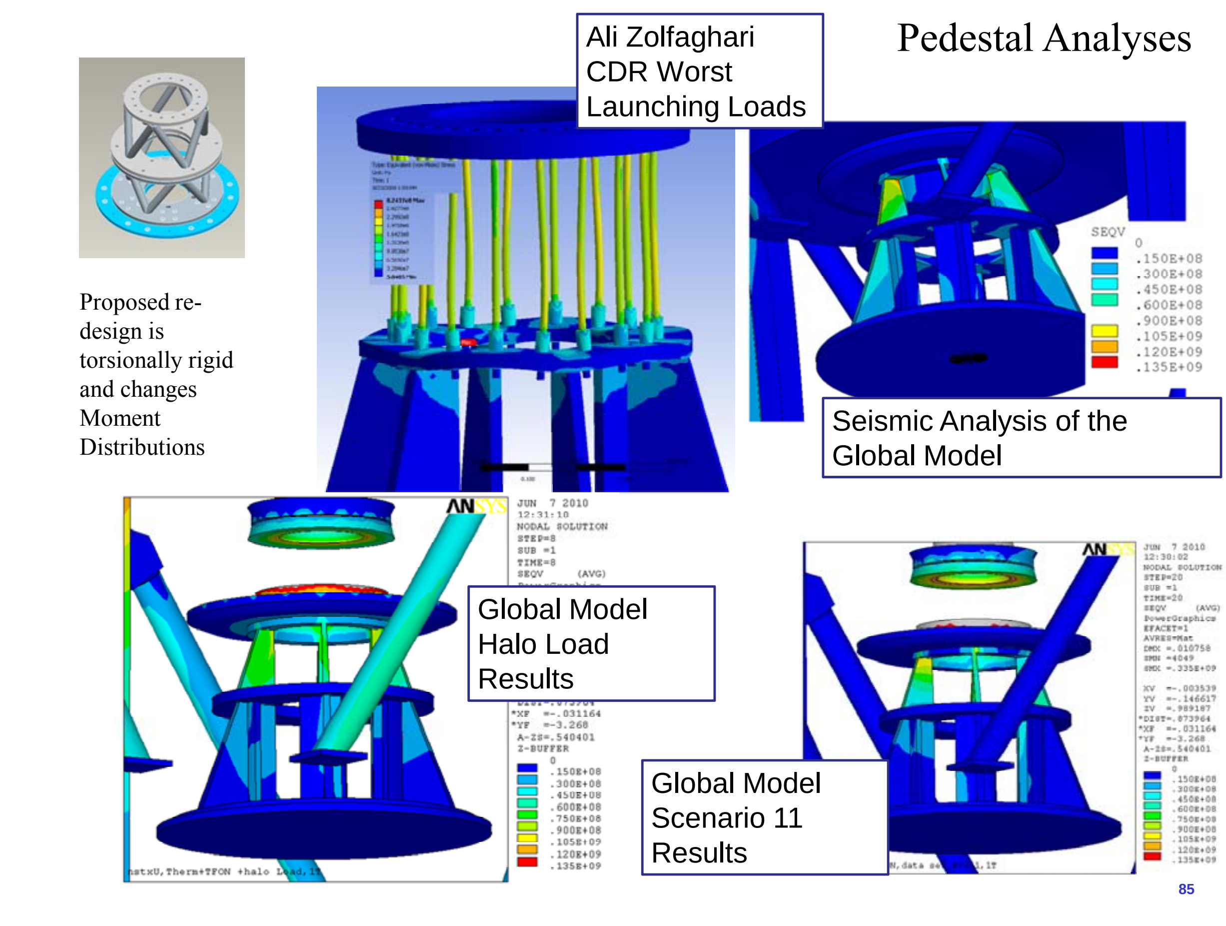

Figure 5.4.6.9-2 Pedistal Analysis Results.

5.4.6.10. PF Coil Hoop Stresses

PF coil hoop stresses(exclusive of the OH coil) are small for all the postulated coil currents, including the worst case power supply currents. The OH coil is the most severely loaded and continues to push the allowable stress.

5.4.6.10-1 shows the “smeared” hoop stresses. Figure 5.4.6.10-61 is representative of the PF coil hoop stress. Figure 5.4.6.10-62 shows the maximum and minimum hoop stresses based on Ron Hatcher’s influence coefficients..

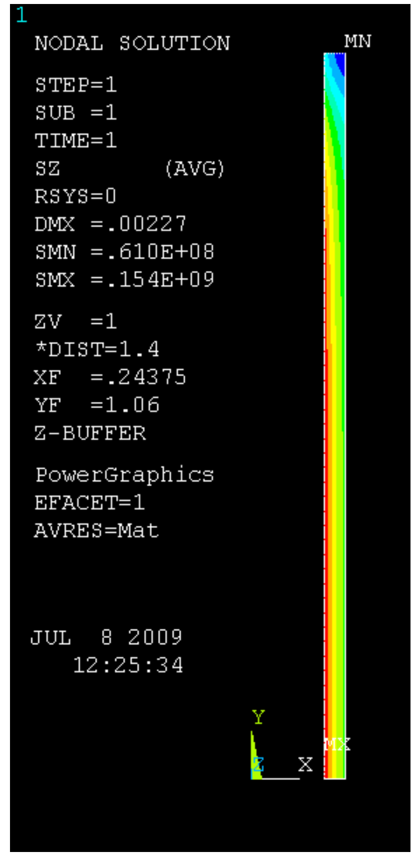

Figure 5.4.6.10-60 - OH “Smeared” Hoop Stress

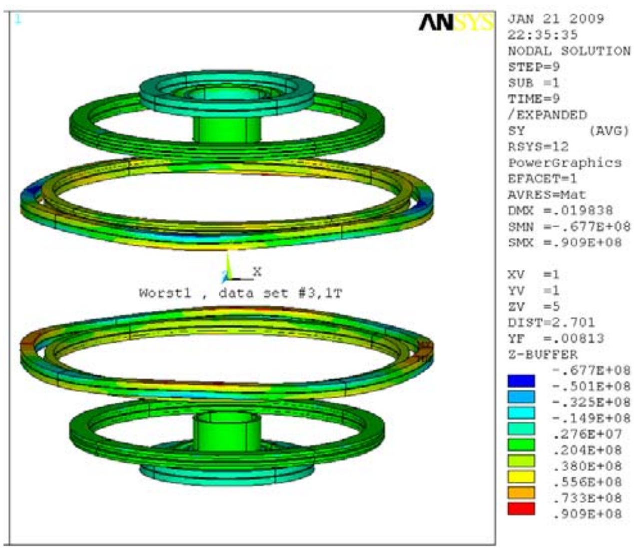

Figure 5.4.6.10-61 .-. Representative PF coil Hoop Stress

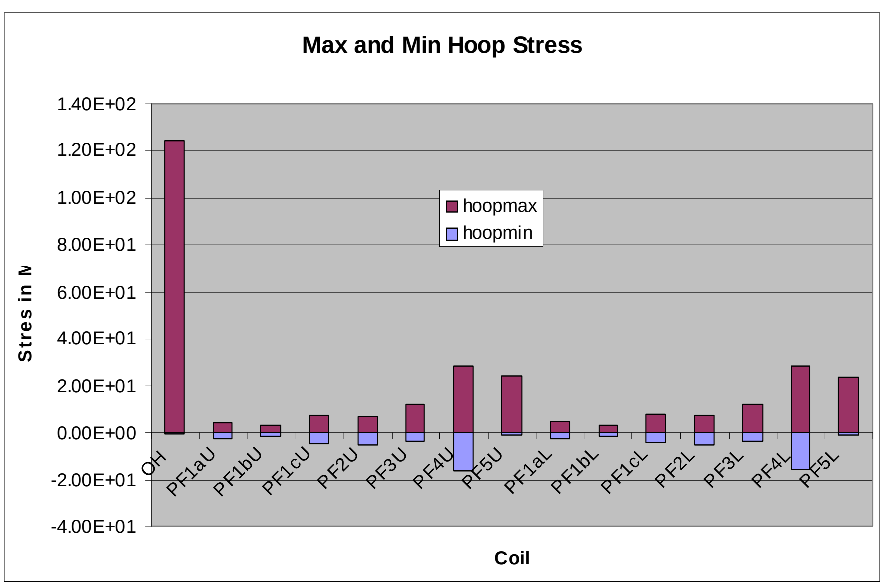

Figure 5.4.6.10-62 – Maximum and Minimum Hoop Stress

5.4.6.9 PF 2 and 3 Supports

5.4.6.9.1 PF 2 Support Design and Analysis

As of the CDR The vessel dome has been analyzed with the maximum loads PF1c and PF2. The stresses are acceptable for these loads (Figure 0-63) but this analysis does not include the full complement of loading - Umbrella loads, global torques etc. The global model includes these.

As of 2010, there are 6 support brackets connecting PF2 to the vessel ribs. There are 11 support ribs and at the original construction of NSTX, Only six supports were necessary.

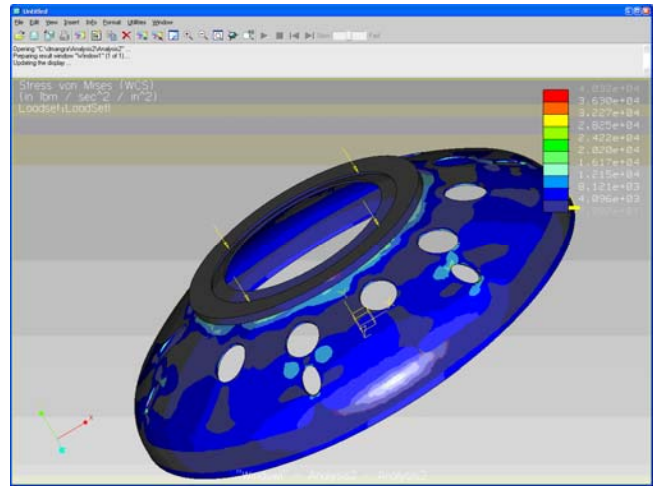

Figure 0-63 PF2 Support Model

PF2 is supported at 6 places with brackets that use four 1/2 inch bolts to clamp the coil. the bolt P/A stress is 47456/6/4/.1416=13,830psi for the 96 scenario max tensile load – if evenly distributed at 6 locations. - but it is not evenly distributed.

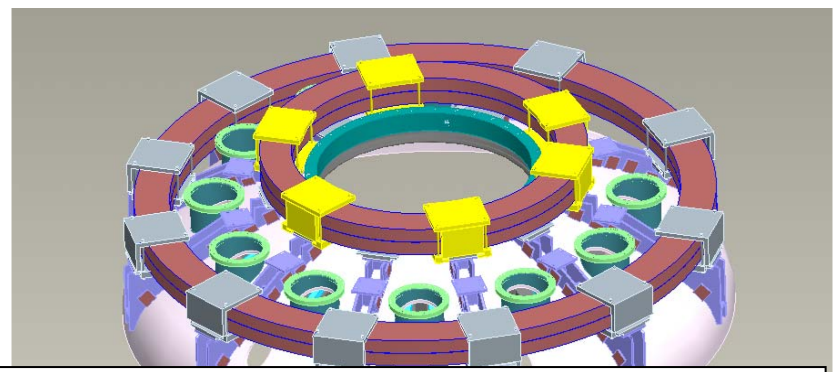

Fz(lbf)	PF2U	PF2L
Min	-41256	-47456
Worst Case Min	-148494	-151752
Max	47456	40174
Worst Case Max	151752	148525

Loads from the June 2010 Design Point

Currently there is one span that looks about 45 degrees. This would distribute the bolt loads more like Fvert/4/4 rather than Fvert/6/4. There would be some rotation as well that might change the loads in the bolt pattern at the clamp and would need some more FEA. This could probably be qualified to the 96 scenario loading, but would have no margin for faulted loads or any headroom for the DCPS. 47456/4/4/.1416 = 20ksi which is OK for standard bolts, but more analysis of one side of the clamp vs. the other (ie. the rotation effect) would be needed.
If you add the 7th support then one side looks like Fvert/6/4 and the other side looks like Fvert/8/4. This is better and doesn't need more analysis to accept.

The weld drawing shows 3/16 inch fillets as under the PF2 support plate. With a weld efficiency of .7 the allowable for a fillet is 14ksi, or 96 MPaThe plate is 9 inches long. There are four 3/16 inch fillets for a total weld area of   4*9*3/16*.707 = 4.77 square inches per pad. There are now six pads. If the loads are evenly distributed this would produce a 6 * 4.77* 14,000 = 400,000 lbs. This would even satisfy the worst case loading.

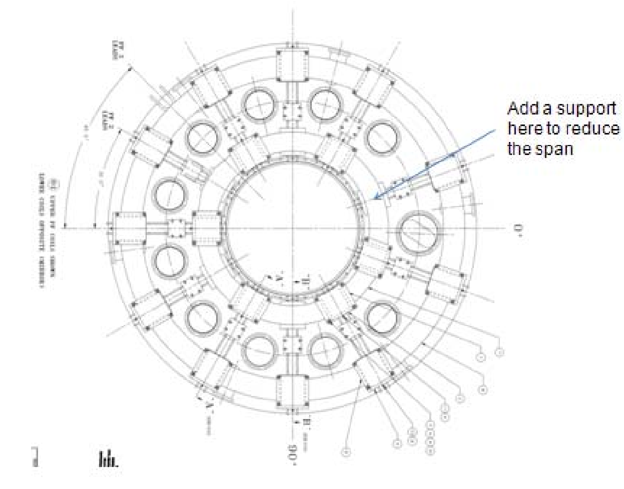

Current (2010) locations of the PF2 supports, and the proposed location of the seventh support

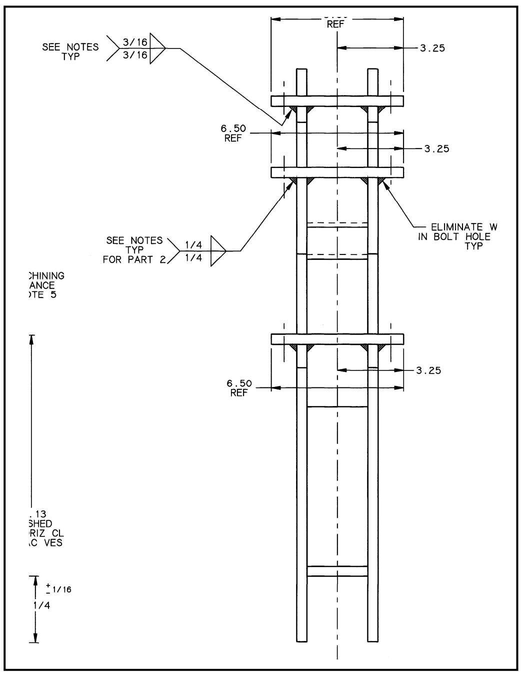

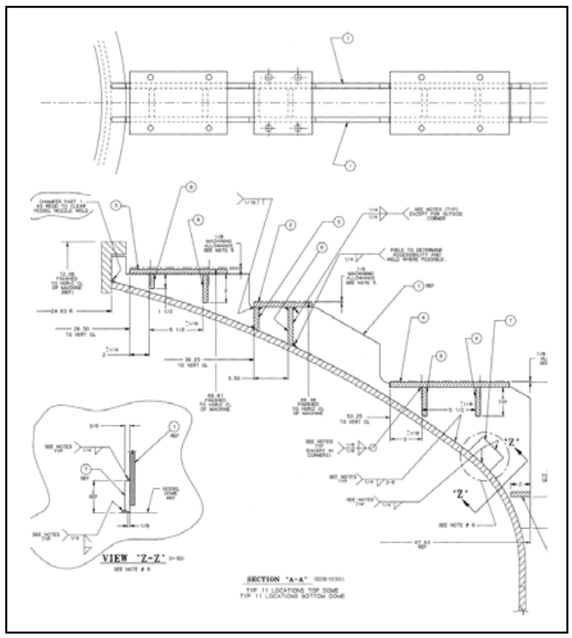

5.4.6.9.2 PF3 Support

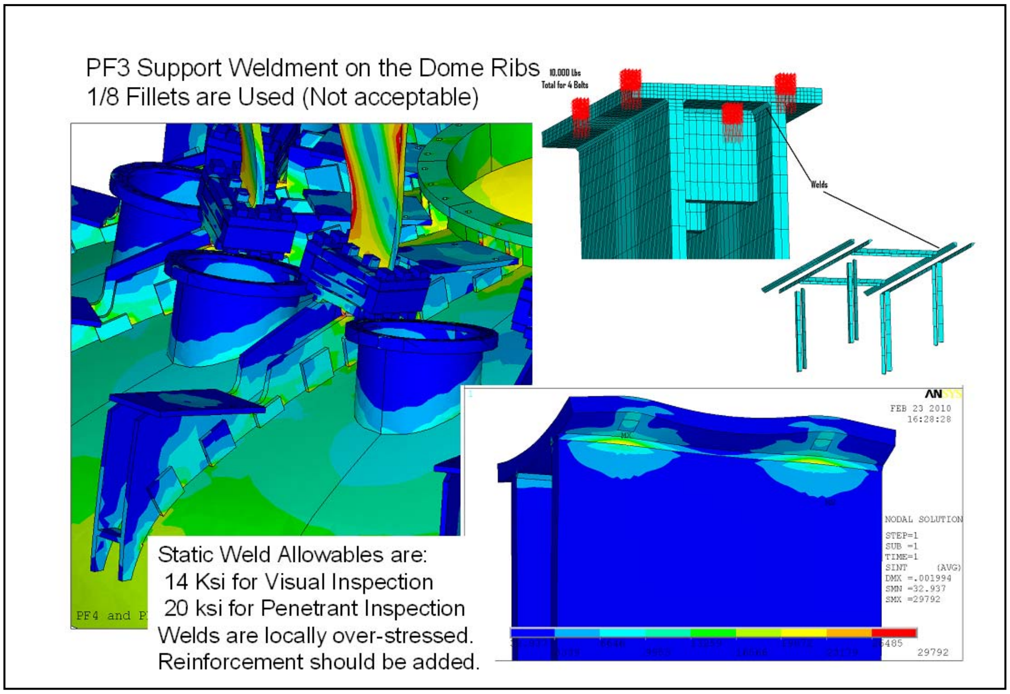

PF 3 is supported by the ribs that are welded to the vessel dome. The connection of the support plate to the ribs is by 1/8 fillets that run around most all of the plate intersections. Average stresses on this weld could be considered acceptable, but the weld size is smaller than recommended by AWS, AISC, and ASME for plates larger than 1/4 inch. The weld concentration under the bolt holes is actually aggravated by starts and stop of the welds. The upgrade plan is to increase the size of these welds. The bolt

5.4.6.12 PF4 and PF5 Supports

5.4.6.12.1 CDR Cage Design

An early outer support frame or cage was an attempt to design the outer PF supports to the extremes of maximum loads resulting from the power supply limits. The max and min vertical loads in the structural elements of the proposed outer PF support cage are presented in Figure . These loads were developed assuming support at the bottom with some sort of column or strut either to the ground or to the vessel support columns/legs. These loads are from the Monte Carlo analysis (Figure) based on worst case PF power supply capabilities. If this concept had not been too costly, it would be worth considering as it de-couples the PF supports from the thermal and mechanical displacements of the vessel. Table shows the vertical load cases for the outer PF supports.

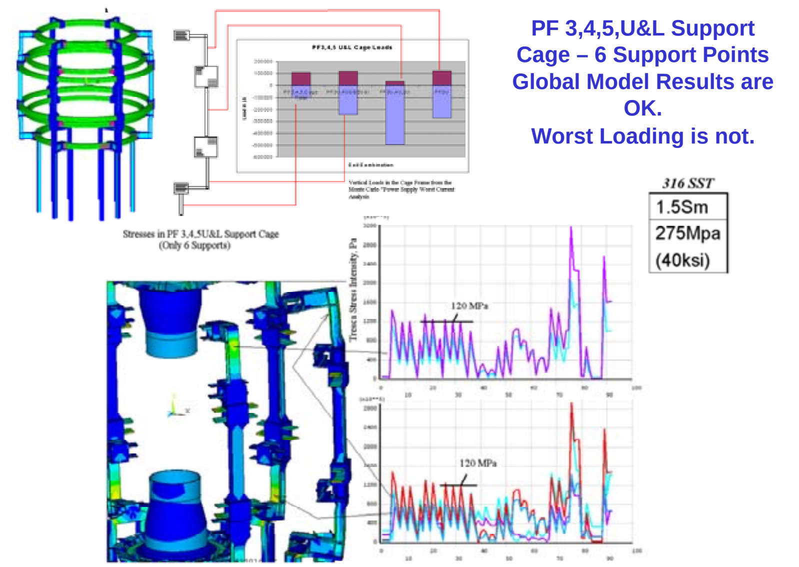

Figure 5.4.6.12.1-1 - Max And Min Vertical Loads in the Structural Elements of the Proposed Outer PF Support Cage

The vessel is not perfectly circular. A survey reported by Danny Mangra showed most locations out of round by no more than .13 inches. Near the ports, the vessel is out of round by about .75 inches. The vessel is made of 2 arcs, each approximately 179 degrees, and 2 flats which join them at the weld seams. One of the goals of the separate cage design, was to separate the alignment of the outer PF coils from the irregularities of the vessel. But since the inner PF coils and centerstack was aligned with the vessel, use of the vessel as the magnetic "fiducial" was preferred.

```
let nam$(numpf+2)="PF3,4,5,Cage"
let vf(numpf+2)=vf(6)+vf(7)+vf(8)+vf(13)+vf(14)+vf(15)  !PF34+5U &L
let nam$(numpf+3)="PF3U,4U&L,5U&L"
let vf(numpf+3)=vf(6)+vf(7)+vf(8)+vf(14)+vf(15)  !PF4&5l+PF3,4+5U
let nam$(numpf+4)="PF3U,4U,5U"
let vf(numpf+4)=vf(6)+vf(7)+vf(8)  !PF3,4+5U
let nam$(numpf+3)="PF3U,4U&L,5U&L"
let nam$(numpf+5)="PF3U"
```

Figure 5.4.6.12.1-2 Monte Carlo Analysis Based on Worst Case PF Power Supply Capabilities

Table 5.4.6.12.1-1 – Vertical Load Cases for the Outer PF Supports

Fz(lbf)	PF3U	PF4U	PF5U	PF5L	PF4L	PF3L
Min	-150417	-216571	-242555	-62432	-91785	-35783
Worst Case Min	-314951	-450863	-541645	-212419	-161901	-272627
Max	103217	91746	62512	242490	198573	150425
Worst Case Max	272631	161856	212552	541490	450422	314965

5.4.6.12.2-PF4 and 5 Support off the Vessel with Added Columns

The expense of the outer PF frame – particularly the effort associated with removing Diagnostics and instrumentation, power and coolant lines, to install the cage structure has led to the investigation of supporting the outer PF coils off the vessel. This is the original support concept used by NSTX. The re-categorization of the worst case current loads as "Extremely Unlikely" as described in the structural criteria document, has allowed consideration of less extensive modifications to the outer PF supports. In the this concept, stronger columns are being added to connect the upper PF4/5 grouping and PF4/5 lower groupings. The location for these six columns is chosen to be between the existing

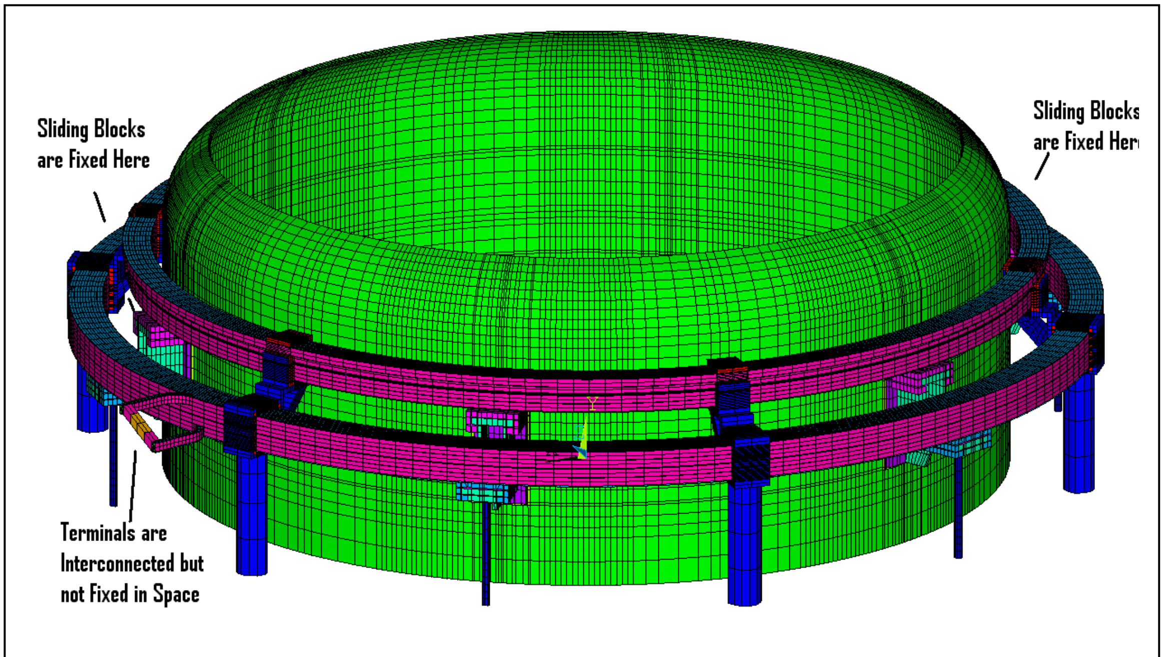

Figure 0-64 PF 4/5 Support Column Upgrade Mounted on the Vacuum Vessel

(small/weak) columns. These locations are judged less congested than the existing attachment points. Figure 0-64 shows the PF 4/5 support column upgrade mounted on the vacuum vessel. Figure 0-65 shows the coil out-of round condition caused by the Joule heating of PF4 and 5 during normal operation.

The support concept must also allow the thermal expansion of the coils to their temperature maximum of 100 degrees C, while maintaining the coil centered on the plasma. The concept utilized here is to allow oval deformations of the coil while holding the coils radially coupled to the vessel near where the terminals exit the coil and 180 degrees opposite this point. Figure 5.4-72 illustrates the support concept and the half symmetry model used to qualify the support scheme.

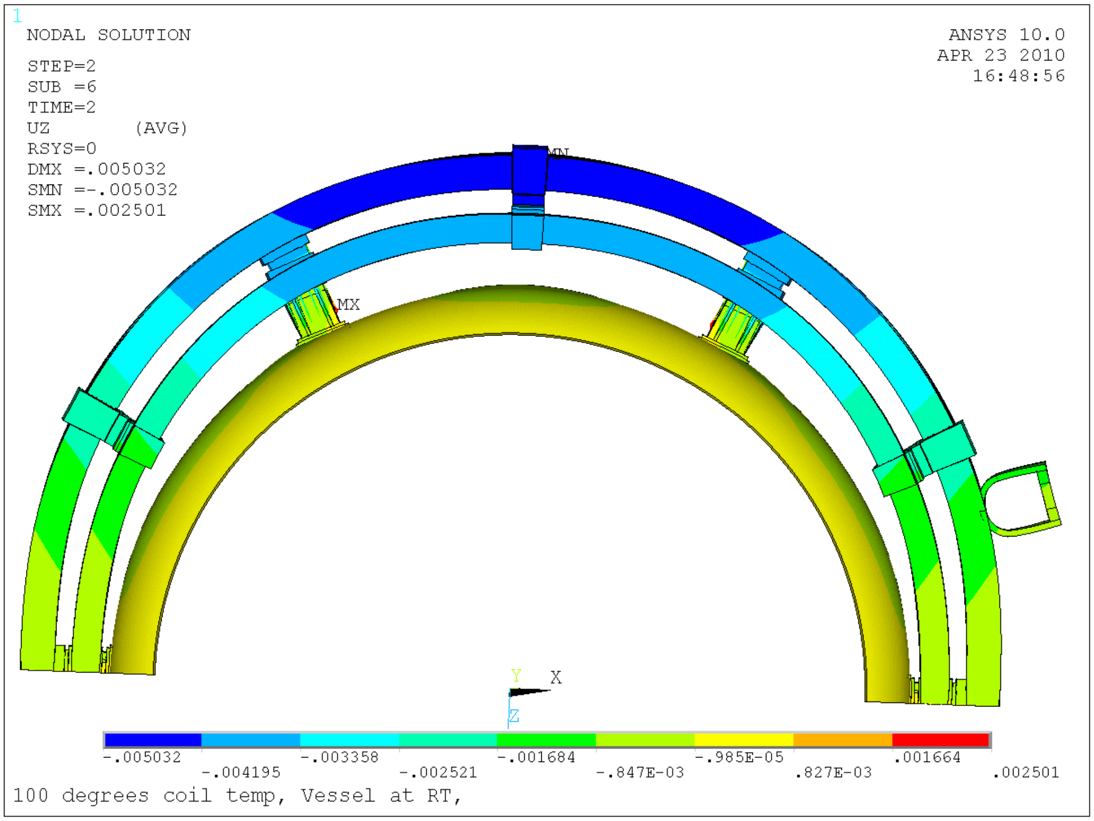

Figure 0-65 Coil out-of-round condition caused by the Joule heating of PF4 and 5 during normal operation.

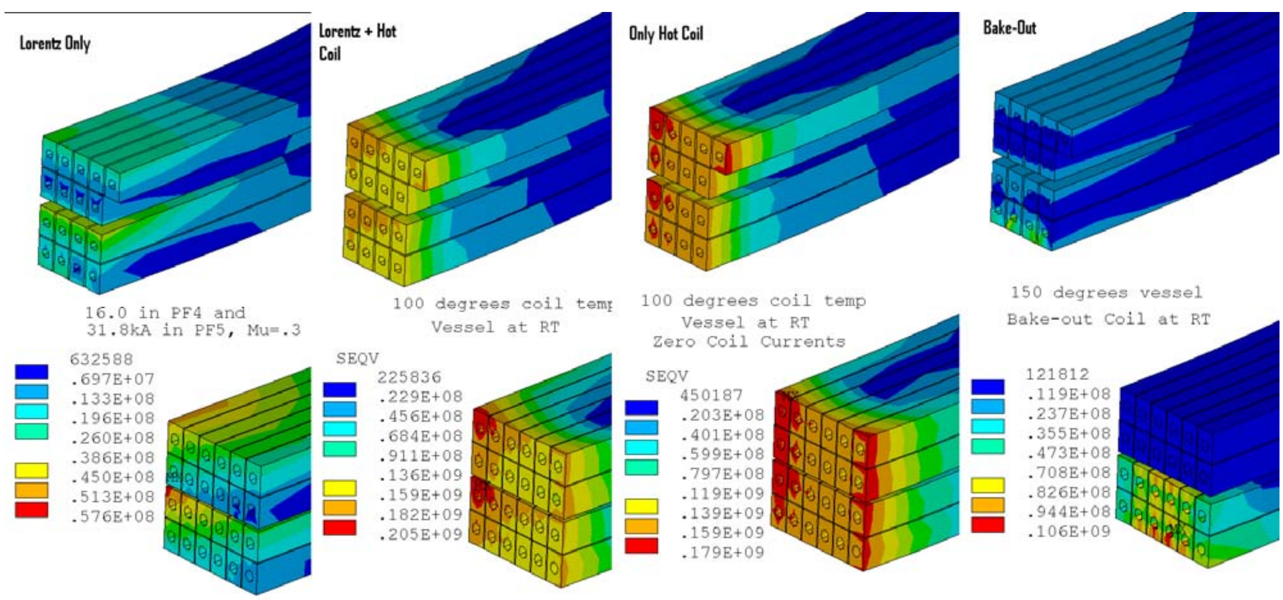

Figure 0-66 PF 4 and 5 Coil Stresses For Various Loading

5.4.6.12.2.1 PF4/5 Support Column and Bracket Hardware Stress

Columns are modeled as 5 inch in diameter and ½ inch with wall thickness

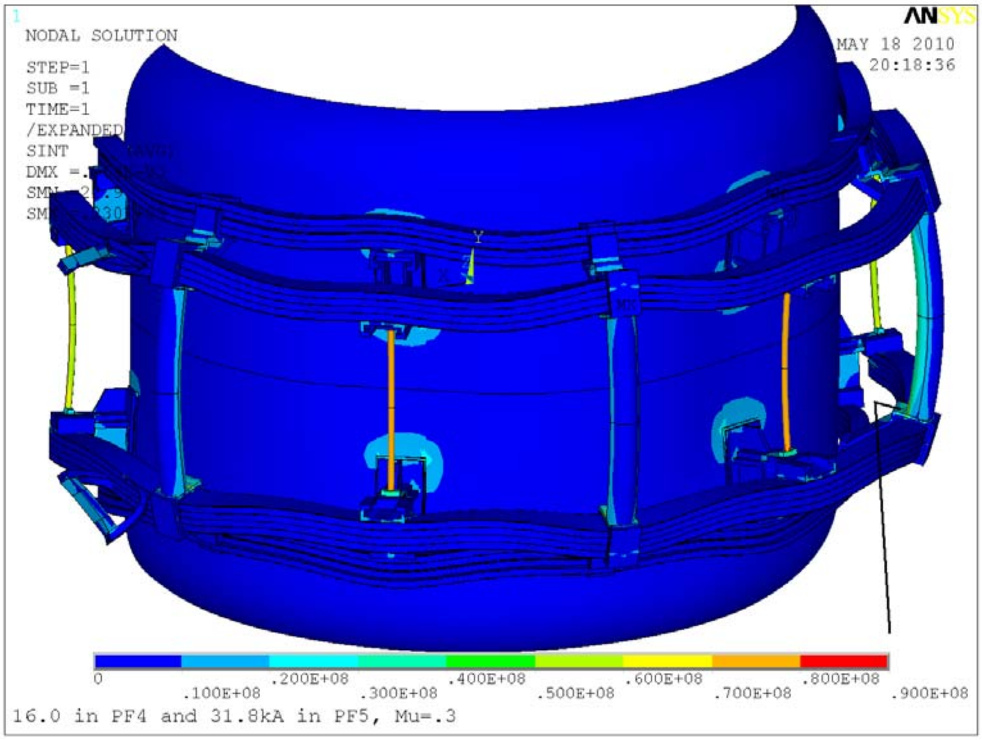

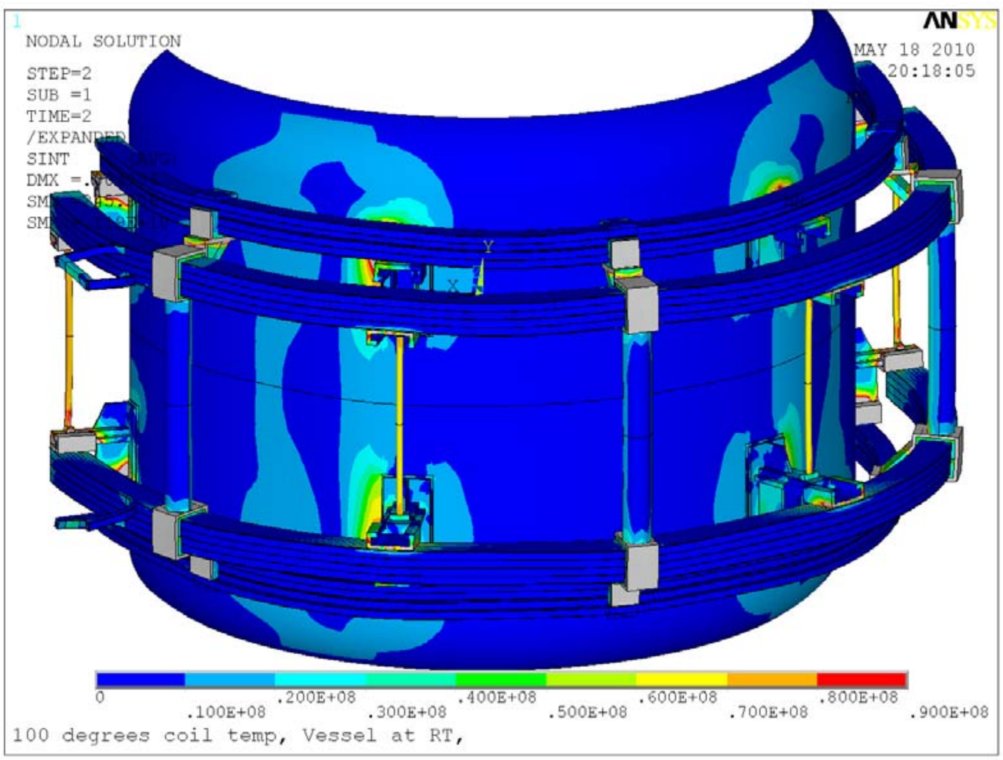

Proposed PF4/5 Column Clamp

5.4.6.12.3- Current Support of PF4 and 5

5.4.6.12.2.2 PF4 and PF5 Bracket Existing Welds

The weld is nominally 5/16, but the QA report recommends that it be treated as an effective ¼ inch weld .To facilitate meshing the weld, an arbitrary cross section is used then the weld stress is scaled by the ratio of the weld section in the model to the actual weld section. In this case, the weld was intended as a fillet, but material has been added to accommodate the vessel curvature, and the resulting weld was derated. The weld is assumed to have a larger cross section than a fillet, so the .707 factor was not applied. The weld allowable is a function of the level of inspection that is applied. At PPPL only visual inspection is routine. ASME would require a weld efficiency of 0.7 or lower.

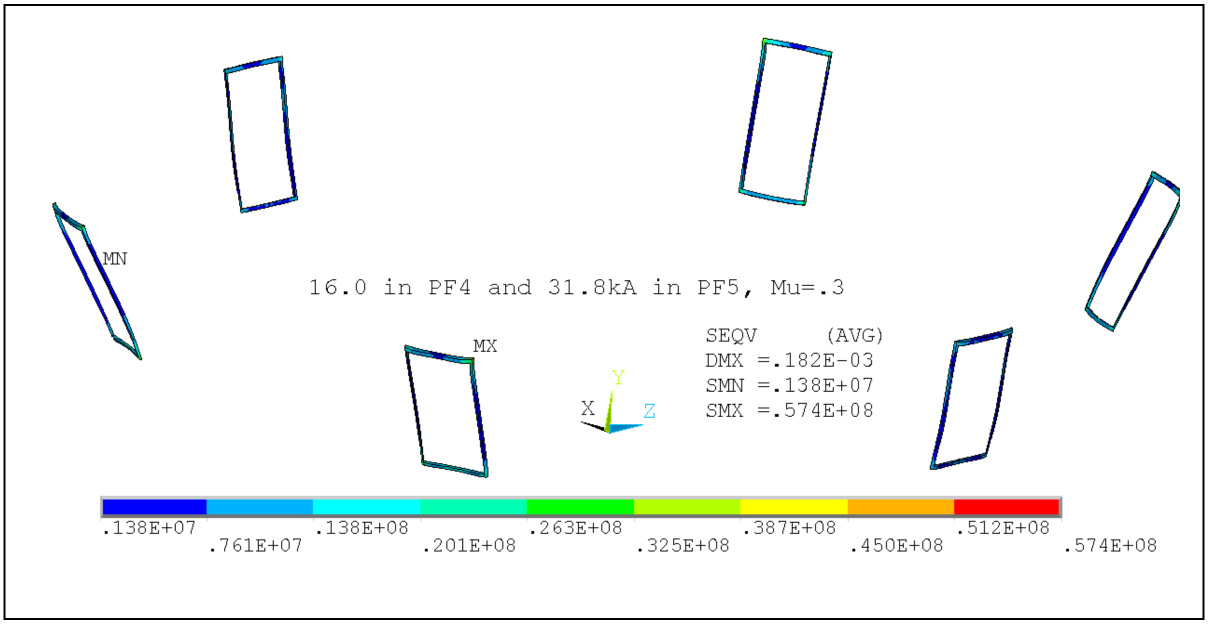

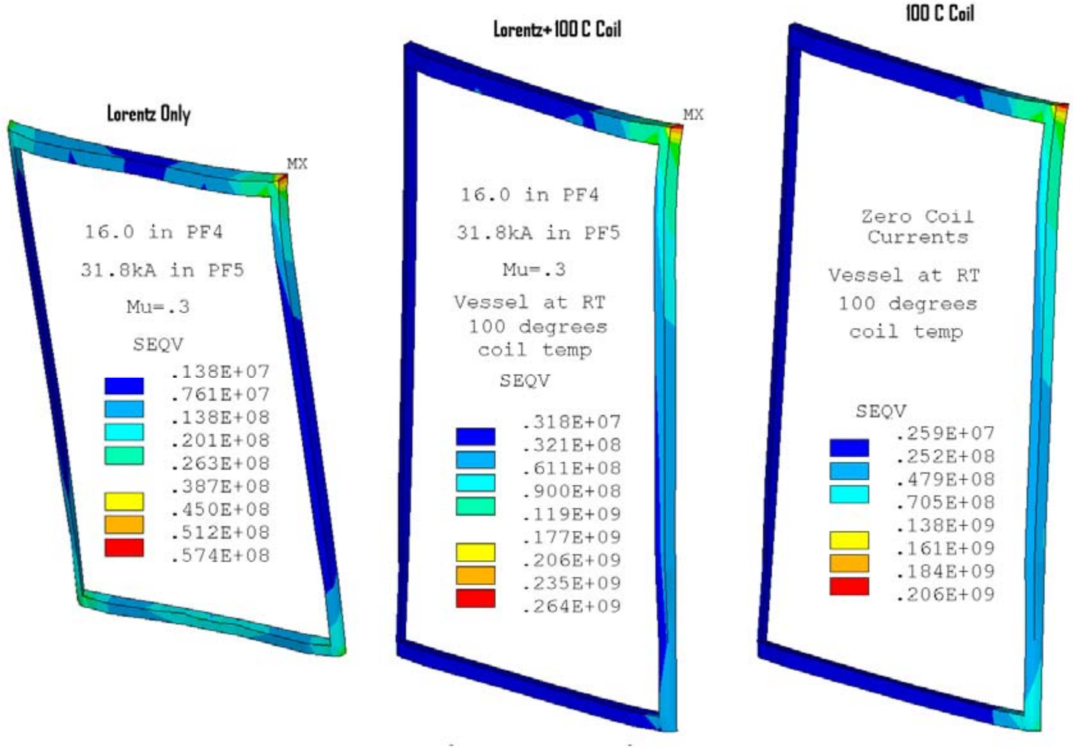

5.4.6.12.2.3 PF 4 and 5 Supports Dynamic Response to Normal Scenario Loading

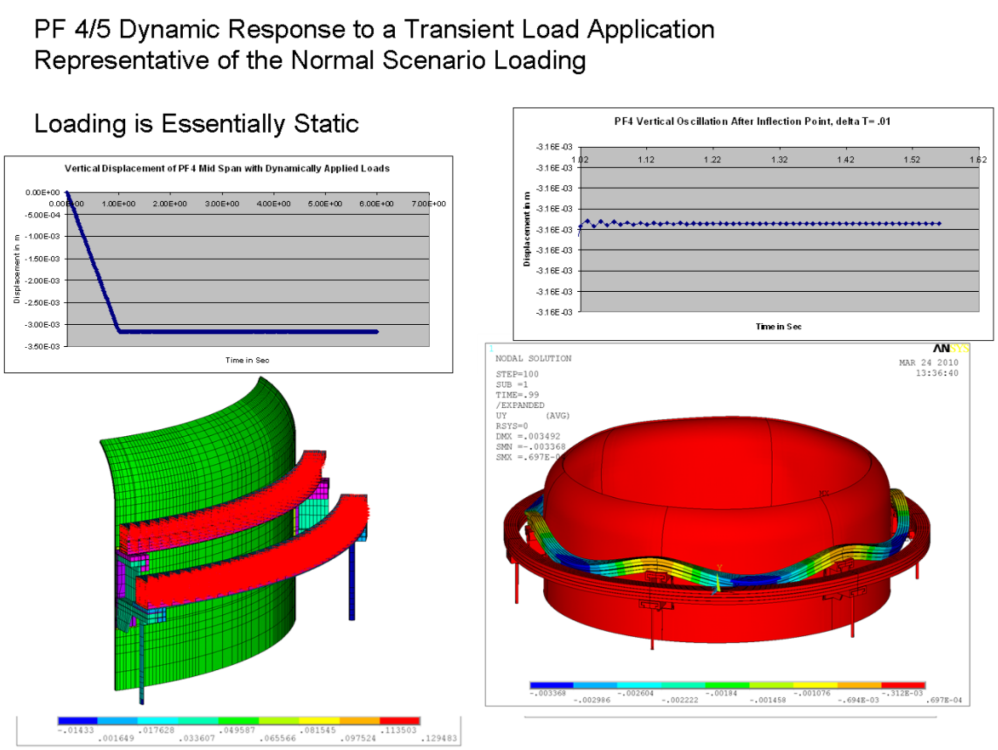

Mode 1 73 Hz PF5 Rotating about a Vertical Axis

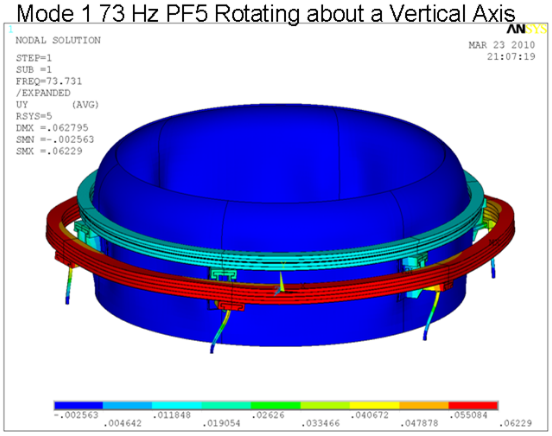

Mode 2 105 Hz PF5 Bending Mode

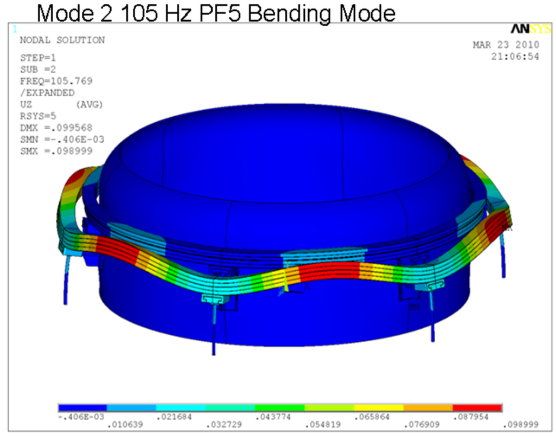

Mode 3 132 Hz PF4 Bending Mode

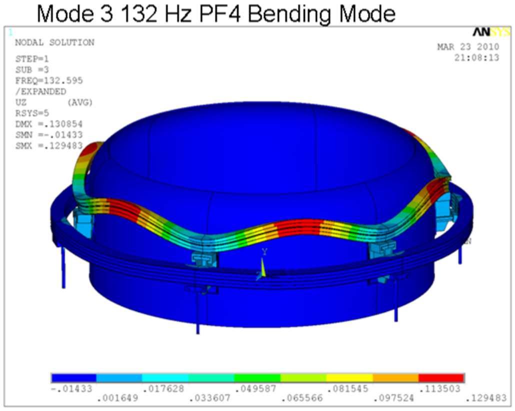

Mode 4 156 Hz PF4 Radial Oscillation

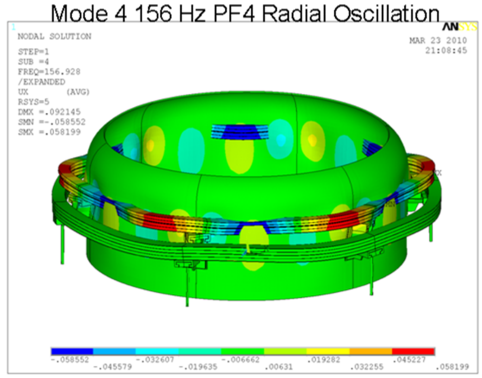

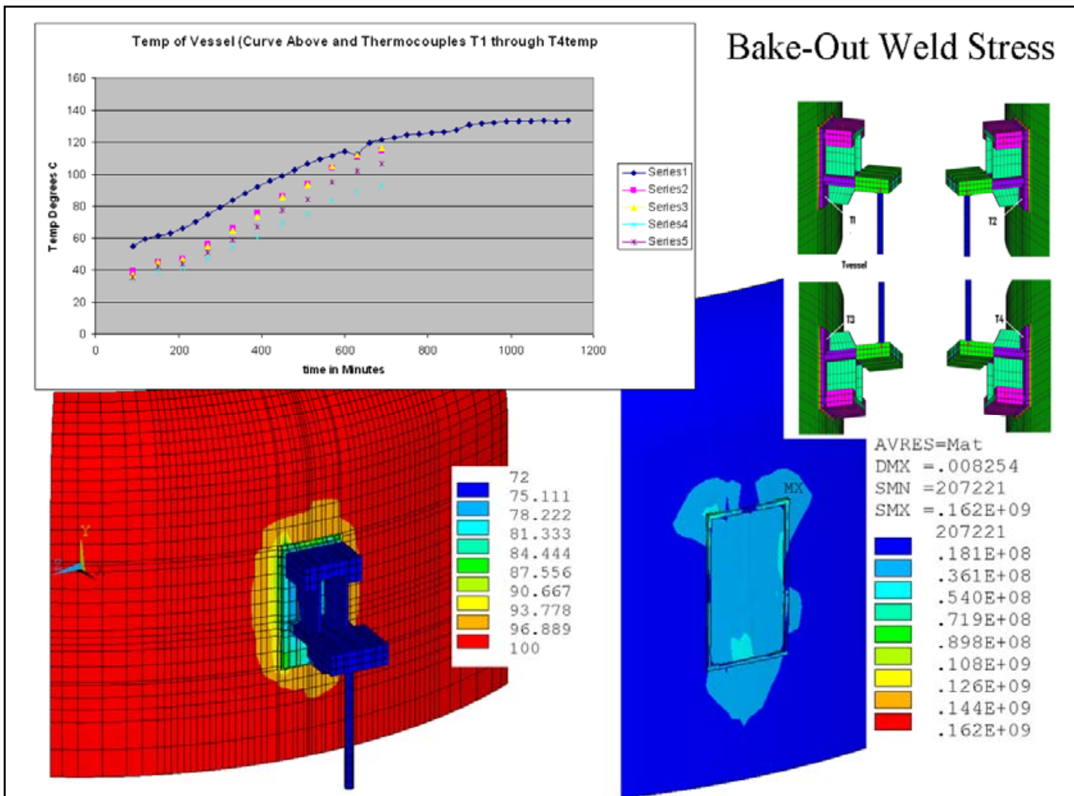

Stresses in the Vessel Shell and Due to Bake-Out Differential Temperature

PF4/5 Support Weldment Stress Algorithm (Appropriate for Fatigue)
Static Application of Loads will not be Based on Peak Stress

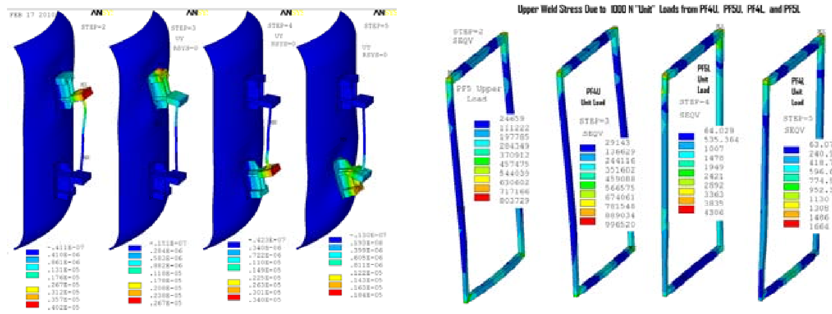

PF4/5 Weldment
Nominal Weld = 5/16 in. QA Effective Weld = 1/4
FEA Weld Model Thick =10mm

Weld Stress to FEA Stress = (.01*39.37)/.25 = 1.57

Weld Allowables are:
14 Ksi for Visual Inspection
20 ksi for Penetrant Inspection

	PF4U	PF5U	PF4L	PF5L
From FEA	996520	803729	4000	1500
Weld Pa/Newton	996.52	803.729	4	1.5
Weld psi/lb	0.964377	0.814102	0.004052	0.00151936

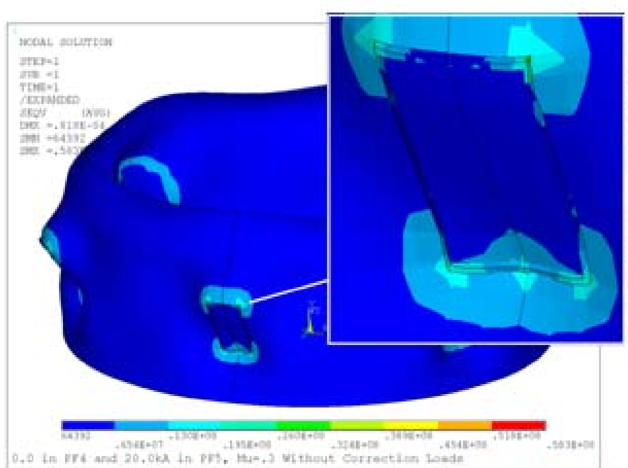

Weique Que told me that the protection system would only allow 18 kA based on my multipliers.

I improved the mesh around the corner – Still has a sharp point, but the stresses are lower.

PF4/5 Weldment
Nominal Weld = 5/16 in. QA Effective Weld = 1/4
FEA Weld Model Thick =10mm

Weld Stress to FEA Stress = (.01*39.37)/.25 = 1.57

~25MPa * 1.57 = 39.25MPa = 5629 psi

Based on the Corner Peak:
58 MPa*1.57 = 13274 psi

14 ksi is allowed with only visual inspection

5.4.9.1 Bus Bar Support Analyses

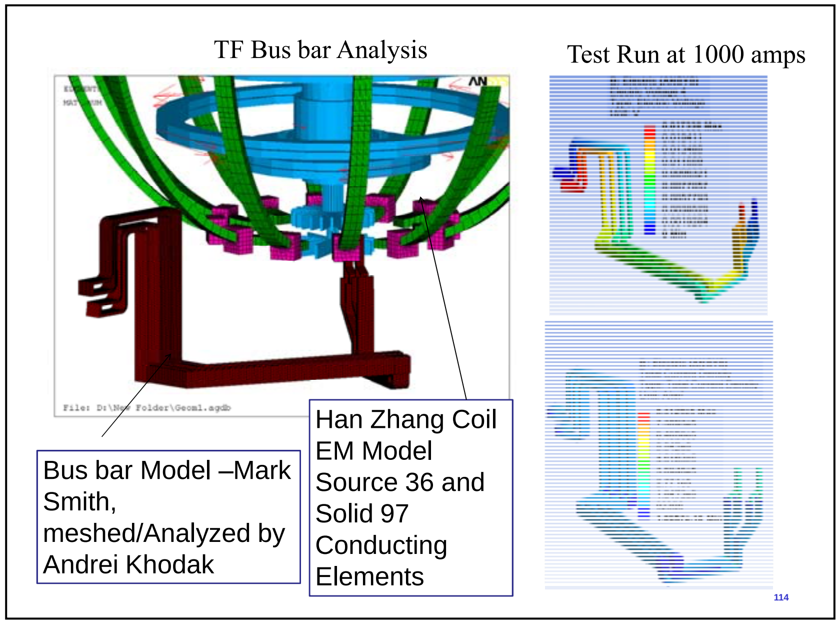

Bus bar analysis has begun during the preliminary design activity. Mark Smith provided ProE models of the TF bus runs. Andei Khodak has used H. Zhang's model of the magnets to calculate the background field and has computed current densities, Lorentz forces and resulting stresses. The magnet model includes conducting elements that model the outboard legs and ANSYS source 36 elements that model the inner TF legs and the poloidal field coils. The solution includes both the background field and self loads from the bus bars. Resulting stresses are modest except at corner bends in the support brackets. Thermal expansion effects have not yet been simulated. Adjustments in the support locations and support bracket design are expected in the final design effort.

The TF bus bars are attached to the most geometrically stable region of the machine. PF 1a and b are mounted on the top of the centerstack casing, which expands with the heating due to a shot. Art Brooks heat balance analyses in section 3 calculates temperatures of components throughout the internals of the vessel including the centerstack casing. expansion was simulated and a stress pass was done. This is discussed in section

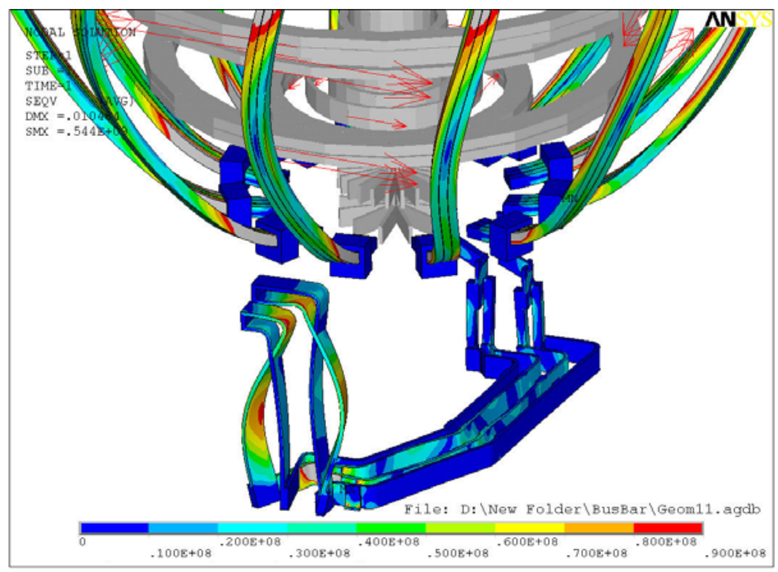

Preliminary Stress results for Scenario #79

Plasma Heating & Current Drive System (WBS 2)

6.1 High Harmonic Fast Wave (HHFW) – WBS 2.1

The NSTX HHFW Antenna has been operating since 1999. For the 2009 run, it was upgraded from a single feed, bottom grounded strap configuration to a double feed, center grounded current strap.

A finite element electromagnetic model of the antenna was generated using the ANSYS code. The model included four of the 12 antennas, and fully represented the important in-vessel components including the straps, backplates, current straps, and Faraday shields. This analysis, performed to satisfy a CHIT from the final design review, indicated that the stresses in the critical areas near the center post of the strap, and the connection of the strap ends to the feed-throughs , were acceptable. Figure 6.1-1 summarizes the disruption analysis of the HHFW antenna.

As part of the NSTX upgrade design, the model was run with ambient fields and plasma current representative of the upgraded NSTX. Critical Hardware details are being evaluated for the higher loads.

Reference Drawings are:

- E-8C3B01, Rev. 2, RF Antenna General Arrangement 12 Antenna Array
- E-8C3B02, Rev. 2, RF Antenna 1 through 12 Assembly

At the CDR, only a mid-plane disruption was modeled. This produces vertical field transients parallel to the straps. During the CDR, a VDE simulation was added to the antenna qualification. Off axis disruptions are being simulated which will have more significant radial Bdot and will load the antenna straps differently than the mid-plane disruption simulation. Loads and stresses are small for the cases analyzed so far, and further analysis is intended mainly to be comprehensive, and little or no design changes are anticipated.

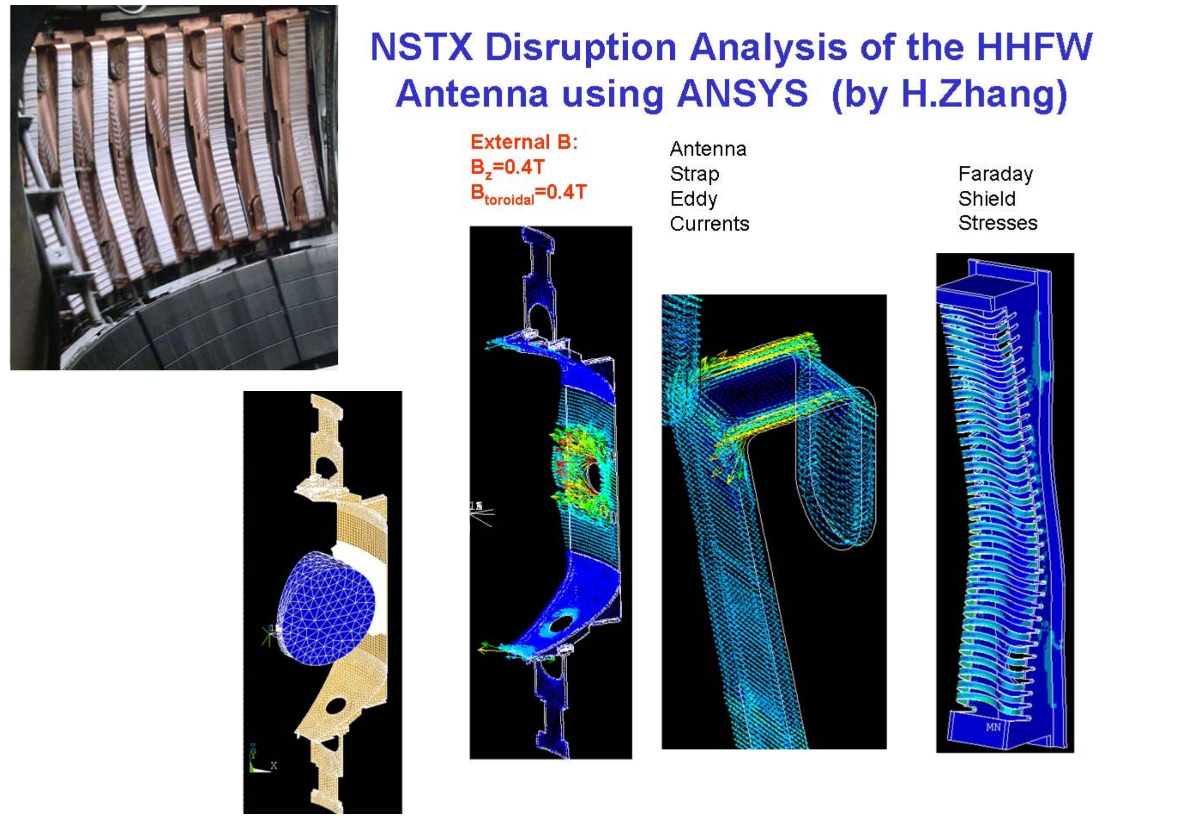

Figure 6.1-1 – HHFW Disruption Analysis

6.2 Electron Cyclotron Heating (ECH) – WBS 2.3

To date, no structural analysis has been performed on the ECH waveguide. This has been carried as a task to recognize that there are many areas in NSTX that may require upgrade to survive the higher background fields.

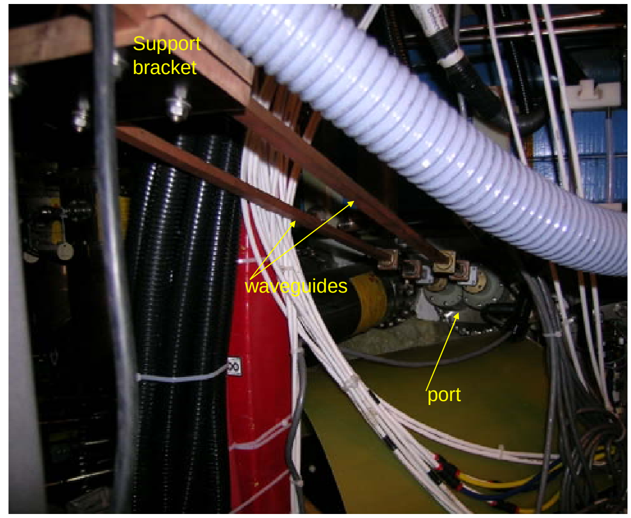

Figure 6.2-1 – ECH Support Details

6.3 Neutral Beam Injection (NBI) – WBS 2.4

6.3.1 Effect of Net Load from NBI Bellows

Based on an e-mail from Danny Mangra, dated November 24, 2009, the following information is available on the effect of the vacuum load on the Neutral Beam Port Bellows.

With the addition of the second neutral beam, the net load due to the uncompensated pressure from the neutral beam bellows might produce enough of a net side load to stress the support columns and braces, or produce unacceptable displacements (Figure 6.3-1) These have been analyzed in a model of the vessel and legs. The Pressure load from two (one existing and one new addition) NB port bellows produces a net load of about 25000 lbs laterally on the tokamak vessel (see table 1). The diagonal braces on the I beam columns help keep the displacements below 2 mm and the column stress is less that 100 MPa. Figure 6.3-5 shows the displacements with and without the neutral beam port covers.

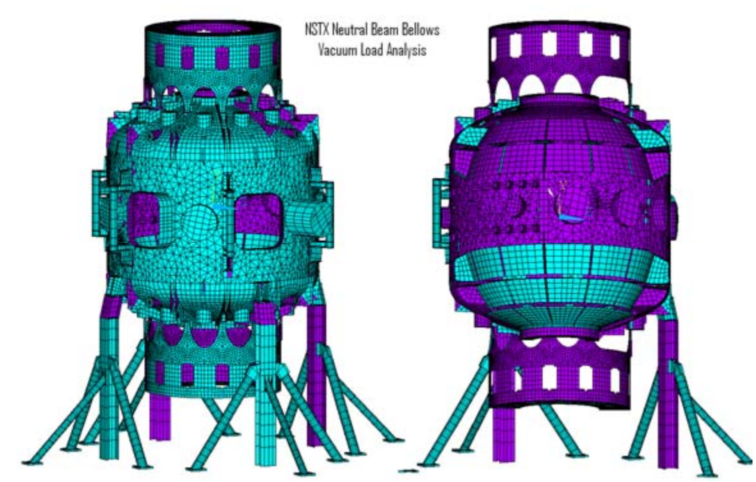

Figure 6.3-1 - The Model Without the Neutral Beam Port Covers is Shown. Blue and Purple Denote the Plate Element Faces

Vacuum loads produce small stresses in the vessel shell. The major radius of the vessel is 1.71m and the thickness is 5/8 inch. For 1 atm or 0.1MPa, the shell stress

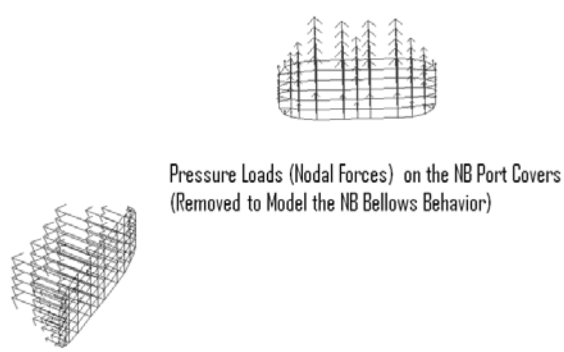

Figure – Loads on the Port Covers (Removed to Model the NB Bellows

is .1*1.71/(5/8/39.37) = 10.8 MPa. – a very small contributor to the global stress. The larger components are those that the vessel must support resulting from Lorentz loads.. The vacuum vessel model portion of the global model was "cleaned-up" with almost all surface normals properly aligned. .All of the big ports and most of the small ports were covered to achieve pressure balance on the model. There are still some residual load imbalances and consequently the model was run with and without the NB ports covered to see the difference in behavior. The displacement range was about 2mm with and without the neutral beam port covers. Figure 1 show the model. The umbrella structure and passive plates were included, but they had no pressure loading. Figure 3 shows the stresses in the vessel and supports, only due to vacuum loads. Note there is a bit more bending stress in the support column (Figure 6.3-3 and 6.3-3)

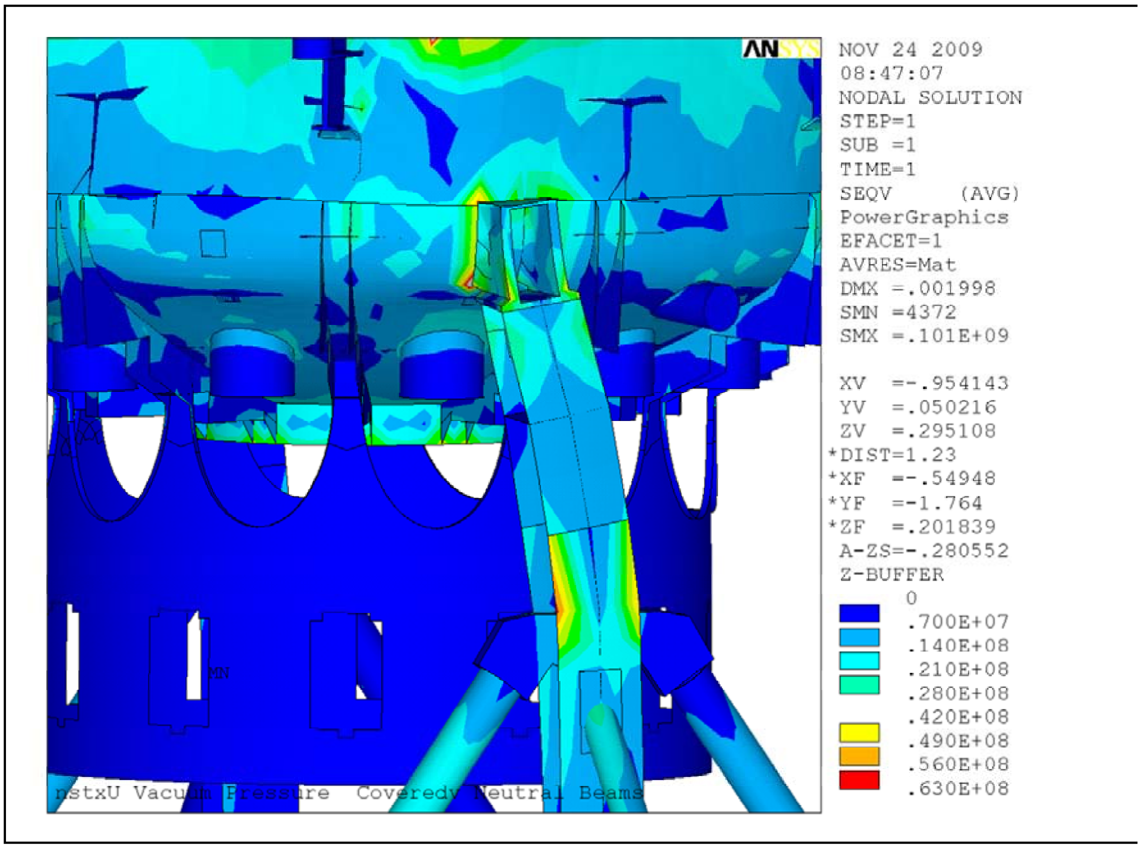

Figure 6.3-2 – Support Column Bending

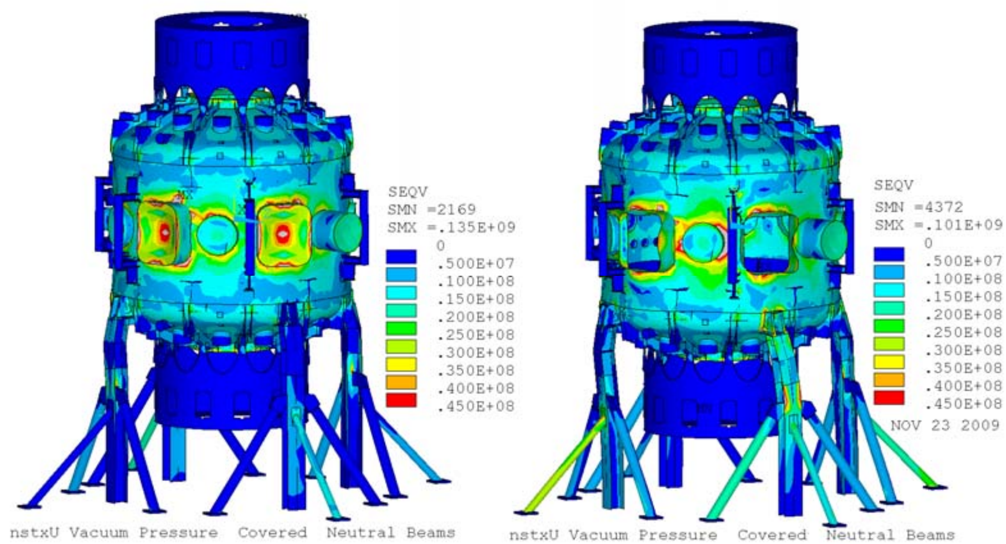

Figure 6.3-3 - Von Mises Stresses With Braces and With and Without the Neutral Beam Port Covers

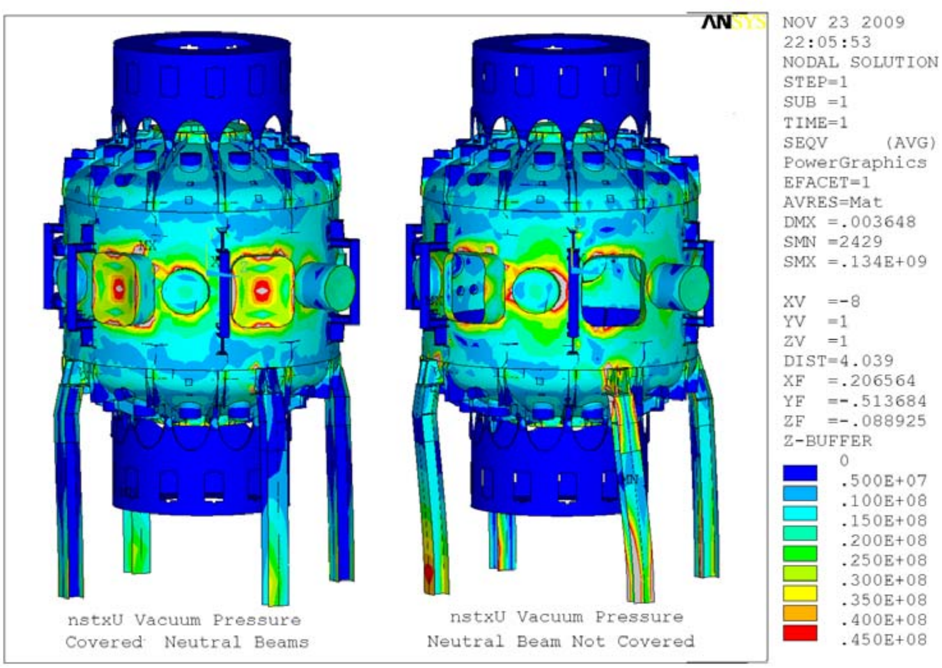

Figure 6.3-4 - Vessel Stresses Without Braces With and Without NB Port Covers

The model was run without the bracing for comparison and the displacements were larger, about 4mm vs the 2mm with the braces. Figure 6.3-5 shows the displacements with and without the NB port covers.

Figure 6.3-4 shows the vessel stresses with and without the NB port covers. Table 6.3-1 shows the details of the force summations from the ANSYS model and load model.

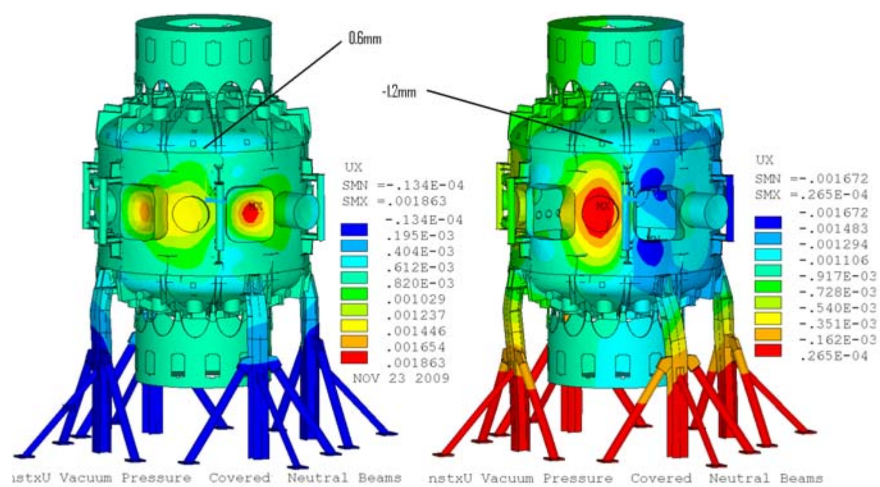

Figure 6.3-5 - Displacements With and Without Neutral Beam Port Covers

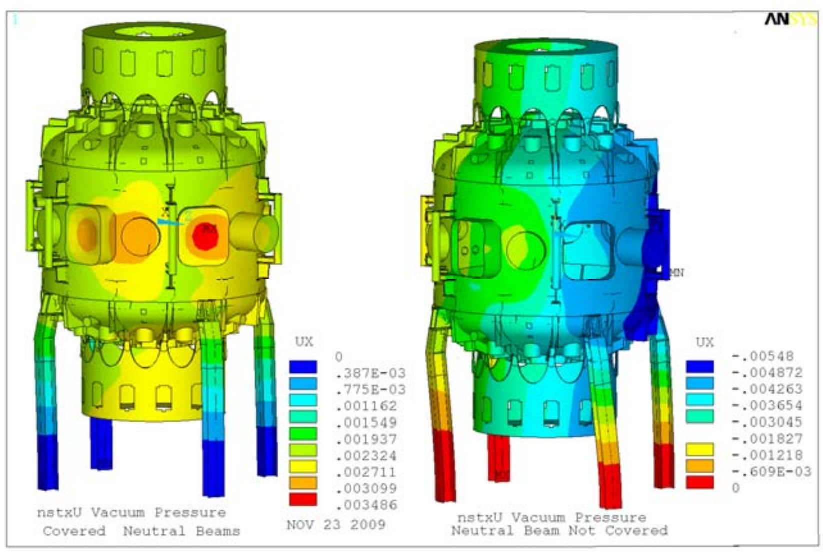

Figure 6.3-6 - Displacements Without Braces, With and Without NB Port Covers

Table 6.3-1 - Force Summations from the ANSYS Model and Load File

	FX	FY(vert)	FZ		SRSS	
No Neutral Beam Port Covers	68786	17011	44665		82015.1	N
With Neutral Beam Covers	-43836	17011	17624		47246.17	N
	112622		-62289		128699.8	N
Net Load from NB Press Load in FEA Model(2 ports)				Press Load (Lbs)(2 ports)	28931.71	
NB1 Port Area	0.6653	m^2		Press Load (Lbs)	15158.83	lb
	0.6653	m^2		Press Load (Lbs)	15158.83	lb
				Press Load (Lbs)(2 ports)	30317.66	lb
Vector Sum NB Press Loads from Model	112622	0	0		112622	N
					25317.43	LB

6.3.2 Neutral Beam Armor Electromagnetic Disruption Analysis

The procedure developed for the passive plate analysis (Section 3.3) was applied to the Neutral Beam Armor plates by Larry Bryant. Static Stress and Transient Dynamic Analyses were performed. Magnetic vector potential data tables from Ron Hatcher's 2-D Opera results were expanded into 3-D through Srinivas Avasarala procedure and e-mail dated 2-29-10. Opera Data for Outboard Displacement encompasses Max disruption load case. ANSYS Element Solid 97 Classic Formulation was used. The Voltage at Vessel Boundary set to be zero potential. All Components are Merged Integral Solids from Pro-Engineer. There are no gaps or other nonlinear material properties. All support structure braces are merged solids. Note: reaction loads and moments are only approximate – not for final design. The transient dynamic analysis assumes 0.5% structural damping. Symmetric boundaries are assigned to cylindrical cuts above and below the armor plate. 304 Stainless steel properties are used throughout. Temperature dependence is not included in this analysis. The Transient Equivalent Stress at Max Current is less than 10 Ksi , and well within the material strength capacity (Based on Merged Solids) The reaction loads are less than 100 lbs at the armor attachment points to the vessel although significant hoop loads (27,997 lbs) are reacted into

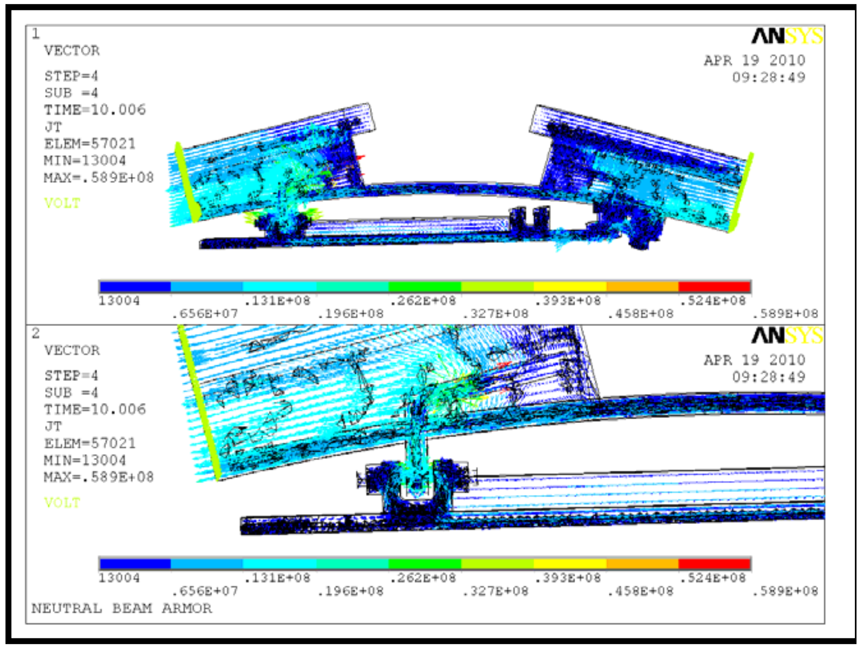

Figure 6.3.2-1 The Eddy Current Profiles Show Current Sharing and Normal Vector Profile at Voltage Boundary Condition

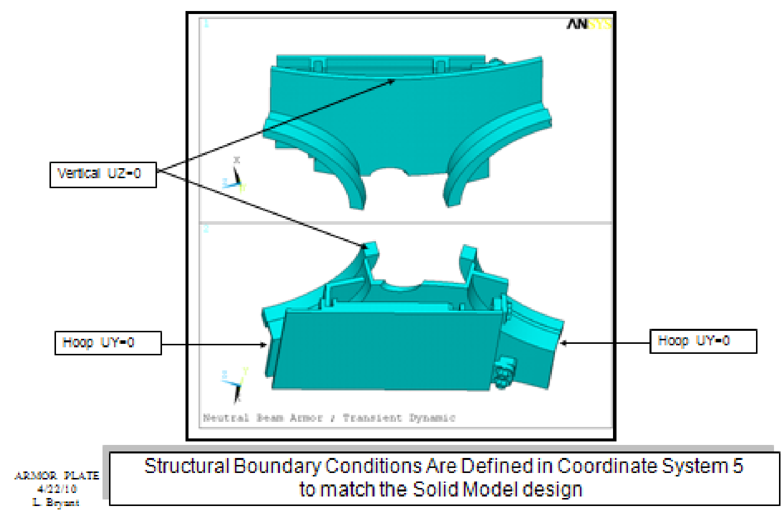

Figure 6.3.2-2 Structural Model Boundary Conditions

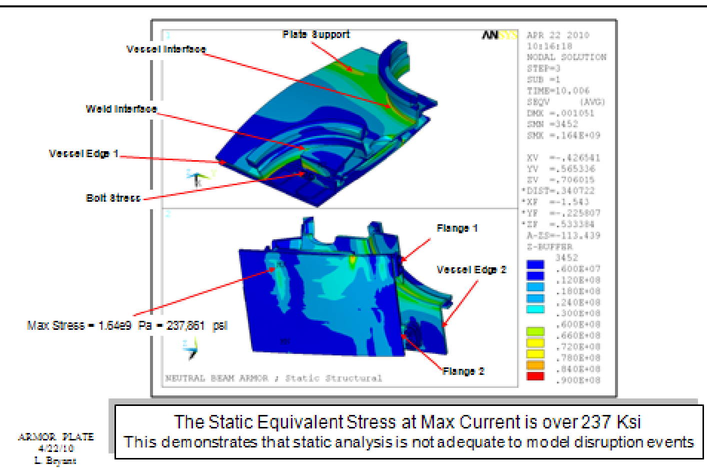

Figure 6.3.2-3 Static Analysis Results

the vessel boundary. This is conservative (although realistic) since we have assumed a symmetry condition. The max current density (3,764 E4 Amps /M^2) occurs 0.006 seconds into the disruption event. The max stress (9,892 psi) and X displacement (7.8 Mils) occurs at 0.009 seconds into the disruption event.

This analysis, like the other disruption analyses is subject to an on-going review of the disruption specifications. The files that were run for the armor plate are the same ones used for the passive plates. These have background fields that were maximized for the passive plate area, and are for a mid plane disruption. These assumptions are good for the neutral beam armor backing plate, but analyses based on the updated disruption files are planned. These results are based on a fully merged solid model of the brackets and bolting that attach the backing plate to the vessel. In the final design activity the local loads in the brackets will be investigated further. Also the tile loads and thermal gradients have not been evaluated. These will need attention in the FDR as well.

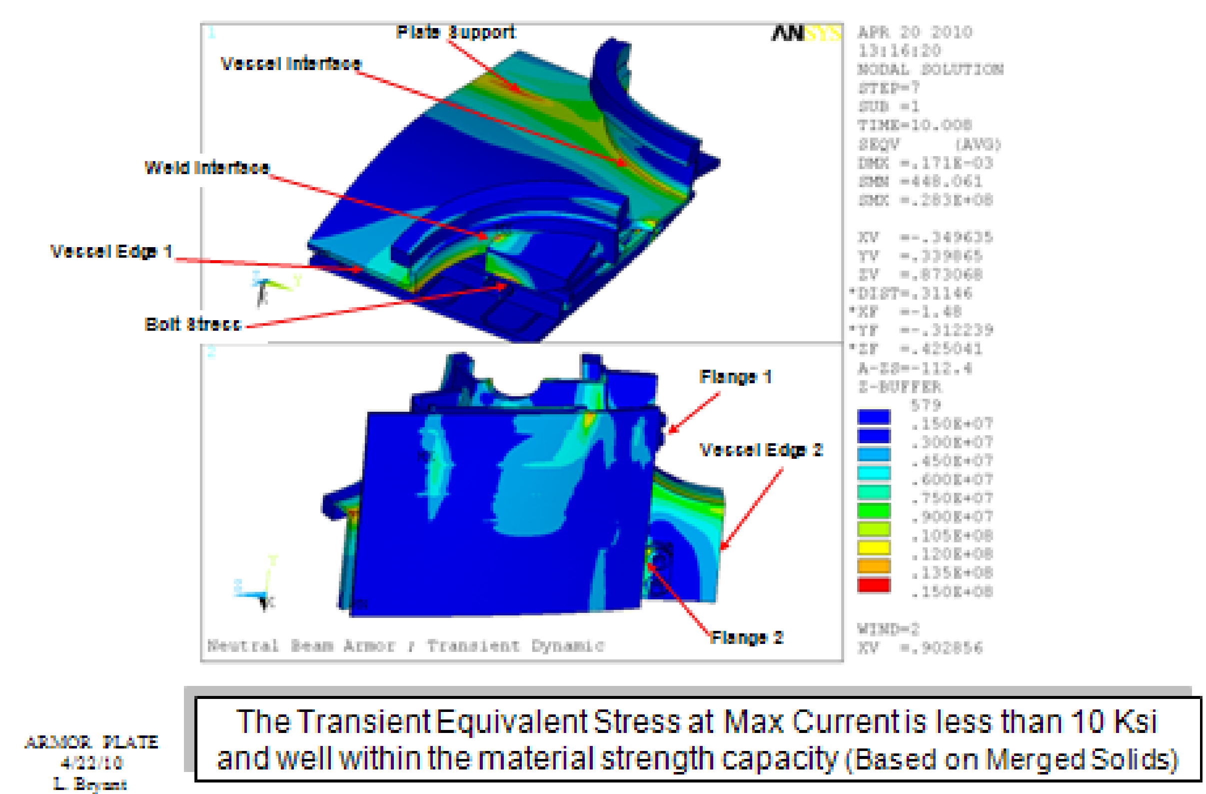

Figure 6.3.2-4 Transient Dynamic Von Mises Stress (Outboard Displacement Disruption)

6.4 Foundation Loads

6.4.1 Angle Brace Hilti Anchor Loads

As of Jan 7 2009, seven of the 12 embedment loads have been post-processed. It takes about an hour and a half per pad to go through the 96 load cases. The load files include bake-out vacuum, including the net side-load from the NB port, 90 of the 96 Current files and some of the extreme scenarios from Han's OOP truss/radius rod analyses. The global model was updated in late December 2009 to include the existing PF4 and 5 supports. It was post-processed to quantify the reaction loads at the brace pads. In order to facilitate the extraction of the reaction loads, the model of the brace structures was redone with real constants from 101 to 112 assigned to each lower pad. An ANSYS macro was used to create the reaction force files with the PRRFOR command. A true basic program was used to strip away the un-necessary text to allow reading the reaction force lists into EXCEL. Loads are in Newton. Hilti anchor loads would be the pad load divided by the number of Hilti's per pad -typically four.

```
ANSYS Macro
Load1=1
load2=108

*do,ireal,101,112
/output,breaction%irea
l%,txt
esel,real,ireal
nelem
nrsel,y,-5,-3.93

*do,ld,load1,load2
set,ld
prrfor
!fsum
*enddo

/output,term

*enddo
```

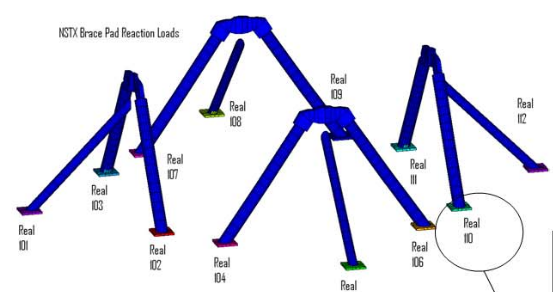

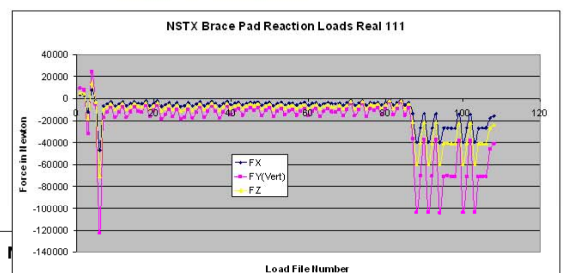

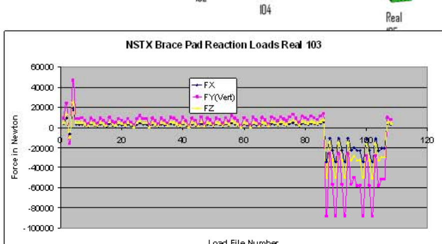

Brace Pad Reactions are ~100,000N
Or 22480 Lbs/pad or
5620 lbs per Hilti
(About the Capacity
of the Hiltis)

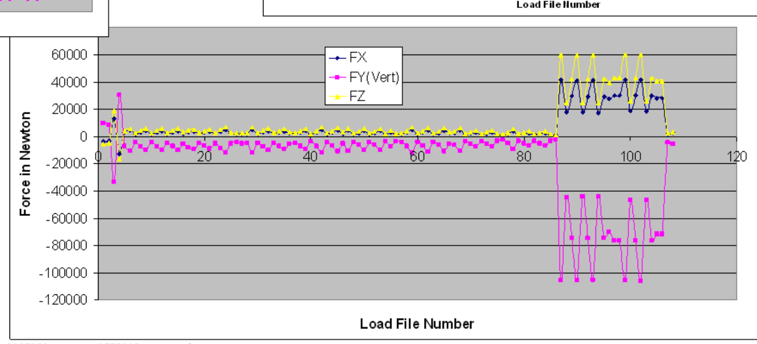

6.5 Seismic Analysis

At the PDR, only a static analysis of the NSTX global model has been done. This is conservative with respect to the original NSTX seismic analysis that was a hand static overturning analysis. In the PDR analysis of the global model, .5 g's lateral were applied v. the original .135 g requirement. The high acceleration was partially intended to address unknown masses (essentially diagnostics) not included in the global model.

Mike Kalish prepared a memo that addressed the seismic requirements for NCSX. Mike spoke with Jerry Levine about the seismic requirements for NSTX. Mike's starting point was the requirements that he wrote for NCSX. This memo started with the Safety Assessment Document and the DOE requirement 1020-2002.

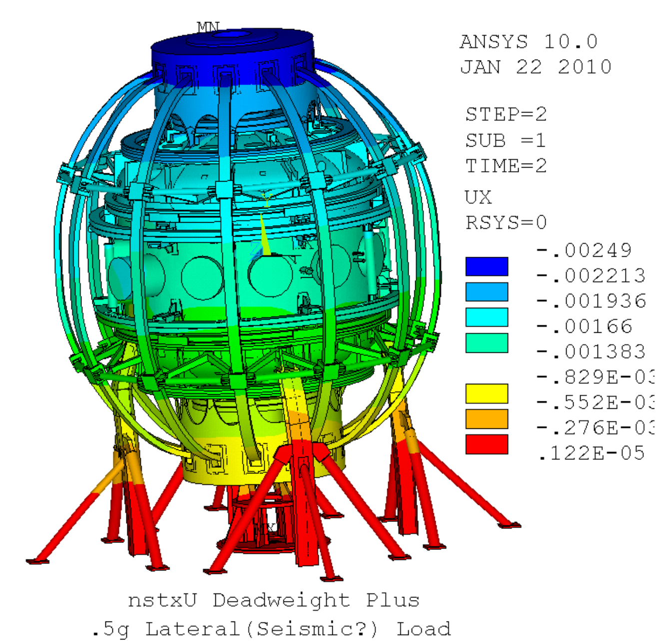

Figure 6.5-1 Lateral displacement for .5 g Lateral Acceleration

"Based on applications of DOE Order O420.1A and DOE Guide G420.1-2, PPPL is required by the Department of Energy to meet the seismic requirements of DOE-STD-1020-2002 Performance Category 1 for Seismic Use Group I. Interpretation of these requirements leads to the adoption of the International Building Code, IBC 2000, with 2/3 the Maximum Considered Earthquake (MCE, site specific) as the standard for PPPL"

It appears that these requirements have not changed since Mike wrote this memo in 2004 so the basic assumptions in the document should be correct. The only caveat is that the evaluation was done using the IBC 2000. To be thorough a more recent IBC might be applicable. The PDR status of the seismic analysis is basically a conservative extension of the original NSTX criteria. This will have to be re-visited during the FDR.

Fp = Z I Cp WP = 0.135 Wp

Where:

Fp = lateral seismic forces
Z = a seismic zone factor.
I = an importance factor.
Cp = a horizontal force factor.
Wp = the weight of element or component

"Z" seismic zone factor: was determined using table 3 of DOE-STD-1024-92 "Probabilistic Hazard Results for DOE sites.

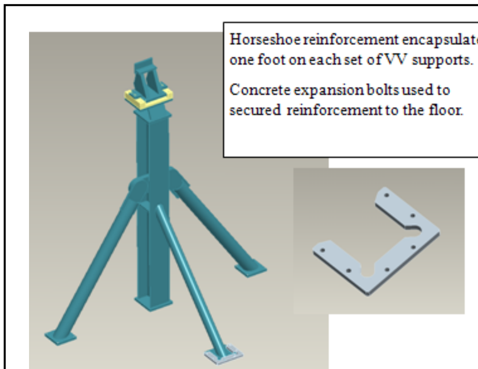

Horseshoe bracing needed at Four of the Brace Feet.

For PPPL, Z = 0.09 g[1]

"I" importance factor: for PC-1, was determined using tables 23-K and 23-L of the Uniform Building Code (UBC)

For PC-1, I = 1.00

"Cp" horizontal force factor: **= (1.5) for non-rigid elements**
= (2.0) for cantilevered walls

[1]U.S. Department of Energy, "Guidelines for Use of Probabilistic Seismic Hazard Curves at Department of Energy Sites", DOE-STD-1024-92 December, 1992

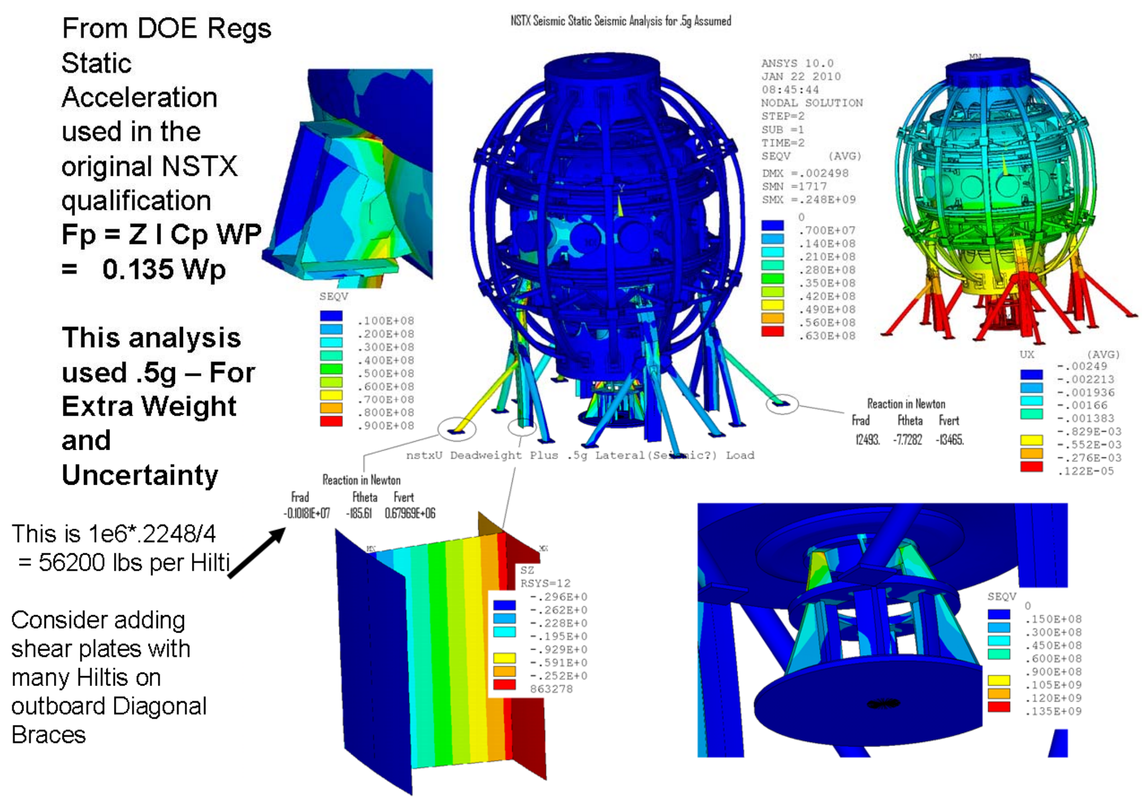

7 Diagnostics Analysis Summary

The purpose of this analysis is to predict any unintended effects that the NSTX-CSU may have on the diagnostic systems, including mechanical failure of the shutters, material degradation from radiation, and any other perceived threats to the diagnostic.

Table 2, below, lists the diagnostics and the most likely cause(s) for concern for each diagnostic if there are any.

Table 2.
List of diagnostics and the most likely cause for concern and relevant comments for each diagnostic.

Diagnostic	Causes for Concern/Comments
"Optical" soft x-ray array	None. Diagnostic is being replaced.
1-D CCD Hα cameras (divertor, midplane)	See General Concerns for Cameras
2-D divertor fast visible camera	See General Concerns for Cameras

Beam Emission Spectroscopy (BES) (32 ch)	Uses forced air cooling for optics during bakeout. If heating becomes a problem, cooling could be used constantly. Glass for optics could be darkened by radiation.
Biased Electrode and Probe (BEAP)	Should be unaffected. Will also be modified before upgrade.
Charge-Exchange Recombination Spectroscopy (CHERS): Ti(R) and VΦ(r) (51 ch)	Optics could be darkened by radiation.
Diamagnetic flux measurement	None. If loop is installed, it will be designed with upgrade in mind.
Divertor bolometer (20 ch)	See General Concerns for Cameras
Edge deposition monitors	Window could be darkened by radiation.
Edge Neutral Density Diagnostic (ENDD)	See General Concerns for Cameras
Edge neutral pressure gauges	None.
Edge Rotation Diagnostics (Ti, VΦ, Vppol)	Optics could darken from radiation.
Fast camera view of RF antennas	See General Concerns for Cameras
Fast ion D-alpha diagnostic	Should check supports for vibrations during disruption.
Fast IR Camera	Already becomes activated. Higher radiation dose will be worse. Also, increase in noise.
Fast lost-ion probe (energy/pitch angle resolving)	Radiation could darken glass.
Fast visible camera	See General Concerns for Cameras
Fission chamber neutron measurement	None.
Gas-puff Imaging (2msec)-midplane and divertor	Shielding for electronics may need to be increased. Fiber optics may darken.
Halo Tile current detectors	Thermally isolated. Could be a problem.
High-n and high-frequency Mirnov arrays	Saturation of digitizers.
Interferometry/forward scattering (1 mm, 1ch)	G10 base could become activated.
IR cameras (30 Hz) (3)	None. Also used on high radiation machines such as DIII-D.
Langmuir probe array-inter-LLD	Designed for 10 MW/m2 for 1 second. May need to be replaced anyway.
Langmuir probes-outboard edge	May need to be replaced when CS is taken out.
Langmuir probes-PFC tiles	On CS. Being replaced.
Langmuir probes-RF antenna	May need to be replaced when CS is taken out.
LLNL EUV spectrometer	None.

LoWEUS	
LLNL EUV spectrometer XEUS	Being relocated. No other concerns.
Locked-mode detectors	Possible saturation of digitizers. Detectors need to be relocated. Extra PF supports may interact with sensors.
Magnetics for equilibrium reconstruction	High heat fluxes may make diagnostics more difficult. Would be a nuisance, but not a problem. Mounting techniques may need to be modified because of high heat fluxes.
Microwave reflectometers (65 GHz backscattering, correlation, FM/CW, fixed frequency)	Window could darken. Copper pipes could bend from larger eddy currents (has happened before). Teflon connector cables could degrade.
Midplane tangential bolometer array	See General Concerns
Motional Stark Effect based on Collisionally-Induced Fluorescence	May need to clean window more often because of longer run time. Noise problems could worsen. Fibers could darken.
Motional Stark Effect based on Laser-Induced Fluorescence	Noise problems may worsen. Sightlines blocked by extension of beam armor.
Multi-pulse Thomson scattering (30 ch, 60 Hz)	May not be able to take measurement at 10 keV at higher temperatures. More noise and saturation problems. G10 components become activated. Vinyl and PVC could degrade.
Neutron detectors (2 uranium and 4 fast scintillator)	Will need to add another channel to accommodate higher neutron flux.
P-CHERS: Vθ(r) (75 ch)	Optics could be darkened.
Plasma TV	See General Concerns for Cameras
RF Antenna (ECH Launcher)	Most of the heat is taken by the boron nitride section.
RF edge magnetic probe	Shielded by tiles. Can be adjusted if they are too close to plasma.
RWM Coils	Should be checked for effects of eddy currents and vibrations.
RWM sensors (n = 1, 2, and 3)	Could be bent by forces induced by halo currents. May saturate digitizers.
Sample probe	Samples may become activated. Can be a nuisance, but not a problem.
Scrape-off layer reflectometer	Similar problems to microwave reflectometer.
SWIFT 2-D flow diagnostic	See General Concerns for Cameras
Tile temperature thermocouple array	Array on center stack will be replaced. Should be designed with upgrade in mind.
Ultra-soft x-ray arrays - tomography	Eddy currents could present a problem. May need stronger supports that can take a larger load. Noise from SPA’s is an issue. Adding more will make it worse.

UV survey spectrometer (SPRED)	To be relocated.
Vertical x-ray crystal spectrometer	None.
Visible (VIPS) survey spectrometer	Fiber optics could darken.
Visible bremsstrahlung detector (1 ch)	Window could be darkened. New beam dump needed (geometrical reasons).
Visible filterscopes	Fiber optics could darken.
VUV transmission grating spectrometer	Currently well-supported, though more supports may be desired. Fast cameras may be added.
Wall coupon analysis	Wall supports should be checked. Activation would be a nuisance.

General Concerns for Diagnostics

Several of the diagnosticians expressed concerns that could affect many of the diagnostics. They are listed below:

- The spa's (fast switching power supplies) create noise for the diagnostics. If more are needed, there will be more noise.
- Wire fatigue could be a problem for vessel-mounted diagnostics from more vibration.
- Saturation of digitizers could occur because of larger magnetic fields.
- More deposition (lithium, carbon, etc.) on glass from longer shots could cause problems for diagnostics.

There was also a concern that does not directly affect diagnostics, but may be important to correct since the radiation levels are expected to rise by a factor of 50. The test cell wall penetrations are drilled straight through (line of sight) the wall, allowing radiation to directly penetrate the wall. The holes should be drilled at angles to prevent radiation from penetrating.

General Concerns for Cameras

There are also concerns that will mostly affect cameras. First, any glass fiber optics or windows may darken much more quickly. If the darkening occurs too quickly, they should be replaced with quartz. Also, any cameras that use a silicon chip may need better shielding to prevent additional noise.

Diagnostic Shutters

The diagnostic shutters are being analyzed for the stresses that develop from eddy currents as well as their deflections due to these stresses. Thermal analyses may also be done to check for deflection. The eddy current analyses are being done in ANSYS using the resistive solution, since this is the worst-case solution. If the stresses that develop due to the resistive solution are too large, the inductive solution will also be checked for a more realistic comparison. The thermal analysis will also be done using ANSYS. The stresses due to thermal expansion are expected to be small, since the shutters are very thin.